Nano Crystal Semiconductor Synthesis, Characterisation and Photodegradation

Thesis submitted
to the University of Calicut for the
adjudge of the degree of

DOCTOR OF PHILOSOPHY IN CHEMISTRY

BINU NAUFAL

DEPARTMENT OF CHEMISTRY
UNIVERSITY OF CALICUT
KERALA- 673635
INDIA

JULY-2017

CERTIFICATE

This is to certify that the thesis entitled “Nano crystal semiconductor synthesis characterisation and photodegradation” submitted by Mr. Binu Naufal to the University of Calicut for the award for the degree of Doctor of Philosophy in Chemistry, is a record of precise research work carried out at the department of Chemistry, University of Calicut under my guidance and supervision. The contents of the thesis have been checked for plagiarism using the software ‘Urkund’ and similarity index falls under permissible limit. I further certify that the thesis or part has not previously formed the basis for the award of any degree, diploma, fellowship, associateship or any other similar title of any other universities or institutions.

Calicut University
January 2018 **Dr. Pradeepan Periyat**

CERTIFICATE

The adjudicators of the thesis entitled "Nano crystal semiconductor synthesis characterisation and photodegradation" submitted by Mr. Binu Naufal, have not suggested any major changes in the scientific content, results and interpretations. However some typographic errors and mild corrections suggested by the examiners are incorporated in the revised thesis.

Calicut University **Dr. Pradeepan Periyat**

January 2018

DECLARATION

I hereby declare that the matter embodied in the thesis is the result of studies carried out by me at the Department of Chemistry, University of Calicut, under the supervision of **Dr. PradeepanPeriyat**, Assistant Professor, Department of Chemistry, University of Calicut and the same has not previously formed the basis for the award of any degree or diploma. Whenever the work described or cited is based on the findings of other researchers, due acknowledgement is made in keeping with the general practice of reporting scientific observations.

Binu Naufal

ACKNOWLEDGEMENT

First of all I am highly grateful to Almighty Lord for his continuous blessing throughout my life.

I wish to express my deep sense of gratitude and indebtedness to my guide Dr. Pradeepan Periyat, Assistant Professor, Department of Chemistry, University of Calicut for his valuable guidance, personal attention, meaningful suggestions, help and encouragement , which would help me in future also.

I would like to express profound gratitude to Dr. P. Raveendran, Head of the Chemistry Department and former heads Dr. K. Muraleedaran and Dr. V. M. Abdul Mujeeb for having provided me with all the facilities to carry out this research work. I am very much grateful to Professor Dr.V. M Abdul Mujeeb for the effort he took for the fond of my fellowship and photoreactor, which are the key factors for completing this research work. I am highly thankful to all the teachers and non-teaching staff members for their timely help.

I wish to express my heartfelt thanks to my teacher Dr. P. Alikutty for his unusual help and support. I express my special thanks to Jaseela, my research group colleagues Shahnas, Jithesh, Dinesh and Dr. Sanjay, co-researchers and friends for their kind assistance rendered throughout my work.

I would like to acknowledge Dr. U. S. Hareesh, Material Science section, NIIST Thiruvananthapuram, Dr. G. M Bhalerao and Dr. Shamima Hussain of the UGC consortium centre Kalpakkam, NIT Calicut, King Abdul Azeez University Saudi Arabia, Physics

department, University of Calicutfor having kind enough for recording different spectra of the research sample.

I thank Divya and Shabeer of Physics Department for spending their valuable time for recording XRD of my samples.

I extend my gratitude to University Grants Commission for providing me the Basic scientific research fellowship.

I must thank from the bottom of my heart to my family members, especially my mother the driver of my life, for their inspiration, affection, prayers, encouragement, endurance and moral support at various stages of my endeavor.

Binu Naufal

To

The Society

"Anyone who can solve the problems of water will be worthy of two Nobel prizes-
one for peace and one for science"

-John. F. Kennedy

CONTENTS

LIST OF TABLES

LIST OF FIGURES

GLOSSARY

TP	:	Titanium tetra isopropoxide
AC	:	Acetic acid
TSm1	:	1% Samarium doped TiO_2
TSm2	:	2% Samarium doped TiO_2
TSm5	:	5% Samarium doped TiO_2
TSm10	:	10% Samarium doped TiO_2
TDy0.5	:	0.5% Dysprosium doped TiO_2
TDy1	:	1% Dysprosium doped TiO_2
TDy2	:	2% Dysprosium doped TiO_2
TDy5	:	5% Dysprosium doped TiO_2
TDy10	:	10% Dysprosium doped TiO_2
TYb1	:	1% Ytterbium doped TiO_2
TYb2	:	2% Ytterbium doped TiO_2
TYb5	:	5% Ytterbium doped TiO_2
TYb10	:	10% Ytterbium doped TiO_2
TNd0.5	:	0.5% Neodymium doped TiO_2
TNd1	:	1% Neodymium doped TiO_2
TNd2	:	2% Neodymium doped TiO_2
TNd5	:	5% Neodymium doped TiO_2
TNd10	:	10% Neodymium doped TiO_2

TEr0.5	:	0.5% Erbium doped TiO_2
TEr1	:	1% Erbium doped TiO_2
TEr2	:	2% Erbium doped TiO_2
TEr5	:	5% Erbium doped TiO_2
TEr10	:	10% Erbium doped TiO_2
FT IR	:	Fourier transform infrared spectroscopy
XRD	:	X-Ray diffraction
DRS	:	Diffuse reflectance spectra
DSC	:	Differential scanning calorimetry
XPS	:	X-Ray photoelectron spectroscopy
SEM	:	Scanning electron microscope
EDS	:	Energy dispersive spectroscopy
TEM	:	Transmission electron microscope
BET	:	Brunaur-Emmett-Teller
PL	:	Photo luminescence
MB	:	Methylene blue
CB	:	Conduction band
VB	:	Valance band
UV	:	Ultra violet
TOC	:	Total organic carbon

ABSTRACT

Nanocrystalline semiconductor oxide TiO_2 and various rare earth metal ions (Sm^{3+}, Dy^{3+}, Er^{3+}, Yb^{3+} and Nd^{3+}) doped TiO_2 were synthesized using a modified sol-gel method. All these materials were well characterised with different techniques such as FT-IR, XRD, Raman spectroscopy, DRS, XPS, SEM and TEM. The photocatalytic activity of nanocrystalline TiO_2 and various rare earth metal ions (Sm^{3+}, Dy^{3+}, Er^{3+}, Yb^{3+} and Nd^{3+}) doped TiO_2 were systematically studied as function of temperature under both UV and sunlight. Chapter 1 explains the subject of nano science and nanomaterials, an introduction to semiconducting nanocrystalline TiO_2, objective and overview of the current thesis. Chapter 2 explains the materials and methods used for carrying out the research work. The working chapter 3, 4, 5, 6 and 7 explains the systematic study on the effect of various rare earth metal ion dopants (Sm^{3+}, Dy^{3+}, Er^{3+}, Yb^{3+} and Nd^{3+}) on nanocrystalline TiO_2 and its photocatalytic activity. Chapter 8 explains the successful demonstration of the self-cleaning and pesticide degradation application of the Sm^{3+}, Dy^{3+}, Er^{3+}, Yb^{3+} and Nd^{3+} doped TiO_2 photocatalyst discussed in chapter 3, 4, 5, 6 and 7 for two practical applications. In first application, a self-cleaning coatings on glass bottle were developed using the above TiO_2 photocatalyst to demonstrate the self-cleaning application of TiO_2 photocatalyst by purifying the organic dye contaminated water under the UV and normal sunlight. In second application explains the degradation of an organo chlorine pesticide “karate” commonly used by the farmers of

Kerala using the Sm^{3+}, Dy^{3+}, Er^{3+}, Yb^{3+} and Nd^{3+} doped TiO_2 photocatalyst. Self-cleaning and degradation activity of pesticide by using above TiO_2 photocatalyst was more effective in sunlight than UV light. These study shows the possibility of using Sm^{3+}, Dy^{3+}, Er^{3+}, Yb^{3+} and Nd^{3+} doped TiO_2 photocatalyst for the practical and industrial applications such as self-cleaning coatings, decomposition of organic pesticides, water purification *etc*.

1 Chapter

Introduction

Contents

1.1 Nanomaterials

Nanomaterials are a set of substances where at least one dimension is less than approximately 100 nanometers. They are classified into - zero dimensional (spheres and clusters), one dimensional (wires and rod), two dimensional (plates and network) and three dimensional (nano material particle)[1,2] as shown in Figure 1.1. It can exist in single, fused, aggregate or agglomerated forms with spherical, tubular and irregular shape.[1] The unique optical, electrical, magnetical properties *etc.* gives nanomaterials a tremendous attention in recent research.[2] These exceptional characteristic of optical, electrical and magnetical properties arises due to the small size and higher surface area exhibited by the nanomaterials and made them an attractive materials and paved to develop a branch of new science called nanoscience.

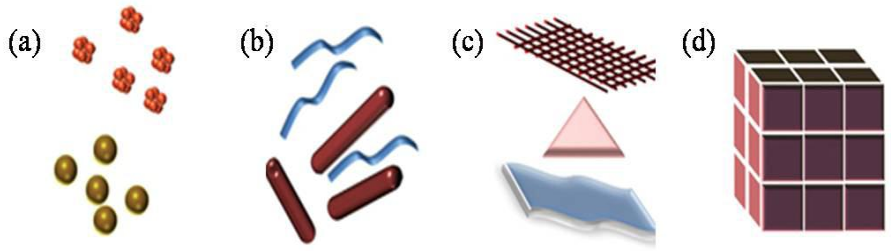

Figure 1.1 Classification of nanomaterials (a) 0D spheres and clusters, (b) 1D nanofibers, wires and rods (c) 2D films, plates and networks (d) 3D nanomaterials.

1.2 Nano science and Nano technology

Nano science is concerned with making, manipulating and imaging materials having at least one spatial dimension in the size range of 1-100 nm. In other words it deals with synthesis, characterization, exploration and exploitation of nanostructured materials having dimension 1-100 nm.[3,4]

Nano technology is the device or machine, product or process based upon individual or multiple integrated nano scale components.[4] Currently nanotechnology is define as a complex fundamental and engineering science that integrates chemistry, physics and biology of nanostructures with material science, electronics and processes technologies focused on a comprehensive research of nano structures.[3] Development of the nanotechnology results in the fabrication and manufacturing of nano devices, nano machines, ultra-low integrated circuits, micro opto-electro-mechanical systems, nano biorobots[3]*etc*. Application of nanomaterials brought a drastic change in the field of electronics, energy and environment *etc.* as shown in Figure 1.2. Nano science developed nanomaterials for the waste water treatment and self-cleaning surfaces with nano semiconductor oxides, which implied a new route in the waste disposal.

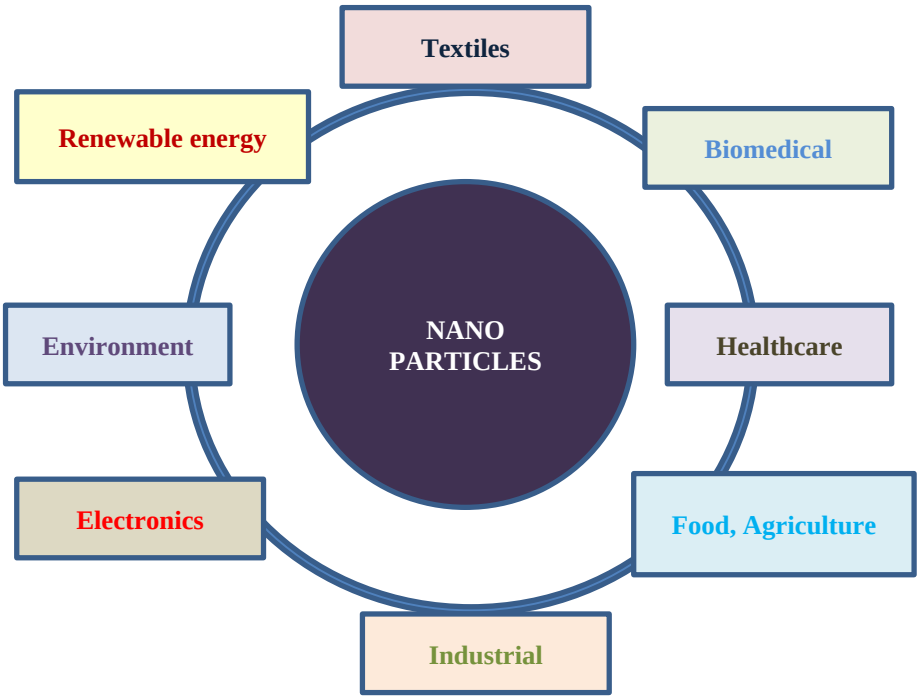

Figure 1.2 Application of Nano particles.

1.3. Nano Semiconductor Oxides

Semiconductor oxides paved the seeds for the development of smart and functional materials, devices and systems. These oxides possess unique features like mixed cation valances and an adjustable oxygen deficiency, which are the bases for creating or bearing many novel materials.[5]Semiconductor oxides such as tin oxide (SnO_2), titanium oxide (TiO_2), zinc oxide (ZnO) *etc.* have been shown to be useful as gas sensor materials for monitoring various pollutant gases like H_2S, NO_x, and NH_3 *etc*. Photodegradation and oxidation capacity of oxides like TiO_2, ZnO, ZrO_3, CeO_2 *etc.* made them interest in the field of

photocatalysis. The most promising among the oxides is TiO_2 and it is due to its electrical and mechanical properties.

1.4. Titanium Dioxide (TiO_2)

$TiO_2$is the naturally occurring oxide of Titanium. It exist in eight forms naturally- Anatase (tetragonal), Rutile(tetragonal), Brookite (orthorhombic) (Figure1.3), synthetically formed meta stable phases- TiO_2 (B) (monoclinic),[6] TiO_2 (H) (tetragonal)[7], TiO_2 (R) (orthorhombic)[8] and high pressure forms-TiO_2 (II) - (α - PbO_2 - like form) (orthorhombic),[9] Baddeleyite - like form (monoclinic),[10] TiO_2 – OI (orthorhombic),[11]cubic form,[12]TiO_2 - OII cotunnite ($PbCl_2$) - like (orthorhombic).[13]

Anatase was named by Rene Just Hauy in 1801 from greek word "anatasis" meaning "extension", since the vertical axis of the crystal being longer than the rutile. It is optically negative, soft, dense and strongly adamantine luster. The unit cell parameters are a =b= 3.7845 A°, c = 9.5143 A°. Its crystals are associated with feldspar, rock-crystal, mica-schist, axinite in crevices, in granite, sandstones, clay and slates as simple acute double pyramids with an indigo-blue to black color and steely luster. This crystal type is abundant at Le Bourg-d' Oisans in Dauphine (France). Honey-yellow to brown colored crystal, having numerous pyramidal faces developed, flatter or sometimes prismatic in habit are seen as attached to the walls of crevices in the gneisses of the Alps, the Binnenthal near Brig in canton Valais, Switzerland.

Rutile is the most common natural form of TiO_2 and it is the second most abundant mineral sand. The name was derived from the Latin *rutilus*, red, in reference to the deep red color observed in some specimens when viewed by transmitted light. It has the highest refractive indices at visible wavelengths of any known crystal, and also exhibits a particularly large birefringence and high dispersion. Commonly seen as an accessory mineral in high - temperature and high-pressure metamorphic rocks and in igneous rocks. Thermodynamically, rutile is the most stable polymorph of TiO_2 at all temperatures, exhibiting lower total free energy than metastable phases of anatase or brookite.[14] Crystal has a body-centered tetragonal unit cell, with unit cell parameters a=b=4.584 A°, and c=2.953 A°.[15]

Brookite was named in 1825 by French mineralogist Armand Lévy for Henry James Brooke (1771–1857), an English crystallographer, mineralogist and wool trader.[16]It is a brittle mineral, with a sub-conchoidal to irregular fracture and poor cleavage in one direction parallel to the 'c' crystal axis.[16,17] Most of the physical properties are between anatase and rutile. Refractive indices are very high, above 2.5, which is even higher than diamond at 2.42. Commonly found in alpine veins, in gneiss and schist as an accessory mineral. The unit cell parameters are a = 5.4558 A°, b = 9.1819 A° and c = 5.1429 A°.

L. Dubrovinsky and co-authors introduced the cotunnite - type phase to be the hardest known oxide with the Vickers hardness of 38 GPa and the bulk modulus of 431 GPa (*i.e.* close to diamond's value of 446 GPa) at atmospheric pressure.[13]

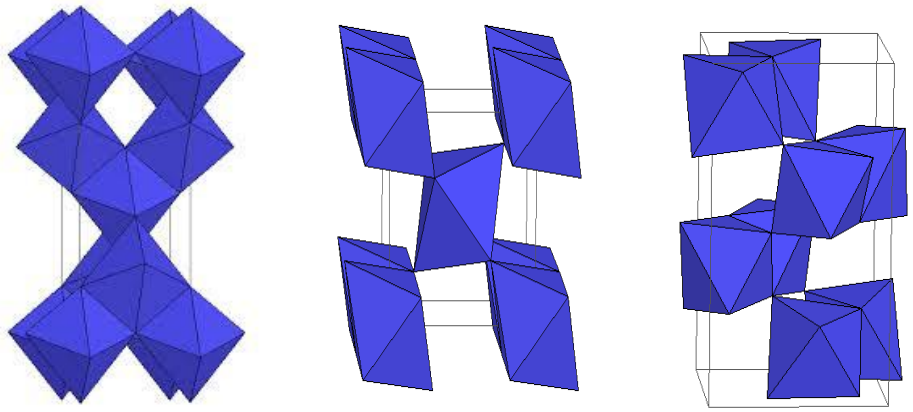

Figure1.3 Crystal structure of (a) Anatase (b) Rutile (c) Brookite.

1.5 Synthesis of TiO_2.

A large distinct synthetic method is reported in the literature to prepare nanocrystalline TiO_2 in the form of powder and coatings. These include sol-gel method,[18,19,20,43] physical vapour deposition,[21,22] chemical vapor deposition,[23-25] sonochemical method,[26-28] solvothermal method,[29-31]direct oxidation method,[32-34] micelle and inverse micelle method,[35-37] hydrothermal method,[38-39] electro-deposition method,[40-42] micro emulsion technique,[43-45] precipitation method,[43,46, 47] biological synthesis[43,48,49] and microwave method.[50-52]In this research sol-gel method was used to synthesis nanocrystalline TiO_2.

1.6 Sol-Gel Method

The sol-gel process is a method for producing solid materials from simpler molecules. Sol may be defined as a colloidal suspension of solids particles in liquids. Colloids are the suspension in which the small particles are dispersed with the Van der Waal's force and surface charges. Process involves the conversion of monomers into a colloidal solution (Sol), which acts as the precursor for an integrated network (Gel) of network polymers or discrete particles. The sol is formed by the hydrolysis and polymerization of the precursors. The commonly used precursors are metal organic compounds such as metal alkoxides[53] ($Ti(OPr)_4$ and $Ti(OC_4H_9)_4$ *etc.*) or inorganic metal salts ($TiCl_4$, $TiOCl_2$, and $TiOSO_4$ *etc.*). The metal alkoxides shows distinguishing properties from other precursors, (1) The lower electronegativity of the transition metals results in more electrophilic and thus less stable towards hydrolysis, condensation and other nucleophilic reactions (2) Transition metals exhibit several stable coordination, and when co-ordinatively unsaturated, they can expand their coordination *via* olation, oxolation, alkoxy bridging or other nucleophilic association mechanisms (3) The greater reactivity of transition metal alkoxides requires control for moisture and conditions of hydrolysis for the preparation of homogenous gel.[20]

Sol-gel synthesis involves hydrolysis of precursors, condensation followed by polycondensation to form particles, gelation and drying process as shown in Figure 1.4.

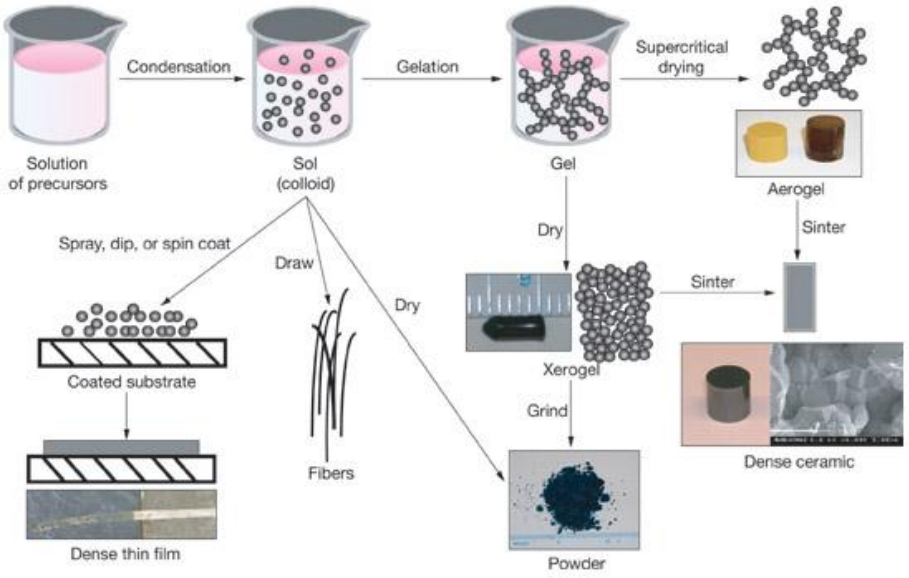

Figure 1.4 Sol-Gel Synthesis route.[54]

1.6.1 Advantages of sol-gel synthesis

1. Better homogeneity from raw materials. [55,56]
2. Better purity from raw materials. [55,56]
3. Lower temperature of preparation. [55,56]
4. Good mixing for multi-component systems. [55,56]
5. Effective control of particle size, shape and properties. [55,56]
6. Better products from the special properties of the gel. [55,56]
7. The creation of special products such as films. [55,56]
8. The creation of new non-crystalline solids outside the range of normal glass formation. [55,56]

9. The fine tuning of chromatographic selectivity *via* the possibility of creating hybrid organic-inorganic materials. [55,56]

10. The possibility of designing the material structure and property through the proper selection of sol-gel precursor and other building blocks. [55,56]

11. The possibility of achieving enhanced stationary phase stability and performance in chromatographic separations. [55,56]

12. Less energy consumption and pollution. [57]

Sol-gel technology has found a large applications in the development of new materials for catalysis,[58,59] chemical sensors,[60,61] membranes,[62] fibers,[63] optical gain media,[64] photochromic and non-linear applications[65,66] and in solid state electrochemical devices.[67] The technology is utilized in the advanced area of scientific and engineering fields, such as the ceramic industry, nuclear field industry and electronic industry.[68] This process facilitate to fabricate ceramic materials such as TiO_2 having a wide variety of forms including ultra-fine shaped powders,[69] thin film coating,[70] fibers,[71]microporous and mesoporous inorganic membranes,[72,73] monolithic[74-76] and extremely porous TiO_2 aerogel.[77-79]

1.6.2 Sol-Gel synthesis of TiO_2

The titanium alkoxides ($Ti(OR)_4$) commonly used as precursor for the synthesis of TiO_2 are titanium isopropoxide $Ti(OC_3H_7)_4$, titanium butoxide $Ti(OC_4H_9)_4$ and titanium ethoxide $Ti(OC_2H_5)_4$. These alkoxides undergo hydrolysis and condensation. Titanium alkoxides (Ti

$(OR)_4$) are very reactive due to the presence of highly electronegative OR groups, which are hard π donors, that stabilize Ti in its highest oxidation state and render Ti very susceptible to nucleophilic attack.[80,20] Rapid hydrolysis and condensation can be attributed to the vacant d orbital in the Titanium which helps in the coordination expansion.[81]

1.6.3 Hydrolysis

Hydrolysis occur by nucleophilic substitution mechanism involves the nucleophilic addition followed by proton transfer from the attacking molecule to an alkoxides or hydroxo-ligand within the transition state and removal of the protonated species as shown in scheme1.1.[20] Here process involves the addition of water, so that the Ti metal will accept the lone pair of electrons from the oxygen of water.[82]

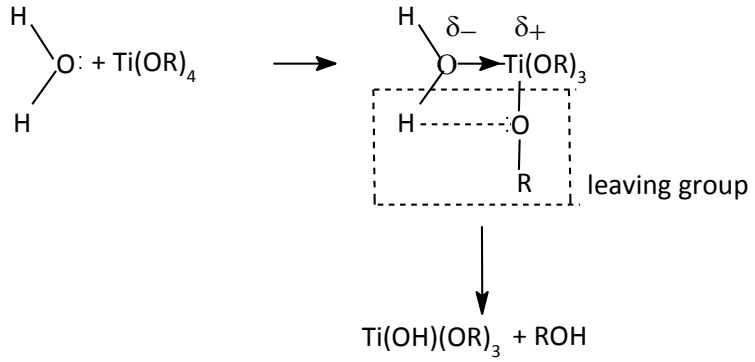

Scheme 1.1 Hydrolysis of titanium alkoxide.

The thermodynamics of hydrolysis depends on

1. The strength of the entering nucleophile
2. The electrophilicity of the metal
3. Partial charge of the leaving group
4. Stability of the leaving group

1.6.4 Condensation

Condensation is the process of removal of water or alcohol from the two partially hydrolysed metal alkoxide molecules. The two Ti atoms link together due to the formation of Ti-O-Ti bond by the removal of water or alcohol.[82,20] The Ti-O-Ti bond formation can continues to build larger and larger molecules by the process of polymerization (Scheme1.2).

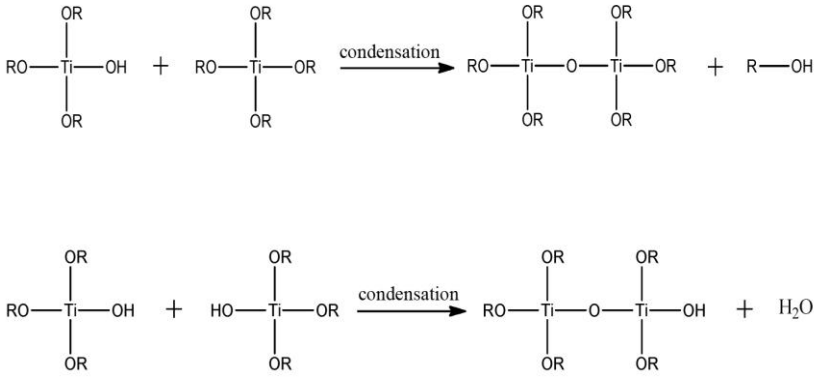

Scheme 1.2 Condensation of hydrolysed metal alkoxides.

The kinetics of condensation depends on

1. The size of the ligand

2. Electron withdrawing capacity of the organic ligand.

1.6.5 Gelation[20]

Hydrolyzed and condensed molecules grow to form clusters until the clusters collide. These clusters link between to form a single giant cluster called gel. The process of forming the gel is called as gelation. As the gel formation begins the clusters in the sol form will progressively get attached to the spanning cluster and get connected to the network, which results in the increase in the stiffness of the gel.

1.6.6 Aging[20]

Gel formed by the gelation is allowed to withstand in same circumstances for a period and that process is termed as aging. The chemical changes that cause gelation continue after the gel point induces strengthening, stiffening and shrinkage of the network. The processes of change during the aging are categorized as polymerization, coarsening and phase transformation. Polymerization is the lengthening of the network produced by condensation reaction. Coarsening or ripening is a process of dissolution and re-precipitation driven by the difference in solubility. The aging leads to an equilibrium size distribution by the growth of smaller particles to larger one.

1.6.7 Drying

Gel is dried at 100 $^{\circ}$C after the gelation. Drying imparts the shrinkage of the gel, which will be equal to the volume of the liquid evaporates. Continues drying makes the gel stiff to shrink and the liquid recedes into the interior which leaves air filled pores in the surface.

1.6.8 Calcination

The dried gel is heated at higher temperature. Volatile impurities, organic matter and moisture present in the sample are expelled on calcination. Calcined sample results in the pure oxide form of metals. It also imparts densification, crystallization, morphological changes and pore shape to the metal oxide.

1.7 Application of TiO_2

TiO_2 has a wide variety of applications in different fields of materials and inorganic chemistry.[2-20] General applications of TiO_2 are shown in Fig. 1.5.

The major applications include

1. Catalytic support[83]
2. Photocatalysts used for antibacterial, antifogging and self-cleaning applications.[84]
3. A major constituent for the preparation of electrochromic display devices.[85]
4. In medical field- dental implantation.[86,87]
5 In electronic industry as capacitors and varistors.[88]

6. Pigment industry where rutile exhibits high light scattering properties.[89]
7. Used as filler in the paper, rubber, textile, plastic and paint industries.[90]
8. The preparation of anti-reflection films due to its high refractive index.[91]
9. In dye sensitized solar cells.[92]
10. Molecular sensing.[87, 93]
11. Energy storage.[94]
12. as bio tracer.[95]
13. Pharmaceuticals (tablet coatings, cosmetic products and tooth pastes).
14. Corrosion resistant coatings.[96]

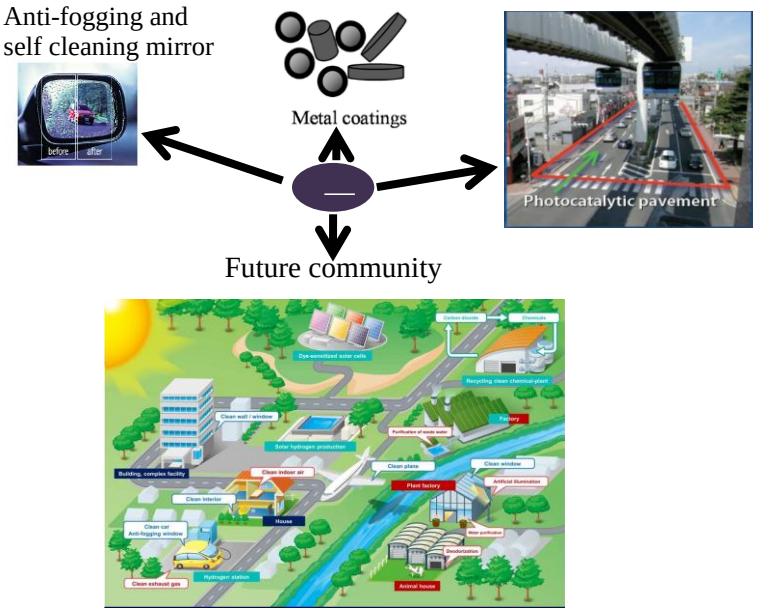

Figure 1.5 Applications of TiO_2.

1.8 TiO_2 as a photocatalyst

Photocatalysis became a remarkable area in heterogeneous catalysis after the discovery of electrolytic splitting of water using TiO_2 electrode by Fujishima and Honda in 1972.[97] Photoinduced molecular transformations or reactions take place at the surface of a catalyst in a heterogeneous photocatalysis system. Photocatalysis can be divided into two classes based on the initial excitation- catalyzed photo reaction and sensitized photoreaction.[98] In catalyzed photoreaction the initial photoexcitation occurs in adsorbate molecule which then interacts with the catalyst substrate and in sensitized photoreaction the initial photoexcitation occurs in the catalyst substrate and the photoexcited catalyst then transfers energy or electron into a ground state molecule.

The anatase and rutile crystal structures of TiO_2 are commonly used for photocatalysis, with anatase showing higher photocatalytic activity.[99] The basic structural unit of anatase and rutile is octahedra. However, the assembly pattern of the octahedron chains and the distortion of each octahedron differ for both crystals of anatase and rutile. This will cause different mass densities and electronic band structures for the two forms, hence shows difference in photocatalytic activity also.[98]

When suitable wavelength radiation from a light source fall on TiO_2 particle, the electron from the valance band of TiO_2 get excited and the electron jump into the conduction band resulting in the formation of a positive charged hole in the valance band and free electron in the conduction band. These photo generated electrons in the conduction band reduces the dissolved dioxygen molecule into superoxide radical

and the hole oxidizes the water into highly reactive hydroxyl radical (Fig1.6). These radicals are highly active and can break the chemical bond, which makes TiO_2 a suitable photo catalyst in the field of self-cleaning coatings, purification of water *etc*.

Anatase TiO_2 with band gap energy 3.2 eV can utilize only UV light normally with wavelength range 380-390 nm. The irradiation of UV light limits the application of TiO_2 because of its possibility, cost and resource *etc*. This research work is focused on utilization of visible light activity of TiO_2 by modifying with doping using metal ions.[99,100] Metal ion doping induce a bathochromic shift *i.e.*, decrease the band gap energy of anatase TiO_2 and shift the absorption to visible region.[101]

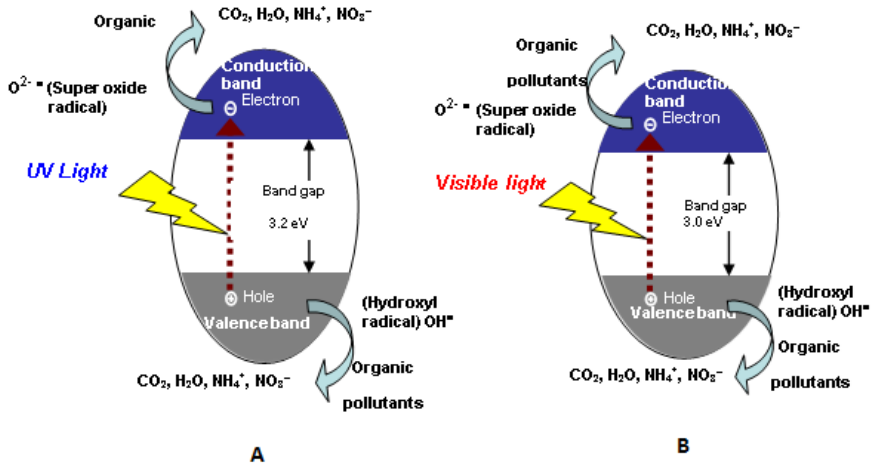

Figure 1.6 Band gap structure of A) UV active anatase TiO_2 B) visible light active doped anatase TiO_2.

1.9 Doping

Doping of metal/non-metal has a key role in band gap engineering of semiconducting TiO_2 material in order to change the optical response of TiO_2 photocatalysts. It may lead to photocatalytic systems that exhibit enhanced efficiency.[102,101] The integrity of the crystal structure of the photocatalyst while changing its electronic structure by doping is desirable to maintain. Ti^{4+} in TiO_2 is easier to replace by a cation than to substitute O^{2-} with another anion, because of the difference in the charge states and ionic radii.[103] Surface modification of TiO_2 nanoparticles appears to be more beneficial than the modified bulk TiO_2 because of their inherent lattice strain.

Doping of TiO_2 with metal cations can improve the anatase phase stability and thereby to control the phase transformation.[104] Metal ion doping for high temperature stabilization of anatase TiO_2 results in the improvement of the photocatalytic activitydue to high crystallinity of anatase phase, surface properties such as high surface area, meso-porosity and pore volume. Anatase stabilization by metal ions depends on their ability to enter into the TiO_2 lattice. Metal ions which enter into interstitial/substitutional sites of TiO_2 resulting in the decrease of oxygen vacancies and therefore the nucleation growth of anatase to rutile is suppressed resulting in the anatase stability.[104]

Main group metals, transition metals and lanthanide ions are used as dopant. Among the main group dopants alumina and silica were considered to be the better dopant to improve the anatase stability and decrease the band gap and show appreciable photocatalytic activity.[105]

Transition metal ions and lanthanide ions can provide additional energy levels within the band gap of a semiconductor. When the metal ions are incorporated into TiO_2 by doping, the impurity energy levels formed in the band gap of TiO_2 lead to an increase in the rate of recombination between photogenerated electrons and holes. Doping at high concentration of metal ions can behave as recombination centre. In other words TiO_2 doping is equivalent to the introduction of defect sites like Ti^{3+} into the semiconductor lattice; the oxidation of Ti^{3+} is kinetically fast compared to oxidation of Ti^{4+}.

1.10 TiO_2 a self-cleaning material

Deposition of dirt, vehicular exhaust, soot and other particulates makes the building surface to be cleaned. Mechanical weakening and even destruction is caused by the growth of organisms such as bacteria, algae and fungi. In order to prevent these, buildings can be coated with a layer of photocatalyst. When light with suitable energy corresponding to the band gap energy falls on the photocatalyst coating, it will break down the organic particles adsorbed on the surface of the coating. The concept of self-cleaning capacity of TiO_2 is well known.[106] If the TiO_2 film is prepared with certain percentage of SiO_2, after UV illumination it acquires super hydrophilic properties. Here similar to normal photcocatalysis the electron and holes are generated but they react in different ways. The electrons reduce the Ti (IV) cations to Ti (III) and the holes oxidize the O^{2-} anions. The oxygen atoms are ejected which results in oxygen vacancies. Water molecules then tend to occupy these oxygen vacancies, producing adsorbed OH groups which tend to make the surface hydrophilic. After irradiating the surface about 30 minutes

under UV light source with moderate intensity, the contact angle approaches zero, which intends that water has a tendency to spread perfectly across the surface.[107]

1.11 TiO_2 an active agent for the removal of pesticide

Over 98% of sprayed insecticides and 95% of herbicides reach a destination other than their target species, because they are sprayed or spread across entire agricultural fields.[108] Runoff can carry pesticides into aquatic environments while wind can carry them to other fields, grazing areas, human settlements and undeveloped areas, potentially affecting other species as shown in Figure 1.7. Other problems emerge from poor production, transport and storage practices.[109] Over time, repeated application increases pest resistance, while its effects on other species can facilitate the pest's resurgence.[110]

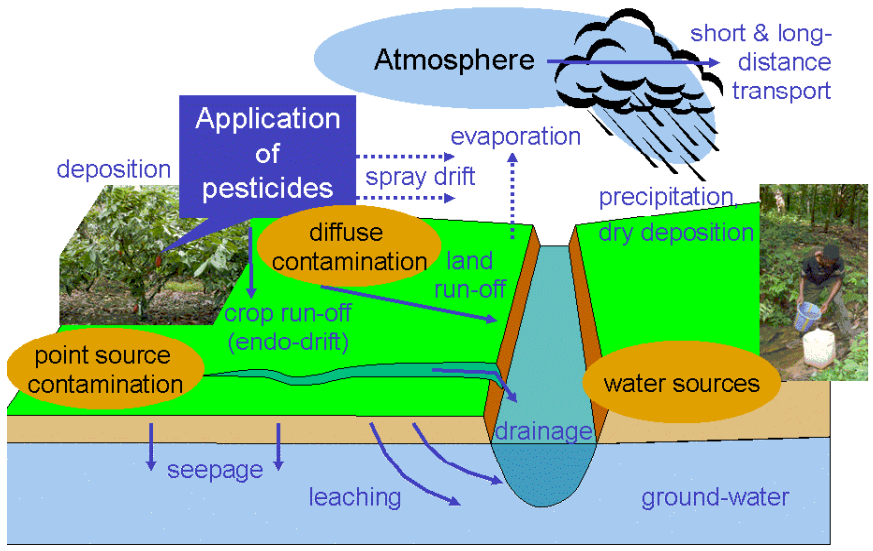

Figure 1.7 Pathway of pesticide pollution.

Pesticides contribute to air pollution, water pollution and soil pollution. It affects the life of plants, aquatic animals, birds, animals, amphibians and the health of human beings (Figure 1.8).

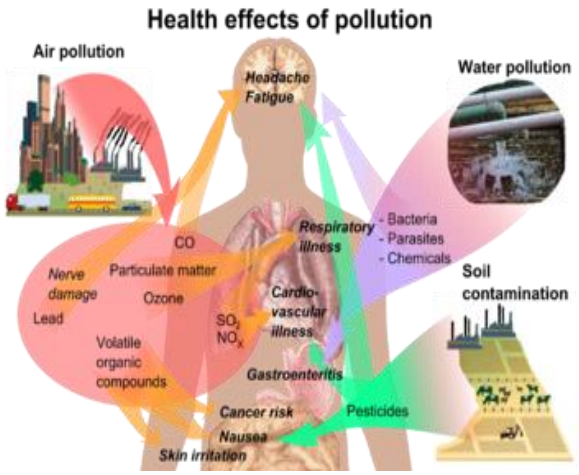

Figure 1.8 Effect of pollution in Human being.

So many alternatives are there to reduce the effects pesticides have on the environment. The alternatives include manual removal, applying heat, covering weeds with plastic, placing traps and lures, removing pest breeding sites, maintaining healthy soils that breed healthy, more resistant plants, cropping native species that are naturally more resistant to native pests and supporting bio-control agents such as birds and other pest predators.[111]Advanced technologies are used for removing the residue from water like nano filtration,[112] photoderadation[113]*etc*. Photodegradation imparts nontoxic byproducts, cheap and easy way.

1.12 Aim and scope of the present research work

This present work focus onthe synthesis of thermally stable anatase TiO_2 photocatalyst and its modifications *via* doping to improve the photocatalytic performance. Finally the active photocatalyst can be used for the photodegradation of fresh water pollutants such as various organic dyes and pesticides. Sol-gel method was identified to synthesise thermally stable TiO_2. Modification of as synthesised TiO_2 was done by doping with lanthanide (M^{3+}) ions of Samarium, Dysprosium, Erbium, Ytterbium and Neodymium. These bare TiO_2 and doped TiO_2 were characterised using various techniques and studied the photocatalytic activity using various coloured organic dyes to identify the best photocatalytic TiO_2 nanomaterials. Using this best photocatalytic TiO_2 sol nanomaterials, coating were made on glass bottle which can degrades the dyes or organic matter and finally can be demonstrated as self-cleaning materials. Pesticide residue which pollutes water will also be tried to remove by using highly active photocatalyst. Present work will attributes a novel, cost effective and eco-friendly process to synthesis TiO_2 based photocatalyst and their modification using lanthanide (M^{3+}) ions to enhance the photocatalytic activity which can finally use to make self-cleaning coatings on different substrate and also can be used to degrade the pesticide present in various sources.

1.13 Objectives of the thesis

The objectives of the present research work are

1. Preparation of nanocrystalline TiO_2 materials and its modification *via* doping with various lanthanide (M^{3+}) ions of Samarium, Dysprosium, Erbium, Ytterbium and Neodymium using sol gel method.

2. Calcination of above TiO_2 materials at various temperature to improve structural as well as textural properties of nano crystalline TiO_2.

3. Characterisation of these materials using various techniques such XRD, FTIR and Raman spectroscopy, DSC, XPS, BET surface area analysis, SEM and TEM.

4. Systematic study of the photocatalytic activity of TiO_2 and various lanthanide (M^{3+}) ions doped under UV and direct sunlight.

5. Making of coating on glass bottle using the above TiO_2 nanomaterials to study the photodegradation under UV and direct sunlight and to demonstrate the self-cleaning activity using best photocatalytically active sample.

6. Study on the photodegradation of commercial pesticide used by common man using the photocatalytically active TiO_2 sample.

1.14 Overview of the experimental work

Sol-gel method was used for the synthesis of TiO_2 and various lanthanide (M^{3+}) ions doped TiO_2 photocatalyst. Structural and textural mmodifications to enhance the photocatalytic properties of bare TiO_2 sample were done successfully using the ions of Samarium, Dysprosium, Erbium, Ytterbium and Neodymium and their detailed characterization and photocatalytic study were discussed in chapter 3, 4, 5, 6 and 7. In order to demonstrate the practical applications of above synthesised nanomaterials, normal glass bottle were coated with the highly active photocatalyst and its self-cleaning ability of TiO_2 coated glass bottle *via* photodegradation were studied. Degradation of common commercial pesticide were also investigated using the above TiO_2 photocatalyst under normal condition. Self-cleaning properties of above mentioned glass bottle coated with active photocatalyst and degradation of pesticide using the same were described in chapter 8.

References

1. A. Alagarais, *Introduction to nanomaterials*, 2011.

2. H. Hofman, *Nanomaterials*, Powder Technology Laboratory 2009.

3. V. Pokropivny, R. Lohmus, I. Hussainova, A. Pokropivny and S. Vlassov,*Tartu University Press*, 2007.

4. G. A. Ozin, A. Arsenault and L. Cademartiri, *RSC publication*, 2009.

5. X.Y. Kong, Z.L. Wang and J. Wu, *Adv. Mater*., 2003, 15, 1445.

6. R. Marchand, L. Brohan and M. Tournoux, *Mater. Res. Bull*, 1980, 15, 1129.

7. M.Latroche, L. Brohan, R. Marchand and Tournoux, *J. Solid State Chem.*, 1989, 81, 78.

8. J. Akimoto, Y.Gotoh, Y.Oosawa, N.Nonose, T.Kumagai, K. Aoki and H.Takei, *J. Solid State Chem.*, 1994, 113, 27.

9. P. Y. Simons and F. Dachille, *Acta Crystallographica*, 1967, 23, 334.

10. H. Sato, S. Endo, M. Sugiyama, T. Kikegawa, O. Shimomura and K. Kusaba, *Science*, 1991, 251, 786.

11. N. A. Dubrovinskaia, L. S.Dubrovinsky, R. Ahuja, V. B. Prokopenko, V. Dmitriev, H. P. Weber, J.M. Osorio-Guillen andB.Johansson, *Phys. Rev. Lett.*, 2001, 87 , 275501.

12. M. Mattesini, J. S. de Almeida, L. Dubrovinsky, L. Dubrovinskaia, B. Johansson and R. Ahuja, *Phys. Rev. B,* 2004, 70, 212101.

13. L.S. Dubrovinsky, N.A. Dubrovinskaia, V.Swamy, J. Muscat, N.M. Harrison, R. Ahuja, B. Holm and B. Johansson, *Nature*, 2001, 410, 653.

14. D. A. H. Hanaor, M. H. N. Assadi, S. Li, A. Yu and C. C. Sorrell, *Computational Mechanics*, 2012, 50 , 185.

15. Diebold and Ulrike, *Surface Sci. Reports*, 2003, 48, 53.

16. Webmineral.com.

17. Handbook of Mineralogy.

18. O. Carp, C. L. Huisman and A. Reller, *Prog. Solid State Chem.*, 2004, 32, 33.

19. X. Chen and S. S. Mao, *Chem. Rev.,* 2007, 107**,** 2891.

20. C. J. Bringer and G. W. Scherer, *Sol-Gel Science*, Academic Press, 1990.

21. a) J. M. Wu, H. C. Shih and W. T. Wu, *Chem. Phys. Lett.*, 2005, 413, 490. b) J. M. Wu, H. C. Shih, W. T. Wu, Y. K. Tseng and I. C. Chen, *J. Cryst. Growth,* 2005, 281, 384.

22. B. Xiang, Y. Zhang, Z. Wang, X. H. Luo, Y. W. Zhu, H. Z. Zhang and D. P. Yu, *J. Phys. D*, 2005, 38, 1152.

23. a) P. Evans, M. E. Pemble and D. W. Sheel, *Chem. Mater.*, 2006, 18, 5750. b) L. A. Brook, P. Evans, H. A. Foster, M. E. Pemble, A. Steele, D. W. Sheel and H. M. Yates, *J. Photochem. Photobio. A: Chem.*, 2007, 187, 53. c) H. M. Yates, M. G. Nolan, D. W. Sheel and M. E. Pemble, *J. Photochem. Photobio. A: Chem.*, 2006, 179, 213. d) M. G. Nolan, M. E. Pemble, D. W. Sheel and H. M. Yates, *Thin Solid Films*, 2006, 515, 1956.

24. a) A. C. Jones, T. J. Leedham, P. J. Wright, M. J. Crosbie, K. A. Fleeting, D. J. Otway, P. O'Brien and M. E. Pemble, *J. Mater. Chem.*,1998, 8, 1773. b) A. C. Jones, P. A. Williams, J. F. Bickley, A. Steiner, H. O. Davies, T. J. Leedham, A. Awaluddin, M. E. Pemble and G. W. Critchlow, *J. Mater. Chem.*, 2001, 11, 1428.

25. [1]a) S. Seifried, M. Winterer and H. Hahn, *Chem. Vap. Deposition,* 2000, 6, 239. b) S. K. Pradhan, P. J. Reucroft, F. Yang and A. Dozier, *J. Cryst. Growth*, 2003, 256, 83. c) J. J. Wu and C. C. Yu, *J. Phys. Chem. B*, 2004, 108, 3377 d) Y. L. Li and T. Ishigaki, *J. Phys. Chem. B*, 2004, 108, 15536.

26. a) W. Huang, X. Tang, Y. Wang, Y. Koltypin and A. Gedanken, *Chem. Commun.,* 2000, 1415. b) Y. Zhu, H. Li, Y. Koltypin, Y. R. Hacohen and A. Gedanken, *Chem. Commun.*, 2001, 2616.

27. a) H. Xia and Q. Wang, *Chem. Mater.*, 2002, 14, 2158. b) J. C. Yu, L. Zhang and J. Yu, *Chem. Mater.*, 2002, 14, 4647. c) J. C. Yu, L. Zhang, Q. Li, K. W. Kwong, A. W. Xu and J. Lin, *Langmuir*, 2003, 19, 7673.

28. a) P. E. Meskin, V. K. Ivanov, A. E.Barantchikov, B. R. Churagulov and Y. D. Tretyakov, *Ultrason. Sonochem.*,2006, 13, 47.b) J. C. Yu, L. Zhang and J. Yu, *New J. Chem.*, 2002, 26, 416. c) J. C. Yu, J. Yu,

L. Zhang and W. Ho, *J. Photochem. Photobiol., A. Chem.*, 2002, 148, 263.

29. a) C. S. Kim, B. K. Moon, J. H. Park, B. C. Choi and H. J. Seo, *J. Cryst. Growth*, 2003, 257, 309 b) C. S. Kim, B. K. Moon, J. H. Park, S. T. Chung and S. M. Son, *J. Cryst. Growth*, 2003, 254, 405.

30. a) X. L. Li, Q. Peng, J. X. Yi, X. Wang and Y. D. Li, *Chem. Eur. J.*, 2006, 12, 2383. b) X. Wang, J. Zhuang, Q. Peng and Y. D. Li, *Nature*, 2005, 437, 121.c) J. Xu, J. P. Ge and Y. D. Li, *J. Phys. Chem. B*, 2006, 110, 2497.

31. a) W. Wang, O. K. Varghese, M. Paulose, C. A. Grimes, Q. Wang and E. C. Dickey, *J. Mater. Res.*, 2004, 19, 417. c) B. Wen, C. Liu and Y. Liu, *Inorg. Chem.*, 2005, 44, 6503 c) B. Wen, C. Liu and Y. Liu, *J. Phys. Chem. B*, 2005, 109, 12372.

32. a) J. M. Wu, *J. Cryst. Growth*, 2004, 269, 347 b) J. M. Wu, T. W. Zhang, Y. W. Zeng, S. Hayakawa, K. Tsuru and A. Osaka, *Langmuir*, 2005, 21, 6995.

33. a) J. M. Wu, S. Hayakawa, K. Tsuru and A. Osaka, *Scripta Mater.*, 2002, 46, 101 b) J. M. Wu, S. Hayakawa, K. Tsuru and A. Osaka, *Scripta Mater.*, 2002, 46, 705.

34. a) J. M. Wu, S. Hayakawa, K. Tsuru and A. Osaka, *Cryst. Growth Des.*, 2002, 2, 147. b) J. M.Wu and T. W. Zhang, *J. Photochem. Photobiol., A Chem.*, 2004, 162, 171.

35. a) S. S. Hong, M. S. Lee, S. S. Park and G. D. Lee *Catal. Today*, 2003, 87, 99. b) K. T. Lim, H. S. Hwang, S. S. Hong, C. Park, W. Ryoo and K. P. Johnston, *Stud. Surf. Sci. Catal.*, 2004, 153, 569.

36. [1]a) K. D. Kim, S. H. Kim and H. T. Kim, *Colloids Surf. A*, 2005, 254, 99 b) G. L. Li and G. H. Wang, *Nanostruct. Mater.*, 1999, 11, 663 c) Y. Li, N. H. Lee, D. S. Hwang, J. S. Song, E. G. Lee and S. J. Kim, *Langmuir*, 2004, 20, 10838. d) K. T. Lim, H. S. Hwang, W. Ryoo and K. P. Johnston, *Langmuir*, 2004, 20, 2466.

37. a) J. Lin, Y. Lin, P. Liu, M. J. Meziani, L. F. Allard and Y. P. Sun, *J. Am. Chem. Soc.*, 2002, 124, 11514 b) J. C. Yu, J. Yu, W. Ho and L. Zhang, *Chem. Commun.*, 2001, 1942. c) D. Zhang, L. Qi, J. Ma and H. Cheng, *J. Mater. Chem.*, 2002, 12, 367.

38. [1] a) D. Vernardou, E. Stratkis, G. Kenanakis, H. M. Yates, S. Couris, M. E. Pemble, E. Koudoumas and N. Katsarakis, *J. Photochem.*

Photobiol. A Chem., 2007, 202, 81. b) J. M. Andersson, L. Oesterlund, S. Ljungstroem and A. Palmqvist, *J. Phys. Chem. B*, 2002, 106, 10674c) S. Y. Chae, M. K. Park, S. K. Lee, T. Y. Kim, S. K. Kim and W. I. Lee, *Chem. Mater.*, 2003, 15, 3326.

39. a) J. Yang, S. Mei and J. M. F. Ferreira, *J. Am. Ceram. Soc.*, 2000, 83, 1361. b) J. Yang, S. Mei and J. M. F. Ferreira, *J. Am. Ceram. Soc.*, 2001, 84, 1696. c) J. Yang, S. Mei and J. M. F. Ferreira, *J. Mater. Res.*, 2002, 17, 2197. d) J. Yang, S. Mei and J. M. F. Ferreira, *J. Colloid Inter. Sci.*, 2003, 260, 82. d) J. Yang, S. Mei and J. M. F. Ferreira, *J. Eur. Ceram. Soc.*, 2003,24, 335.

40. J.H. Lee, H.S. Choi, J.H. Lee, Y. J. Kim, S. J. Suh, C.S. Chi and H.J. Oh, *J. Cryst. Growth.* 2009, 311, 638.

41. J. Liu, J. Xu, R. Che, H. Chen, M. Liu and Z. Liu, *Chem – A. Eur. J.* 2013, 19, 6746.

42. M. M. Byranvand, A. N. Kharat, L. Fatholahi and Z. M. Beiranvand, *J.Nano Struct*, 2013, 3, 1.

43. S. M. Gupta and M. Tripathi, *Cent. Eur. J. Chem*., 2012, 10, 279.

44. F.A. Deorsola and D. Vallauri, *Powd. Tech*. 190, 2009, 304.

45. V. Chhabra, V. Pillai, B. K. Mishra, A. Morrone and D.O. Shah, *Langmuir*,1995,11, 3307.

46. T. Sato, Y. Aita, M. Komatsu and S. Yin, *J. Mater. Sci.*, 2006, 41, 1433.

47. H. E. Namin, H. Hashemipour and M. Ranjbar, *Inter. J. Mod. Phys. B*, 2008, 22, 3210.

48. A.V. Kirthi, A.A. Rahuman, G. Rajakumar, S. Marimuthu, T. Santhoshkumar, C. Jayaseelan, G. Elango, A. AbduzZahir, C. Kamaraj and A. Bagavan, *Mater. Letters*, 2011, 65, 2745.

49. M. Sundrarajan and S. Gowri, *Chalcogenide Lett.*, 2011, 8, 447.

50. A. B. Corradi, F. Bondioli, B. Focher, A. M. Ferrari, C. Grippo, E. Mariani and C. Villa, *J. Am. Ceram. Soc.*, 2005, 88, 2639.

51. a) E. Gressel-Michel, D. Chaumont and D. Stuerga, *J. Colloid Inter. Sci.,* 2005, 285, 674. b) V. G. Pol, Y. Langzam and A. Zaban, *Langmuir,* 2007**,** 23, 11211.

52. G. Ma, X. Zhao and J. Zhu, *Int. J. Mod. Phys. B,* 2005, 19, 2763.

53. P.C. R. Varma, P. Periyat, M. Oubaha, C. Mc. Donagh and B. Duffy, *Surface & Coatings Technol,* 2011, 205, 3992.

54. Lawrence livemore national laboratory, Science and Technology, Review, magazine, University of California, may, 2005.

55. J. D. MacKenzie, J. *Sol-Gel Sci. Techn*. 2003, 26, 23.

56. T. K. Tseng, Y. S. Lin, Y. J. Chen and H. Chu, *Int. J. Mol. Sci*. 2010, 11, 2336.

57. S.K. Kulkarni, Capital Publishing Company, 2007. ISBN 978-3-319-09171-6.

58. U. Schubert, New *J. Chem*., 1994, 18, 1049.

59. J. Blum, A. Rosenfeld, F. Gelman, H. Schumann and D. Avnir, *J. Mol. Catal*. 1999, 146, 117.

60. P. Banet, C. Cantau, C. Rivron, T. H. Tran-Thi, *Actual. Chim*., 2009, 331, 30.

61. J. Lin and C.W. Brown, *Trends Anal. Chem.,* 1997, 16, 200.

62. G. Xomeritakis, C.Y. Tsai, Y. B. Jiang and C. J. Brinker, *J. Membrane Sci.* 2009, 341, 30.

63. Z. R. Zeng, W. L. Qiu, M. Yang, X. Wei, Z. F. Huang, F. Li, *J. Chromatogr.*, 2001, 934, 51.

64. R. Gvishi, U. Narang, G. Ruland, D. N. Kumar and P.N. Prasad, *Appl. Organomet. Chem.* 1997, 11, 107.

65. D. Levy and L. Esquivias, *Adv. Mater.*, 1995, 7, 120.

66. D. Levy, *Mol. Crys. Liq. Crys. A*, 1997, 297, 31.

67. B. Dunn, G.C. Farrington and B. Katz, *Solid State Ionics*, 1994, 70, 3.

68. C. J. Brinker and G.W. Scherer, *Academic Press: Boston*, MA, USA, 1990.

69. H. Liu, W. Yang, Y. Ma, Y. Cao, J. Yao, J. Zhang and T. Hu, *Langmuir,* 2003**,** 19, 3001. b) J. H. Schattka, D. G. Shchukin, J. Jia, M. Antonietti and R. A. Caruso, *Chem. Mater.,* 2002**,** 14, 5103.

70. K. Wang, M. A. Morris and J. D. Holmes, *Chem. Mater.*, 2005, 17, 1269.

71. W. S. Chae, S. W. Lee and Y. R. Kim, *Chem. Mater.***,** 2005**,** 17, 3072.

72. a) H. Choi, A. C. Sofranko and D. D. Dionysiou, *Adv. Funct. Mater.,* 2006, 16, 1067 b) H. Choi, E. Stathatos and D. D. Dionysiou, *Appl. Cata. B: Environ.,* 2006, 63, 60.

73. a) S. Y. Kwak, S. H. Kim and S. S. Kim, *Environ. Sci. Technol.*, 2001, 35, 2388. b) D. S. Bae, K. S. Han and S. H. Choi, *Solid State Ionics*, 1998, 109, 239.

74. a) J. Konishi, K. Fujita and K. Nakanishi, *Chem. Mater.*, 2006, 18, 6069 b) W. Q. Shen, F. Liu, J. Qiu and B. D. Yao, *Nanotechnology*, 2009, 20, 105605.

75. a) P. Avila, A. Bahamonde and J. Blance, *Appl. Cata. B: Environ.,* 1998, 17, 75. b) S. Backlund, J. H. Smatt and J. B. Rosenholm, *J. Dispersion Sci. and Tech.*, 2007, 28, 115. c) J. Ren, J. Zhong, C. Zhang and Q. Hang, *Chinese J. Chem.*, 2006, 24, 955.

76. a) W. I. Kim and L. K. Hong, *J. Ind. Eng. Chem.*, 2003, 9, 728. b) B. D. Yao and L. D. Zhang, *J. Mater. Sci.*, 1999, 34, 5983.

77. a) G. Dagan and M. Tomkiewicz, *J. Phys. Chem.*, 1993, 97, 12651 b) G. Dagan and M. Tomkiewicz, *J. Non-Cryst. Solids*, 1994, 175, 294. c) Z. Zhu, M. Lin, G. Dagan and M. Tomkiewicz, *J. Phys. Chem.*, 1995, 99, 15950. d) Z. Zhu, L. Y. Tsung and M. Tomkiewicz, *J. Phys. Chem.*, 1995, 99, 15945.

78. a) S. Kelly, F. H. Pollak and M. Tomkiewicz, *J. Phys. Chem. B*, 1997, 101, 2730 b) M. Schneider and A. Baiker, *Catal. Today*, 1997, 35, 339 c) J. M. Watson, A. T. Cooper and J. R. V. Flora, *Environ. Eng. Sci.,* 2005, 22, 666.

79. M. T. Dulay, J. P. Quirino, B. D. Bennett and R. N. Zare, *J. Sep. Sci*. 2002, 25, 3.

80. L. G. Hubart - Pfalzgraf, *New. J. Chem.*, 1987, 11,663.

81. U. Schubert, *J. Mater. Chem.*, 2005, 15, 3701.

82. J. Livage, M. Henry and C. Sanchez, *Pro. Solid State Chem.*, 1998, 18, 259.

83. M. A. Fox and M. T. Dulay, *Chem. Rev.*, 1993, 93, 341.

84. A. Fujishima, X. Chang and D. A. Tryk, *Surf. Sci. Reports*, 2008, 63, 515.

85. D. C. Cronemeyer, *Phys. Rev.*, 1959, 113, 1222.

86. W.E. Yang, M.L. Hsu, M.C. Lin, Z.H. Chen, L.K. Chen, H.H. Huang, *J. Alloys Compd*., 2009, 479, 642.

87. D. P. Macwan, P. N. Dave and S. Chaturvedi, *J. Mater Sci.*, 2011 46, 3669.

88. C.P. Li, J.F. Wang, W.B. Su, H.C. Chen, Y.J. Wang and D. X. Zhuang, *J. Mater. Sci.*, 2003, 57, 1400.

89. a) C. Feldmann, *Adv. Mater.*, 2001, 13, 1301. b) C. Feldmann and H. O. Jungk, *Angew. Chem., Int. Ed.*, 2001, 40, 359.

90. A. E. Jacobsen, *Ind. Eng. Chem.*, 1949, 41, 523.

91. a) L. A. Pranger, R. Tannenbaum, Z. L. Wang and C. J. Summers, *Adv. Mater.*, 2005, 17, 2103. b) J. S. King, E. Graugnard and C. Summers, *Adv. Mater.*, 2005, 17, 1010. c) S. M. Prokes, J. L. Gole, X. B. Chen, C. Burda and W. E. Carlos, *Adv. Funct. Mater.*, 2005, 15, 161.

92. A. Hagfeldt and M. Grätzel, *Chem. Rev.*, 1995, 95, 49.

93. a) J. Watson and K. Ihokura, *Mater. Res. Soc. Bull.*, 1999, 6, 14 b) Y. Zhu, J. Shi, Z. Zhang, C. Zhang and X. Zhang, *Anal. Chem.* 2002, 74, 120 c) D. Morris and R. G. Egdell, *J. Mater. Chem.*, 2001, 11, 3207.

94. a) C. A. Grimes, *J. Mater. Chem.*, 2007, 17, 1451. b) G. K. Mor, O. K. Varghese, M. Paulose, K. Shankar and C. A. Grimes, *Sol. Energy Mater. Sol. Cells*, 2006, 90, 2011.

95. T. Paunesku, T. Rajh, G. Wiederrecht, J. Maser, S. Vogt, N. Stojicevic, M. Protic, B. Lai, J. Oryhon, M. Thurnauer and G. Woloschak, *Nature Mater.*, 2003, 2, 343.

96. T. Liu, F. Zhang, C.Xue, L. Li andY. Yin, *Surf. Coat. Technol.*, 2010, 205, 2335.

97. A. Fujishima and K. Honda, *Nature*, 1972, 37, 238.

98. A. L. Linsebigler, G. Lu, T. John and Jr. Yates, *Chem. Rev*. 1995, 95, 735-75.

99. P. Periyat, S. C. Pillai, D. E. McCormack, J. Colreavy and S. J. Hinder, *J. Phys. Chem.C*, 2008, 112, 7644.

100. S. Bingham and W. A. Daoud, *J. Mater. Chem.*, 2011, 21, 2041.

101. G. S. Mital and T. Manoj, *Chinese. Sci. Bul*, 2011, 56, 1639.

102. O. Carp, C. L. Huissman and A. Reller, *Prog.in solid state chem.*, 2004, 32, 33.

103. G.K. Mor, O.K. Varghese and M. Paulose, *Solar Energ mater. Solar cell*, 2006, 90, 2011.

104. P. Periyat, B. Naufal and S.G. Ullattil, *Material science forum, Trans Tech Pub*., 2016, 855, 78.

105. C. Anderson and A. J. Bard, *J. Phys. Chem.*, 1995, 99, 9882.

106. A. Mills, S. Hodgen and S. K. Lee, *Res. Chem. Intermed*, 2005, 31, 295.

107. A. Fujishima, T.N. Rao and D.A Tryk, *J.Photochem.Photobio. C Photochem. Rev.*, 2000, 1, 1.

108. G. T. Miller, *Sustaining the Earth: An Integrated Approach. Thomson/Brooks/Cole*., 2004, 1, 211.

109. Tashkent (1998), Part 1. Conditions and provisions for developing a national strategy for biodiversity conservation, 2007.

110. C. A. Damalas, I. G. Eleftherohorinos, *Inter. J. Environ.* 2011, 8, 1402.

111. Take Action! How to Eliminate Pesticide Use. *National Audubon Society*., 2003, 1.

112. R. Boussahel , S. Bouland , K.M. Moussaoui , A. Montiel, J. Desalination, 2000, 132, 205.

113. T.Katagi, *Rev Environ Contam Toxicol*, 2004, 182, 1.

2 Chapter

Experimental procedures and characterization techniques

Contents

2.1 Experimental procedures.

This chapter discusses the procedure used for the synthesis of the titania (TiO_2) samples under investigation and the various techniques used for characterization of the materials. First part of the chapter, section 2.2 explains the procedure for the preparation of TiO_2 and Samarium ion (Sm^{3+}), Dysprosium ion (Dy^{3+}), Erbium ion (Er^{3+}), Ytterbium ion (Yb^{3+}) and Neodymium ion (Nd^{3+}) modified TiO_2. In the second part section 2.3, explain thesynthesis pathway of TiO_2 modified sol and its coating on glass bottles. In the third part 2.4, the photocatalysis procedure under both UV and direct sunlight is discussed. The final part of the chapter 2.5 describes the different techniques used for the characterization of the synthesised materials. The spectroscopic, thermal, optical and surface characterization techniques used for describing the properties of bare and modified TiO_2. (The details of chemicals used are tabulated in the Table 2.1.).

Table 2.1. List of chemicals used for synthesis and characterization

Chemical name	Abbreviations	Company	Purity
Titanium Tetra isopropoxide	TP	Sigma Aldrich	97%
Acetic Acid	AC	Sigma Aldrich	99.8%
Samarium Nitrate	Sm_3NO_3	Sigma Aldrich	99.90 %
Dysprosium Nitrate	Dy_3NO_3	Sigma Aldrich	99.90 %
Erbium Nitrate	Er_3NO_3	Sigma Aldrich	99.90 %
Ytterbium Nitrate	Yb_3NO_3	Sigma Aldrich	99.90 %
Neodymium Nitrate	Nd_3NO_3	Sigma Aldrich	99.90 %
Methylene Blue	MB	Merck	99%
Tween 80	Tween 80	Merck	
Pesticide(Karate-Commercial)	Karate	Syngenta	
Hydrochloric acid	HCl		
Nitric acid	HNO_3		
Potassium Bromide	KBr	Sigma Aldrich	

2.2 Preparation of nano titanium dioxide powder *via* sol gel method.[1]

Titanium isopropoxide (TP) and glacial acetic acid (AC) were used as received. In a typical experiment to synthesize nano TiO_2, the reagents were mixed with the ratio 1:10:100. 35.6 mL of titanium isopropoxide was mixed with 71.56 mL of glacial acetic acid followed by the addition of 225 mL of distilled water in small quantity with constant stirring. The

homogenous solution was stirred for 3 hours. It was dried at 100 °C on water bath for 12 hours. The dried powder was calcined at various temperatures (300, 500 and 700 °C) at a heating rate of 5 °C per minute and held at this temperature. The synthesis procedures were summarized in scheme 2.1.

2.2.1 Sm^{3+} doped TiO_2 preparation

The reagents used were titanium isopropoxide, glacial acetic acid and samarium nitrate. The reagents were used as such without any further purification. In a typical experiment to synthesize nano TiO_2 sol, the reagents were mixed with the ratio 1:10:100. 35.6 mL of titanium isopropoxide was mixed with 71.56 mL of glacial acetic acid followed by the addition of 200 mL of distilled water in small quantity with constant stirring. A white sol of TiO_2 is formed and sol was stirred for 3 hours. To this TiO_2 sol, calculated quantity of samarium nitrate (for 1 wt %) is added and stirred for another 3 hours. The stirred solution was dried at 100 °C on a water bath for 12 hours. The dried powder was calcined at various temperatures (300, 500 and 700 °C) at a heating rate of 5 °C per minute and held at this temperature. The similar procedure was followed for the synthesis of 2, 5 and 10% Sm^{3+} doped TiO_2. The samples were named as TSm1, TSm2, TSm5 and TSm10.

2.2.2 Dy^{3+} doped TiO_2 preparation

The reagents used were titanium isopropoxide, glacial acetic acid and dysprosium nitrate. The reagents were used as such without any further purification. In a typical experiment to synthesize nano TiO_2, the reagents were mixed with the ratio 1:10:100. 35.6 mL of titanium

isopropoxide was mixed with 71.56 mL of glacial acetic acid followed by the addition of 200 mL of distilled water in small quantity with constant stirring. A white sol of TiO_2 is formed and sol was stirred for 3 hours. To this TiO_2 sol, calculated quantity of dysprosium nitrate (1 wt %) is added and stirred for another 3 hours. The stirred solution was dried on a water bath for 12 hours. The dried powder was calcined at various temperatures (300, 500 and 700 $^{\circ}$C) at a heating rate of 5 $^{\circ}$C per minute and held at this temperature. The similar procedure was followed for the synthesis of 0.5, 2, 5 and 10% Dy^{3+} doped TiO_2. The samples were named as TDy0.5, TDy1, TDy2, TDy5 and TDy10.

2.2.3 Er^{3+} doped TiO_2 preparation

The reagents used were titanium isopropoxide, glacial acetic acid and erbium nitrate. The reagents were used as such without any further purification. In a typical experiment to synthesize nano TiO_2, the reagents were mixed with the ratio 1:10:100. 35.6mL of titanium isopropoxide was mixed with 71.56 mL of glacial acetic acid followed by the addition of 200 mL of distilled water in small quantity with constant stirring. A white sol of TiO_2 is formed and sol was stirred for 3 hours. To this TiO_2 sol, calculated quantity of erbium nitrate (1 wt %) is added and stirred for another 3 hours. The stirred solution was dried on a water bath for 12 hours. The dried powder was calcined at various temperatures (300, 500 and 700 $^{\circ}$C) at a heating rate of 5 $^{\circ}$C per minute and held at this temperature. The similar procedure was followed for the synthesis of 0.5, 2, 5 and 10% Er^{3+}doped TiO_2. The samples were named as TEr0.5, TEr1, TEr2, TEr5 and TEr10.

2.2.4 Yb^{3+} doped TiO_2 preparation

The reagents used were titanium isopropoxide, glacial acetic acid and ytterbium nitrate. The reagents were used as such without any further purification. In a typical experiment to synthesize nano TiO_2 sol, the reagents were mixed with the ratio 1:10:100. 35.6 mL of titanium isopropoxide was mixed with 71.56 mL of glacial acetic acid followed by the addition of 200 mL of distilled water in small quantity with constant stirring. A white sol of TiO_2 is formed and sol was stirred for 3 hours and to this TiO_2 sol, calculated quantity of ytterbium nitrate (1 wt%) in is mixed and stirred for another 3 hours. The stirred solution was dried on a water bath for 12 hours. The dried powder was calcined at various temperatures (300, 500 and 700 $^{\circ}$C) at a heating rate of 5 $^{\circ}$C per minute and held at this temperature. The similar procedure was followed for the synthesis of 2, 5 and 10% Yb^{3+} doped TiO_2. The samples were named as TYb1, TYb2, TYb5 and TYb10.

2.2.5 Nd^{3+} doped TiO_2 preparation

The reagents used were titanium isopropoxide, glacial acetic acid and neodymium nitrate. The reagents were used as such without any further purification. In a typical experiment to synthesize nano TiO_2 sol, the reagents were mixed with the ratio 1:10:100. 35.6mL of titanium isopropoxide was mixed with 71.56 mL of glacial acetic acid followed by the addition of 200 mL of distilled water in small quantity with constant stirring. A white sol of TiO_2 is formed and sol was stirred for 3 hours. To this TiO_2 sol, calculated quantity of neodymium nitrate (1 wt %) is added and stirred for another 3 hours. The stirred solution was

dried on a water bath for 12 hours. The dried powder was calcined at various temperatures (300, 500, 700 and 800 °C) at a heating rate of 5 °C per minute and held at this temperature. The similar procedure was followed for the synthesis of 0.5, 2, 5 and 10% Nd^{3+} doped TiO_2 and calcined at the temperatures (300, 500 and 700 °C). The samples were named as TNd0.5, TNd1, TNd2, TNd5 and TNd10.

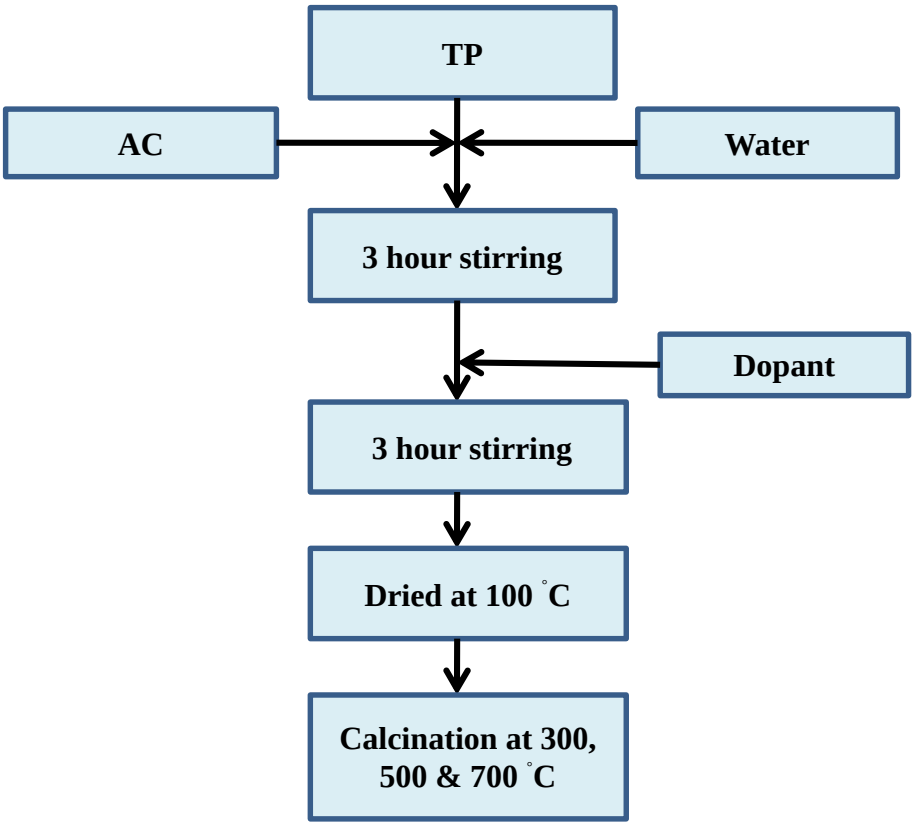

Scheme 2.1. Flow chart of synthesis of TiO_2 and various lanthanide ion (M^{3+}) doped TiO_2.

2.3 Self-cleaning coating on bottle using cashew gum / Tween 80

In order to make the nano coating on glass bottle, the best photoactive sol sample was used. 50 ml of the sol was taken in 100 ml beaker with cashew gum (used as a binder) in the ratio 10:1 and stirred for further 3 hours. Then the solution was poured into the glass bottle to obtain the coating and kept for 1 hour. After 1 hour the sol was poured out back and the empty bottle was dried in an oven at 80 ˚C and then calcined at 500 ˚C at a heating rate of 5 ˚C per minute and held at this temperature for 1 hour.

In the case of tween 80, 30 ml of the sol was taken in 100 ml beaker with Tween 80 (used as a binder) in the ratio 30:1 and stirred for further 3 hours. Then the solution was poured into the glass bottle to obtain the coating and kept for 1 hour. After 1 hr the sol was poured out back and the empty bottle was dried in an oven at 80 ˚C and then calcined at 500 ˚C at a heating rate of 5 ˚C per minute and held at this temperature for 1 hour.

2% Sm^{3+} doped TiO_2 calcined at 500 ˚C was coated on the bottle using cashew gum as a binder. Tween 80 was the binding agent used for Dy^{3+}, Er^{3+}, Yb^{3+} and Nd^{3+} doped TiO_2 samples. 1% Dy^{3+} doped, 1% Er^{3+}doped and 2% Yb^{3+} doped TiO_2 calcined at 500 ˚C and 1% Nd^{3+} doped TiO_2 calcined at 700 ˚C were coated using the above procedure.

2.4 Photocatalysis studies

For the photocatalytic studies, 0.1 g calcined sample was dispersed in 50 mL of methylene blue solutions prepared in deionised water having a concentration of $1x10^{-4}$ M. This solution was stirred for 30 minutes in dark for the chemisorption on the surface of the catalyst to avoid any

adsorption error. The methylene blue solution containing catalyst was then irradiated under UV photo reactor (LZC-4x Luzchem Photo reactor, Fig 2.2) with continuous and uniform stirring. The degradation of methylene blue dye was monitored by taking 5 mL aliquots at different intervals of time. These aliquots were centrifuged at 4500 rpm for 15 minutes and absorption spectra of the samples were recorded using UV/Visible spectrophotometer. The rate of degradation was assumed to obey first order kinetics and hence the rate constant for degradation k was obtained from the first order plot using equation 2.1.

$$\ln (A_o/A) = kt \qquad \textbf{(2.1)}$$

Where A_o is the initial absorbance, A is the absorbance after a time, t and k is the first order rate constant.

Figure 2.2. Photoreactor used for photo catalytic experiment.

The photo catalytic activity in the presence of sunlight was determined by carrying out the reaction under direct normal sunlight. The intensity of the sunlight during the experiment was determined with 75000 – 76000 lux intensity at Calicut University Campus, Kerala, India

(Altitude: 11° 7′ 34″ North 75° 53′ 25″ East, Time: 11.00-13.00, Temperature: 27 ± 1 °C). 50 mL of the methylene blue dye with concentration of $1x10^{-4}$ was taken in a 100 mL beaker. 0.1g of the catalyst was loaded and stirred in dark for 30 minutes. Then the sample was exposed to direct sunlight on a magnetic stirrer with uniform stirring. The degradation of methylene blue dye was monitored by taking 5 mL aliquots at different intervals of time. Degradation was then studied by the same procedure that used in UV.

Photocatalytic activity of coated bottle were investigated using UV chamber (LZC-4x Luzchem Photo reactor) and under direct sunlight. 10 mL of methylene blue was taken in the coated bottle and irradiate with UV Light and direct sunlight. Dye degradation was recorded using photography through color change during different time intervals.

Pesticide degradation was studied under the same photoreactor and under direct sunlight with uniform stirring. 50 mL of the 1% karate solution in water was taken and 0.1g, 0.2g and 0.3g active catalyst were loaded. The degradation was studied using the photography through color change at different time intervals.

2.5 Characterization techniques used

2.5.1 FT-IR technique

The FT-IR spectra of samples were recorded using Jasco-FT/IR-4100 spectrometer (Fig.2.3) with a wave number range of 4000-400 cm^{-1}. The spectra were measured with 70 scan per sample. Small quantity of sample was mixed with high grade KBr in the ratio 1:10 and ground

well. Pellet of the mixture was prepared using the dye of pelletize. The samples were scanned and the spectrum was recorded.

Figure 2.3. Jasco-FT/IR-4100 spectrometer.

2.5.2 FT Raman spectroscopy

Raman measurements of the calcined powder samples were taken using a MultiRAM spectrometer (Fig2.4). Spectrometer provides range 3600 to 50 cm^{-1} and is suited for Raman measurements with a laser excitation 1064 nm (standard) or 785 nm (optional). MultiRam spectrometer is specified as laser class 3B according to EN60825-1:10-2007. It is equipped with Rayleigh filters, primary filters, room temperature 'InGaAs' detector and 'Si' avalanche detector. Highly stable Raman light source is used.

Figure 2.4. MultiRAM spectrometer.

2.5.3 X-ray diffraction technique (XRD)

X-ray diffraction technique gives the idea about the crystallinity of materials. It is based on the Bragg's equation.

$$n\lambda = 2d\sin\theta \qquad \textbf{(2.2)}$$

Where 'n' is an integer, 'λ' is the wavelength, 'd' is the distance between the atomic layers in a crystal and 'θ' is the angle of diffraction. X-ray diffraction (XRD) patterns of the calcined gels were obtained with Rigaku Miniflex 600 X-ray diffractometer with CuKα radiation, λ=1.54 A°, Voltage 40 KV and current 15 mA in the diffraction angle range 2θ = 10–70°. The spectra were plotted and compared with data from the joint committee powder diffraction standards (JCPDS) for analysis. The

(101) peak (2θ=25.2˚) of anatase was used for analysis. The crystallite size (τ) was calculated using Scherer equation[2]

$$\tau = \frac{0.9\lambda}{\beta \mathrm{Cos}\theta} \qquad \textbf{(2.3)}$$

Where, 'λ' is the X-ray wave length, β the full width at half maxima and θ the Bragg angle.

Figure 2.5. Rigaku Miniflex 600X-ray Diffractometer.

2.5.4 Diffuse reflectance spectra

The diffuse reflectance spectra (DRS) of the semiconducting TiO_2 nanomaterials in the wavelength range of 200-800 nm were obtained using a UV-Vis reflectance spectrophotometer using a Jasco-V-550 UV/VIS spectrophotometer (Figure 2.5). Radiations from UV to IR region passed through monochromator are allowed to fall on the sample.

The sample reflects or absorbs certain wavelength and transmits the rest which is detected and recorded.The band gap energy was calculated from the DRS spectra by plotting $[f(R)\ h\nu]^{½}$ against hν, where 'h' is the Planck's constant. The Kubelka-Munk function f(R) was calculated using the following equation[3]

$$f(R) = \frac{(1-R)^2}{2R} \qquad \textbf{(2.4)}$$

Where 'R' is the reflectance.

Figure 2.6. Jasco-V-550 UV/VIS spectrometer.

2.5.5 X-Ray Photoelectron Spectroscopy (XPS)

X-ray photoelectron spectroscopy (XPS) analyses were performed on a SpecsLab2, Version 2.76-r26050 (Fig.2.6). The instrument employs an analyzer PHOIBOS HSA3500 DLSGED150 R7 [HW Type 30:100] DLSGED and monochromated AlKα X-ray source (hν = 1486.74*eV*) which was used at 1.5KV. The area of analysis was medium and analysis slit with a dimension of 5:7 x 20\2: open. For the survey of spectra pass energy of 20 *eV* and a 0.1 *eV* step size were employed.

Figure 2.7. SpecsLab2 Version 2.76-r26050.

2.5.6 Differential scanning calorimetry[4]

Differential scanning calorimetry (DSC) measurements were carried out using a TA Instrument DSC Q20 V24.11 Build 124 (Fig. 2.7). A sample and a reference material (alumina crucible used as a reference) were placed in holders in the instrument. They were heated at a required temperature at a specific rate (10 ˚C/min). The difference in the heat flow between the sample and the reference material is measured.

A graph was plotted with heat flow *Vs* temperature. In the experiments a small amount of accurately weighed sample was heated from room temperature to 500 ˚C at a constant heating rate of 10 ˚C/min.

Figure 2.8. DSC Q20 V24.11 Build 124.

2.5.7 Scanning Electron Microscope[5]

The SEM image of the samples was taken by using a Scanning Electron Microscope Hitachi SU-6600 Analytical VP FEG-SEM. A new and versatile Field Emission SEM which utilizes advanced Variable Pressure (VP) technology and an improved Schottky field emission electron source that provides exceptional imaging and high probe current with great stability. The vapour pressure mode allows the operator to change vacuum conditions in the sample chamber from high vacuum (≤10 – 4 Pa) to low vacuum (10 ~ 300 Pa) operation. The back scattered electrons or secondary electrons are detected. The fine beam of electrons focused on the target using electrostatic lenses is scanned and the amplified signal generates the image of sample surface. Vacuum conditions were used in order to avoid oxidation, contamination of filament and reduce the collision between air molecules and electrons.

Figure 2.9. Hitachi SU-6600 Analytical VP FEG-SEM.

2.5.9 Energy Dispersive Spectroscopy5

Energy Dispersive Spectroscopy (EDS) is done using the microscope Hitachi SU-6600 Analytical VP FEG-SEM. The composition of the sample is obtained using the technique known as Energy Dispersive Analysis of X-rays (EDAX). The high energy electrons striking the sample produce characteristic X-rays of atoms with which they interact. The intensities of X-rays are compared and the composition is recorded.

2.5.8 Transmission Electron Microscope5

The Transmission electron microscope (TEM) image was recorded using LIBRA 200 TEM (M/s Carl Zeiss, Germany). Electrons are transmitted through the specimen in the microscope. Electric field of 120 and 200 kV is applied. Instrument investigates the nanomaterials with a resolution of 0.7 eV. TEM can not only obtain the images of the specimen but also the diffraction patterns, which enables to make the detailed crystal structure analysis of the sample. It require vacuum environment for their operation.

The sample thickness should be less than 300 nm in order to transmit sufficient electrons. Jet thinning is used for metallic samples and ion milling for non-conducting samples for limiting the thickness.

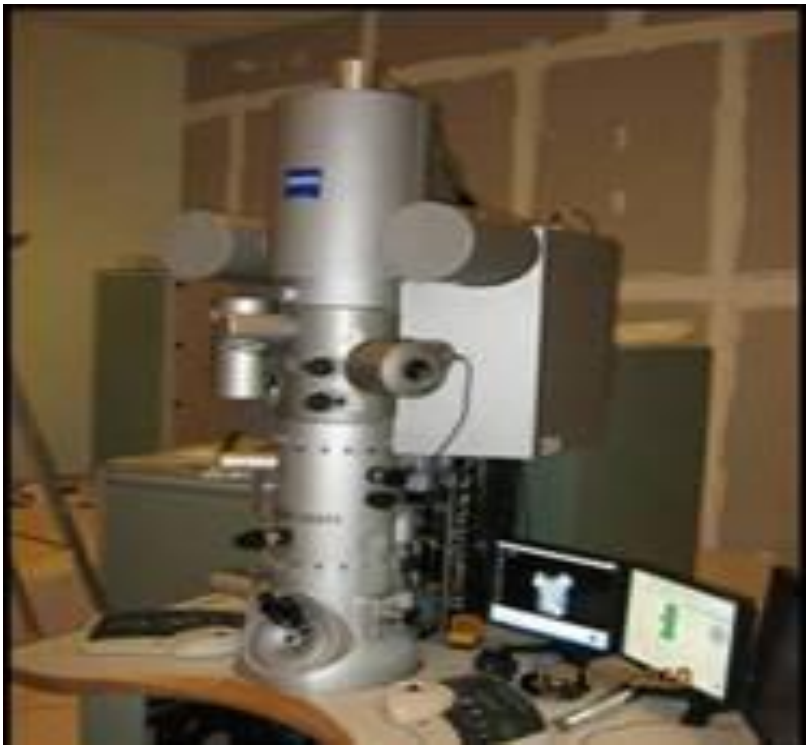

Figure 2.10. LIBRA 200 TEM.

2.5.9 Reference

1. C. P. Sibu, S. Rajesh Kumar, P. Mukundan, K. G. K. Warrier, *Chem. Mater.*, 2002**,** 14, 2876.

2. A. Guinier and D.L. Dexter, *Interscience (Wiley)*, 1963

3. J. B. M. Goodall, S. Kellici, D. Illsley, R. Lines, J. C. Knowlesd, J. A. Darr, *RSC Adv.*, 2014,4, 31799.

4. D. A. Skoog, F. J. Holler and S. R. Crouch, *Principals of Instrumental Analysis*, Thomson Brooks/Cole, USA, 2007.

5. S. K. Kulkarni, *capital Publishing company*, 2007.

3 Chapter

Samarium ion (Sm^{3+}) doped TiO_2 synthesis, characterization and photodegradation.

Contents

3.1 Introduction

In this chapter an efficient and straight-forward method for the preparation of samarium ion (Sm^{3+}) doped photocatalytically active, anatase TiO_2 is discussed. TiO_2 has mainly two drawbacks in achieving high photocatalytic efficiency, the fast electron hole recombination and the limited absorption in the solar spectrum. To reduce the recombination of photogenerated electrons and holes on TiO_2, and also to extend its light absorption into the visible region, TiO_2 has been doped with transition metal ions,[1,2,3,4,5,6] coupled semiconductor systems,[7,8] noble metals deposition,[9] nonmetals[10,11,12,13,14,15] and rare earth ions.[16,17,18,19]

Various synthetic routes like sol–gel method,[17] hydrothermal method,[18] co-precipitation-peptization method[19] have been studied for the preparation of metal ion doped TiO_2 nanocrystals. Rare earth metals having incompletely occupied 4f and empty 5d orbitals often serve as catalyst or promoter for catalysis.[20] It has been already discussed that the photocatalytic activity of TiO_2 can be improved by doping with rare earth metals.[21,22,23] Liang *et.al.* reported the photocatalytic activity of rare earth ions (Sm^{3+}, Nd^{3+}, Pr^{3+}) doped TiO_2 catalysts for Orange I degradation under both UV and visible light irradiations.[24] Xiao *et.al.* reported the synthesis of Sm^{3+} doped TiO_2 nanocrystallites under visible light by auto-combustion technique shift to longer wavelengths as compared to bare TiO_2 sample.[25] Shi *et.al.* developed a series of Sm^{3+} doped TiO_2 for the photocatalytic degradation of methyl orange.[26] Park *et.al.* reported that the

photoluminescence emission of Sm^{3+}doped TiO_2 nano tubes with UV light irradiation.[27] However, all these method required expensive chemicals, templates for structure direction of TiO_2, harsh chemical/heat treatment for removal of the template to obtain pure TiO_2 and induce crystallinity into TiO_2. In this work a simple modified sol-gel method was used to synthesize TiO_2 and Sm^{3+} doped TiO_2 and characterized with XRD, FTIR, DRS, SEM and TEM. Photocatalytic activity of these samples was studied by photo degradation of methylene blue under UV and direct sun light. The effect of calcination temperatures on the photo catalytic activity was also been discussed. This modified sol-gel method using acetic acid as a stabilizing agent leads to a highly homogeneous distribution of the Sm^{3+}dopant in the TiO_2 host matrix with nano sized powders. This method also offers a uniform particle size distribution and other advantages such as excellent compositional control, homogeneity of dopant distribution on the molecular level due to the mixing of liquid precursor and lower crystallization temperature for the formation of TiO_2.

3.2 Results and Discussion

3.2.1 FT-IR Spectroscopy

The FTIR spectra of TSm1, TSm2, TSm5, TSm10 and bare TiO_2 calcined at 300, 500 and 700 ˚C were recorded. A representative example of the FTIR spectra of TSm2 dried at 100 ˚C and 500 ˚C and bare TiO_2 calcined at 500 ˚C was shown in Figure 3.1. In both spectra of TiO_2 and TSm2, the absorption band at 3500-3000 cm^{-1} indicates hydroxyl group stretching vibration and surface adsorbed water molecule. The peak at 1627 cm^{-1} indicates the hydroxyl group bending vibration and the peak at 2920 and 2855 cm^{-1} is the asymmetric C-H

stretching vibration.[28]Absorbed CO_2 on the surface is indicated by the peak at 2338 cm^{-1}.[29]The presence of peak at 1120 cm^{-1} in Sm^{3+}doped TiO_2 sample is due to the Ti-O-Sm stretching vibrations. The peak at 1425 and 1532 cm^{-1} in both TiO_2 and Sm^{3+} doped TiO_2 is due to the symmetric and asymmetric stretching vibration of acetate groups. Both TiO_2 and Sm^{3+} doped TiO_2 sample possess strong and broad band in the range of 400-700 cm^{-1} which were attributed to Ti-O stretching and Ti-O-Ti bridging stretching modes, which is a characteristic peaks of anatase phase of TiO_2.[30]The peak at 477 cm^{-1} for Sm^{3+} doped TiO_2 is due to the vibration modes of anatase skeletal O-Ti-O and Ti-O-Sm bonds.[31,32,33,34]A new band at 478 cm^{-1} was observed in the spectra of Sm^{3+}doped TiO_2 samples. This band is attributed to the Sm–O bond.[35]Similar type of observation was also seen in the FTIR spectra of TiO_2 and Sm^{3+} doped TiO_2 calcined at 500 and 700 ˚C.

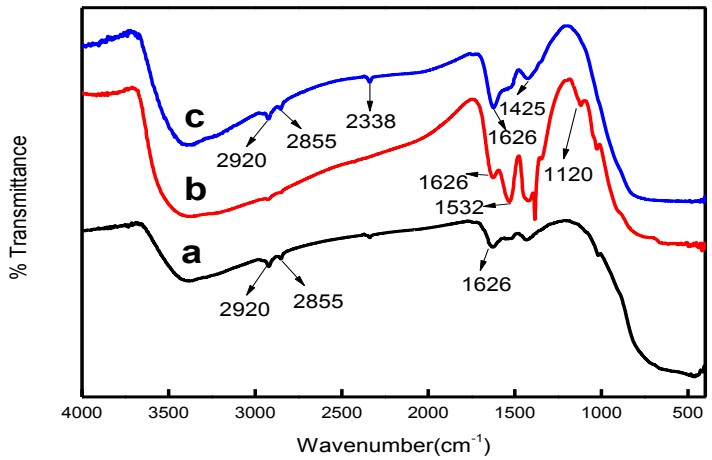

Figure 3.1. FTIR spectra of a) TiO_2 calcined at 500 ˚C b) TSm2 dried at 100 ˚C c) TSm2 calcined at 500 ˚C.

3.2.2 XRD

XRD patterns of pure TiO_2 and TSm1, TSm2, TSm5, TSm10 calcined at 300, 500 and 700 ˚C were recorded. The XRD of TiO_2 and Tsm2 at 300, 500 and 700 ˚C were shown in Figure 3.2 A, 3.2 B and 3.2 C respectively. From the figure it is clear that all samples are in the anatase phase. The particle characteristics of the TiO_2 and Sm^{3+} doped TiO_2 samples under different weight percentage and temperature are summarized in Table 3.1 A. The relative intensity of (101) peaks were broadened and reduced in the Sm^{3+}doped TiO_2, in comparison with pure TiO_2 calcined at the same temperature (Figure.3.3). It can be seen that no peaks from samarium oxide (Sm_2O_3) were observed in any of the doped sample which implies that Sm^{3+} ions are incorporated in the crystal lattice of TiO_2.When the crystallite sizes of the Sm^{3+} doped TiO_2 samples were calculated using the Scherrer formula (Table 3.1), it was found that the crystallite size was reduced by Sm^{3+} ion doping. It is due to the segregation of the dopant cations at the grain boundary of TiO_2, and the growth of nanocrystalline TiO_2 is then prevented. These smaller crystallite of TSm2 may delay the transformation of anatase to rutile structure and also have the larger surface area compared to pure TiO_2,[36,37] which is accordance to the data obtained from the BET surface area isotherm (Figure 3.2 D & 3.2 F, Table 3.1 B), where TSm2 shows a surface area of 68.07 m^2/g while that of TiO_2 is only 1.14 m^2/g.

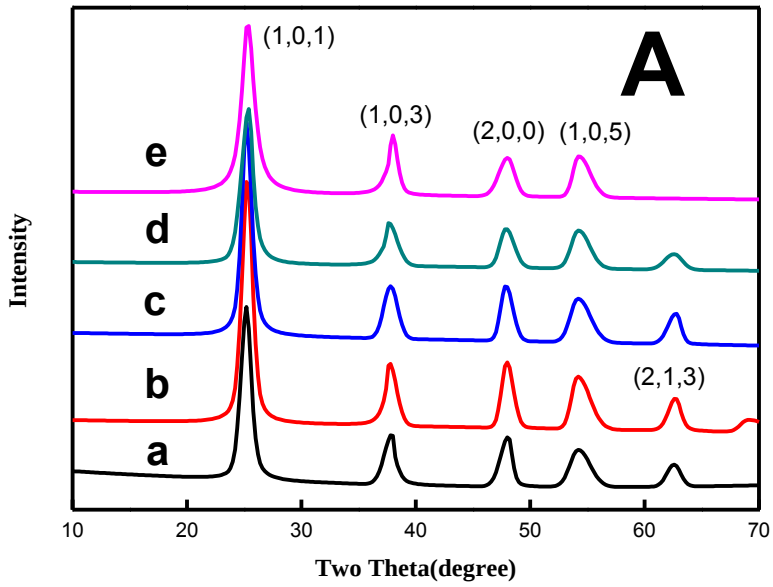

Figure 3.2 A) XRD patterns of a) TiO_2 b) TSm1 c) TSm2 d) TSm5 and e) TSm10 calcined at 300 ˚C.

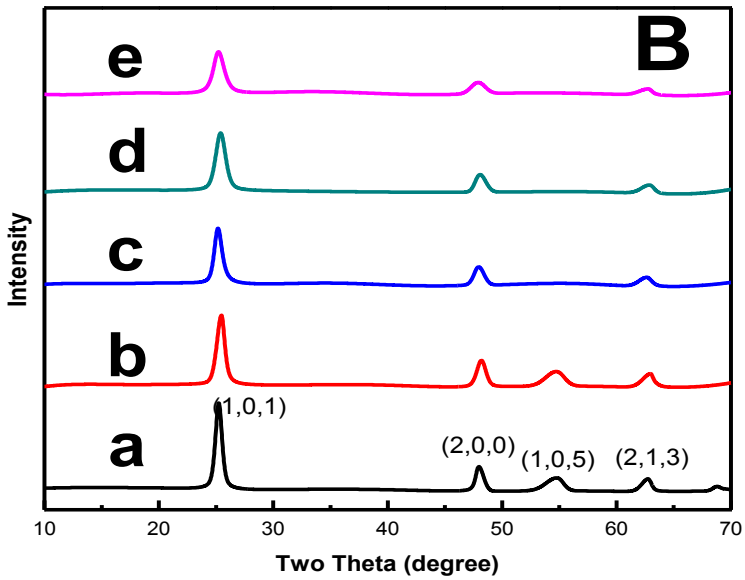

Figure 3.2 B) XRD patterns of a) TiO_2 b) TSm1 c) TSm2 d) TSm5 and e) TSm10 calcined at 500 ˚C

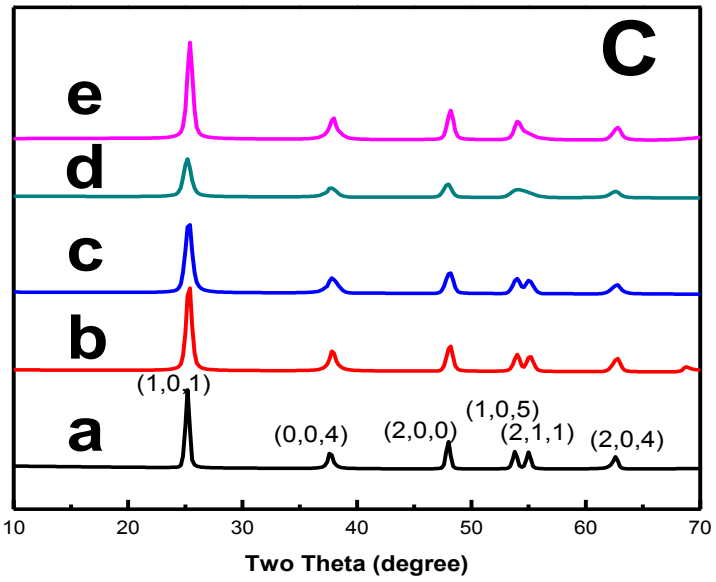

Figure 3.2 C) XRD patterns of a) TiO_2 b) TSm1 c) TSm2 d) TSm5 and e) TSm10 calcined at 700 ˚C

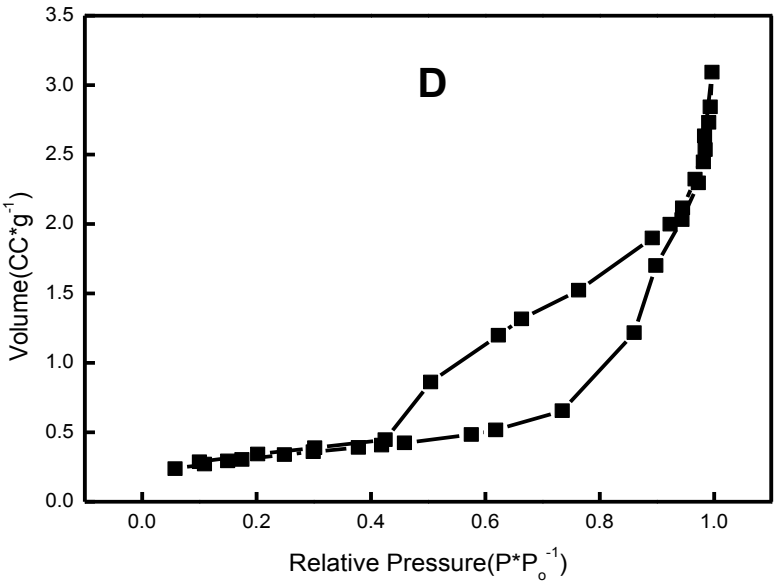

Figure 3.2 D) BET adsorption Isotherm of TiO_2 calcined at 500 ˚C.

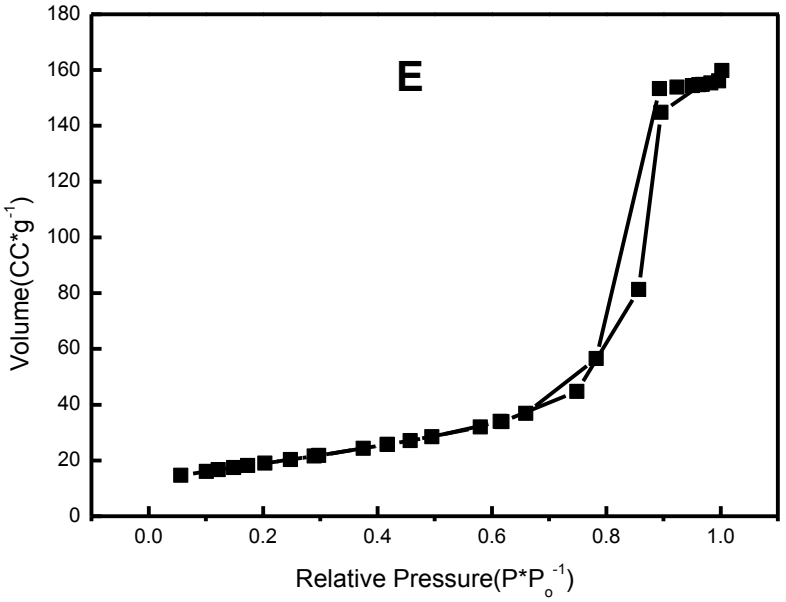

Figure 3.2 E) BET adsorption Isotherm of TSm2 calcined at 500 ˚C.

Table 3.1 A. Crystal size of anatase TiO_2, TSm1, TSm2, TSm5 and TSm10 calcined at 300, 500 and 700 ˚C.

Sample	300 ˚C	500 ˚C	700 ˚C
TiO_2	8.4	12.6	21.7
TSm1	7.79	10.6	15
TSm2	7.7	10.5	12.4
TSm5	6.96	8.4	11.4
TSm10	6.5	7.6	11.1

Table 3.1 B. BET surface Area Analysis of TiO_2 and TSm2 at 500 ˚C.

Material	Surface area
TiO_2	1.14 m^2/g
TSm2	68.07 m^2/g

3.2.3 Raman Spectroscopy

Raman spectra of TSm1, TSm2, TSm5, TSm10 and pure TiO_2 calcined at 300, 500 and 700 ˚C were recorded. A representative example of the Raman spectra of TiO_2 and TSm2 calcined at 500 ˚C was shown in Figure 3.3. The spectrum reveals the anatase phase purity of synthesized TiO_2 nanoparticles. The peaks are present at 145 (E_g), 395 (B_{1g}), 514 (B_{1g}) and 639 cm^{-1} (E_g) which are the characteristics of anatase phase of TiO_2.[38] The major peak of anatase is decreasing as the doping was introduced confirms the incorporation of Sm^{3+} into the crystal lattice and thereby decrease in crystallinity which has been explained in XRD spectra (Figure 3.2). It can also be confirmed that, in addition to decrease in peak intensity the peak broadening increases, which attributes to the oxygen vacancies and thereby Ti^{3+} doping occurred as a result of doping.[39]

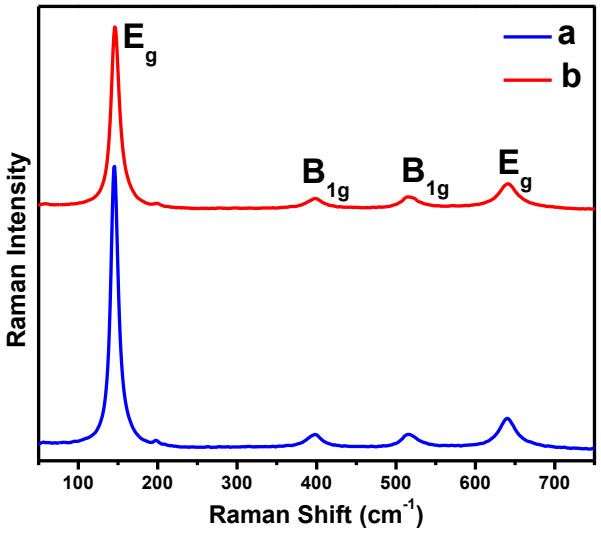

Figure 3.3. Raman Spectra of a) TiO_2 and b) TSm2 calcined at 500 ˚C.

3.2.4 Differential scanning calorimetry (DSC)

Differential scanning calorimetry (DSC) studies were carried out (Figure 3.4) to investigate the amorphous to crystalline transition of the TiO_2 precursor samples of both TiO_2 and TSm2 samples. Endothermic peak at 92 ˚C was observed for the TiO_2 sample and 94 ˚C for the TSm2 and these peaksare due to the removal of adsorbed water molecules. The exothermic peak at 309 ˚C of TSm2 sample shows the amorphous to crystalline transition.[40]The presence of an endothermic peak at 405 ˚C shows desorption of water molecules from the TiO_2.[41]

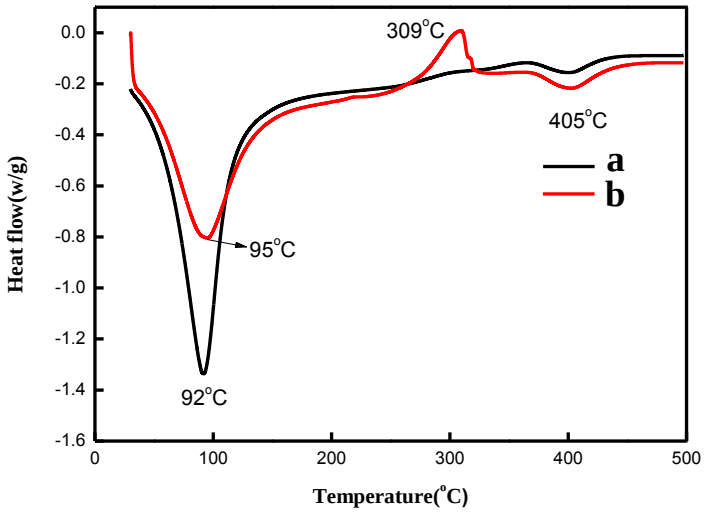

Figure 3.4. Differential scanning calorimetry of a) TiO_2 b) TSm.

3.2.5 Diffuse reflectance spectroscopy (DRS)

Diffuse reflectance spectroscopy (DRS) in the range 200-800 nm of TiO_2 and TSm1, TSm2, TSm5 and TSm10 calcined at different temperature were investigated to study the optical absorption properties. The DRS spectra of TiO_2 and TSm2 calcined at 500 and 700 ˚C were shown in the Figure 3.5, and it is clear that TSm2 shows an absorption band in the range 400-500 nm. It also observed that when doping concentration increased 1 to 10 percent, the absorption edge of sample shifts to higher wavelength. This red shift can be attributed to the charge-transfer transition between the *f* electrons of Sm^{3+} ion and the TiO_2 conduction band[33,34]which help in the generation of electron and hole under visible light irradiation. Which is in accordance with the Photoluminescence spectra obtained (Figure 3.6), where it can be observed that the intensity of the emission peak is

quenched. Similar red shift absorption profile is observed with an increase in calcined temperature. The band gap energies were calculated by using UV-Vis DRS spectra with Tauc equation are shown in the Table 3.2. The band gap energies of Sm^{3+} doped samples are lower than that of TiO_2 due to the red shift that occurred as a result of Sm^{3+} doping.

Table 3.2. Band gap energies of TSm1, TSm2, TSm5, TSm10 and TiO_2 calcined at different temperatures.

Sample	Band Gap (eV)		
	300 ˚C	**500 ˚C**	**700 ˚C**
iO2	3.1	3.02	3.00
TSm1	2.54	2.45	2.25
TSm2	2.50	2.28	2.30
TSm5	2.54	2.43	2.28
TSm10	2.59	2.44	2.29

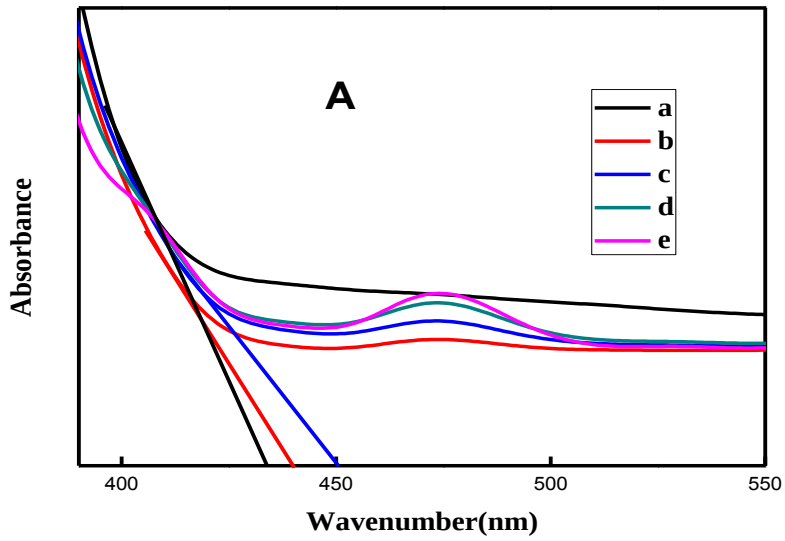

Figure 3.5 A) Absorbance of a) TiO_2 b) TSm1 c) TSm2 d) TSm5 and e) TSm10 calcined at 500 ˚C.

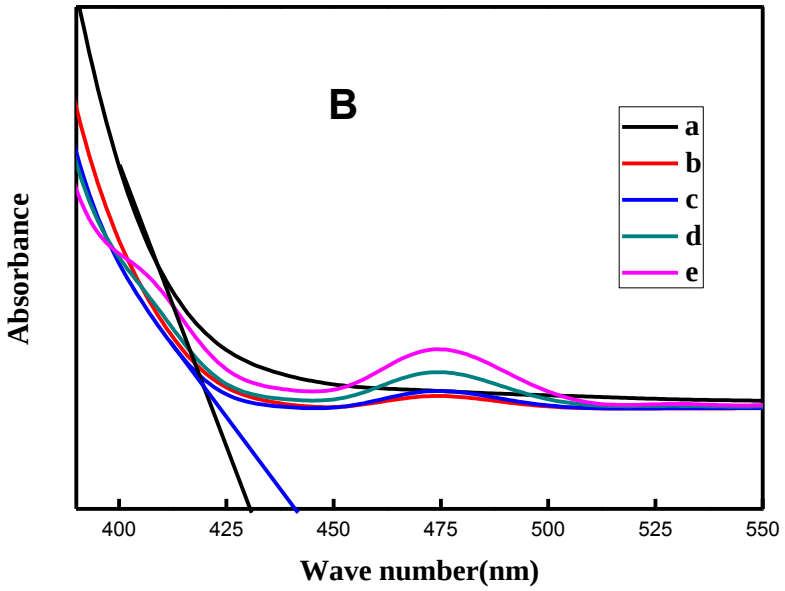

Figure 3.5 B) Absorbance of a) TiO_2 b) TSm1 c) TSm2 d) TSm5 and e) TSm10 calcined at 700 ˚C.

.

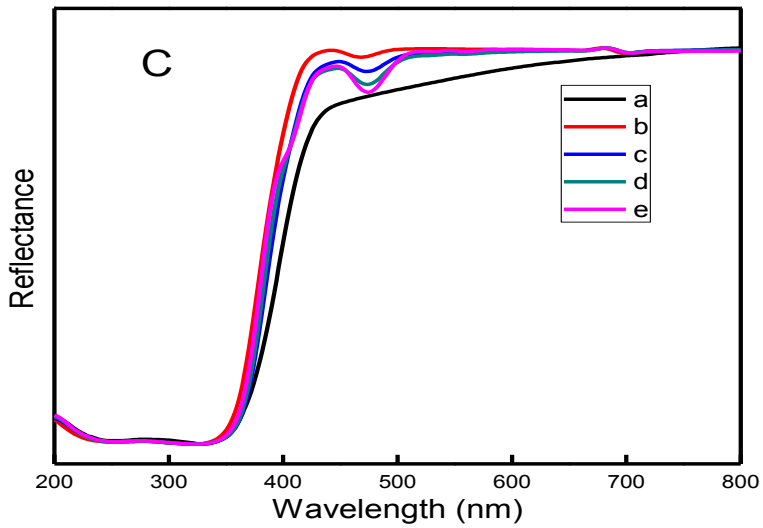

Figure 3.5 C) Reflectance of a) TiO_2 b) TSm1 c) TSm2 d) TSm5 and e) TSm10 calcined at 500 ˚C.

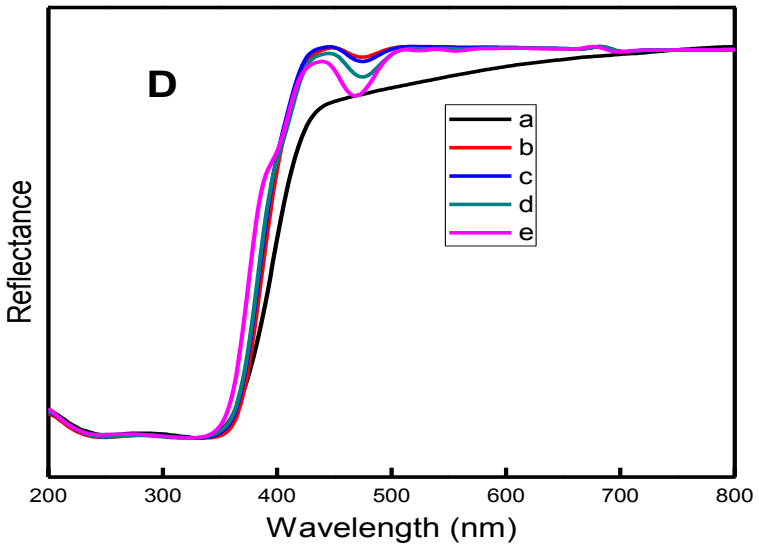

Figure 3.5 D) Reflectance of a) TiO_2 b) TSm1 c) TSm2 d) TSm5 and e) TSm10 calcined at 700 ˚C.

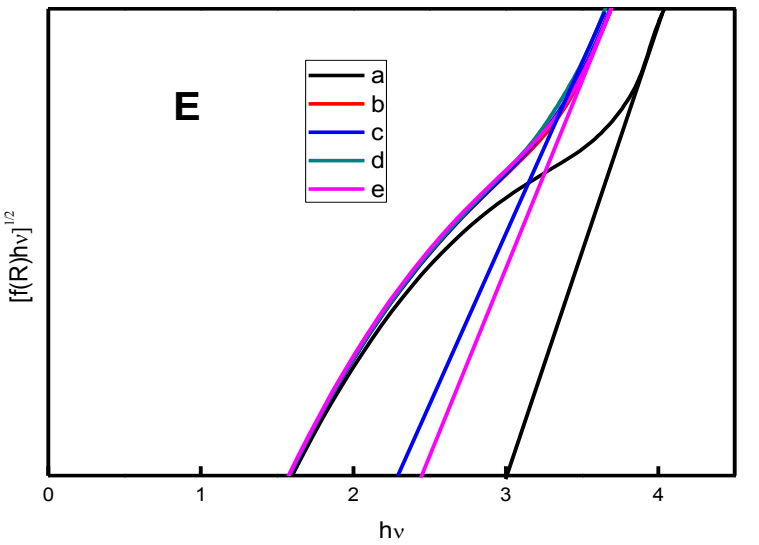

Figure 3.5 E) Tauc plot of a) TiO_2 b) TSm1 c) TSm2 d) TSm5 and e) TSm10 calcined at 500 ˚C.

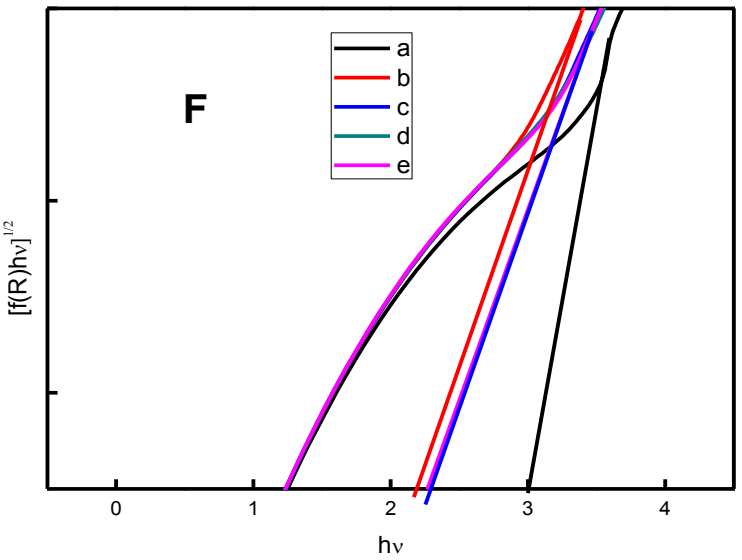

Figure 3.5 F) Tauc plot of a) TiO_2 b) TSm1 c) TSm2 d) TSm5 and e) TSm10 calcined at 700 ˚C.

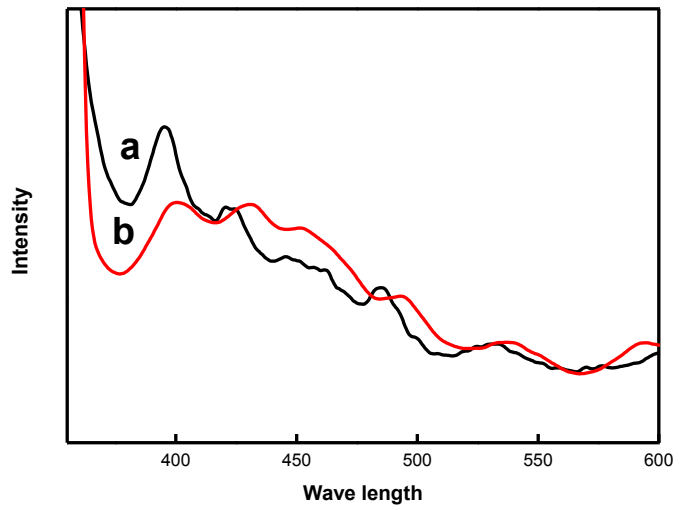

Figure 3.6 PL spectra of a) TiO_2 and b) TSm2 calcined at 500 ˚C.

3.2.6 X-ray Photoelectron Spectroscopy (XPS)

XPS of TiO_2 and TSm2 calcined at 500 ˚C were recorded. Spectrum reveals the incorporation of Sm^{3+} into the lattice of TiO_2. Notable peak changes are occurred on the surface of TiO_2. The $2p_{3/2}$ and $2p_{1/2}$ peaks of TiO_2 were observed at 460.2 eV and 466 eV for bare TiO_2 (Figure 3.7A). The peak 460.2 eV is attributed to the oxygen richness.[42] The splitting was found in both the samples at 5.8 eV, which attributes the anatase phase purity of both TiO_2 samples.[43]Surface defects originate when Sm^{3+} enters in to the lattice of TiO_2 and which is confirmed by the blue shifting in the binding energy *i.e.* 457.6 eV ($2p_{3/2}$) and 463.2 eV ($2p_{1/2}$). The peak at 457.6 eV reveals the presence of Ti^{3+}.[42]At the same time the decrease in valency of Ti explain the presence of oxygen vacancies. These relevant explanations reveal the transformation of oxygen rich environment to oxygen deficient environment. From the O1s XPS (Figure 3.7B) it can be seen that the peak at 531.5 eV blue shifted to 528.7 eV indicates the change in oxygen environment.[30] Figure 3.7C, the Sm3d XPS reveals the incorporation of Sm^{3+} into the crystal lattice. As evidenced from XRD, even though the ionic radius of Sm^{3+} (109.8pm) is far greater than Ti^{4+} (74.5pm), Sm^{3+} entered into the crystal lattice of TiO_2 and those ions occupy the interstitial position of TiO_2. The distinct doublets at 1081.5 and 1106 eV coming from $Sm3d_{5/2}$ and $Sm3d_{3/2}$ attribute the presence of Sm-O-Ti bond.[44]

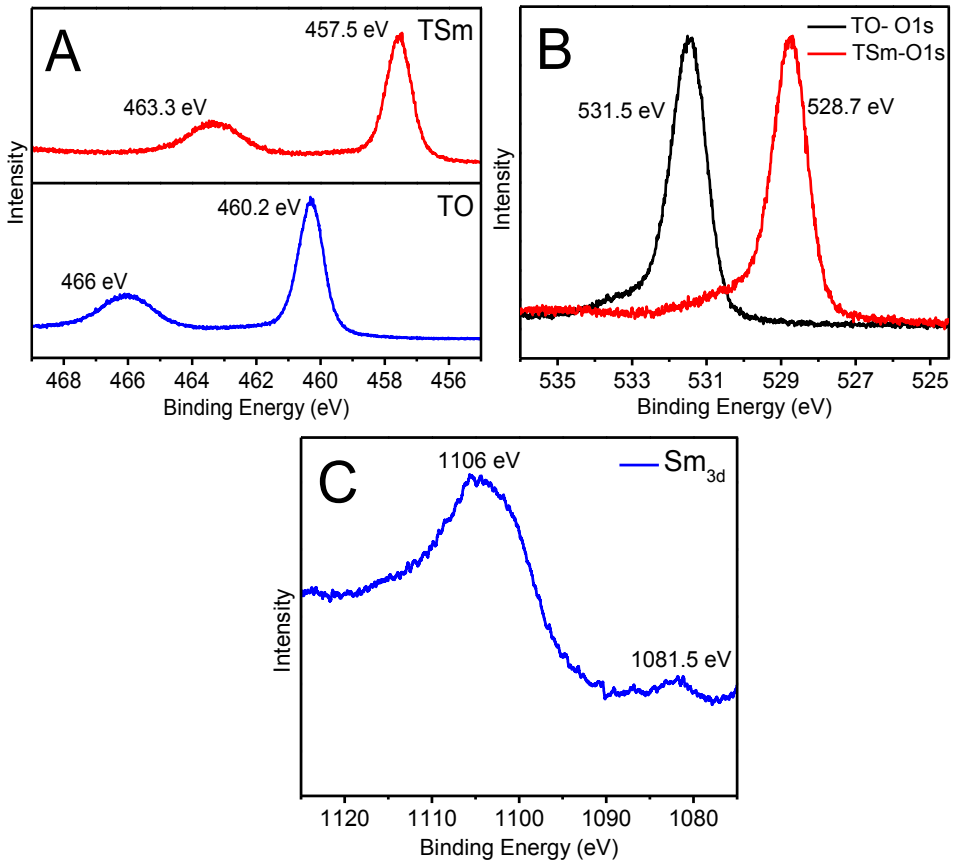

Figure 3.7. XPS of A) Ti2p B) O1s and C) Sm3d.

3.2.7 Scanning Electron Microscopy (SEM)

The morphology of the TiO_2 and Sm^{3+} doped TiO_2 sample was analyzed using Scanning Electron Microscopy (SEM). SEM images of TiO_2 and TSm2 doped TiO_2 calcined at a temperature 500 °C showed in the Figure 3.8A. SEM analysis indicates that the particles undergo agglomeration in both TiO_2 and Sm^{3+} doped TiO_2 samples. It is clear from Figure 3.8A that the particle size of Sm^{3+} doped TiO_2 sample is lower than that of TiO_2. This observation is in agreement with the

crystalline size calculation from XRD where TiO_2 showed a crystalline size of 12.6 nm whereas TSm2 showed only 10.6 nm (Table 3.2) at a calcination temperature 500 ˚C. That means the Sm^{3+} ion doping could hinder the increase of crystallite size during calcinations. Also SEM images showed the uniform nature of particles with no change in particle morphology due to Sm^{3+} doping with well-defined clear boundaries. EDS analysis (Figure 3.8B and Table 3.3) was carried out for the TiO_2 and TSm2 to determine the chemical composition. Strong X-ray peaks associated with Ti and oxygen are present in TiO_2 whereas strong peaks of samarium were found in the Sm^{3+} doped TiO_2 along with Ti and oxygen. Quantitative analysis by the EDS software package was used to determine the respective weight percentages of each element in the TiO_2 and TSm2 shown in Table 3.3 confirms the presence of both Ti and Sm in the lattice of Sm^{3+} doped TiO_2.

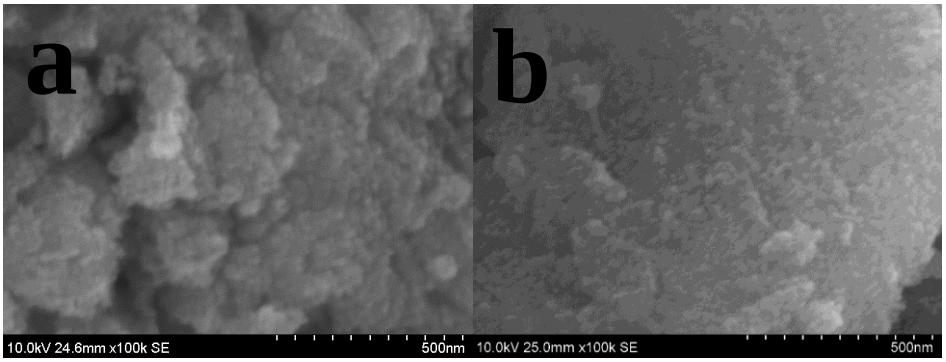

Figure 3.8A. SEM image of a) TiO_2 b) TSm2 calcined at 500 ˚C.

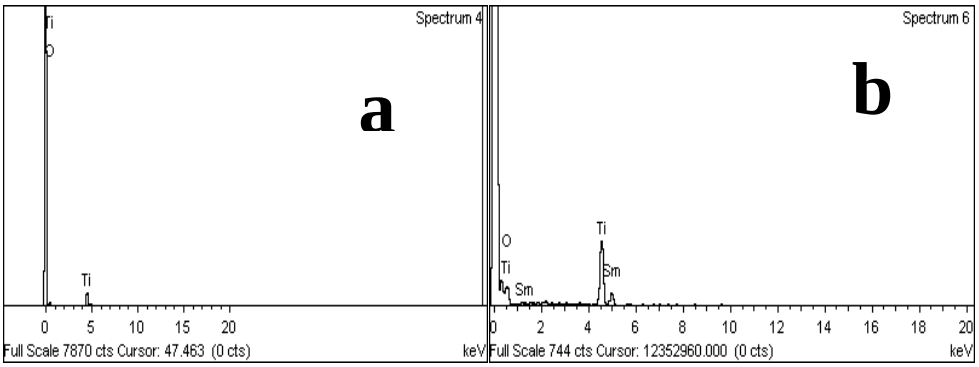

Figure 3.8 B. Energy Dispersive Spectroscopy (EDS) of a) TiO_2 and b) TSm2 at 500 ˚C.

Table 3.3. Energy Dispersive Spectroscopy (EDS) elementary analysis TiO_2 and TSm2 calcined at 500 ˚C.

Element	TSm2		TiO_2	
	Weight %	Atomic%	Weight %	Atomic%
TiK	57	80.03	57.39	80.13
OK	42.40	19.88	42.61	19.87
SmL	0.61	0.09	Nil	Nil

3.2.8 Transmission Electron Microscopy (TEM)

TEM images of TiO_2 and TSm2 calcined at 500 ˚C were recorded.TiO_2 shows a particle size of 19-23 nm (Figure.3.9a) at 500 ˚C. On the other hand, the TSm2 has a particle size of 10-12 nm (Figure. 3.9b), and thus the TEM observations support the conclusions derived from the XRD data. The selected area electron diffraction (SAED) image of Sm^{3+} doped TiO_2 calcined at 500 ˚C shows broad band due to the Scherrer line broadening which is attributed to the small crystalline size[45,46]

however TiO_2, at same temperature, showed distinct spots due to the high crystallinity and larger size of the crystals.

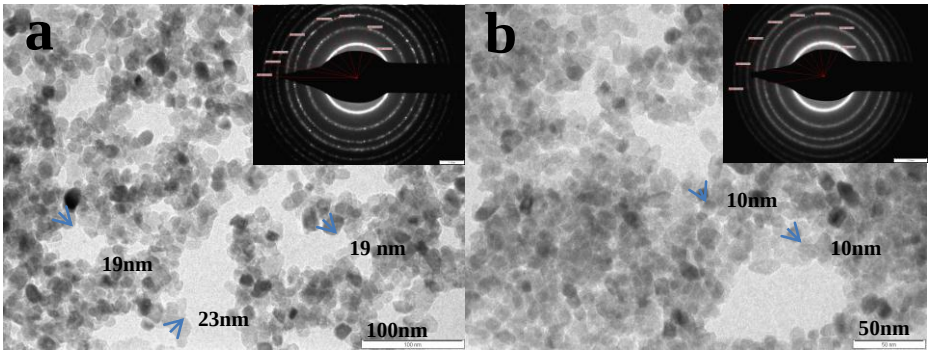

Figure 3.9. TEM images of a) TiO_2 and b) TSm2 at 500 ˚C.

3.3 Photocatalysis

Photocatalytic activity of both TiO_2 and TSm2 calcined at 500 ˚C for methylene blue degradation under UV and sunlight were carried and the rate constant obtained from the degradation kinetics were summarized in Table 3.4. Figure 3.10 shows the degradation efficiency of methylene blue under the UV and sunlight irradiation using TiO_2 and TSm1, TSm2, TSm5 and TSm10 calcined at 500 ˚C. From Table 3.4 it can be seen that calcined temperature influence on photocatalytic activity of pure TiO_2 and TSm. The optimum calcination temperature was at 500 ˚C. Rate of degradation under direct sunlight irradiation is more compared to UV light irradiation. This is because upon Sm^{3+} ion doping, the light absorption capacity of TiO_2 increases from UV to visible region in accordance with band gap narrowing. From the Table 3.4, it is observed that TSm sample shows greater photocatalytic activity than TiO_2 under UV light except the lower temperature and

lower concentration of Sm^{3+} (TSm1). The rate constant obeys the first order kinetics and the values are summarized in the Table 3.4, among the different TSm, highest activity was obtained for TSm2 calcined at 500 ˚C,with a rate constant of 0.092 min^{-1}, which is 2.5 times higher than the bare TiO_2 (0.037 min^{-1}). Absorption spectra of methylene blue dye degradation under UV light using TiO_2 and Sm^{3+} doped TiO_2 at 500 ˚C were shown in Figure 3.11 and 3.12. TSm2 calcined at 500 ˚C degraded completely within 40 minutes. From the results it can be concluded that the TSm2 calcined at 500 ˚C is the best photocatalyst among the samples under UV light irradiation.

The visible light activity of TiO_2 and TSm under direct sunlight using the methylene blue degradation experiment was carried out and the time taken for degradation of methylene blue using TiO_2 and TSm under sunlight was also shown in Table 3.4. From the Table 3.4, it is found that Sm^{3+} doped TiO_2 sample undergo methylene blue degradation much faster than compared to TiO_2 at all calcinations temperatures under sunlight irradiation. The rate constant was calculated from the first order kinetics and is shown in Table 3.4. Among the doped samples highest activity was obtained for TSm2 sample calcined at 500 ˚C with a rate constant of 0.103 min^{-1} which is 10 times higher than the pure TiO_2 (0.013 min^{-1}). Absorption spectra of methylene blue dye degradation under visible light using TiO_2 and 2% Sm^{3+} doped TiO_2 at 500 ˚C were shown in Figure 3.13 and 3.14. TSm2 calcined at 500 ˚C degraded completely within 25 minutes. The results point out that TSm2 calcined at 500 ˚C is the best photocatalyst among samples under visible light irradiation.

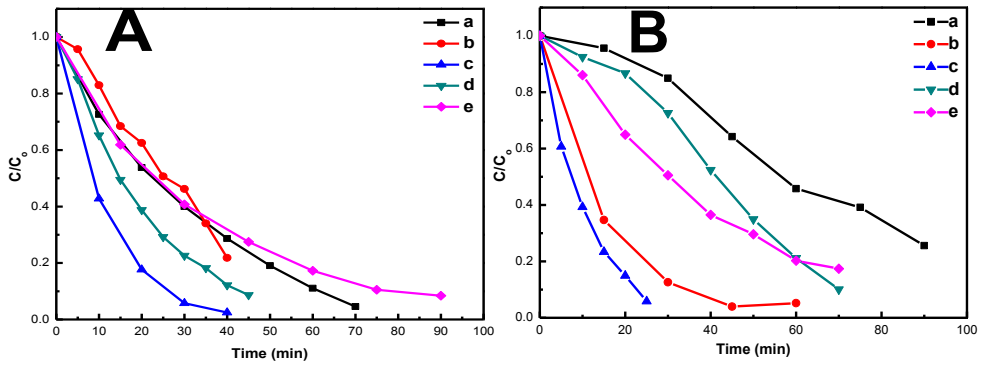

Figure 3.10. Degradation curve of a) TiO_2 b) TSm1 c) TSm2 d) TSm5 and e) TSm10 calcined at 500 ˚C A) UV light B) Sunlight.

Table 3.4. Rate constant (min^{-1}) of TiO_2 and TSm calcined at different temperatures.

UV light				Sunlight			
Sample	**300 ˚C**	**500 ˚C**	**700 ˚C**	**Sample**	**300 ˚C**	**500 ˚C**	**700 ˚C**
TiO_2	0.021	0.036	0.002	TiO_2	0.007	0.013	0.004
TSm1	0.007	0.03	0.014	TSm1	0.003	0.059	0.28
TSm2	0.007	**0.092**	0.073	TSm2	0.004	**0.103**	0.091
TSm5	0.009	0.051	0.066	TSm5	0.005	0.024	0.026
TSm10	0.012	0.028	0.023	TSm10	0.013	0.025	0.020

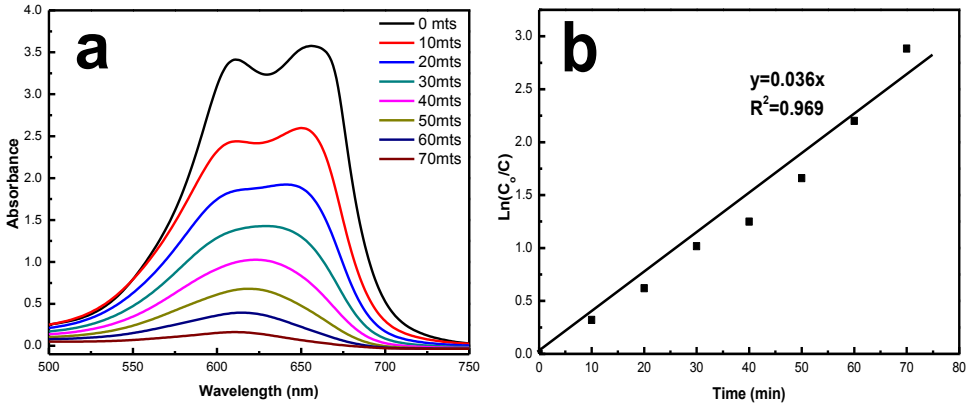

Figure 3.11. Absorption spectra and Kinetic study of methylene blue dye degradation under UV using TiO_2 sample calcined at 500 ˚C.

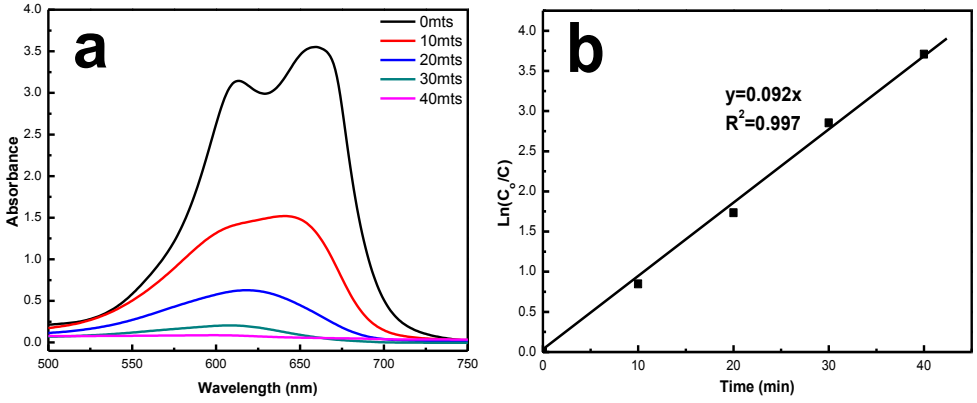

Figure 3.12. Absorption spectra and Kinetic study of methylene blue dye degradation under UV usingTSm2 calcined at 500 ˚C.

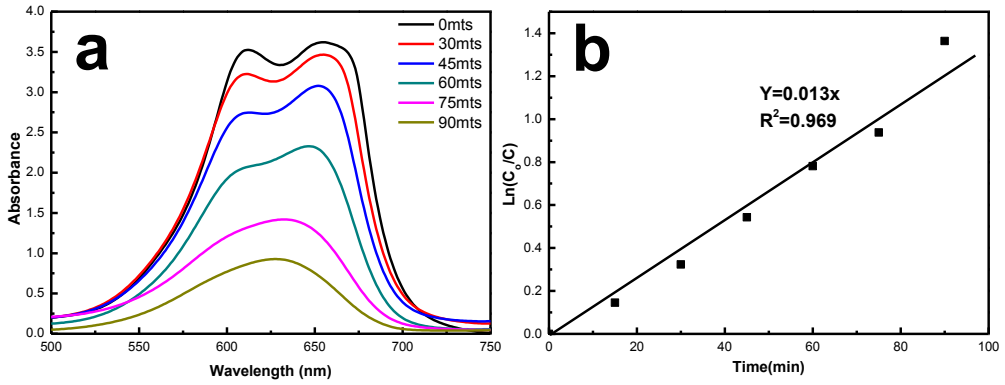

Figure 3.13. Absorption spectra and Kinetic study of methylene blue dye degradation under direct sunlight using TiO_2 sample calcined at 500 ˚C.

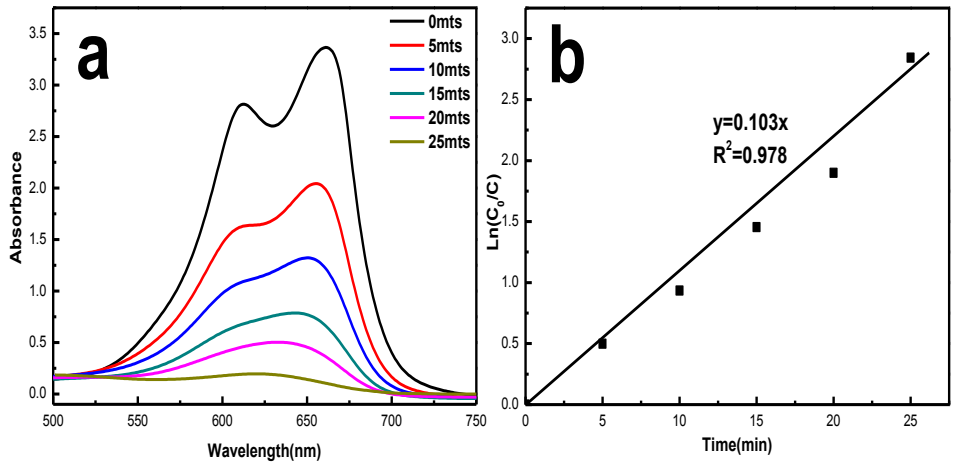

Figure 3.14. Absorption spectra and Kinetic study of methylene blue dye degradation under direct sun light using TSm2 sample calcined at 500 ˚C.

3.3.1 Proposed photocatalytic mechanism of Sm^{3+} doped anatase TiO_2

TSm doped sample showed higher visible light activity than the TiO_2 can be explained as follows. The methylene blue dye gets adsorbed as well as complexes with the Sm^{3+}ions on the surface of the anatase TiO_2 catalyst. When the dye molecule get excited by absorption of a suitable visible light photon, the electrons of excited dye molecule can be injected into conduction band (CB) of TiO_2 as shown in Scheme 3.1. The Sm^{3+} species can act as an effective electron scavenger to trap the conduction band electrons of TiO_2, which were injected from the excited dye molecule. The electrons trapped in Sm^{2+} sites were subsequently transferred to the adsorbed O_2 by oxidation process leading to generation of effective oxidative superoxide radical species ($O_2^{\bullet-}$) capable of attacking the nearby dye molecules. Since Sm^{2+} with six f-electron is unstable; the electrons can be easily de-trapped and transferred to the oxygen molecules. Therefore it reduced the recombination rate of the photogenerated electron and hole, which enhanced the photocatalytic degradation rate of methylene blue dye. Ti2p XPS clearly explains the presence of Ti^{3+} species originated after Sm doping. Presence of Ti^{3+} means the oxygen vacancy rich environment. The defective surface always results in the VB maxima increase and conduction band minima decrease. As a result of Sm doping there must be VB tailing *i.e.* the presence of surface oxygen vacancy states arise due to O2s states.[47]The Ti^{3+} can also form a defect level and act as the hole-trap to promote the charge transfer. These defects on the TiO_2 surface can suppress the recombination of

electron–hole pairs and hence extend their lifetime and thereby improves the photocatalytic efficiency. The aforementioned processes can be summarized as

$Dye + h\upsilon \rightarrow Dye^{*}$

$Dye^{*} + TiO_2 \rightarrow Dye + TiO_2(e^{-})$ (electron injection)

$Sm^{3+} + e^{-} \rightarrow Sm^{2+}$ (electron trapping)

$Sm^{2+} + O_2 \rightarrow Sm^{3+} + O_2^{\bullet -}$ (electron trapping)

$O_2^{\bullet -} + 2\,H^{+} \rightarrow 2\,{}^{\bullet}OH$ (Generation of oxidative species)

$Ti^{4+} + e^{-} \rightarrow Ti^{3+}$

$Ti^{3+} + h^{+} \rightarrow Ti^{4+}$

As shown in scheme 3.1, there is a possibility for the light absorption directly by the anatase titania photocatalyst leading to the photoexcitation of electron from the valence band to the conduction band. The process provides electron-hole separation and thereby effective photocatalysis as shown in Scheme 3.1. In this case the holes that are generated get react with water molecules forming $^{\bullet}OH$. Also the electrons that are present in the conduction band of anatase simultaneously react with oxygen molecules directing towards $O_2^{\bullet -}$ (super oxide radical anion). The so formed $^{\bullet}OH$ and $O_2^{\bullet -}$ mineralize the methylene blue dye facilitate effective photocatalysis. In the case of Sm^{3+} doped TiO_2 the photoexcitation is more feasible due to the narrowed band gap arose due to the donor levels that are formed by

Sm^{3+} doping and thus photodegradation rate was more as depicted in Figure 3.14.

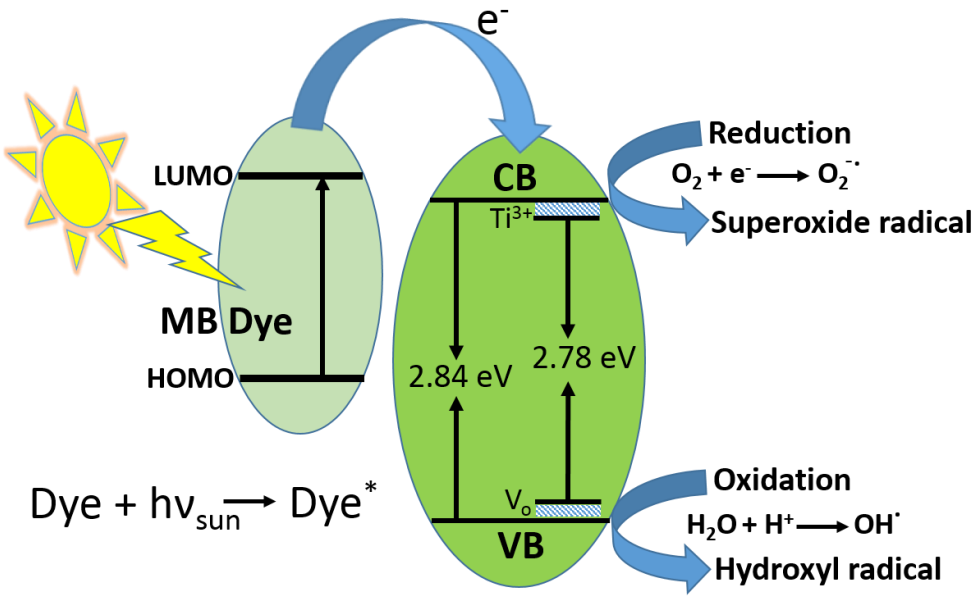

Scheme 3.1. Photocatalytic mechanism of Sm^{3+} doped anatase TiO_2.

3.4 Conclusions

A modified sol-gel strategy has been developed for the synthesis of TiO_2 and Sm^{3+} doped TiO_2 nanoparticles. On introducing Sm^{3+} into the crystal lattice of oxygen rich TiO_2 nanocrystals environment was changed from oxygen richness to oxygen deficiency *i.e.* Sm^{3+} induced oxygen deficiency in the crystal lattice of TiO_2. These TiO_2 nanoparticles with oxygen richness and oxygen deficiency (doped and undoped) were subjected photocatalytic degradation of methylene blue dye under UV and solar illuminations and degradation kinetics were

systematically examined. It was found that TSm2 calcined at 500 ˚C has shown the maximum photoactivity under both UV and sunlight illumination. The augment activity was connected to the change of surface structure of TiO_2, the raise of $\cdot OH$ radicals produced by the unbalance charge, and the production of sub-band gap by doping Sm^{3+}.

3.5 References

1. J. G. Yu, J. C. Yu, M. K. P. Leung, W. K. Ho, B. Cheng and X. J. Zhao, *J. Catal.*, *2003*, 217, 69.

2. J. G. Yu, H. G. Yu, B. Cheng, X. J. Zhao, J. C. Yu and W. K. Ho, *J. Phys. Chem. B*, 2003, 107, 13871.

3. A. D. Paola, G. Marci, L. Palmisano, M. Schiavello, K. Uosaki and S.Ikeda, *J. Phys. Chem. B*, 2002, 106, 637.

4. W. Choi, A. Termin and M. R. Hoffmann, *J. Phys. Chem.*, 1994, 98, 13669.

5. J. A. Wang, R. L. Ballesteros, T. Lopez, A. Moreno, R. Gomez and O. X. Novaro, *J. Phys. Chem. B*, 2001, 105, 9692.

6. S. Jin and F. Shiraishi, *J. Chem. Eng.*, 2004, 97, 203.

7. A. Hattori, Y. Tokihisa, H. Tada and S. Ito, *J. Electrochem. Soc.*, 2000, 147, 2279.

8. C. Wang and B. Q. Xu, *J. Solid State Chem.*,2005, 178, 3500.

9. V. Iliev, D.Tomova, L. Bilyarska, A. Eliyas and L. Petrov, *Appl. Catal. B: Environ.*, 2006, 63, 266.

10. V. Vaiano, O. Sacco, D. Sannino, P. Ciambelli, S. Longo, V. Venditto and G. Guerra, *J. Chem. Technol. Biotechnol.*, 2014, 89, 1175.

11. G.Shang, H.Fu, S. Yang, and T.Xu, *INT J PHOTOENERGY*, 2012, 2012.

12. K. Li, H.Wang, C. Pan, J.Wei, R. Xiong, and J. Shi, *INT J PHOTOENERGY*, 2012, 2012.

13. O. Sacco, V. Vaiano, Changseok Han, D. Sannino and D. D. Dionysiou, *Appl.Catal B-Environ.*, 2015, 164, 462.

14. J. C. Yu, J. G. Yu, and J. C. Zhao, *App. Catal.*, 2002, 36, 31.

15. V. Vaiano, O. Sacco, M. Stoller, A. Chianese, P. Ciambelli and D. Sannino, *Int. J. Chem. React. Eng.*, 2014, 12, 63.

16. K. T. Ranjit, I. Willner, S. H. Bossmann and A. M. Braun, *J. Catal.*, 2001, 204, 305.

17. Y. Zhang, H. Xu, Y. Xu, H. Zang and Y. Wang, *J. Photochem. Photobiol. A: Chem.*, 2005, 170, 279.

18. Y. Xiaoli, J. He, D. G. Evans, X. Duan and Y. Zhu, *Appl. Catal. B: Environ.*, 2005, 55, 243.

19. Y. B. Xie, C. W. Yuan and X. Z. Li, *Appl. Catal. B: Environ.*, 2005, 55, 243.

20. P. Yang, C .Lu and N. P. Hua, *Mater. Lett.*, 2002,57, 794.

21. Y. B. Xie and C. W. Yuan, *Appl. Catal. B: Environ.*, 2003, 46, 251.

22. Y. B. Xie and C. W. Yuan, *Mater. Res. Bull.*, 2004, 39, 533.

23. W. Y. Zhou, Y. Zhou and S. Q. Tang, *Mater. Lett.*, 2005, 59, 3115.

24. C. H. Liang, F. B. Li, C. S. Liu, J. L. Lu and X. G. Wang, *Dyes Pigm.*, 2008,76, 477.

25. Q. Xiao, Z. Si, Z. Yu and G. Qiu, *Mater. Sci.Eng. B.*, 2007, 137, 189.

26. J. Shi, J. Zheng, Y. Hu and Y. Zhao, *Environ. Eng.*, 2008, 25, *451*.

27. D. J. Park, T. Sekino, S. Tsukuda and S. Tanaka, *Res. Chem. Intermed.,* 2013, 39, 1581.

28. A. Pawlak and M. Mucha, *Thermochim. Acta*, 2003, 396, 153.

29. X. Zou, F. Zhang, S. Thomas, Prof. G. Zhu, V. Valtchev and S. Mintova, *Chem. Eur. J.*, 2011, 17, 12076.

30. D. G. Huang, S. J. Liao, W. B. Zhou, S. Q. Quan, L. Liu, Z. J. He and J. B. Wan, *J. Phys. Chem. Solids*, 2009, 70, 853.

31. K. M. Parida and N. Sahu, *Appl. Catal. A*, 2008, 287, 151.

32. G. J. de A. A. Soler-Illia, A. Louis and C. Sanchez, *Chem. Mater.*, 2002**,** 14, 750.

33. J. Yu, L. Zhang, Z. Zheng and J. Zhao, *Chem. Mater.*, 2003,15, 2280.

34. K. Karakitsou and X. Verykios, *J. Phys. Chem.*, 1993, 97, 1184.

35. X. A. Wu, Y. Gao and H. Q. Liu, *J. Catal.*, 2002, 207, 151.

36. M. F. Hou, F. B. Li, R. F. Li, H. F. Wan, G. Y. Zhou and K. C. Xie, *J. Rare Earths*, 2004, 22, 542.

37. C. H. Liang, F. B. Li, C. S. Liu, J. L. Lu and X. G. Wang, *Dyes Pigm.*, 2008, 76, 477.

38. J. Yan, G. Wu, N. Guan, L. Li, Z. Li and X. Cao, *Phys. Chem. Chem. Phys.*, 2013, 15, 10978.

39. Z. Lu, C. T. Yip, L. Wang, H. Huang and L. Zhou, *Chem. Plus. Chem.*, 2012, 77, 991.

40. C. Suresh, V. Biju, P. Mukundan and K.G. K. Warrier, *Polyhedron*, 1998, 17, 3131.

41. D. Mohanta, ethesis, 2010.

42. S. G. Ullattil and P. Periyat, *Nanoscale*, 2015, 7, 19184.

43. R. Ren, Z. Wen, S. Cui, Y. Hou, X. Guo and J. Chen, *Sci. Rep.*, 2015, 5, 10714.

44. Y. Ma, J. Zhang, B. Tian, F. Chen and L. Wang, *J. Hazard. Mater.*, 2010, 182, 386.

45. E. Borgarello, J. Kiwi , M. Gratzel, E. Pelizzetti , M. Visca, *J. Am. Chem. Soc.*,1982,104, 2996.

46. K. V. Baiju, C. P. Sibu, K. Rajesh, P. K. Pillai, P. Mukundan, K. G. K. Warrier, W. Wunderlich, *Mater. Chem. Phys.*, 2005, 90, 123.

47. Xiao bo Chen, Lei Liu, Fuqiang Huang, *Chem. Soc. Rev.*, 2015, 44, 1861.

4 Chapter

Dysprosium ion (Dy^{3+}) doped TiO_2 via modified sol-gel method.

Contents

4.1. Introduction

In this chapter a photocatalytic active, thermally stable dysprosium ion (Dy^{3+}) doped anatase TiO_2 synthesized using modified sol-gel method is discussed. TiO_2 is an ample photocatalytic material for photochemical water splitting and environmental purification due to its prime properties, such as low cost, availability, nontoxicity, long-term stability and high oxidative power.[1,2,3]As is generally known, anatase and rutile are the two most closely examined phases of TiO_2. Besides, anatase shows higher photocatalytic activity than that of rutile, and thus is the most commonly practiced crystal phase of TiO_2 for photocatalysis.[4,5]Though, a large intrinsic band gap of TiO_2 (3.2 eV for the anatase structure[6] and 3.0 eV for the rutile structure[7]) allows only the UV portion (λ< 385 nm) of the solar spectrum to be absorbed, which persuades to a poor solar energy utilization. Different efforts have been made to modify the electronic properties of TiO_2, so that it could expand its response to visible light and enhance its visible-light photocatalytic activity.

Rare earth ions are well known for their capability to form complexes with various Lewis bases in the interaction of these functional groups with the f-orbital.[8] Thus, the incorporation of the rare earth ions into TiO_2 crystal matrices could provide a potential means to inhibit the photohole and photoelectron combination and to expand the light adsorption of the semiconductor, and therefore to enhance the visible light photocatalytic activity, such as Eu-TiO_2 nanocrystalline, [9]

Ln_2O_3/TiO_2 (Ln = Eu, Pr, or Yb),[10] La-TiO_2, Pr-TiO_2, Nd-TiO_2,[11] N-Ce/TiO_2.[12]The results indicates that the photocatalytic activity of TiO_2 could be significantly enhanced by doping with the rare earth ions because the doped rare earth ions can form complexes with various organic molecules by f-orbital.

In this workTiO_2 and Dy^{3+}dopedTiO_2 were synthesized *via* modified sol-gel method. The photocatalytic effect under both UV and direct sunlight were studied using the bare and doped TiO_2 calcined at 300, 500 and 700 ˚C**.**

4.2 Results and Discussion

4.2.1. FTIR Spectroscopy

FTIR spectra of the samples calcined at 300, 500 and 700 ˚C have been recorded. A representative example of the FTIR spectra of TDy1 dried at 100 ˚C and 500 ˚C and bare TiO_2 calcined at 500 ˚C was shown in Figure 4.1. The absorption band at 3500-3000 cm^{-1} in both spectra indicates hydroxyl group stretching vibration and surface adsorbed water molecule. The peak at 1635 cm^{-1} indicates the hydroxyl group bending vibration. The peak at 2910 and 2855 cm^{-1} is the asymmetric C-H stretching vibration.[13] The bands at 1422 cm^{-1} are due to the vibration of CO_3^{2-} anions, indicating the absorption of CO_2 molecules on the surface of the samples.[14] The broad peak in the range 400-700 cm^{-1} is due to Ti-O stretching vibration modes, which can be observable in the anatase phase of TiO_2.[14] The peak at 410 cm^{-1} for Dy^{3+} doped TiO_2 is due to the vibration modes of anatase skeletal O-

Ti-O and O-Ti-O-Dy bonds.[15]Band at 543 cm^{-1} observed, attributes the Dy-O bond.

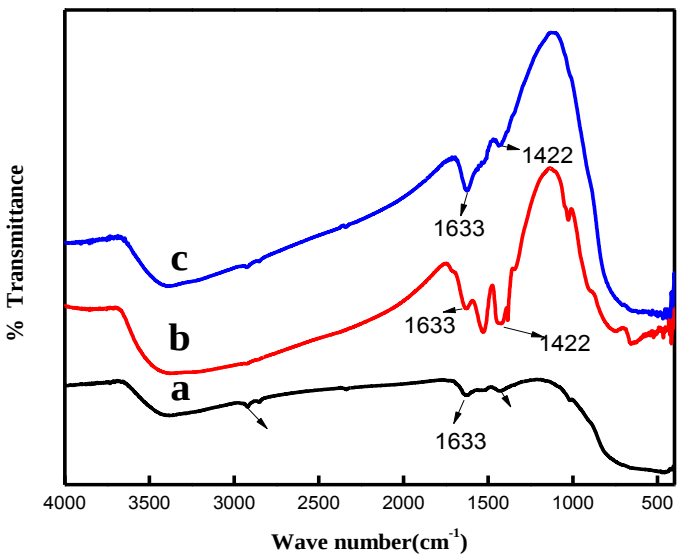

Figure 4.1 FTIR spectra of a) TiO_2 calcined at 500 ˚C b) TDy1 dried at 100 ˚C c) TDy1 calcined at 500 ˚C.

4.2.2. XRD

XRD patterns of pure TiO_2 and 1,2,5 and 10% Dy^{3+}-TiO_2 powders calcined at 300, 500, 700 ˚C were showed in Figure 4.2 A, 4.2 B and 4.2 C. From the figure it is clear that all catalysts were dominated by the anatase structure, which indicates that Dy^{3+} doping inhibits the crystal phase transformation of TiO_2. Comparing the relative intensity of 101 peaks of Dy^{3+}doped TiO_2 and pure TiO_2 calcined at the same temperature, the relative intensity of (101) peak get broadened in doped sample. However, XRD did not show any peaks for dysprosium

oxide (Dy_2O_3). This implies that Dy^{3+} ions are incorporated into the crystal lattice of TiO_2.When the crystallite size of the Dy^{3+}-TiO_2 samples were calculated using the Scherrer formula, it was found that the crystallite size was reduced by doping. It may be ascribed to the segregation of the dopant cations at the grain boundary, and the growth of nanocrystallite in the nanoparticles is prevented. The particle characteristics of the samples under different weight percentage and temperature used in this study are summarized in Table 4.1. It was concluded that Dy^{3+} ion doping could hinder crystal transformation and decrease crystallite size generally. This smaller crystalline size for Dy^{3+}could lead to larger surface area,[16,17] which will improve the photocatalytic performance of Dy^{3+} doped TiO_2 compared to bare TiO_2.

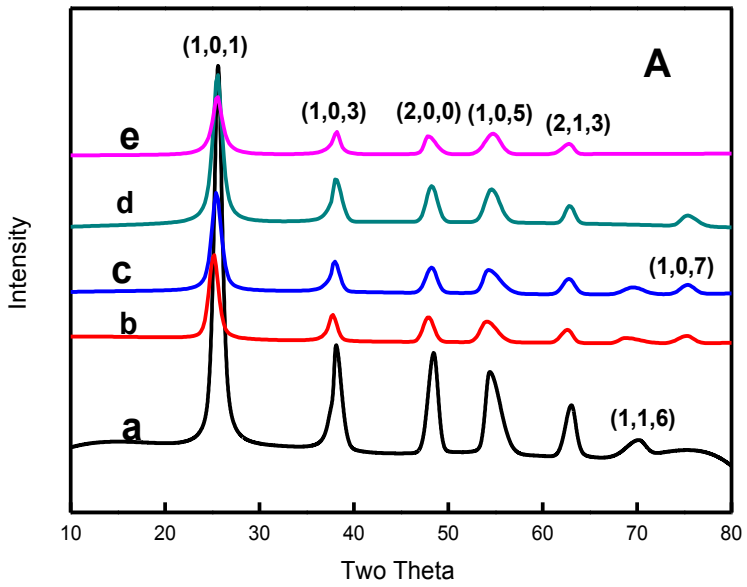

Figure 4.2 A. XRD patterns of a) TDy0.5 b) TDy1 c) TDy2 d) TDy5 and e) TDy10 calcined at 300 ˚C.

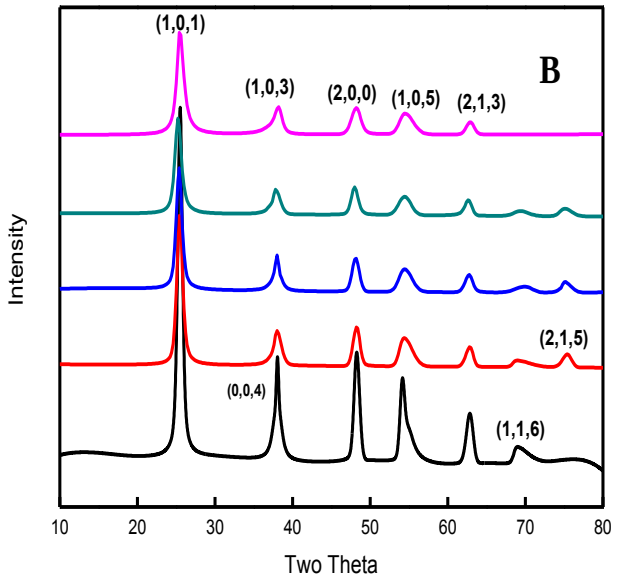

Figure 4.2 B. XRD patterns of a) TDy0.5 b) TDy1 c) TDy2 d) TDy5 and e) TDy10 calcined at 500 ˚C

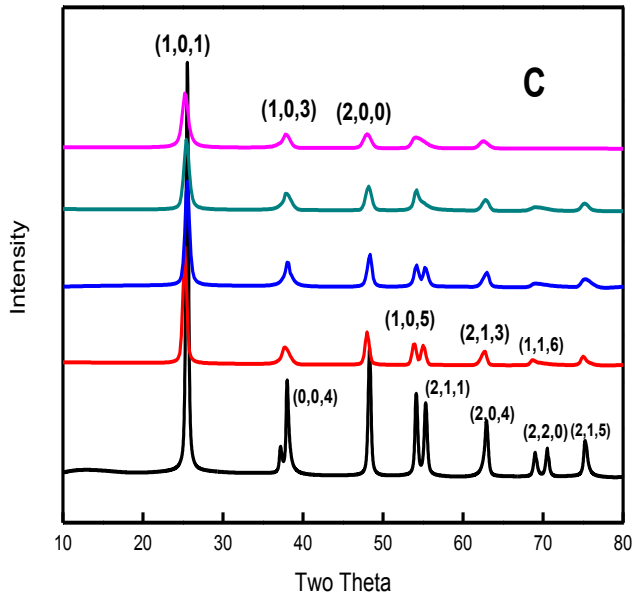

Figure 4.2 C. XRD patterns of a) TDy0.5 b) TDy1 c) TDy2 d) TDy5 and e) TDy10 calcined at 700 ˚C

Table 4.1. Crystal size of anatase TiO_2, TDy0.5, TDy1, TDy2, TDy5 and TDy10 calcined at 300, 500 and 700 ˚C.

Sample	300 ˚C	500 ˚C	700 ˚C
TiO_2	7.84	12.6	21.7
TDy0.5	8.26	11.8	20.7
TDy1	7.20	9.80	15.6
TDy2	7.19	9.80	11.1
TDy5	7.01	8.60	11.1
TDy10	6.90	8.10	9.90

4.2.3 Raman Spectroscopy

Raman spectra of TDy0.5, TDy1, TDy2, TDy5, TDy10 and pure TiO_2 calcined at 300, 500 and 700 ˚C were recorded. Raman spectra of TiO_2 and TDy1calcined at 500 ˚C were shown in Figure 4.3. The spectrum reveals the anatase phase purity of synthesized TiO_2 nanoparticles. The peaks are present at 146 (E_g), 397 (B_{1g}), 517 (B_{1g}) and 639 cm^{-1} (E_g) which are the characteristics of anatase phase of TiO_2.[18,19] The major peak of anatase is decreasing as the doping was introduced confirms the incorporation of Dy^{3+} into the crystal lattice of TiO_2 and thereby decrease in crystallite size which has been explained in XRD spectra (Figure 4.2). It can also be confirmed that, in addition to decrease in peak intensity the peak broadening increases, which attributes to the presence of oxygen vacancies as a result of Dy^{3+}doping.[20]

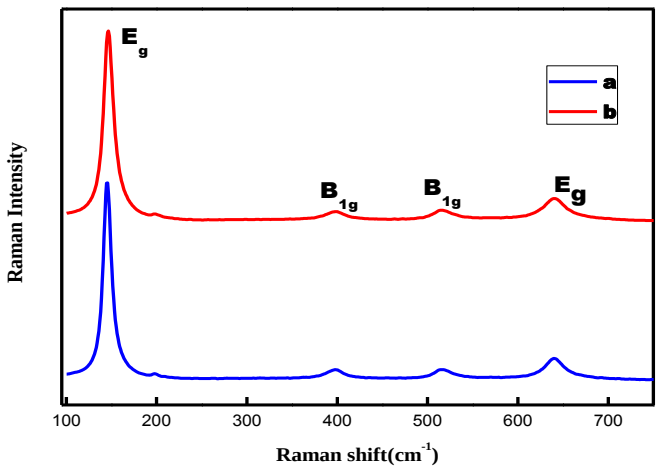

Figure 4.3. Raman Spectra of a) TiO_2 and b) TDy1 calcined at 500 ˚C.

4.2.4 Diffuse reflectance spectroscopy (DRS)

Diffuse reflectance spectroscopy (DRS) in the range 200-900 nm of TiO_2 and Dy^{3+} doped TiO_2 calcined at different temperature were investigated to study the optical absorption properties. The DRS spectra of TiO_2 and TDy1 at 500 and 700 ˚C were shown in the Figure 4.4. From the Figure 4.4 Dy^{3+} doped TiO_2 shows an absorption band higher than pure TiO_2. It was also observed that at calcination temperature of 500 ˚C, TDy1 shows the maximum absorption edge and shifts to higher wavelength. This red shift can be attributed to the charge-transfer transition between the *f* electrons of Dy^{3+} ion and the TiO_2 conduction band which help in the generation of electron and hole under visible light irradiation. The red shift absorption profile is observed with an increase in calcined temperature from 300 to 700 ˚C. The band gap energies were calculated by using DRS spectra with Tauc equation and condensed in the Table 4.2. The

band gap energies of Dy^{3+} doped samples are lower than that of TiO_2 due to the red shift that occurred as a result of Dy^{3+} doping.

Table 4.2. Band gap energies of TiO_2, TDy0.5, TDy1, TDy2, TDy5 and TDy10 calcined at different temperatures.

Sample	Band Gap (eV)		
	300 ˚C	**500 ˚C**	**700 ˚C**
TiO_2	3.1	3.02	3.00
TDy0.5	2.86	2.8	2.73
TDy1	2.85	2.74	2.71
TDy2	2.65	2.62	2.60
TDy5	2.54	2.51	2.49
TDy10	2.42	2.38	2.36

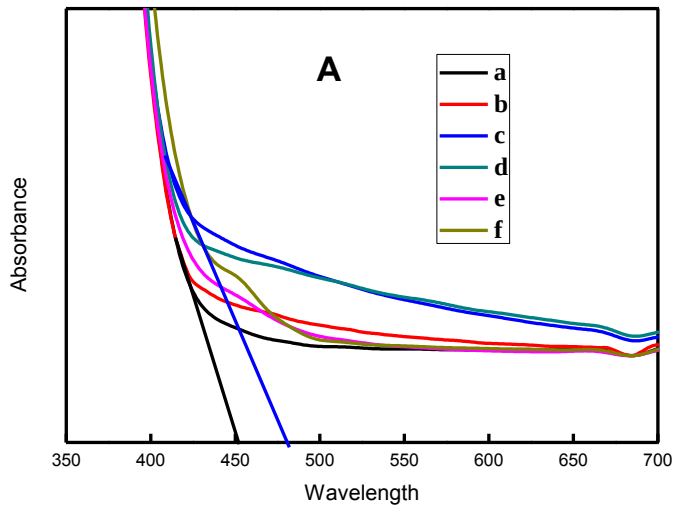

Figure 4.4. A) Absorbance plot of a) TiO_2 b) TDy0.5 c) TDy1 d) TDy2 e) TDy5 and f) TDy10 calcined at 500 ˚C.

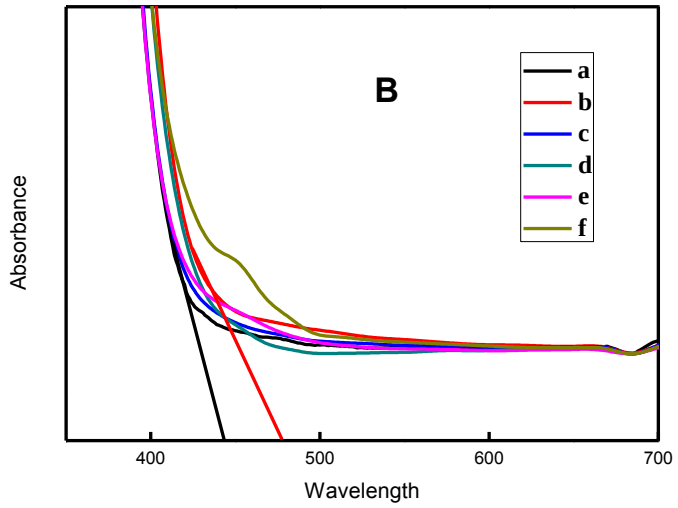

Figure 4.4 B) Absorbance plot of a) TiO_2 b) TDy0.5 c) TDy1 d) TDy2 e) TDy5 and f) TDy10 calcined at 700 ˚C.

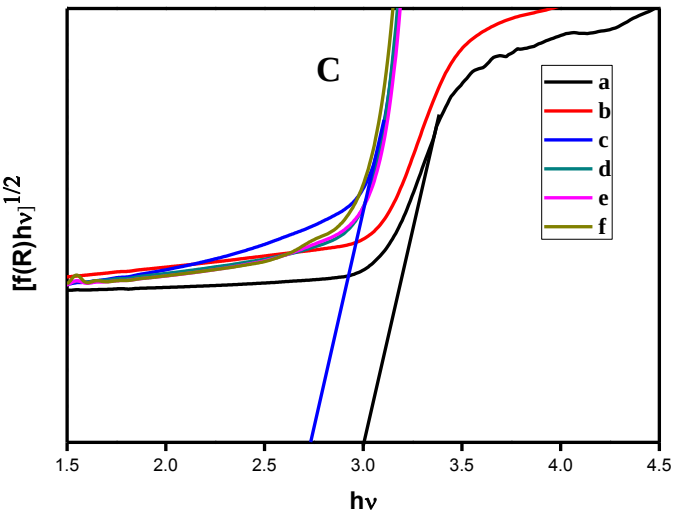

Figure 4.4 C) Tauc plot of a) TiO_2 b) TDy0.5 c) TDy1 d) TDy2 e) TDy5 and f) TDy10 calcined at 500 ˚C.

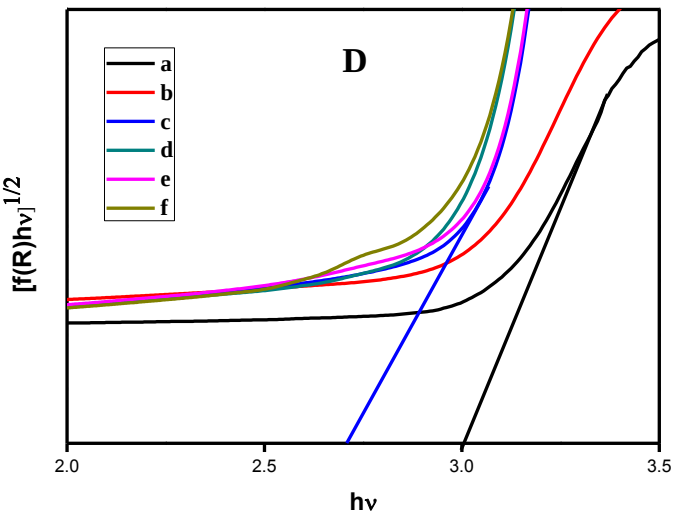

Figure 4.4 D) Tauc plot of a) TiO_2 b) TDy0.5 c) TDy1 d) TDy2 e) TDy5 and f) TDy10calcined at 700 ˚C.

4.2.5. X-ray Photoelectron Spectroscopy (XPS)

XPS of TiO_2 and TDy1 calcined at 500 ˚C were recorded. Spectrum reveals the association of Dy^{3+} ion into the lattice of TiO_2. There is some peak changes are occurred on the surface of TiO_2. The $2p_{3/2}$ and $2p_{1/2}$ peaks of Ti^{4+} were observed at 460.2 eV and 466 eV for bare TiO_2 (Figure 4.5A) whereas for Sm^{3+} doped TiO_2 peaks are obtained at 459 and 465 eV. The peak 460.2 eV (in bare TiO_2) attributes to the oxygen richness.[21] The splitting difference was found around 6 eV almost similar for bare and Sm^{3+} doped TiO_2, which attributes the anatase phase purity of both TiO_2 samples.[22]Surface defects originate when Dy^{3+} enters in to the lattice of TiO_2 and which is confirmed by the blue shifting in the binding energy *i.e.* 459 eV ($2p_{3/2}$) and 465 eV ($2p_{1/2}$). The peak at 459 eV reveals the presence of Ti^{3+}.[21]The decrease in valency of Ti explains the presence of oxygen vacancies, which

reveal the transformation of oxygen rich environment to oxygen deficient environment. From the O1s XPS (Figure 4.5B) it can be seen that the peak at 531.5 eV blue shifted to 530.3 eV indicates the change in oxygen environment. Figure 4.5C, the Dy4d XPS reveals the incorporation of Dy^{3+} into the crystal lattice. The Dy4d peak had a greater degree of complex peak shape than based on the simple spin–orbit splitting, due to final state multiplet splitting effects arising from interactions of 4d and 4f states,[23]very large due to the same principal quantum number of the two shells.[24,25]The main band was centered at an average BE of 158.2 eV. The BE of the absolute maximum is relatively close to the values reported for Dy (III) oxide.[23, 25] As evidenced from XRD, even though the ionic radius of Dy^{3+} (105.2 pm) is far greater than Ti^{4+} (74.5 pm), Dy^{3+} entered into the crystal lattice of TiO_2 and those ions occupy the interstitial position of TiO_2.

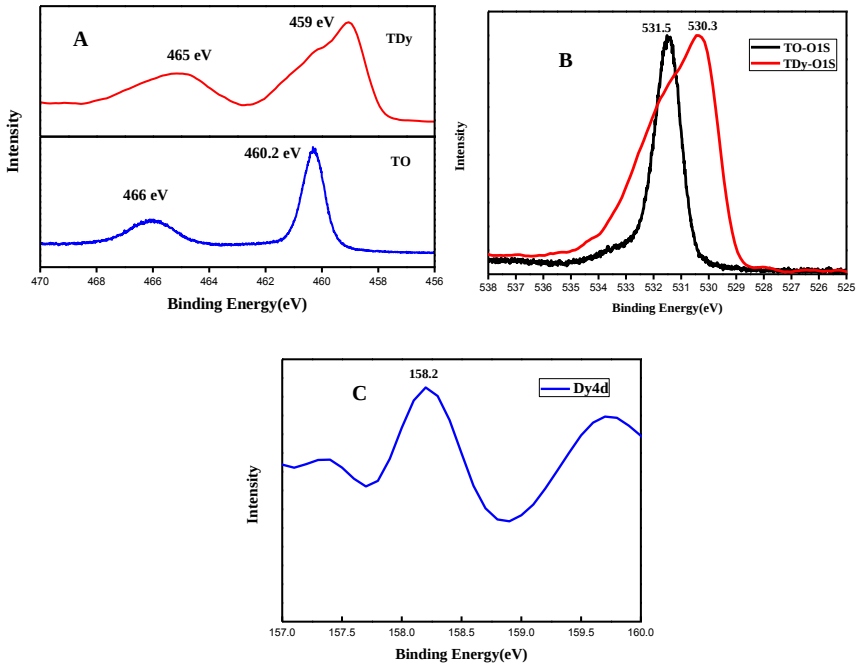

Figure 4.5. XPS of A) Ti2p, B) O1s and C) Dy4d.

4.2.6. Transmission Electron Microscopy (TEM)

Figure 4.6 shows TEM images of TiO_2 and TDy1 calcined at 500 ˚C. TiO_2 shows a particle size of 20-28 nm (Figure 4.6a) at 500 ˚C. On the other hand, the Dy^{3+} doped TiO_2 has a particle size of 7-12 nm (Figure 4.6b), and thus the TEM observations support the conclusions derived from the XRD data that the particle size will decrease as a result of Dy^{3+} doping into TiO_2 lattice. The electron diffraction image of TDy1 calcined at 500 ˚C shows broad band due to the Scherrer line broadening which is attributed to the small crystalline size[26,27] however TiO_2, at same temperature, showed distinct spots due to the high crystallinity and larger size of the crystals.

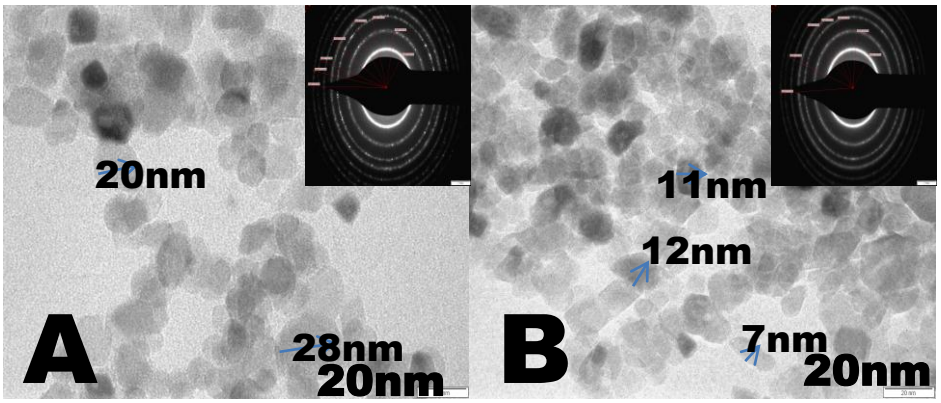

Figure 4.6. TEM image of a) TiO_2 and b) TDy1 at 500 ˚C.

4.2.7. Energy Dispersive Spectroscopy (EDS)

Chemical composition of TiO_2 and TDy1 was determined using EDS analysis (Figure 4.7). Strong X-ray peaks associated with Ti and oxygen are present in TiO_2 where as strong peaks of Dy were found in

the TDy1 along with Ti and oxygen confirms the presence of both Ti and Dy in the lattice of TDy1.

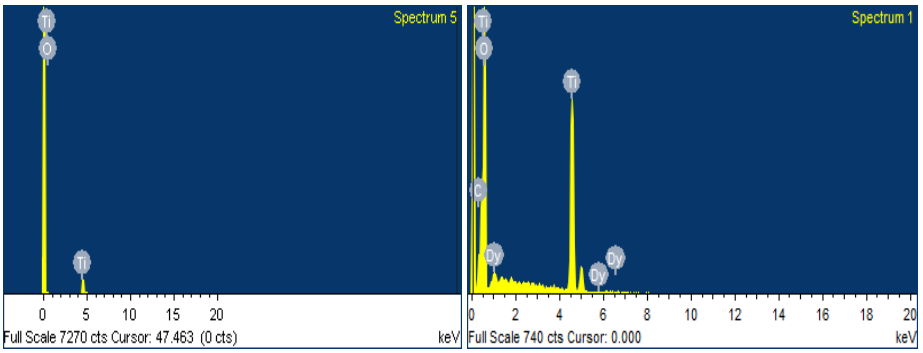

Figure 4.7. Energy Dispersive Spectroscopy (EDS) of a) TiO_2 and b) TDy1 at 500 ˚C.

4.3 Photocatalysis

Photocatalytic activity of both TiO_2 and TDy1 calcined at 500 ˚C for methylene blue degradation under UV and sunlight were carried out and the rate constant obtained from the degradation kinetics were briefed in Table 4.3. From Table 4.3 it can be seen that photocatalytic activity of pure TiO_2 and TDy is influenced by the calcination temperature. Rate of degradation under direct sunlight irradiation and UV light irradiation of Dy^{3+}doped TiO_2 is more than that of bare TiO_2 except in lower temperature. This is because upon Dy^{3+} ion doping, the light absorption capacity of TiO_2 increases from UV to visible region in accordance with band gap lowering. The rate constant obeys the first order kinetics and the values are summarized in the Table 3,among the different TDy, highest activity was obtained for TDy1 calcined at 500 ˚C, with a rate constant of $0.145min^{-1}$and is approximately 4 times

higher than the bare TiO_2 (0.036 min^{-1}). Absorption spectra of methylene blue dye degradation under UV light using TiO_2 and Dy^{3+} doped TiO_2 at 500 ˚C were shown in Figure 4.8 and 4.9. TDy1 calcined at 500 ˚C degraded completely within 25 minutes. From the results it can be concluded that the TDy1 calcined at 500 ˚C is the best photocatalyst among the samples under UV light irradiation.

The visible light activity of TiO_2 and TDy under direct sunlight using the methylene blue degradation experiment was carried out and the time taken for degradation of methylene blue using TiO_2 and TDy under sunlight were also shown in Table 4.3. From the Table 4.3, it is found that Dy^{3+} doped TiO_2 sample undergo methylene blue degradation much faster than compared to TiO_2 at all calcinations temperatures under sunlight irradiation. The rate constant was calculated from the first order kinetics and is shown in Table 4.3. Among the doped samples highest activity was obtained for TDy1sample calcined at 500 ˚C with a rate constant of 0.141 min^{-1} which is almost 11 times higher than the pure TiO_2 (0.013 min^{-1}). Absorption spectra of methylene blue dye degradation under visible light using TiO_2 and TDy1 doped TiO_2 at 500 ˚C were shown in Figure 4.10 and 4.11. TDy1 calcined at 500 ˚C degraded completely within 25 minutes. The results point out that TDy1 calcined at 500 ˚C is the best photocatalyst among samples under sunlight irradiation.

Table 4.3. Rate constant of TiO_2 and TDy calcined at different temperatures.

UV light				Sunlight			
Sample	300 ˚C	500 ˚C	700 ˚C	Sample	300 ˚C	500 ˚C	700 ˚C
TiO_2	0.021	0.036	0.002	TiO_2	0.007	0.013	0.004
TDy0.5	0.038	0.098	0.052	TDy0.5	0.006	0.070	0.064
TDy1	0.008	**0.145**	0.123	TDy1	0.005	**0.141**	0.119
TDy2	0.009	0.060	0.067	TDy2	0.08	0.044	0.022
TDy5	0.007	0.051	0.070	TDy5	0.011	0.038	0.042
TDy10	0.012	0.037	0.028	TDy10	0.012	0.028	0.037

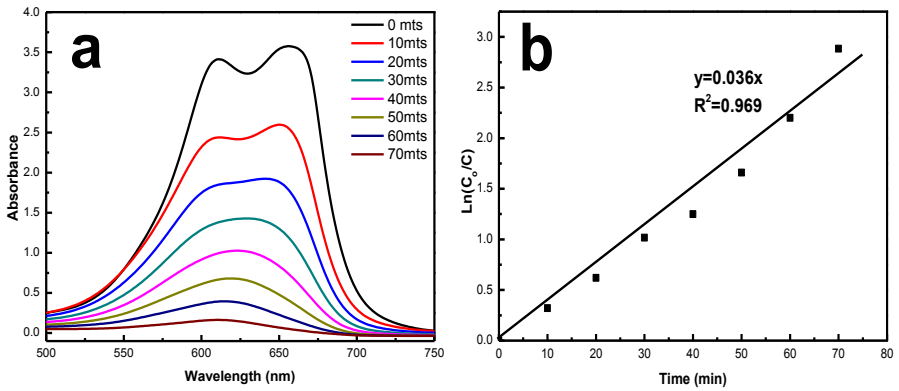

Figure 4.8. Absorption spectra and Kinetic study of methylene blue dye degradation under UV using TiO_2 sample calcined at 500 ˚C.

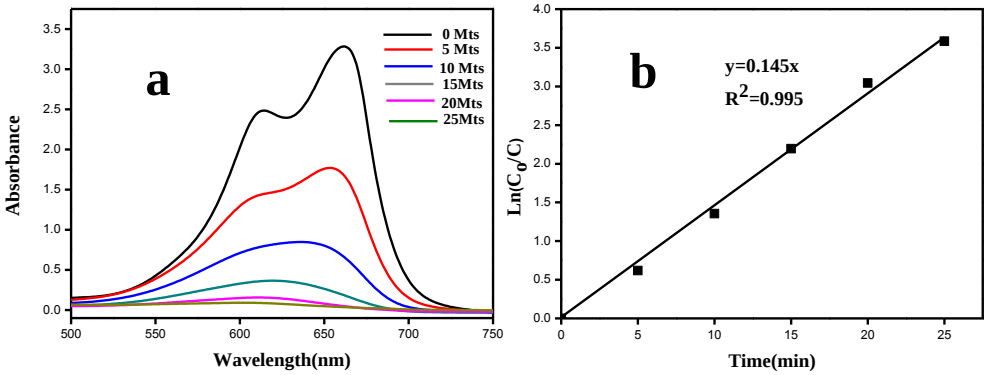

Figure 4.9. Absorption spectra and Kinetic study of methylene blue dye degradation under UV using TDy1 sample calcined at 500 ˚C.

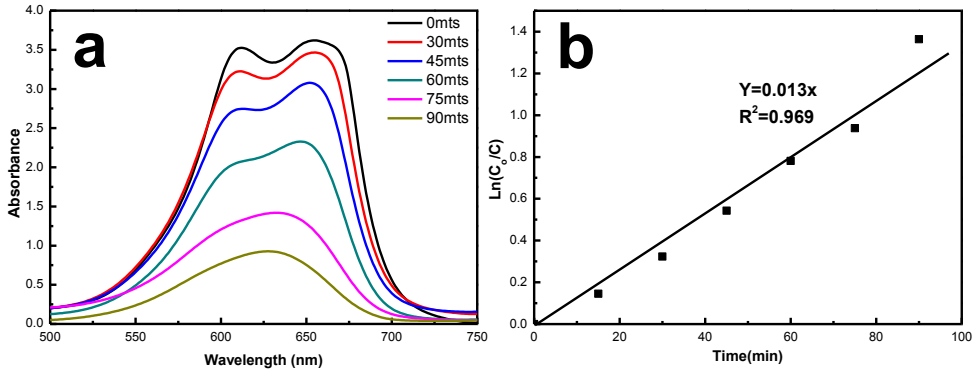

Figure 4.10. Absorption spectra and Kinetic study of methylene blue dye degradation under direct sunlight using Ti sample calcined at 500 ˚C.

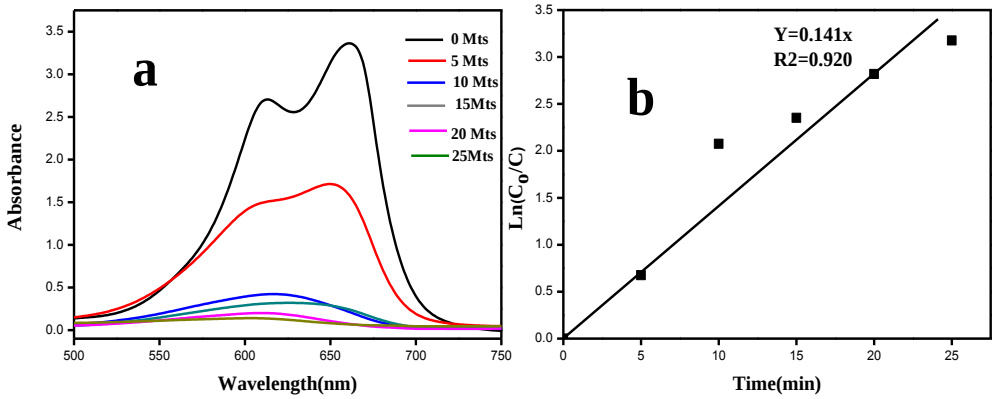

Figure 4.11. Absorption spectra and Kinetic study of methylene blue dye degradation under direct sunlight using TDy1sample calcined at 500 ˚C.

4.4 Conclusions

A modified sol-gel strategy was developed for the synthesis of TiO_2 and Dy^{3+} doped TiO_2 nanoparticles. As synthesised nanomaterials are well characterised with XRD, FT-IR and Raman spectroscopy, DRS, XPS, SEM and TEM. Crystallite size calculation from XRD showed that the crystallite size is decreased as a result of Dy^{3+} doping and is further supported by TEM also. XPS result showed that on introducing Dy^{3+} into the crystal lattice of oxygen rich TiO_2 nanocrystals the environment was changed from oxygen richness to oxygen deficiency. Dy^{3+} doping induced oxygen deficiency in the crystal lattice of TiO_2. These TiO_2 nanoparticles and Dy^{3+} doped TiO_2 with doped and undoped were subjected to various calcination temperatures and their photocatalytic degradation under UV and solar illuminations were systematically examined. Among the various samples TDy1 calcined at 500 ˚C has shown the maximum photoactivity under both UV and sunlight illumination.

4.5 References

1. A. Fujishima and K. Honda, *Nature,* 1972, 238, 37.

2. B. O'regan and M. Grfitzeli, *Nature*, 1991, 353, 737.

3. B. Naufal, P. K. Jaseela and P. Periyat, *Mater. Sci. Forum*., 2016, 855, 78.

4. S.W. Lee, J.H. Noh, H.S. Han, D.K. Yim, D. H. Kim, J. K. Lee, J.Y. Kim, H. S. Jung and K.S.Hong, *J. Phys. Chem. C.*, 2009, 113, 6878.

5. P. Periyat, B. Naufal and S. G. Ullattil, *Mater. Sci. Forum*. 2016, 855, 33.

6. H. Tang, F. Levy, H. Berger and P.E. Schmid, *Phys. Rev. B.*, 1995, 52, 7771.

7. F. Arntz and Y. Yacoby, *Phys. Rev. Lett*., 1966, 17, 857.

8. H. Shi, T. Zhang , T.An , B. Li and X. Wang, *J. Colloid Inter. Sci*., 2012, 380, 121.

9. Y. Zhang, H. Zhang, Y. Xu and Y. Wang, *J. Mater. Chem.*, 2013, 13, 2261.

10. K.T. Ranjit, I. Willner, S. H. Bossmann and A.M. Braun, *Environ. Sci. Technol*., 2001, 35, 1544.

11. K. M. Parida and N. Sahu, *J. Mol. Catal. A: Chem*., 2008, 287,151.

12. X. Z. Shen, Z. C. Liu, S.M. Xie and J. Guo, *J. Hazard. Mater*., 2009, 162, 1193.

13. A. Pawlak and M. Mucha, *Thermochim. Acta*, 2003,396, 153.

14. D. R. Zhang, H. L. Liu, R. H. Jin, N. Z. Zhang, Y. X. Liu and Y.S. Kang, *J. Ind. Eng. Chem*.2007, 13, 92.

15. G. B. Kumar and S. Buddhudu, *Ceram. Inter.*, 2009, 35, 521.

16. M. F. Hou, F. B. Li, R. F. Li, H. F. Wan, G. Y. Zhou and K. C. Xie, *J. Rare Earths*, 2004, 22, 542.

17. C. H. Liang, F. B. Li, C. S. Liu, J. L. Lu and X. G. Wang, *Dyes Pigm.*, 2008, 76, 477.

18. J. Yan, G. Wu, N. Guan, L. Li, Z. Li and X. Cao,. *Chem. Chem. Phys.*, 2013, 15, 10978.

19. W. Ma, Z. Lu and M. Zhang, *Appl. Phys. A*, 1998, 66, 621.

20. Z. Lu, C. T. Yip, L. Wang, H. Huang and L. Zhou, *Chem. Plus. Chem*, 2012**,** 77, 991.

21. S. G. Ullattil and P. Periyat, *Nanoscale*, 2015, 7, 19184.

22. R. Ren, Z. Wen, S. Cui, Y. Hou and X. Guo, *J. Chen, Sci. Rep.*, 2015, 5, 10714.

23. H. Ogasawara, A. Kotani and B. T. Thole, *Phys. Rev. B: Condens.Matter*, 1994, 50, 12332.

24. D. Barreca, A. Gasparotto, A. Milanov, E. Tondello, A. Devi and R.A. Fischer, *Surf. Sci*., 2007, 14, 52.

25. A. P. Milanov, R. W. Seidel, D. Barreca, A. Gasparotto, M. Winter, J. Feydt, S. Irsen, H.W. Becker and A. Devi, *Dalton Trans*., 2011, 40, 62.

26. E. Borgarello, J. Kiwi , M. Gratzel, E. Pelizzetti and M. Visca, *J. Am. Chem. Soc.*,1982, 104, 2996.

27. K. V. Baiju, C. P. Sibu, K. Rajesh, P. K. Pillai, P. Mukundan, K. G. K. Warrier and W. Wunderlich, *Mater. Chem. Phys*, 2005, 90, 123.

5 Chapter

Solar active Ytterbium ion (Yb^{3+}) doped TiO_2 by way of sol-gel method.

Contents

5.1. Introduction

In this chapter a solar active thermally stable ytterbium ion (Yb^{3+}) doped anatase TiO_2 synthesized using modified sol-gel method is discussed. Heterogeneous photocatalysis, in presence of TiO_2, has been comprehensively studied for the degradation of hazardous pollutants in air and water under ultraviolet (UV) or solar light for last few years.[1,2,3,4] When TiO_2 get illuminated with an appropriate range of irradiation, the pairs of electrons and holes are generated inside photocatalyst crystal lattice. The major problem in its practical application is a wide band gap which requires a high energy UV light for its excitation (*e.g.* 3.2 eV). A large number of studies have been under gone to develop a photocatalytic system which can be activated under visible light irradiation.[5,6,7]

Recently, it was reported that the loading of rare earth (RE) elements into the semiconductor photocatalysts can alter the surface adsorption properties, prevents electron–hole recombination [8] as well as the complexation of the organic contaminants through their f-orbitals to bring effective for the environmental remediation. [9, 10] Several techniques can be used to prepare advanced photocatalytic materials and the sol–gel can be highlighted among all of them.[11,12]Recently, this method is popular to greater degree as a straight forward preparation process to produce nanosized crystallized powders of high purity at relatively low temperature. Moreover, it is also applicable in stoichiometry controlled synthesis, preparation of composite or

homogeneous materials *etc*.[13]The sol–gel method is economic, simple and reproducible way of synthesis.[14]

In this scrutiny TiO_2 and ytterbium ion (Yb^{3+}) doped solar active TiO_2 were synthesized with modified sol-gel method. The photocatalytic effect under both UV and direct sunlight were studied using the bare and doped TiO_2 calcined at 300, 500 and 700 ˚C.

5.2 Results and Discussion

5.2.1. FT-IR Spectroscopy

FTIR spectra of all the samples dried at 100 ˚C and calcined at 300, 500 and 700 ˚C were recorded. A representative example of the FTIR spectra of TYb2 dried at 100 ˚C, bare TiO_2 and TYb2 calcined at 300 ˚C were shown in Figure 5.1. The absorption band at 3500-3000 cm^{-1} denote the hydroxyl group stretching vibration and surface adsorbed water molecule and 1629 cm^{-1} indicates the hydroxyl group bending vibration. The peak at 2922 and 2852 cm^{-1} point out the asymmetric C-H stretching vibration,[15] the bands at 1425 cm^{-1} are due to the vibration of CO_3^{2-} anions, signifying the absorption of CO_2 molecules on the surface of the samples.[16]The peak on 2338 cm^{-1} also designate the absorbed CO_2 on the surface.[17] The broad peak in the range 400-700 cm^{-1} is due to Ti-O stretching vibration modes, which is observable in the anatase phase of TiO_2.[16]The peak at 409 cm^{-1} for Yb^{3+} doped TiO_2 is due to the vibration modes of anatase skeletal O-Ti-O and O-Ti-O-Yb bonds,[18] Band at 567 cm^{-1} designate the Yb-O bond.

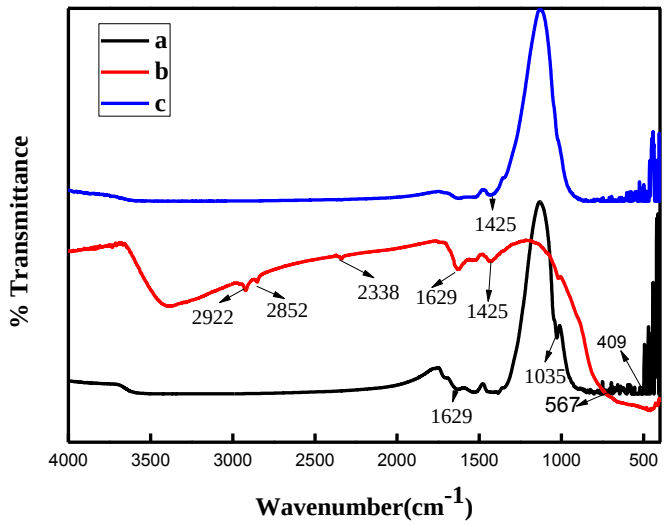

Figure 5.1. FTIR spectra of a) TYb2 calcined at 100 ˚C b) TiO_2 c) TYb2 calcined at 300 ˚C.

5.2.2XRD

XRD patterns of pure TiO_2 and TYb1, TYb2, TYb5 and TYb10 powders calcined at 300, 500

and 700 ˚C were carried out. The sample at 300,500 and 700 ˚C of TYb2 were shown in Figure 5.2 A, 5.2 B and 5.2 C. From the figure it is lucid that all TiO_2 samples were completely in the anatase phase. The particle characteristics of the TiO_2 and Yb^{3+} doped TiO_2 samples under different weight percentage and temperature are resumed in Table 5.1. In comparison with pure TiO_2 the relative intensity of (101) peaks were broadened in the Yb -doped TiO_2 at the same calcination temperature (Table 5.1). The crystallite sizes of the Yb^{3+} doped TiO_2 samples were calculated using the Scherer formula (Table 5.1) and it was perceived that the crystallite size was reduced along with Yb^{3+} ion doping. It is owing to the segregation of the dopant cations at the grain

boundary of TiO_2. The growth of nanocrystallineTiO_2 is thus prevented. It was concluded in this study that Yb^{3+} doping decreases the crystallite size and hinder the growth of anatase TiO_2. Anatase to rutile structure transformation is delayed as a result of smaller crystallite size of the material.[19,20]

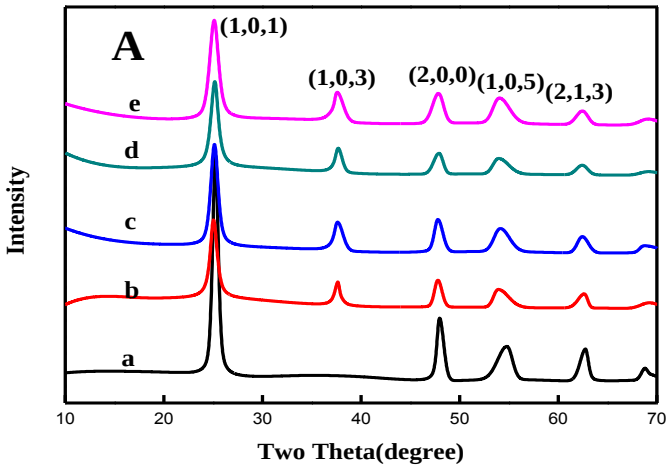

Figure 5.2 A. XRD patterns of a) TiO_2 b) TYb1 c) TYb2 d) TYb5 and e) TYb10 calcined at 300 ˚C.

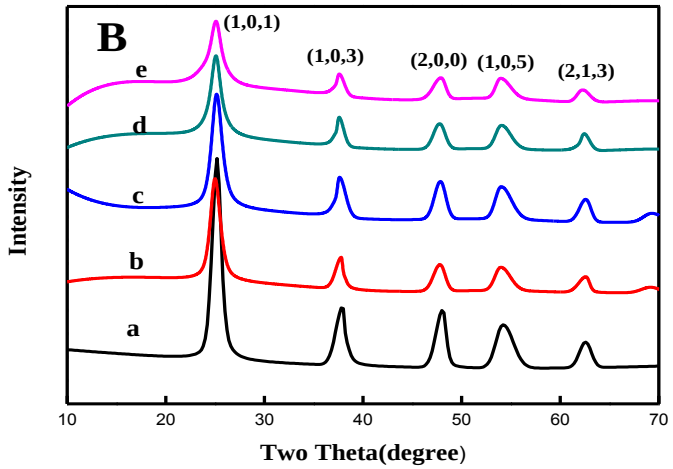

Figure 5.2 B. XRD patterns of a) TiO_2 b) TYb1 c) TYb2 d) TYb5 and e) TYb10 calcined at 500 ˚C.

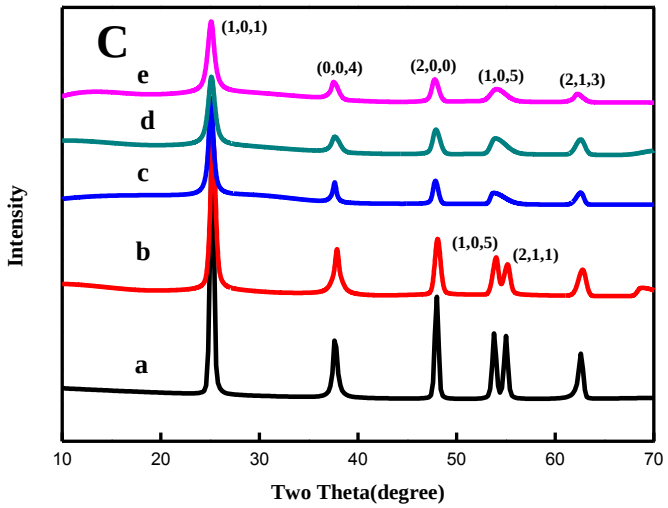

Figure 5.2 C. XRD patterns of a) TiO_2 b) TYb1 c) TYb2 d) TYb5 and e) TYb10 calcined at 700 ˚C.

Table 5.1. Crystal size of anatase of TiO_2,TYb1, TYb2, TYb5 and TYb10 calcined at 300, 500 and 700 ˚C.

Sample	300 ˚C	500 ˚C	700 ˚C
TiO_2	7.84	12.6	21.7
TYb1	7.00	10.2	15.2
TYb2	6.60	9.60	13.6
TYb5	6.70	9.50	10.6
TYb10	5.70	7.90	10.5

5.2.3. FT- Raman Spectroscopy

As shown in Figure 5.3 the Raman spectra of TiO_2 and TYb2 calcined at 500 ˚C were recorded. Raman spectra disclose the anatase phase purity of as synthesized TiO_2 nanoparticles. The peaks are present at 145 (E_g), 395 (B_{1g}), 514 (B_{1g}) and 639 cm^{-1} (E_g) which are the

characteristics of anatase phase of TiO_2.[21] The major peak of anatase get decreased with doping confirms the incorporation of Yb^{3+} into the crystal lattice. Crystallite size also gets reduced and is accordance with the result explained in XRD spectra (Figure 5.1). In addition to decrease in peak intensity and the peak broadening also gets increased, which attributes the oxygen vacancies as a result of Yb^{3+}doping.[22]

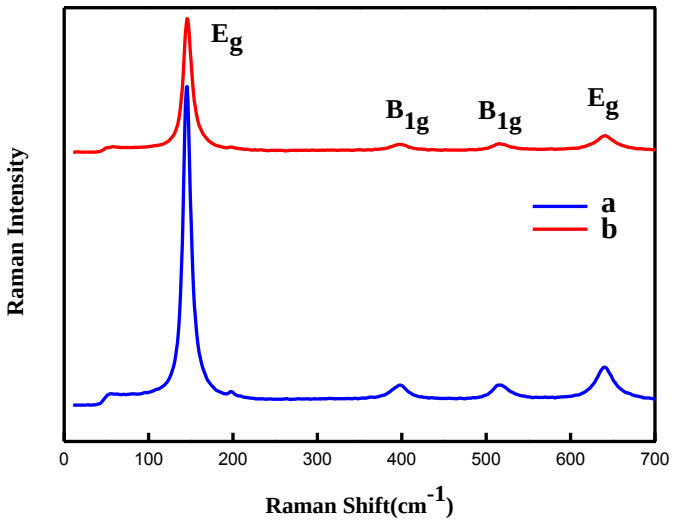

Figure 5.3. Raman Spectra of a) TiO_2 and b) TYb2 calcined at 500 ˚C.

5.2.4 Diffuse Reflectance Spectroscopy (DRS)

Diffuse reflectance spectroscopy (DRS) in the range 200-900 nm of TiO_2 and Yb^{3+} doped TiO_2 calcined at different temperature were investigated to study the optical absorption properties. The DRS spectra of TiO_2 and TYb at 500 and 700 ˚C were shown in the Figure 5.4. From the Figure 5.4, TYb shows an absorption band higher than pure TiO_2. It was also observed that at calcination temperature of

500°C, TYb2 shows the maximum absorption edge and shifts to higher wavelength, *i.e.* visible light region. This red shift can be attributed to the charge-transfer transition between the *f* electrons of Yb^{3+} ion and the TiO_2 conduction band which help in the formation of electron and hole under visible light irradiation. The red shift absorption profile is observed with an increase in calcined temperature from 300 to 700 ˚C. The band gap energies were calculated by using UV-Vis DRS spectra with tauc equation and catalogued in the Table 5.2. The band gap energies of Yb^{3+} doped samples are lower than that of TiO_2 due to the red shift that occurred as a result of Yb^{3+} doping.

Table 5.2. Band gap energies of TiO_2, TYb1, TYb2, TYb5 and TYb10 calcined at different temperatures.

Sample	**Band Gap (eV)**		
	300 ˚C	**500 ˚C**	**700 ˚C**
TiO_2	3.10	3.02	3.00
TYb1	2.87	2.85	2.72
TYb2	2.84	2.83	2.67
TYb5	2.79	2.75	2.64
TYb10	2.72	2.69	2.61

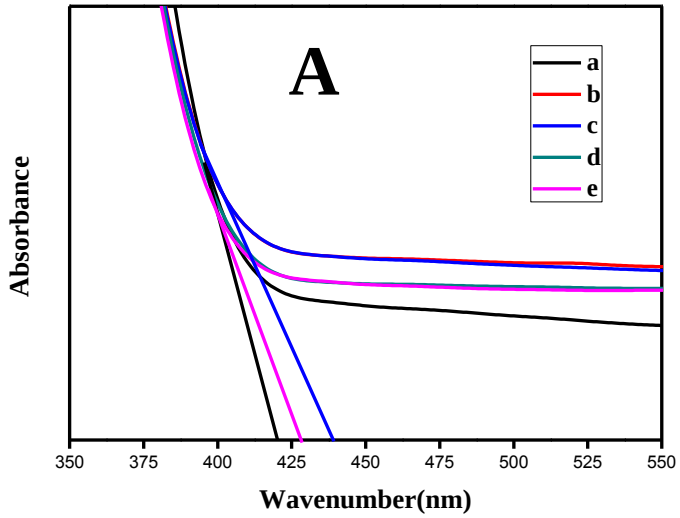

Figure 5.4 A) Absorbance of a) TiO_2 b) TYb1 c) TYb2 d) TYb5 and e) TYb10 calcined at 500 ˚C.

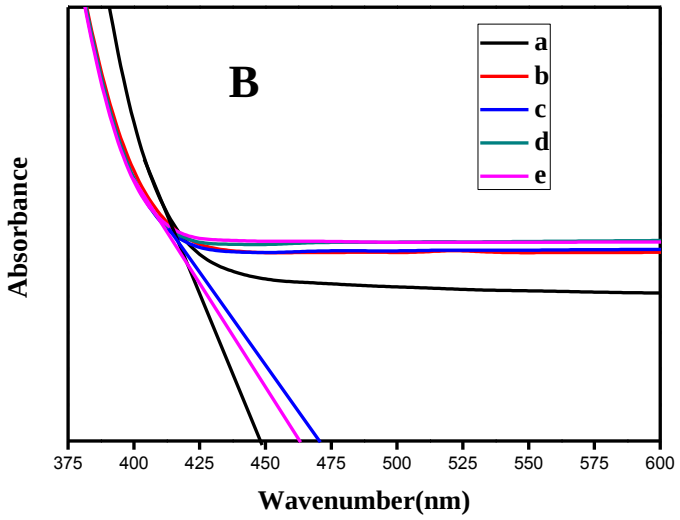

Figure 5.4 B) Absorbance D) Tauc plot of a) TiO_2 b) TYb1 c) TYb2 d) TYb1 and e) TYb10 calcined at 700 ˚C.

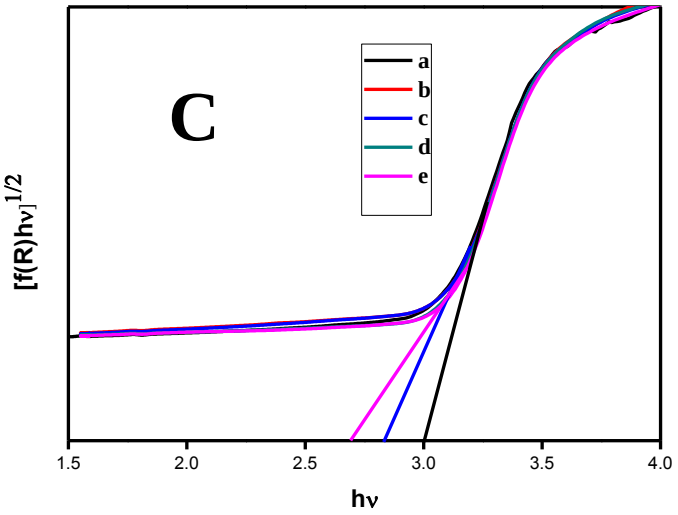

Figure 5.4 C) Tauc plot of a) TiO_2 b) TYb1 c) TYb2 d) TYb5 and e) TYb10 calcined at 500 ˚C

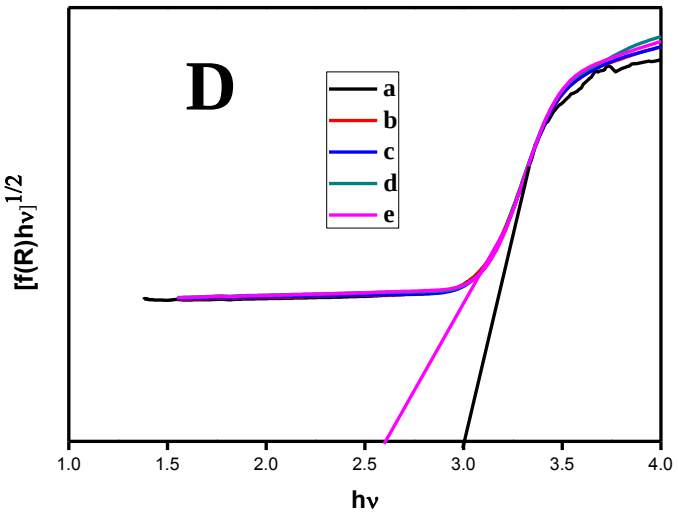

Figure 5.4 D. Tauc plot of a) TiO_2 b) TYb1 c) TYb2 d) TYb1 and e) TYb10 calcined at 700 ˚C.

5.2.5. X-ray Photoelectron Spectroscopy (XPS)

XPS of TiO_2 and TYb2 calcined at 500 ˚C were recorded. XPS study showed the presence of Yb^{3+} doping in TiO_2 lattice and it is evidenced from the remarkable peak changes as a result of Yb^{3+}doping. The $2p_{3/2}$ and $2p_{1/2}$ peaks of Ti^{4+} in bare TiO_2 were observed at 460.2 and 466 eV (Figure 5.5A). Here the peak 460.3 eV attributes to the oxygen richness.[23] Whereas in the case of Yb^{3+} doped TiO_2, the Ti^{4+} peaks were obtained at 458.8 and 464.4 eV. The splitting difference of $2p_{3/2}$ and $2p_{1/2}$ peaks were found to be 5 eV in both TiO_2 and Yb^{3+} doped TiO_2, which attributes the anatase phase purity of both TiO_2 samples.[24] Surface defects originate when Yb^{3+} enters into the lattice of $TiO_2$and which is confirmed by the blue shifting in the binding energy *i.e.* 458.8 eV ($2p_{3/2}$) and 464.6 eV ($2p_{1/2}$). The peak at 458.8 eV reveals the presence of Ti^{3+}.[23]The decrease in valency of Ti explains the presence of oxygen vacancies, which reveal the transformation of oxygen rich environment to oxygen deficient environment. From the O1s XPS (Figure 5.5B) it can be seen that the peak at 531.5 eV blue shifted to 530 eV indicates the change in oxygen environment. Figure 5.5C, the Yb4d XPS reveals the incorporation of Yb^{3+} into the crystal lattice. The Yb4d photopeak had a greater degree of complex peak shape range from188-198 eV. It is based on the simple spin–orbit splitting, due to final state multiplet splitting effects arising from interactions of 4d and 4f states,[25] and is very large due to the same principal quantum number of the two shells.[26,28] The main band was centered at an average BE of 192.3 eV, which corresponds to Yb in trivalent state.[27] The BE of the absolute maximum is relatively close to the values

reported for Yb (III) oxide[28,29]As evidenced from XRD, even though the crystal radius of Yb^{3+}(100.8 pm) is far greater than Ti^{4+} (74.5 pm), Yb^{3+} entered into the crystal lattice of TiO_2 and those ions occupy the interstitial position of TiO_2.

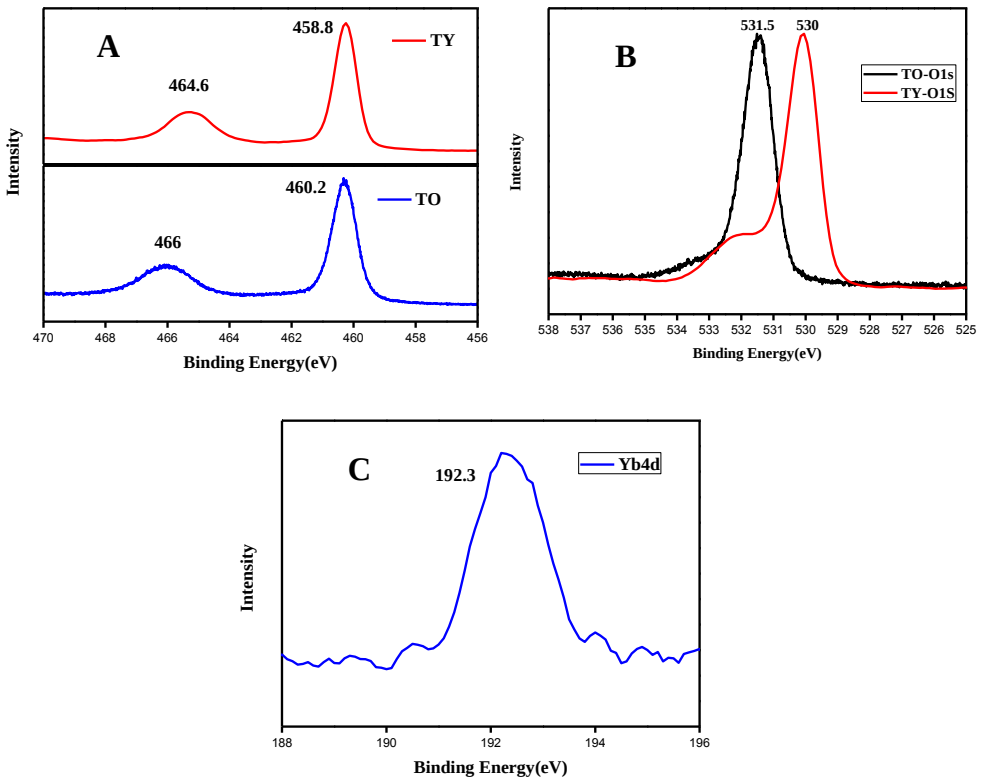

Figure 5.5. XPS of A) Ti2p, B) O1s and C) Yb4d.

5.2.6. Transmission Electron Microscopy (TEM)

Figure 5.6 shows TEM images of TiO_2 and TYb2 calcined at 500 ˚C. TiO_2 shows a particle size in the range of 19-23 nm (Figure 5.6a) at 500 ˚C. On the other hand, the Yb^{3+} doped TiO_2 has a particle

size of 7-14 nm (Figure 5.6b). Thus the TEM observations support the conclusions derived from the XRD data where the crystallite size is reduced as a result of doping. The electron diffraction image of TYb2 calcined at 500 ˚C shows broad band due to the Scherrer line broadening which is attributed to the small crystalline size[30,31] however TiO_2, at same temperature, showed distinct spots due to the high crystallinity and larger size of the crystals.

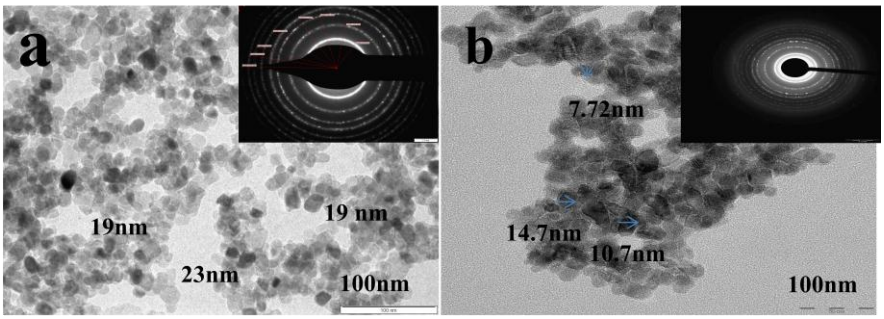

Figure 5.6. TEM images of a) TiO_2 and b) TYb2 at 500 ˚C.

5.2.7. Energy Dispersive Spectroscopy (EDS)

Chemical composition of TiO_2 and TYb2 was determined using EDS analysis (Figure 5.7). Strong X-ray peaks associated with Ti and oxygen are present in TiO_2 whereas peaks of Yb were found in the TYb2 along with Ti and oxygen. This confirms the presence of both Ti and Yb in the lattice of TYb2 as a result of doping.

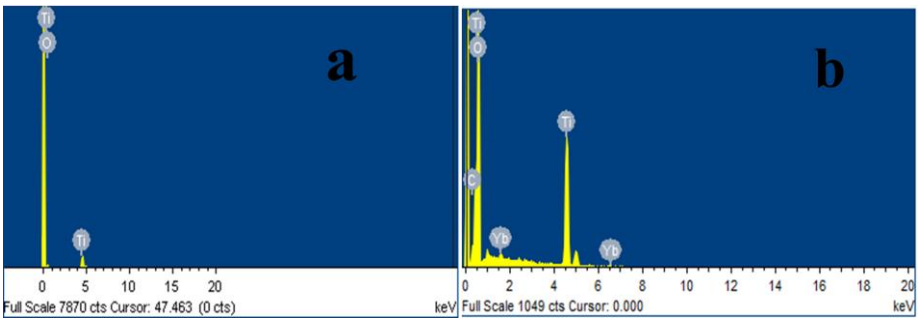

Figure 5.7. Energy Dispersive Spectroscopy (EDS) of a) TiO_2 and b) TYb2 at 500 ˚C.

4.3 Photocatalysis

Photocatalytic activity of both TiO_2 and TYb2 calcined at 500 ˚C for methylene blue degradation under UV and sunlight were carried out and the rate constant obtained from the degradation kinetics were listed in Table 5.3. From Table 5.3 it can be seen that photocatalytic activity of pure TiO_2 and TYb got influenced by the calcination temperature. Rate of degradation under direct sunlight irradiation is more compared to UV light irradiation and it is because of the fact that upon Yb^{3+} ion doping, the light absorption capacity of TiO_2 increases from UV to visible region in accordance with band gap lowering (Table 5.2). The rate constant obeys the first order kinetics and the values are summarized in the Table 5.3, among the different TYb, highest activity was obtained for TYb2 calcined at 500 ˚C, with a rate constant of 0.149 min^{-1}, which is more than 4 times higher than the bare TiO_2 (0.036 min^{-1}). Absorption spectra of methylene blue dye degradation under UV light using TiO_2 and TYb2 calcined at 500 ˚C were shown in Figure 5.8 and 5.9.TYb2 calcined at 500 ˚C degraded completely within 25 minutes. From the results it can be concluded that the TYb2

calcined at 500 ˚C is the best photocatalyst among the samples under UV light irradiation. The visible light activity of TiO_2 and TYb under direct sunlight using the methylene blue degradation experiment was carried out and the time taken for degradation of methylene blue using TiO_2 and TYb under visible light was also shown in Table 5.3. From the Table 5.3, it is found that Yb^{3+} doped TiO_2 sample undergo methylene blue degradation much faster than compared to TiO_2 at all calcinations temperatures under visible light irradiation. The rate constant was calculated from the first order kinetics and is shown in Table 5.3. Among the doped samples highest activity was obtained for TYb2sample calcined at 500 ˚C with a rate constant of 0.151 min^{-1} which is more than11 times higher than the pure TiO_2 (0.013 min^{-1}). Absorption spectra of methylene blue dye degradation under visible light using TiO_2 and TYb2 doped TiO_2 at 500 ˚C were shown in Figure 5.10 and 5.11. TYb2 calcined at 500 ˚C degraded completely within 25 minutes and the results point out that TYb2 calcined at 500 ˚C is the best photocatalyst among samples under visible light irradiation.

Table 5.3. Rate constant of TiO_2 and TYb calcined at different temperatures.

UV light				**Sunlight**			
Sample	300 ˚C	500 ˚C	700 ˚C	Sample	300 ˚C	500 ˚C	700 ˚C
TiO2	0.021	0.036	0.002	TiO2	0.007	0.013	0.004
TYb1	0.010	0.141	0.119	TYb1	0.008	0.135	0.54
TYb2	0.006	**0.149**	0.135	TYb2	0.011	**0.151**	0.073
TYb5	0.005	0.075	0.077	TYb5	0.010	0.038	0.042
TYb10	0.001	0.040	0.044	TYb10	0.009	0.028	0.037

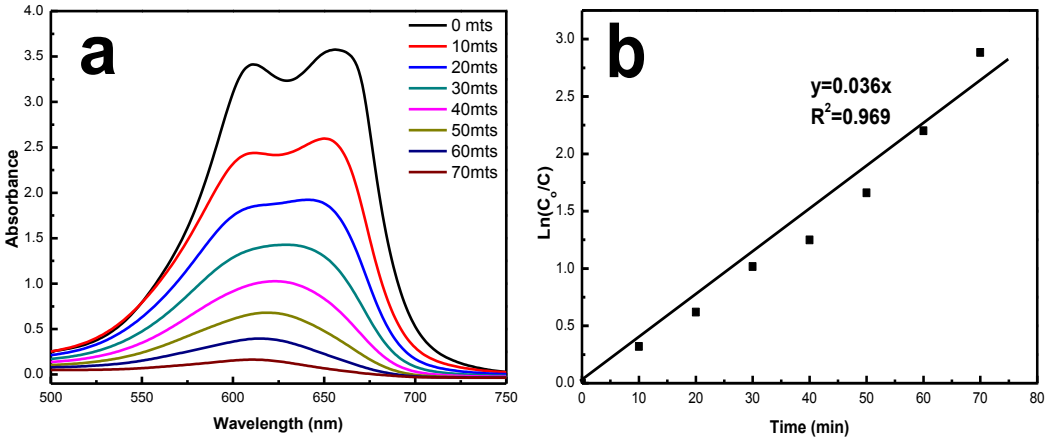

Figure 5.8. Absorption spectra and Kinetic study of methylene blue dye degradation under UV using TiO_2 sample calcined at 500 ˚C.

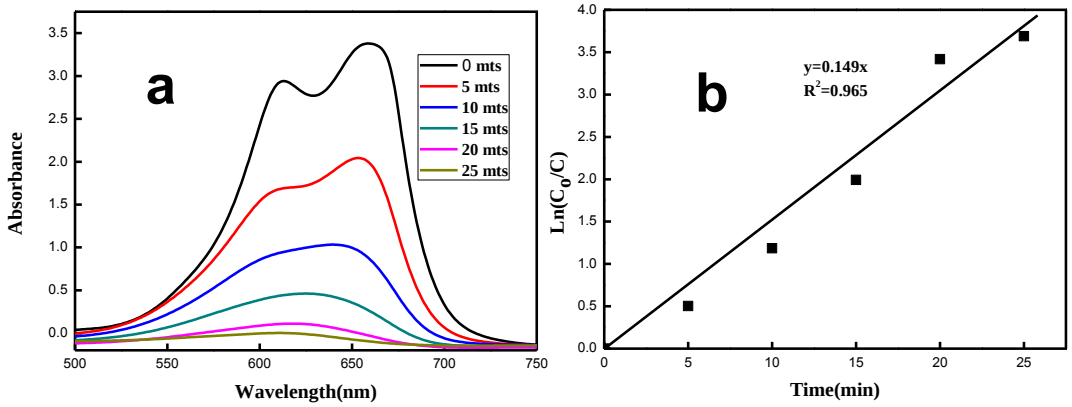

Figure 5.9. Absorption spectra and Kinetic study of methylene blue dye degradation under UV using TYb_2 sample calcined at 500 ˚C.

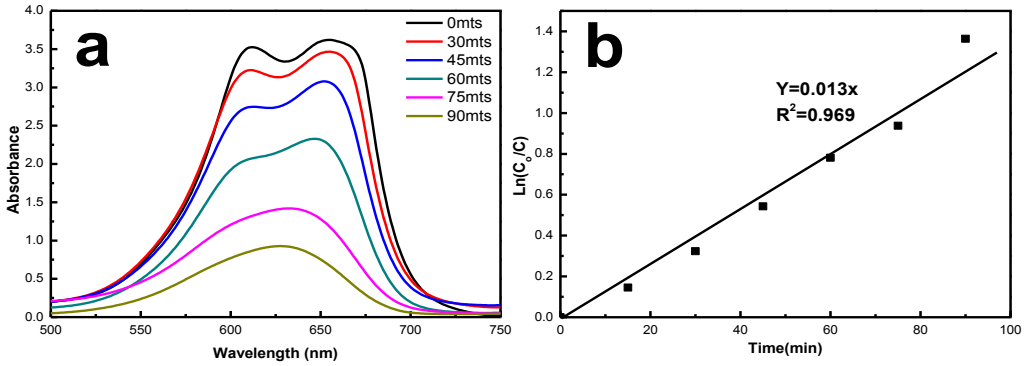

Figure 5.10. Absorption spectra and Kinetic study of methylene blue dye degradation under direct sun light using TiO_2 sample calcined at 500 ˚C.

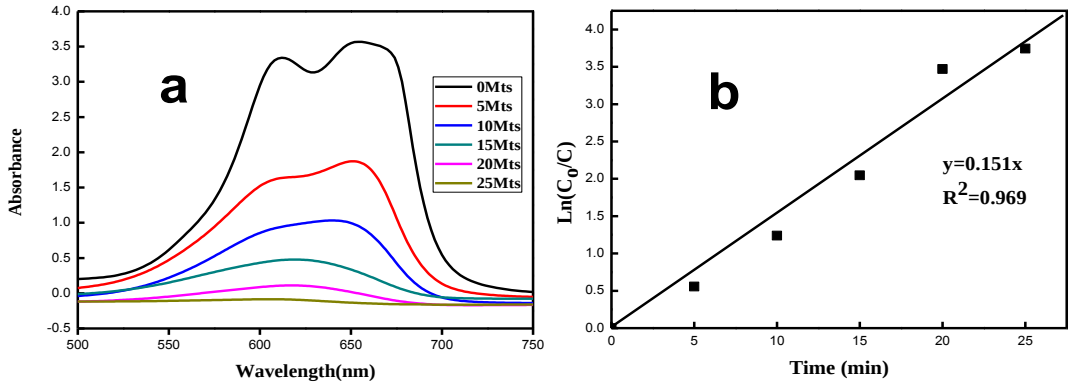

Figure 5.11. Absorption spectra and Kinetic study of methylene blue dye degradation under direct sun light using TYb2 sample calcined at 500 ˚C.

5.3. Conclusion

Nanocrystalline anatase TiO_2 and Yb^{3+} doped TiO_2 was synthesized by a room-temperature aqueous sol–gel process using titanium isopropoxide, acetic acid and ytterbium (III) nitrate as precursors. These TiO_2 nanoparticles were subjected to various calcination temperatures and characterisation were done using technique such as XRD, Raman, FT IR, XPS, SEM and TEM analysis. The investigation confirmed the Yb^{3+} doping improved the anatase phase stability of bare TiO_2. The crystallite sizes of the Yb^{3+} doped TiO_2 samples were reduced along with Yb^{3+} ion doping in comparison with bare TiO_2. XPS results showed that on introducing Yb^{3+} into the crystal lattice of oxygen rich TiO_2 nanocrystals, the environment was changed from oxygen richness to oxygen deficiency *i.e.* Yb^{3+} induced oxygen deficiency in the crystal lattice of TiO_2. These TiO_2 nanoparticles with oxygen richness and oxygen deficiency were subjected to photocatalytic activity under UV and solar illuminations systematically. It was found that TYb2 at 500 ˚C has shown the maximum photoactivity activity under both UV and sunlight illumination. The Photocatlytic activity of TYb2 is more in direct sunlight than in UV, which inference that the light absorption capacity of TiO_2 gets enhanced.

5.4. References.

1. A. Rapsomanikis, A. Apostolopoulou, E. Stathatos and P. Lianos, *J. Photochem.Photobiol. A*, 2014, 280, 46.

2. M. Nischk, P. Mazierski, M. Gazda and A. Zaleska, *Appl. Catal. B.*, 2013, 144,674.

3. S.G. Ghugal, S.S. Umare and R. Sasikala, *Mater. Res. Bull.*2015, 61 298.

4. A. Krukowska, J. Reszczynska and A. Zaleska, *Physicochem. Probl. Miner. Process*.2014, 50, 551.

5. M. Kralova, P. Dzik, M. Vesely and J. Cihlar, *Catal. Today*, 2014, 230, 188.

6. B. Naufal, P.K.Jaseela and P.Periyat, *Mater. Sci. Forum*., 2016, 855, 78.

7. E.Kowalska, M. Janczarek, L. Rosa, S. Juodkazis and B. Ohtani, *Catal. Today*, 2014, 230,131.

8. Y. Xin and H. Liu, *J. Solid State Chem.*, 2011, 184, 3240.

9. P. Sathishkumar, R.V. Mangalaraja, O. Rozas, H.D. Mansilla, M.A. Gracia-Pinilla and S. Anandan, *Ultrason. Sonochem*., 2014, 21, 1675.

10. S. Ramya, S.D. R. Nithila, R.P. George, D. N. G. Krishna, C. Thinaharan and U.K. Mudali, *Ceram. Int*,. 2013,39, 1695.

11. M. Saif, S.M.K. Aboul-Fotouh, S.A. El-Molla, M. M. Ibrahim and L.F.M. Ismail, *Spectrochim. Acta Part A*., 2014,128, 153.

12. H. Shi, T. Zhang, T. An, B. Li and X. Wang, *J. Colloid Interface Sci*., 2012,380, 121.

13. U.G. Akpan and B.H. Hameed, *Appl. Catal. A*, 2010, 375, 1.

14. J. Reszczy´nska, T. Grzyb, J.W. Sobczak, W. Lisowski, M. Gazda, B. Ohtani and A.Zaleska, *Appl. Surf. Sci.*, 2014, 307, 333.

15. A. Pawlak and M. Mucha, *Thermochim. Acta*, 2003, 396, 153.

16. D. G. Huang, S. J. Liao, W. B. Zhou, S. Q. Quan, L. Liu, Z. J. He and J. B. Wan, *J. Phys. Chem. Solids*, 2009, 70, 853.

17. X. Zou, F. Zhang, S. Thomas, Prof. G. Zhu, V. Valtchev and S. Mintova, *Chem. Eur. J.*, 2011,17, 12076.

18. K. M. Parida and N. Sahu, *Appl. Catal. A*, 2008, 287, 151.

19. M. F. Hou, F. B. Li, R. F. Li, H. F. Wan, G. Y. Zhou and K. C. Xie, *J. Rare Earths*, 2004, 22, 542.

20. C. H. Liang, F. B. Li, C. S. Liu, J. L. Lu and X. G. Wang, *Dyes Pigm.* 2008, 76, 477.

21. J. Yan, G. Wu, N. Guan, L. Li, Z. Li and X. Cao, *Phys. Chem. Chem. Phys.*, 2013, 15, 10978.

22. Z. Lu, C. T. Yip, L. Wang, H. Huang and L. Zhou, *Chem. Plus. Chem*, 2012, 77, 991.

23. S. G. Ullattil and P. Periyat, *Nanoscale*, 2015, 7, 19184.

24. R. Ren, Z. Wen, S. Cui, Y. Hou and X. Guo, *J. Chen. Sci. Rep.*, 2015, 5, 10714.

25. H. Ogasawara, A. Kotani and B. T. Thole, *Phys. Rev. B: Condens.Matter*, 1994, 50, 12332.

26. D. Barreca, A. Gasparotto, A. Milanov, E. Tondello, A. Devi and R.A. Fischer, *Surf. Sci*., 2007, 14, 52.

27. F. Wu, H. Su, X.Zhu , K. I. Wang , Z. Zhang and W. Wong, *J. Mater. Chem. B*, 2016, 4, 6366.

28. T. M. Pan and W.S. Huang, *Appl. Surf. Sci*.,2009,255,4979.

29. H. M. Wang, M.C. Simmonds, J.M. Rodenburg, *J. Mater. Chem. Phys.*, 2003,77,802

30. E. Borgarello, J. Kiwi , M. Gratzel, E. Pelizzetti and M. Visca, *J. Am. Chem. Soc.*,1982,104, 2996.

31. K. V. Baiju, C. P. Sibu, K. Rajesh, P. K. Pillai, P. Mukundan, K. G. K. Warrier and W. Wunderlich, *J.Mater. Chem. Phys,*. 2005, 90, 123.

6 Chapter

Neodymium ion (Nd^{3+}) doped TiO_2 an eminent solar photocatalyst.

Contents

6.1. Introduction

This chapter explains high temperature stable and photocatalytic activity of neodymium ion (Nd^{3+}) doped anatase TiO_2 synthesized using modified sol-gel method. Dye waste water excretes into nature mainly by dyestuff, textile industry, and some artificial way causes severe ecological problems. These compounds are highly colored and can contaminate water source in a large extent. Chemical oxidation method for dye wastewater treatment is too costly and physical adsorption method often results in secondary pollution. [1] Many attempts have been carried out to develop efficient biological methods to decolorize these effluents but they have not been very successful. In this regard, the semiconductor photocatalysis appears more competent than the conventional chemical oxidation methods for the decomposition of toxic compounds to non-hazardous products[2]. Metal oxides (e.g. TiO_2, ZnO, and SnO_2) and chalcogenides (e.g.CdS, ZnS) are generally considered for the investigation of semiconductor photocatalysis.[3]TiO_2 is the most widely used photocatalyst because of its high photocatalytic activity, non-toxicity, photochemical stability, optical properties, including a high refractive index leading to a hiding powerand whiteness, relatively low production cost and high efficiency.[4,5] However, the light energy used for excitation must be equal to or exceed the bandgap of 3.2 eV for anatase TiO_2, thus, ultraviolet light with wavelength (λ) shorter than 387 nm is required as excitation source.[4] Rare earth ions are known for their f-orbitals to

form complexes with various Lewis bases and their oxides having characteristics of adsorption selectivity and thermal stability.[6]A. Burns *et.al.* synthesized Nd doped TiO_2 nanostructured thin films on a quartz substrate for the photodegradation of 2-chlorophenol.[7]Y.Xue-ling*et.al.* prepared neodymium doped TiO_2 on silicon dioxide (Nd/TiO_2-SiO_2) to study the photocatlytic activity on methyl orange.4

In this investigation a series of Nd^{3+} doped TiO_2 and bare TiO_2 were synthesized through modified sol-gel method. These TiO_2 photocatalysts having different percentage (0.5, 1, 2, 5 and 10%) of dopants were calcined at different temperature and characterized by various techniques such as XRD, FT-IR and Raman Spectroscopy, SEM, TEM and XPS analysis and finally subjected to photocatalytic studies under UV and sunlight.

6.2 Results and Discussion

6.2.1. FTIR Spectroscopy

FTIR spectra of the TiO_2 and Nd^{3+} doped TiO_2 sample dried at 100 ˚C and calcined at 300, 500 and 700 ˚C have been recorded. A representative example of the FTIR spectra of TNd1dried at 100 ˚C, bare TiO_2 and TNd1 calcined at 300 ˚C were shown in Figure 6.1.The absorption band at 3500-3000 cm^{-1} in both spectra indicate hydroxyl group stretching vibration and surface adsorbed water molecule and 1626 cm^{-1} indicates the hydroxyl group bending vibration. The peak at 2920 and 2855 cm^{-1} is the asymmetric C-H stretching vibration.[8] The bands at 1425 cm^{-1} are due to the vibration of CO_3^{2-} anions, indicating the absorption of CO_2 molecules on the surface of the samples.[9] The

broad peak in the range 400-700 cm^{-1} is due to Ti-O stretching vibration modes, which can be observable in the anatase phase of TiO_2.9 The peak at 654 cm^{-1} for Nd^{3+} doped TiO_2 is due to the vibration modes of anatase skeletal O-Ti-O and O-Ti-O-Nd bonds.[10]

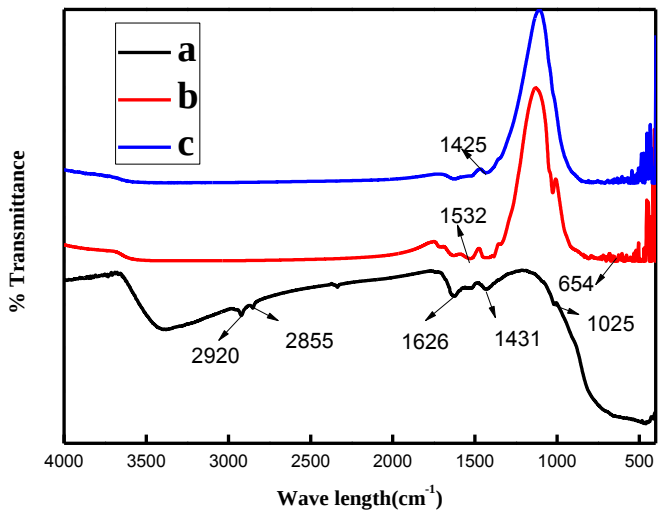

Figure 6.1. FTIR spectra of a) TiO_2 calcined at 300 ˚C b) TNd1 dried at 100 ˚C c) TNd1 calcined at 300 ˚C.

6.2.2 XRD

XRD patterns of pure TiO_2 and 0.5,1,2,5 and 10% Nd^{3+}-TiO_2 powders calcined at 300,500, 700 ˚C were shown in Figure 6.2A, 6.2B and 6.2C respectively. From the figure it is obvious that all catalysts are in the anatase phase. The particle characteristics of the TiO_2 and various Nd^{3+} doped TiO_2 samples at different temperatures are summarized in Table 6.1A. It can be seen from the Figure 6.2that no peaks for neodymium

oxide (Nd_2O_3) were observed in any of the doped sample which implies that Nd^{3+} ions are incorporated in the crystal lattice of TiO_2.The crystallite size was calculated using Scherrer formula and vivid that the crystallite size gets reduced by Nd^{3+} ion doping (Table 6.1). It is due to the insulation of the dopant cations at the grain boundary of TiO_2, which prevent the growth of nanocrystallineTiO_2. It was deduced that rare earth ion doping could hinder crystal transformation and decrease crystallite size. Generally smaller crystalline size could lead to larger surface area.[11,12] These factors may contribute positively towards the greater photocatalytic activity of Nd^{3+} doped TiO_2 in comparison to bare TiO_2.

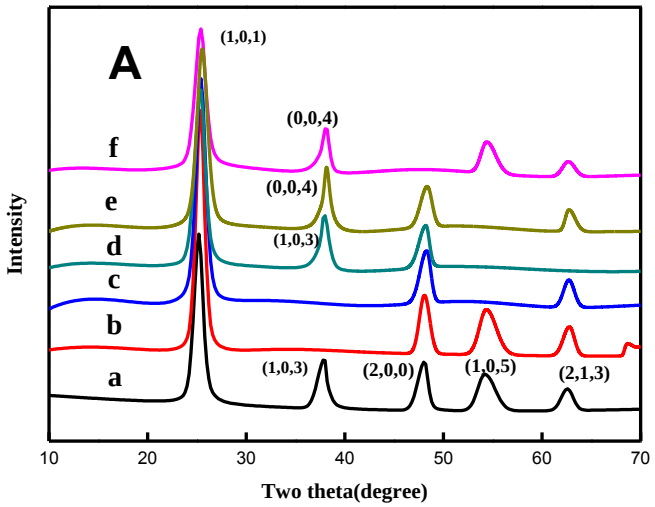

Figure 6.2 A. XRD patterns of a) TNd0.5 b) TNd1 c) TNd2 d) TNd5 and e) TNd10 calcined at 300 ˚C.

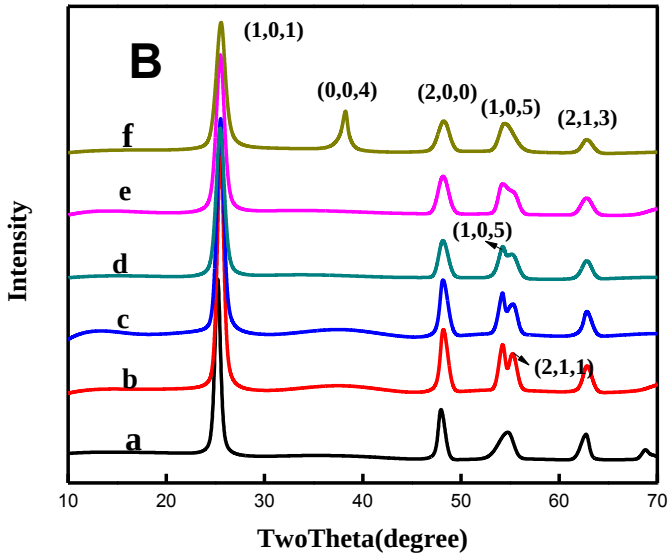

Figure 6.2 B. XRD patterns of a) TNd0.5 b) TNd1 c) TNd2 d) TNd5 and e) TNd10 calcined at 500 ˚C.

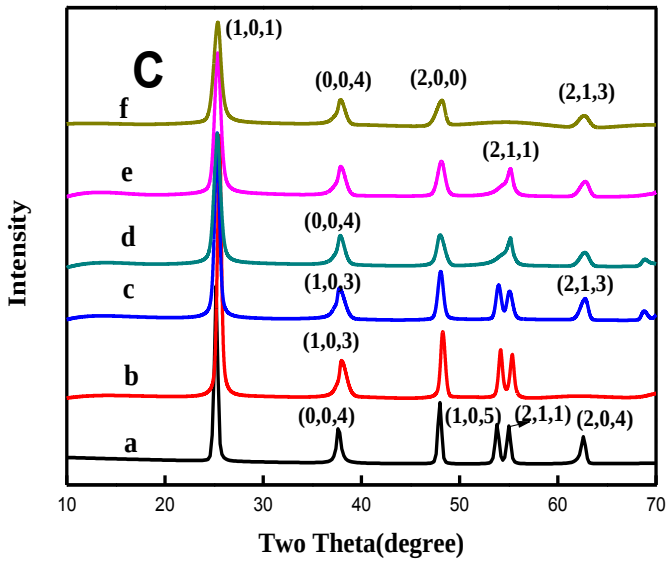

Figure 6.2 C. XRD patterns of a) TNd0.5 b) TNd1 c) TNd2 d) TNd5 and e) TNd10 calcined at 700 ˚C.

Table 6.1. Crystal size of anatase TiO_2, TNd0.5, TNd1, TNd2, TNd5 and TNd10 calcined at 300, 500 and 700 ˚C

Sample	300 ˚C	500 ˚C	700 ˚C
TiO_2	7.84	12.6	21.7
TNd0.5	8.26	11.2	18.6
TNd1	7.30	10.1	15.1
TNd2	6.83	8.68	11.0
TNd5	6.60	8.50	11.0
TNd10	6.60	7.80	9.80

6.2.3 Raman Spectroscopy

Raman spectra of pure TiO_2 and TNd calcined at 300, 500 and 700 ˚C were recorded. A representative example of the Raman spectra of TiO_2 and TNd1calcined at 700 ˚C was shown in Figure 6.3A and 6.3B respectively. The spectrum reveals the anatase phase purity of synthesized TiO_2 nanoparticles. The peaks are present at 145 (E_g), 397 (B_{1g}), 517 (B_{1g}) and 640 cm^{-1} (E_g) which are the characteristics of anatase phase of TiO_2.[13] The major peak of anatase is diminishing as the doping was commenced strengthen the incorporation of Nd^{3+} into the crystal lattice and thereby decrease in crystallite size which has been explained in XRD spectra (Figure 6.3). It can also be confirmed that, in addition to decrease in peak intensity the peak broadening increases, which attributes to the oxygen vacancies occurred as a result of doping.[14]

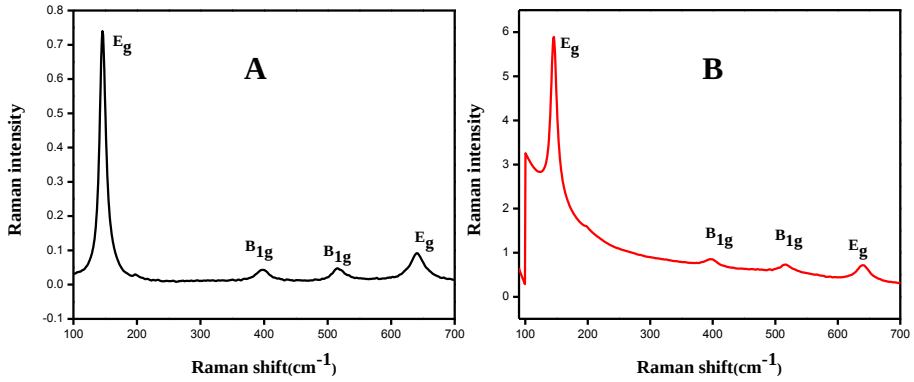

Figure 6.3. Raman Spectra of A) TiO_2 and B) TNd1 calcined at 700 ˚C.

6.2.4 Differential Scanning Calorimetry (DSC)

Differential scanning calorimetry (DSC) studies were carried out (Figure 6.4) to explore the amorphous to crystalline transition of the TiO_2 precursor samples of both TiO_2 and TNd1 samples. Endothermic peak at 92 ˚C was observed for the TiO_2 sample and 106 ˚C for the TNd1 and these peaks are due to the thermal decomposition of the precursor. The exothermic peak at 288 ˚C of TNd1 sample shows the amorphous to crystalline transition. The presence of an endothermic peak at 405 ˚C and 415 ˚C show the desorption of water molecules from the TiO_2 and TNd1 respectively.

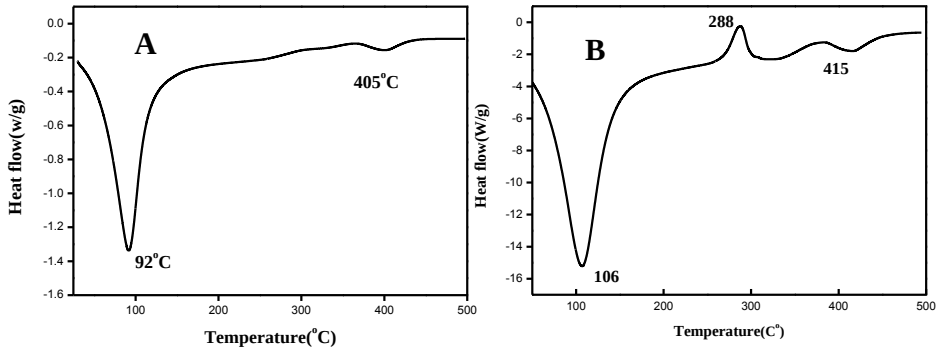

Figure 6.4. Differential scanning calorimetry of A) TiO_2 B) TNd1.

6.2.5. Diffuse reflectance spectroscopy (DRS)

Diffuse reflectance spectroscopy (DRS) in the range 200-900 nm of TiO_2 and TNd calcined at different temperature were investigated to study the optical absorption properties. The DRS spectra of TiO_2 and TNd at 500 and 700 ˚C were shown in the Figure 6.5. From the Figure 6.5, Nd^{3+}doped TiO_2 shows an absorption band higher than pure TiO_2. It was also observed that at 700 ˚C TNd1 shows the maximum absorption edge and alters to higher wavelength. This red shift can be attributed to the charge-transfer transition between the *f* electrons of Nd^{3+} ion and the TiO_2 conduction band which help in the generation of electron and hole under visible light irradiation. The red shift absorption profile is observed with an increase in calcined temperaturefrom 300 to 700 ˚C. The band gap energies were calculated by using UV-Vis DRS spectra with Tauc equation and consolidated in the Table 6.2. The band gap energies of Nd^{3+} doped samples are lower than that of TiO_2 due to red shift.

Table 6.2. Band gap energies of TNd0.5, TNd1, TNd2, TNd5, TNd10, and TiO_2 calcined at different temperatures.

Sample	Band Gap (eV)		
	300 ˚C	**500 ˚C**	**700 ˚C**
TiO_2	3.10	3.02	3.00
TNd0.5	2.96	2.92	2.88
TNd1	2.88	2.85	2.82
TNd2	2.81	2.80	2.76
TNd5	2.74	2.72	2.71
TNd10	2.70	2.69	2.68

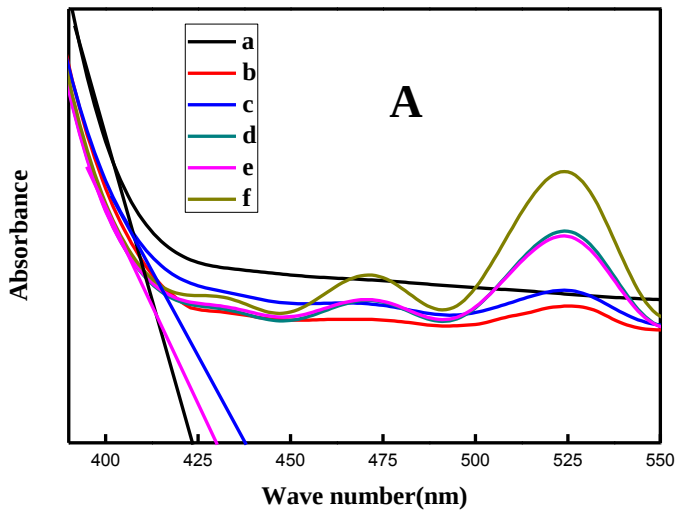

Figure 6.5 A) Absorbance plot of a) TiO_2 b) TNd0.5 c) TNd1 d) TNd2 e) TNd5 and f) TNd10 calcined at 500 ˚C.

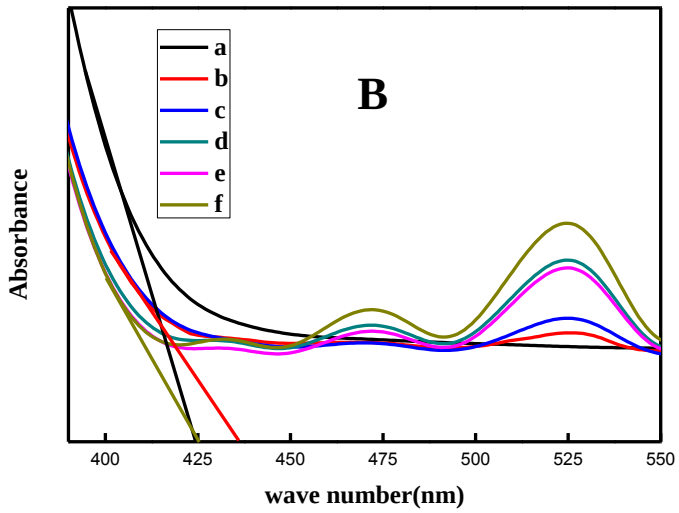

Figure 6.5 B) Absorbance plot of a) TiO_2 b) TNd0.5 c) TNd1 d) TNd2 e) TNd5 and f) TNd10 calcined at 700 ˚C.

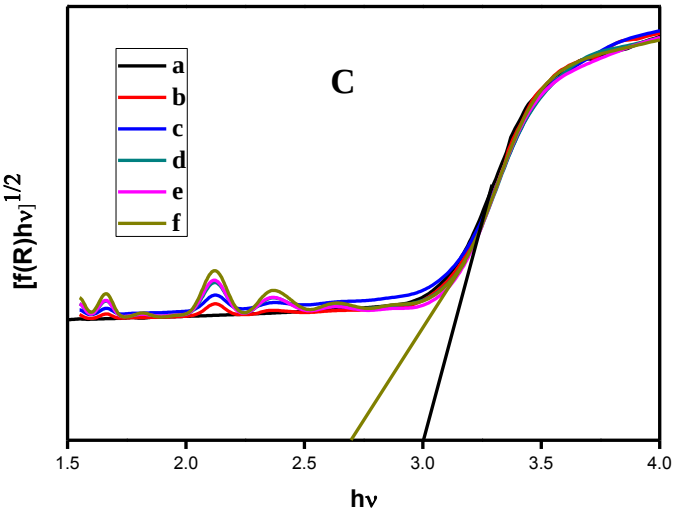

Figure 6.5C) Tauc plot of a) TiO_2 b) TNd0.5 c) TNd1 d) TNd2 e) TNd5 and f) TNd10 calcined at 500 ˚C.

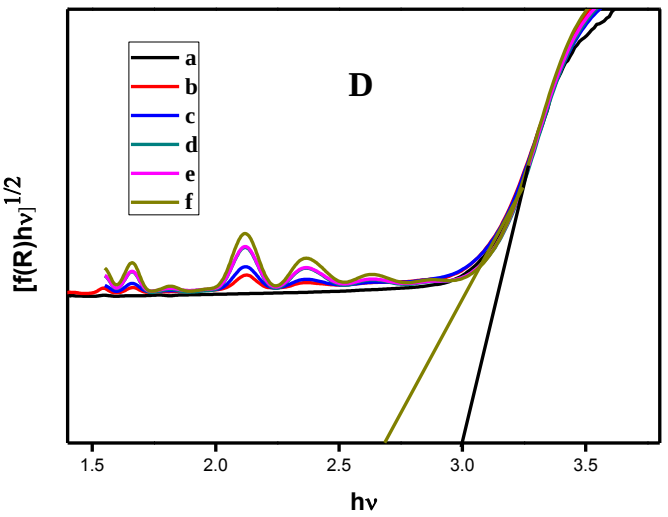

Figure 6.5 D) Tauc plot of a) TiO_2 b) TNd0.5 c) TNd1 d) TNd2 e) TNd5 and f) TNd10 calcined at 700 ˚C.

6.2.6. X-ray Photoelectron Spectroscopy (XPS)

XPS of TiO_2 and TNd1 calcined at 500 ˚C were recorded. XPS study reveals that the presence of Nd^{3+} ion doped into the lattice of TiO_2. As a result of Nd^{3+} doping in TiO_2, there is a considerable change in the peak position of Ti^{4+} in Nd^{3+} doped TiO_2 in comparison to the Ti^{4+} peaks of bare TiO_2. The $2p_{3/2}$ and $2p_{1/2}$ peaks of Ti^{4+} were observed at 460.2 eV and 466 eV for bare TiO_2 (Figure 6.6A). The peak 460.2 eV attributes to the oxygen richness.[15]Whereas in the case Nd^{3+} doped TiO_2, the Ti^{4+} peaks were obtained at 458 and 464 eV. The splitting energy difference of $2p_{3/2}$ and $2p_{1/2}$ in both bare and doped sample approximately equal to 6 eV, which attributes the anatase phase purity of both TiO_2 samples.[16] Surface defects originate when Nd^{3+} enters in to the lattice of TiO_2 and which is confirmed by the blue shifting in the binding energy *i.e.* 458eV ($2p_{3/2}$) and 464 eV ($2p_{1/2}$). The peak at

458 eV reveals the presence of Ti^{3+}.[15] The decrease in valency of Ti explains the presence of oxygen vacancies, which reveal the transformation of oxygen rich environment to oxygen deficient environment. From the O1s XPS (Figure 6.6B) it can be seen that the peak at 531.5 eV blue shifted to 529.9 eV indicates the change in oxygen environment. The peak at 531.5 attributes to the Nd-O bond.[17] Figure 6.6C, the Nd3d XPS reveals the incorporation of Nd^{3+} into the crystal lattice. The Nd3d band was centered at an average BE of 994.3 eV. The BE of the absolute maximum is relatively close to the values reported for Nd (III) oxide.[18] As evidenced from XRD, even though the ionic radius of Nd^{3+} (112.3pm) is greater than Ti^{4+} (74.5pm), Nd^{3+} entered into the crystal lattice of TiO_2 and those ions occupy the interstitial position of TiO_2.

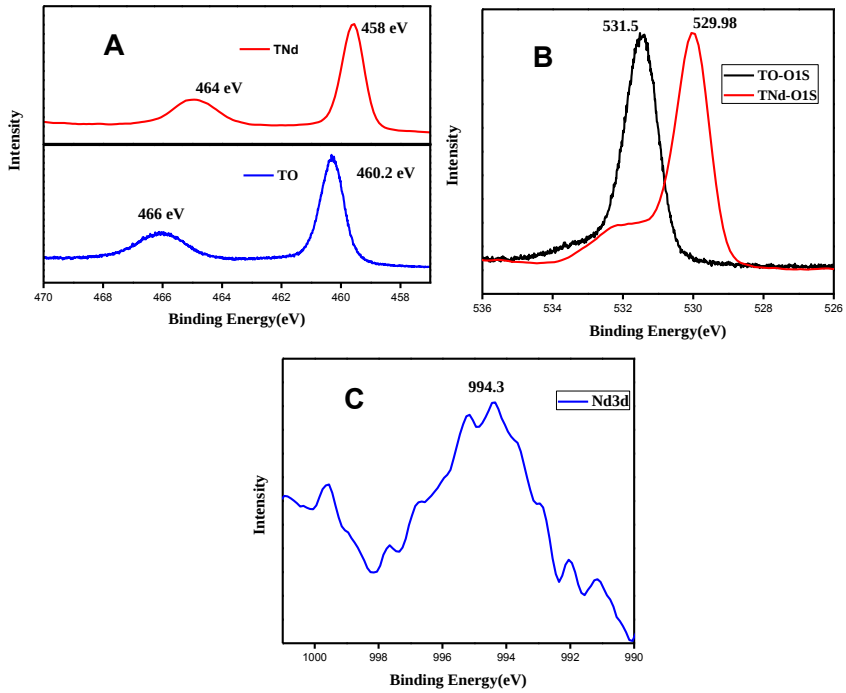

Figure 6.6. XPS of A) Ti2p, B) O1s and C) Nd3d.

6.2.7. Transmission Electron Microscopy (TEM)

TEM images of TiO_2 and TNd1 calcined at 700 ˚C is shown in Figure 6.7. TiO_2 shows a particle size around19-26 nm (Figure 6.7a) at 500 ˚C. On the other hand, the Nd^{3+} doped TiO_2 has a particle size around 8-16nm (Figure 6.7b). This TEM observations support the conclusions derived from the XRD data where the crystallite size is decreased as a result of Nd^{3+} doping in TiO_2. The electron diffraction image of TNd1 calcined at 700 ˚C shows broad band due to the Scherrer line broadening which is attributed to the small crystalline size,[19,20] however in TiO_2, at same temperature, showed distinct spots due to the high crystallinity and larger size of the crystals.

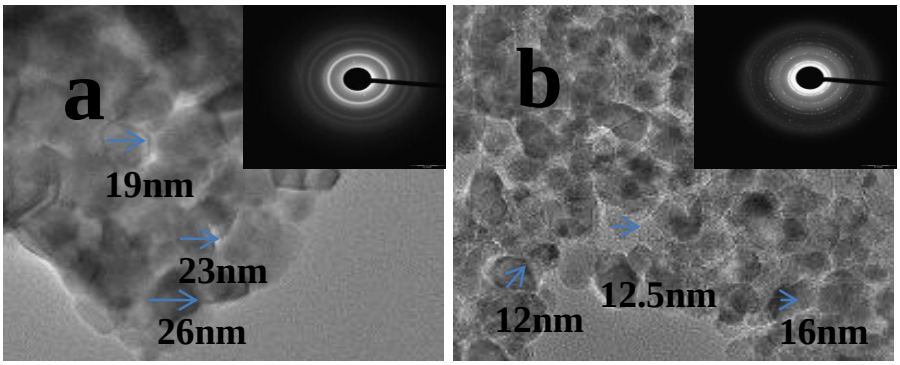

Figure 6.7. TEM image of a) $TiO_2$and b) TNd1 at 700 ˚C.

6.2.8. Energy Dispersive Spectroscopy (EDS)

Chemical composition of TiO_2 and TNd1 was determined using EDS analysis (Figure 8). Strong X-ray peaks associated with Ti and oxygen are present in TiO_2 where as strong peaks of Nd were found in the TNd1 along with Ti and oxygen. This assures the presence of both Ti and Nd^{3+} ion in the lattice.

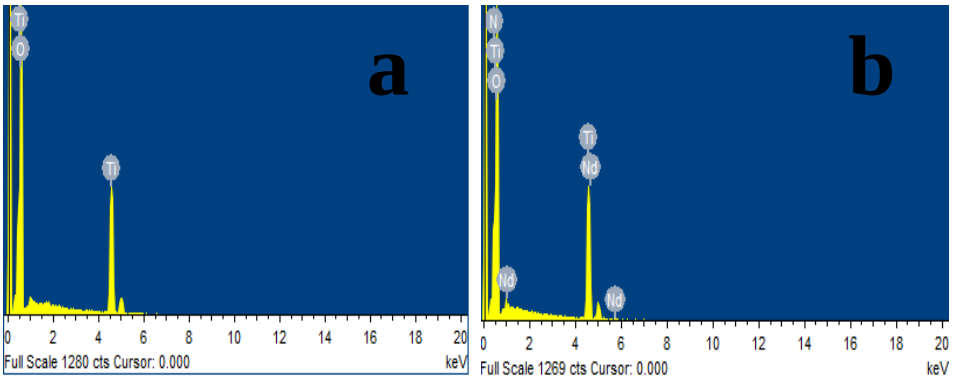

Figure 8. Energy Dispersive Spectroscopy (EDS) of a) TiO_2 and b) TNd1 at 700 ˚C.

6.3 Photocatalysis

Photocatalytic activity of both TiO_2 and TNd calcined at 300, 500, 700 and 800 ˚C for methylene blue degradation under UV and sunlight were carried out and the rate constant obtained from the degradation kinetics were briefed in Table 6.3. From Table 6.3 it can be seen that photocatalytic activity of pure TiO_2 and TNd is influenced by the calcination temperature. Rate of degradation under direct sunlight irradiation and UV light irradiation of Nd^{3+} doped TiO_2 is more than that of bare TiO_2 except in lower temperature. This is because upon Nd^{3+} ion doping, the light absorption capacity of TiO_2 increases from UV to visible region in accordance with band gap lowering. The rate constant obeys the first order kinetics and the values are summarized in the Table 6.3, among the different TNd, highest activity was obtained for TNd1 calcined at 700 ˚C,with a rate constant of 0.128 min^{-1} which is 40 times higher than the bare TiO_2 (0.003 min^{-1}). Absorption spectra of methylene blue dye degradation under UV light using TiO_2 and Nd^{3+} doped TiO_2 at 700 ˚C were shown in Figure 6.9 and 6.10. TNd1

calcined at 700 ˚C degraded completely within 25 minutes. From the results it can be concluded that the TNd1 calcined at 700 ˚C is the best photocatalyst among the samples under UV light irradiation.

The visible light activity of TiO_2 and TNd under direct sunlight using the methylene blue degradation experiment was carried out and the time taken for degradation of methylene blue using TiO_2 and TNd under visible light was also shown in Table 6.3. From the Table 6.3, it is found that Nd^{3+} doped TiO_2 sample undergo methylene blue degradation much faster than compared to TiO_2 at all calcinations temperatures under visible light irradiation. The rate constant was calculated from the first order kinetics and is shown in Table 6.3. Among the doped samples highest activity was obtained for TNd1 sample calcined at 700 ˚C with a rate constant of 0.123 min^{-1} which is almost 30 times higher than the pure TiO_2 (0.004 min^{-1}). Absorption spectra of methylene blue dye degradation under visible light using TiO_2 and TNd1 doped TiO_2 at 700 ˚C were shown in Figure 6.11 and 6.12.TNd1 calcined at 700 ˚C degraded completely within 30 minutes. The results point out that TNd1 calcined at 700 ˚C is the best photocatalyst among samples under visible light irradiation.

Table 3. Rate constant (min^{-1}) of TiO_2 and TNd calcined at different temperatures.

UV light					Sunlight				
Sample	**300 ˚C**	**500 ˚C**	**700 ˚C**	**800 ˚C**	**Sample**	**300 ˚C**	**500 ˚C**	**700 ˚C**	**800 ˚C**
TiO_2	0.021	0.036	0.003		TiO_2	0.007	0.013	0.004	
TNd0.5	0.038	0.026	0.041		TNd0.5	0.006	0.037	0.044	
TNd1	0.007	0.112	**0.128**	0.029	TNd1	0.005	0.98	**0.123**	0.44
TNd2	0.008	0.074	0.091		TNd2	0.08	0.036	0.040	
TNd5	0.008	0.068	0.058		TNd5	0.011	0.026	0.028	
TNd10	0.011	0.029	0.028		TNd10	0.012	0.028	0.029	

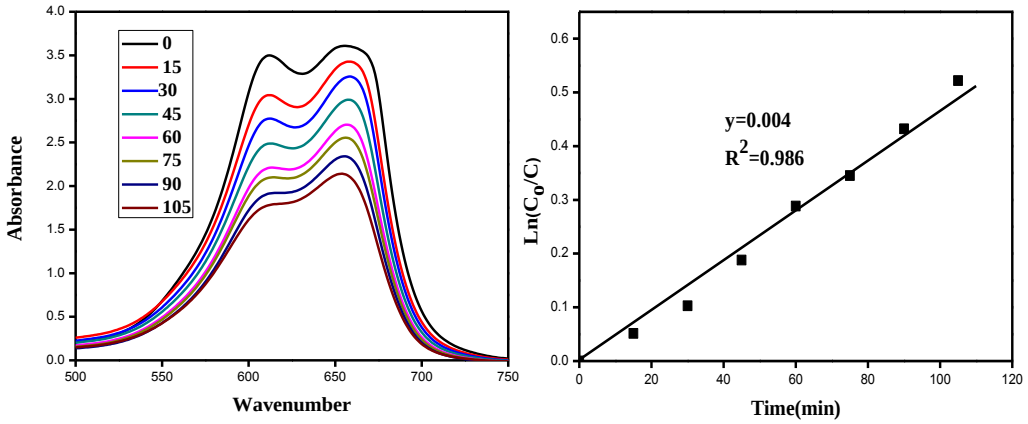

Figure 6.9. Absorption spectra and Kinetic study of methylene blue dye degradation under UV using TiO_2 sample calcined at 700 ˚C.

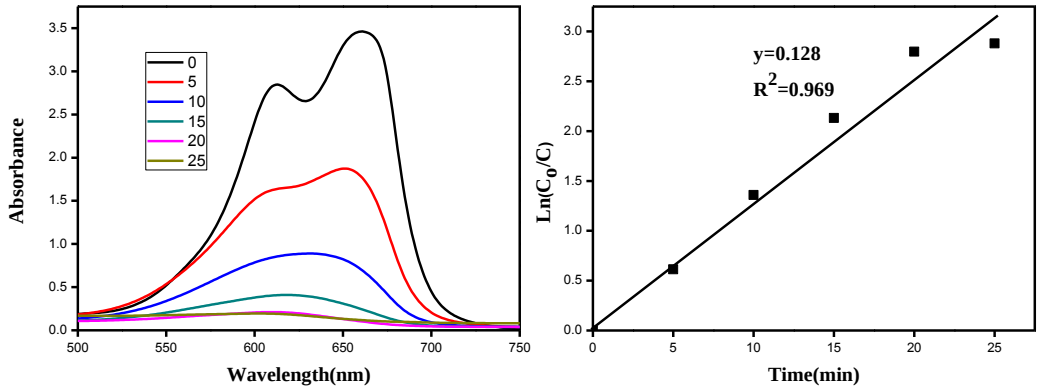

Figure 6.10. Absorption spectra and Kinetic study of methylene blue dye degradation under UV using TNd1 sample calcined at 700 ˚C.

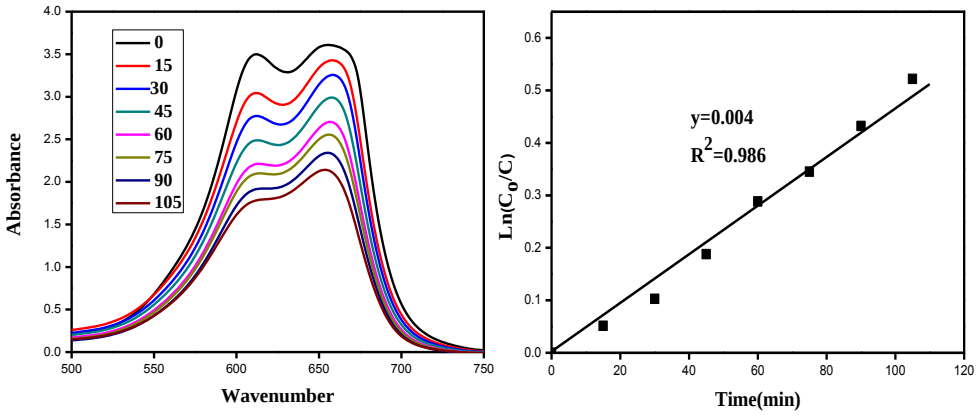

Figure 6.11. Absorption spectra and Kinetic study of methylene blue dye degradation under direct sun light using TiO_2 sample calcined at 700 ˚C.

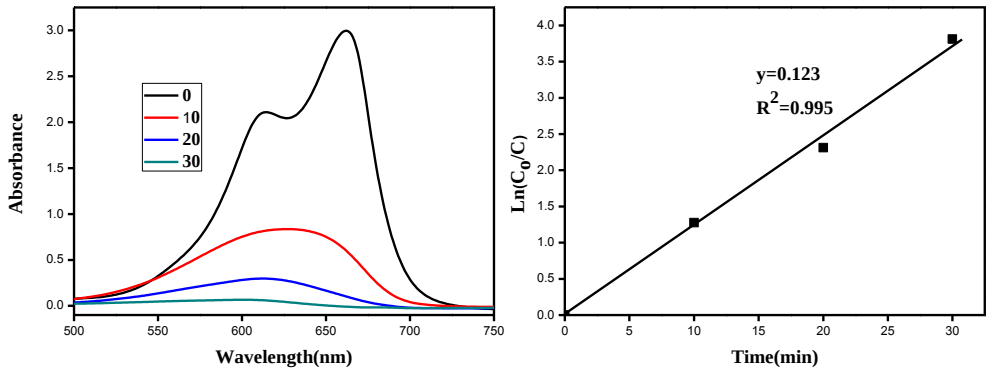

Figure 6.12. Absorption spectra and Kinetic study of methylene blue dye degradation under direct sunlight using TNd1 sample calcined at 700 ˚C.

6.4 Conclusions

Employing a modified sol-gel strategy nanocrystalline TiO_2 and Nd^{3+} doped TiO_2 were synthesised. As synthesised sample were calcined at various temperatures 300, 500, 700 and 800 ˚C and characterised using XRD, FT-IR and Raman Spectroscopy, XPS, SEM and TEM. XRD study showed that all calcined sample were crystalline in nature with anatase TiO_2 phase structure. It also showed that as a result of doping of Nd^{3+}, crystalline size ofNd^{3+}doped TiO_2 sample were reduced considerable in comparison with bare TiO_2. XPS study showed that on introducing Nd^{3+} in to the crystal lattice of TiO_2 nanocrystals the environment was changed from oxygen richness to oxygen deficiency. These TiO_2 and Nd^{3+} doped TiO_2nanoparticles calcined at various temperatures were subjected to photocatalytic under UV and solar illuminations. These nanocrystalline TiO_2 showed high photocatalytic activity and stability at higher temperature due to high degree of crystallinity. It was found that TNd1 calcined at 700 ˚C has shown the maximum photoactivity under both UV and sunlight illumination.

6.5. Reference

1. Y. Xie, C. Yuan and X. Li, *Colloids Surf*, 2005, 252, 87.

2. W. Xiaohong, S. Peibo, L. Huiling and Q. Lili, *J. Rare Earths*, 2009,27,939.

3. J. Peral, X. Domenech and D. F. Ollis, *J. Chem. Technol. Biotechnol.*, 1997,70,117.

4. Y. Xue-ling, Z. Li, Y. Le-min, Z. Wu-yi and X.Yue-Hua, *Trans. Nonferrous Met. Soc. China*, 2011, 21, 335.

5. B. Shahmoradi, I. A. Ibrahim, N. Sakamoto, S. Ananda, R. Somashekar, T. N. Gururow and K. Byrappa, *J. Environ. Sci. Health A*, 2010, 45, 1248.

6. C. Jun-tao, L. Xin-jun, Y. Ying, W. Liang-yan and H. Ming-xing, *J. Catal.*, 2004, 25, 397.

7. A. Burns, W. Li, C. Baker and S.I. Shah,*Mat. Res. Soc. Symp. Proc*, 2002,703.

8. A. Pawlak and M. Mucha, *Thermochim. Acta*, 2003, 396, 153.

9. D.R. Zhang, H.L. Liu, R. H. Jin, N. Z. Zhang, Y. X. Liu and Y.S. Kang, *J. Ind. Eng. Chem*. 2007, 13, 92.

10. G. D. Dhamale, V. L. Mathe , S. V. Bhoraskar , S. N. Sahasrabudhe , S. D. Dhole and S. Ghorui, *Nanotechnology*, 2016, 27, 85603.

11. M. F. Hou, F. B. Li, R. F. Li, H. F. Wan, G. Y. Zhou and K. C. Xie, *J. Rare Earths*, 2004, 22, 542.

12. C. H. Liang, F. B. Li, C. S. Liu, J. L. Lu and X. G. Wang, *Dyes Pigm.*, 2008, 76, 477.

13. J. Yan, G. Wu, N. Guan, L. Li, Z. Li and X. Cao, *Phys. Chem. Chem. Phys.*, 2013, 15, 10978.

14. Z. Lu, C. T. Yip, L. Wang, H. Huang and L. Zhou, *Chem. Plus. Chem.*, 2012, 77, 991.

15. S. G. Ullattil and P. Periyat, *Nanoscale*, 2015, 7, 19184.

16. R. Ren, Z. Wen, S. Cui, Y. Hou and X. Guo, *J. Chen, Sci. Rep.*, 2015, 5, 10714.

17. D. Nassoko, Yan-Fang Li, Jia-Lin Li, Xi Li and Y. Yu, *Int. J. Photoenergy*, 2012, 716087.

18. X. Fan, H. Liuand C. Fei, *Mater. Res. Express*, 2014, 1, 4.

19. E. Borgarello, J. Kiwi , M. Gratzel, E. Pelizzetti and M. Visca, *J. Am. Chem. Soc.*,1982, 104 2996.

20. K. V. Baiju, C. P. Sibu, K. Rajesh, P. K. Pillai, P. Mukundan, K. G. K. Warrier and W. Wunderlich, *Mater. Chem. Phys*,. 2005,90, 123.

7 Chapter

Erbium ion (Er^{3+}) doped TiO_2 via sol-gel method.

Contents

7.1. Introduction

Photocatalysis come in sight as an efficient pollution control technology because of its destructivity, lower energy consumable, milder condition, easy controllability and handy operation.[1,2] From the discovery of photocatalyst in 1972,[3] TiO_2 is considered to be an encouraging photocatalyst for the removal of various organic and inorganic pollutants from the contaminated water and air. However, its utilization in the solar light is restrained by the fact that it absorbs only the ultraviolet light due to its broadband-gap and the UV light composes only 3–5 % of the solar light energy.[3] Many reformative methods have been accepted such as the surface sensitization, noble metal deposition, metal ion doping and non-metal ion doping the combination of narrow band-gap semiconductors and the aggradations of noble metals.[2,4]

Among them, the metal ion doping method is simple and is more advantageous to improve the photocatalytic potency. Rare-earth elements have rich electronic energy levels and hence in recent years used to modify the TiO_2 (*e.g.* La & Ce) to improve its photocatalytic activity, up-conversion emission efficiency and other properties.[5,6] Erbium is a rare earth element with high up conversion of infrared to visible light because of a favorable electronic level scheme with equally spaced, long-lived excited states.[7] Yali Zheng *et al.* prepared Er^{3+}doped TiO_2 nano-fibers and investigated its photo-degradation of methyl orange.[8] Jie Zhang *et al.* obtained the TiO_2: Er^{3+}nanocrystals with a mixture of anatase and pyrochlore, and a mixture of rutile and

pyrochlore at different annealing temperatures.[9] Xinguang Mao *et al.* reported that the highest up-conversion efficiency could be achieved by doping Er^{3+}into TiO_2 thin films prepared by RF magnetron sputtering.[10]Yinchang Lia *et al.* prepared TiO_2 nanotubes which was doped with erbium ions in ethylene glycol organic electrolyte through ion doping method. [11] R. Xu *et al.* two new photocatalysts of Er^{3+}:$YAlO_3$/Fe and co-doped TiO_2 coated composites were prepared by the sol–gel process to extend the photocatalytic performance of TiO_2.[2]
In this chapter TiO_2 andEr^{3+} doped TiO_2 were synthesized *via* modified sol-gel method. All these samples were calcined at 300, 500, 700 ˚C and its properties were compared with bare TiO_2. The photocatalytic effect under both UV and direct sunlight and effect of calcination temperature were studied using the bare and Er^{3+} doped TiO_2 were also carried out.

7.2 Results and Discussion

7.2.1. FT-IR Spectroscopy

The FT-IR spectra of all the samples of TiO_2 and Er^{3+} doped TiO_2were recorded. Spectra TEr1 uncalcined and calcined at 300 and 500 ˚C were demonstrated in Figure 7.1. Peak commonly seen at 3300-3500 cm^{-1} indicates hydroxyl group stretching vibration and surface adsorbed water molecule, while at 1625cm^{-1} the hydroxyl group bending vibration. Absorbed CO_2 on the surface is shown by the peak at 2337 cm^{-1}.[12] The band at 1422 cm^{-1} is due to the vibration of CO_3^{2-} anions, which designate the absorption of CO_2 molecules on the surface of the samples. Both TiO_2 and Er^{3+} doped TiO_2 sample hold strong and broad band in the range of 400-700 cm^{-1}, which assign to Ti-O stretching and Ti-O-Ti bridging modes. These are the characteristic peaks of anatase

phase of TiO_2.[13]The peak at 462 and 566 cm^{-1} for Er^{3+} doped TiO_2 is due to the vibration modes of anatase skeletal O-Ti-O and Ti-O-Er bonds. Similar observation was seen in the FTIR spectra of TiO_2 and Er^{3+} doped TiO_2 calcined at 500 and 700 ˚C.

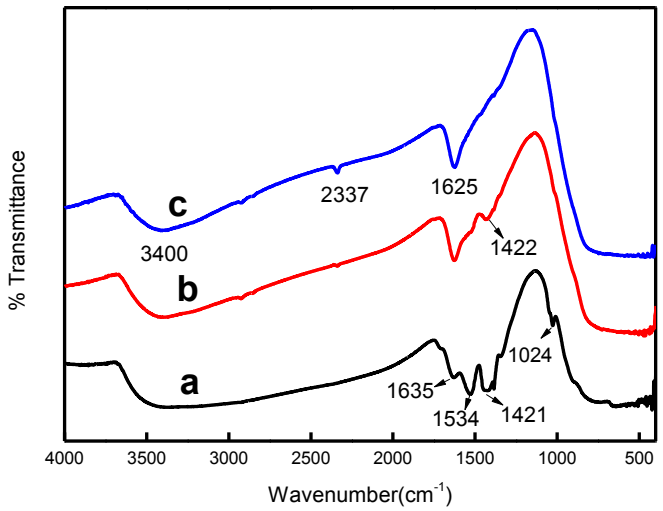

Figure 7.1 FTIR spectra of a) TiO_2 calcined at 500 ˚C b) TEr1 dried at 100 ˚C c) TEr1 calcined at 500 ˚C.

7.2.2XRD

XRD patterns of bare TiO_2 and 1,2,5 and 10% Er^{3+} doped TiO_2 powders calcined at 300, 500, 700 ˚C were shown in Figure 7.2A, 7.2B, 7.2C. From the Figure it is clear that all samples were present in anatase structure, which indicates that Er^{3+}doping inhibits the crystal phase transformation of TiO_2. Er^{3+} doped TiO_2 when compared with pure TiO_2 calcined at the same temperature, the relative intensity of (101) peaks get broadened and reduced by Er^{3+} doping. It is clearly evident from XRD that no peaks from erbium oxide (Er_2O_3) were observed. This implies that Er^{3+} ions are incorporated into the crystal lattice of TiO_2. When the crystallite sizes of the Er^{3+} doped TiO_2 samples were calculated using the Scherrer formula, it was found that the crystallite size was reduced by Er^{3+} ion doping. It may be assign to the segregation of the dopant cations at the grain boundary, and the growth of nanocrystallite in the nanoparticles is prevented. The particle characteristics of the samples under different weight percentage and temperature used in this study are concise in Table 7.1.It was concluded that Er^{3+} ion doping could obstruct crystal transformation and decrease crystallite size. Generally, smaller crystalline size could lead to larger surface area which may positively contribute towards the improvement in the photocatalytic activity of Er^{3+} doped TiO_2.[14,15]

Table 1. Crystal size of anatase TiO_2, TEr0.5, TEr1, TEr2, TEr5 and TEr10 calcined at 300, 500 and 700 ˚C.

Sample	300 ˚C	500 ˚C	700 ˚C
TiO_2	7.84	12.6	21.7
TEr0.5	8.4	11.6	19.8
TEr1	7.8	10.1	15.6
TEr2	7.4	9.8	15.1
TEr5	6.4	8.6	12.2
TEr10	6.1	7.7	9.6

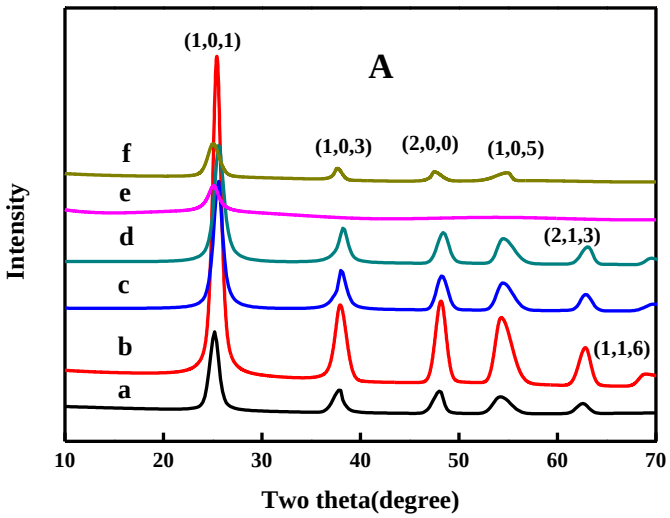

Figure 7.2 A. XRD patterns of a) TEr0.5 b) TEr1 c) TEr2 d) TEr5 and e) TEr10 calcined at 300 ˚C.

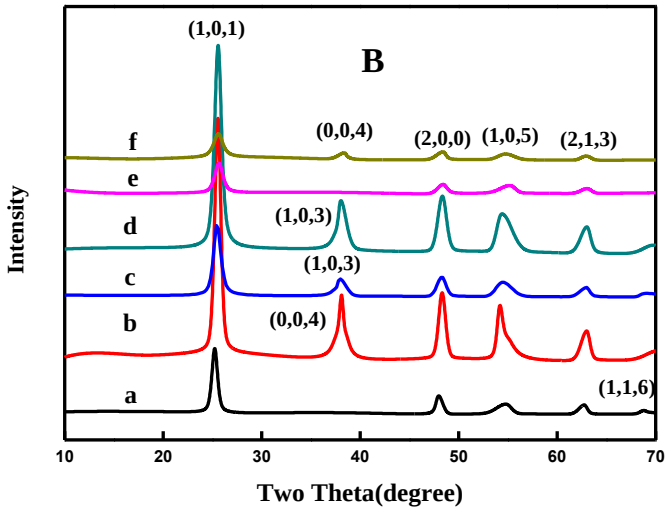

Figure 7.2 B. XRD patterns of a) TEr0.5 b) TEr1 c) TEr2 d) TEr5 and e) TEr10 calcined at 500 ˚C.

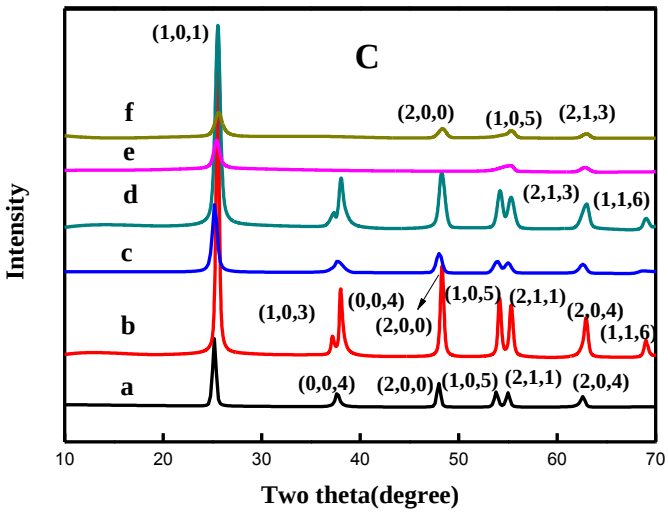

Figure 7.2 C. XRD patterns of a) TEr0.5 b) TEr1 c) TEr2 d) TEr5 and e) TEr10 calcined at 700 ˚C.

7.2.3 Raman Spectroscopy

Raman spectra of TEr0.5, TEr1, TEr2, TEr5, TEr10 and pure TiO_2 calcined at 300, 500 and 700 ˚C were recorded. A representative example of the Raman spectra of TiO_2 and TEr1 calcined at 500 ˚C were shown in Figure 7.3. The spectrum discloses the anatase phase purity of synthesized TiO_2 nanoparticles. The peaks are present at 146 (E_g), 397 (B_{1g}), 517 (B_{1g}) and 639 cm^{-1} (E_g) which are the characteristics of anatase phase of TiO_2.[16,17] The major peak of anatase is decreasing as the doping was introduced assure the incorporation of Er^{3+} into the crystal lattice and thereby decrease in crystallite size which has been explained in XRD spectra (Figure 7.2). It can also be confirmed that, in addition to decrease in peak intensity the peak broadening increases, which attributes to the oxygen vacancies as a result of doping in TiO_2 lattice.[18]

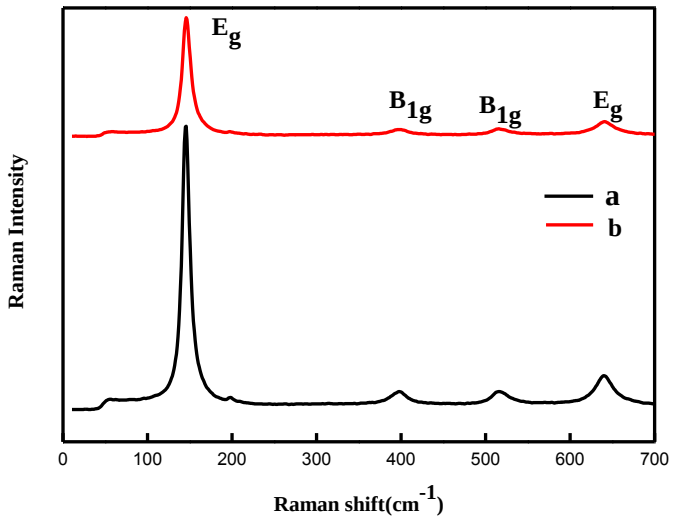

Figure 3. Raman Spectra of a) TiO_2 and b) TEr1 calcined at 500 ˚C.

7.2.4 Diffuse reflectance spectroscopy (DRS)

Diffuse reflectance spectroscopy (DRS) in the range 200-900 nm of TiO_2 and Er^{3+} doped TiO_2 calcined at different temperature were investigated to study the optical absorption properties. The DRS spectra of TiO_2 and TEr1 at 500 and 700 ˚C were shown in the Figure 7.4. From the Figure 7.4, Er^{3+}doped TiO_2 shows an absorption band higher than pure TiO_2.The absorption peaks at 488, 522 and 653 nm are characteristic for Er^{3+} dopant and could be identified with the transition from the $^4I_{15/2}$ ground state to the excited states of erbium ions $^4F_{7/2}$, $^2H_{11/2}$ and $^4F_{9/2}$.[19] It was also noticed that at calcination temperature of 500 ˚C, TEr1 shows the maximum absorption edge and shifts to higher wavelength. This red shift can be ascribed to the charge-transfer transition between the *f* electrons of Er^{3+} ion and the TiO_2 conduction band which help in the generation of electron and hole under visible light irradiation. The red shift absorption profile is observed with an increase in calcined temperature from 300 to 700 ˚C. The band gap energies were calculated by using UV-Vis DRS spectra with Tauc equation and condensed in the Table 7.2.The band gap energies of Er^{3+} doped samples are lower than that of TiO_2 due to the red shift that occurred as a result of Er^{3+} doping.

Table 7.2. Band gap energies of TEr0.5, TEr1, TEr2, TEr5, TEr10, and TiO_2 calcined at different temperatures.

Sample	Band Gap (eV)		
	300 ˚C	**500 ˚C**	**700 ˚C**
TiO_2	3.1	3.02	3.00
TEr0.5	2.96	2.91	2.87
TEr1	2.86	2.80	2.78
TEr2	2.79	2.76	2.75
TEr5	2.75	2.74	2.72
TEr10	2.73	2.71	2.70

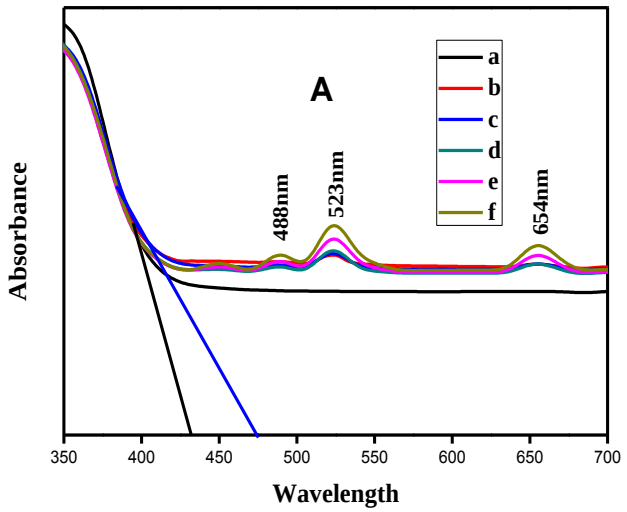

Figure 7.4 A) Absorbance plot of a) TiO_2 b) TEr0.5 c) TEr1 d) TEr2 e) TEr5 and f) TEr10 calcined at 500 ˚C.

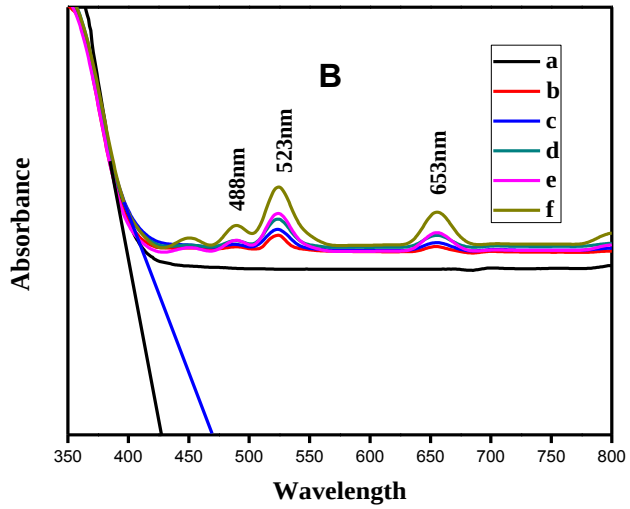

Figure 7.4 B) Absorbance plot of a) TiO_2 b) TEr0.5 c) TEr1 d) TEr2 e) TEr5 and f) TEr10 calcined at 700 ˚C.

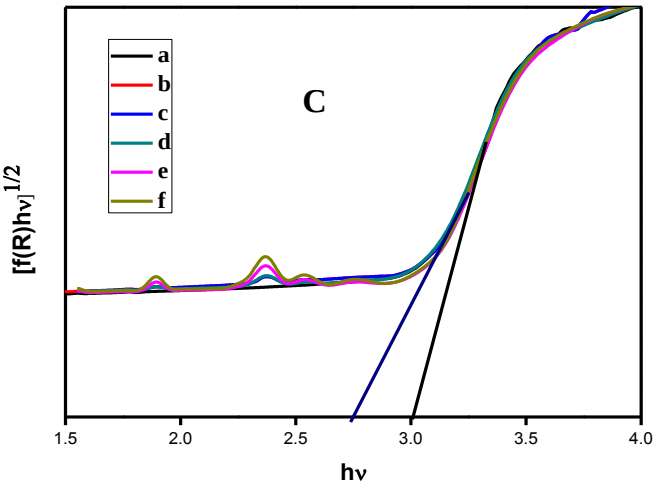

Figure 7.4 C) Tauc plot of a) TiO_2 b) TEr0.5 c) TEr1 d) TEr2 e) TEr5 and f) TEr10 calcined at 500 ˚C.

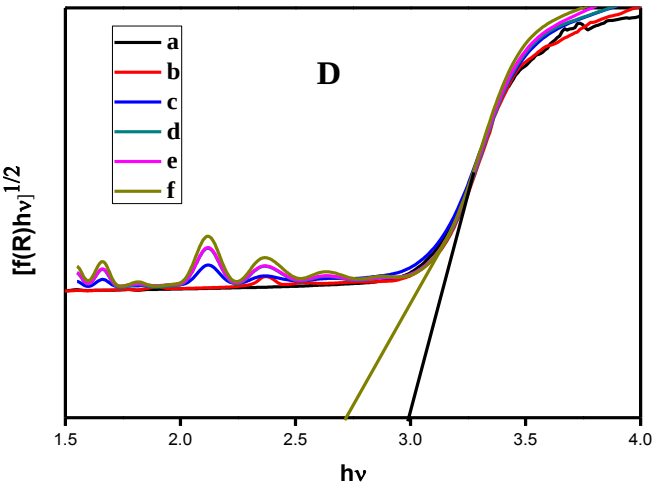

Figure 7.4 D) Tauc plot of a) TiO_2 b) TEr0.5 c) TEr1 d) TEr2 e) TEr5 and f) TEr10 calcined at 700 ˚C.

7.2.5. X-ray Photoelectron Spectroscopy (XPS)

XPS of TiO_2 and TEr1 calcined at 500 ˚C were recorded to study the effect doping of Er^{3+} in TiO_2. Remarkable peak changes are occurred on the Er^{3+} doped TiO_2 in comparison to the bare TiO_2. In bare TiO_2, the $2p_{3/2}$ and $2p_{1/2}$ peaks of Ti^{4+} were observed at 460.3 and 466 eV whereas in Er^{3+} doped TiO_2, the corresponding Ti^{4+} peaks are obtained at 458.9 and 464.7 eV (Figure 7.5A). In Figure 7.5A for bare TiO_2, the peak 460.3 eV attributes to the oxygen richness whereas in Er^{3+} doped TiO_2 same peak reduced to a value of 458.9 eV showing a reduction in oxygen vacancy.[20] The splitting of $2p_{3/2}$ and $2p_{1/2}$were found in both the samples at around 5.7-5.8 eV, which attributes the anatase phase purity of both TiO_2 samples.[21] Surface defects originate when Er^{3+} enters into the lattice of $TiO_2$and which is confirmed by the blue shifting in the binding energy *i.e.* 458.9 eV ($2p_{3/2}$) and 464.7 eV ($2p_{1/2}$). The peak at 458.9 eV reveals the presence of Ti^{3+}.[20] The decrease in valency of Ti explains the

presence of oxygen vacancies, which reveal the transformation of oxygen rich environment to oxygen deficient environment. From the O1s XPS (Figure 7.5B) it can be seen that the peak at 531.5 eV blue shifted to 530.13 eV indicates the change in oxygen environment. Figure 7.5C, the Er4d XPS reveals the incorporation of Er^{3+} into the crystal lattice. The Er4d peak had a greater degree of complex peak shape than that based on the simple spin–orbit splitting, due to final state multiplet splitting effects arising from interactions of 4d and 4f states,[22]very large due to the same principal quantum number of the two shells.[23,24] The main band was centered at an average BE of 169.9 eV. The BE of the absolute maximum is relatively close to the values reported for Er (III) oxide.[22,24]As evidenced from XRD, even though the ionic radius of Er^{3+} (103pm) is far greater than Ti^{4+} (74.5pm), Er^{3+} entered into the crystal lattice of TiO_2 and those ions occupy the interstitial position of TiO_2.

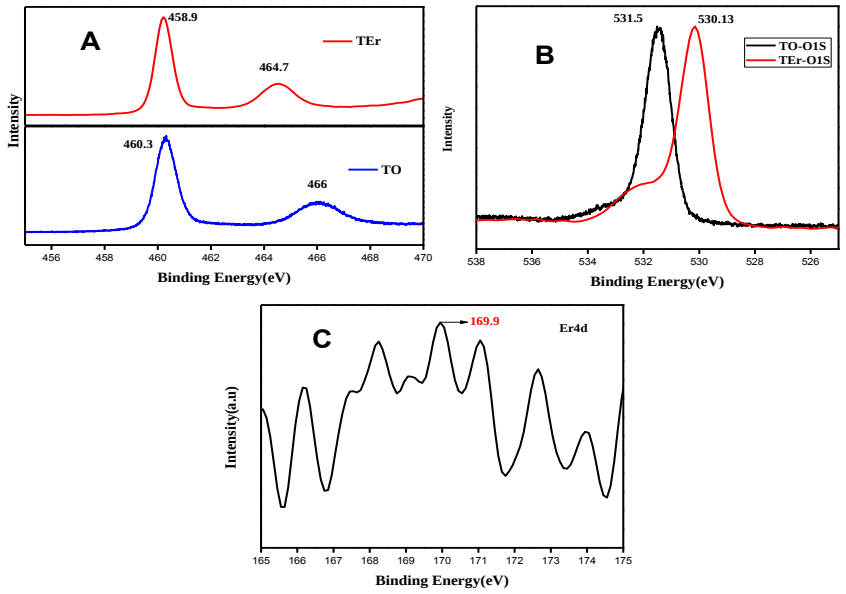

Figure 7.5. XPS of A) Ti2p, B) O1s and C) Er4d.

7.2.6. Transmission Electron Microscopy (TEM)

Figure 7.6 shows TEM images of TiO_2 and TEr1 calcined at 500 ˚C. TiO_2 shows a particle size of 19-23 nm (Figure 7.6a) at 500 ˚C. On the other hand, the Er^{3+} doped TiO_2 has a particle size of 7-13 nm (Figure 7.6b), and thus the TEM observations support the conclusions derived from the XRD data *i.e.* the particle size is reduced as result of Er^{3+} doping in TiO_2. The electron diffraction image of TEr1 calcined at 500 ˚C shows broad band due to the Scherrer line broadening which is attributed to the small crystalline size,[25,26] however TiO_2, at same temperature, showed distinct spots due to the high crystallinity and larger size of the crystals.

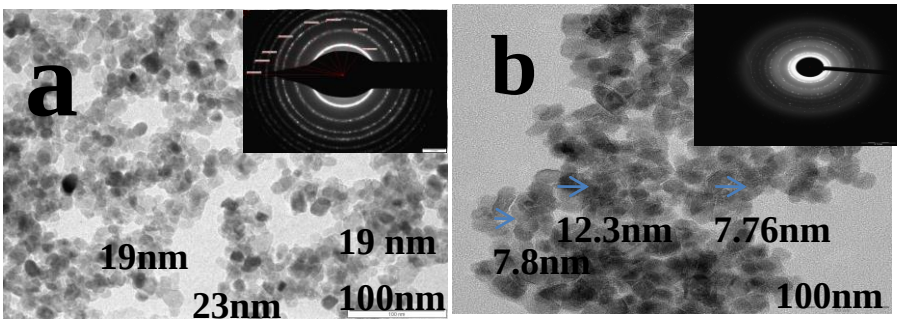

Figure 7.6. TEM image of a) TiO_2 and b) TEr1 at 500 ˚C.

7.2.7. Energy Dispersive Spectroscopy (EDS)

Chemical composition of TiO_2 and TEr1wasdetermined using EDS analysis (Figure 7.7). Strong X-ray peaks associated with Ti and oxygen are present in TiO_2 where as strong peaks of Er were found in the TEr1 along with Ti and oxygen. That confirms the presence of both Ti and Er in the lattice of TEr1.

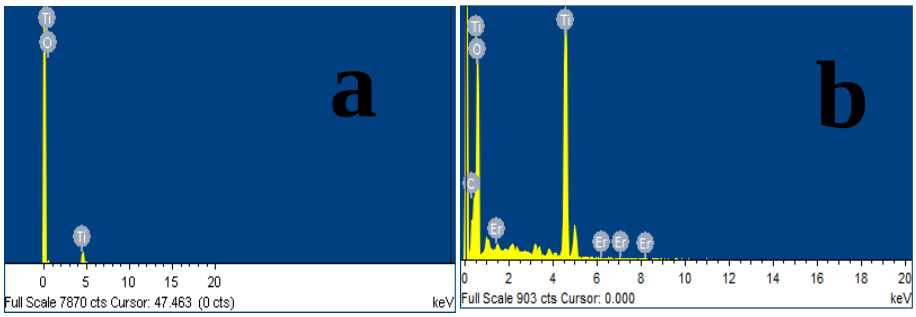

Figure 7.7. Energy Dispersive Spectroscopy (EDS) of a) TiO_2 and b) TEr1 at 500 ˚C.

7.3 Photocatalysis

Photocatalytic activity of both TiO_2 and TEr1 calcined at 500 ˚C for methylene blue degradation under UV and sunlight were carried out and the rate constant obtained from the degradation kinetics were briefed in Table 7.3. From Table 7.3 it can be seen that photocatalytic activity of pure TiO_2 and TEr is influenced by the calcination temperature. Rate of degradation under direct sunlight irradiation and UV light irradiation of Er^{3+} modified $TiO_2$is more than that of pure TiO_2 except in lower temperature. This is because upon Er^{3+} ion doping, the light absorption capacity of TiO_2 increases from UV to visible region in accordance with band gap lowering. The rate constant obeys the first order kinetics and the values are summarized in the Table 7.3, among the different TEr, highest activity was obtained for TEr1 calcined at 500 ˚C, with a rate constant of 0.121 min^{-1}. Which is more than 3 times higher than the bare TiO_2 (0.036 min^{-1}). Absorption spectra of methylene blue dye degradation under UV light using TiO_2 and Er^{3+} doped TiO_2 at 500 ˚C were shown in Figure 7.8and 7.9. TEr1 calcined at 500 ˚C degraded completely within 25 minutes. From the results it can be concluded that

the TEr1 calcined at 500 ˚C is the best photocatalyst among the samples under UV light irradiation.

The visible light activity of TiO_2 and TEr under direct sunlight using the methylene blue degradation experiment was carried out and the time taken for degradation of methylene blue using TiO_2 and TEr under visible light was also shown in Table 7.3. From the Table 7.3, it is found that Er^{3+} doped TiO_2 sample undergo methylene blue degradation much faster than compared to TiO_2 at all calcinations temperatures under visible light irradiation. The rate constant was calculated from the first order kinetics and is shown in Table 7.3. Among the doped samples highest activity was obtained for TEr1 sample calcined at 500 ˚C with a rate constant of 0.123 min^{-1} which is almost 10 times higher than the pure TiO_2 (0.013 min^{-1}). Absorption spectra of methylene blue dye degradation under visible light using TiO_2 and TEr1 doped TiO_2 at 500 ˚C were shown in Figure 7.10 and 7.11. TEr1 calcined at 500 ˚C degraded completely within 30 minutes. The results point out that TEr1 calcined at 500 ˚C is the best photocatalyst among samples under visible light irradiation.

Table 7.3. Rate constant of TiO_2 and TEr calcined at different temperatures.

UV light				**Sunlight**			
Sample	**300 ˚C**	**500 ˚C**	**700 ˚C**	**Sample**	**300 ˚C**	**500 ˚C**	**700 ˚C**
TiO_2	0.021	0.036	0.003	TiO_2	0.007	0.013	0.004
TEr0.5	0.038	0.102	0.052	TEr0.5	0.006	0.074	0.067
TEr1	0.017	**0.121**	0.119	TEr1	0.005	**0.123**	0.098
TEr2	0.009	0.111	0.062	TEr2	0.08	0.091	0.060
TEr5	0.007	0.081	0.070	TEr5	0.011	0.067	0.064
TEr10	0.012	0.042	0.037	TEr10	0.012	0.044	0.038

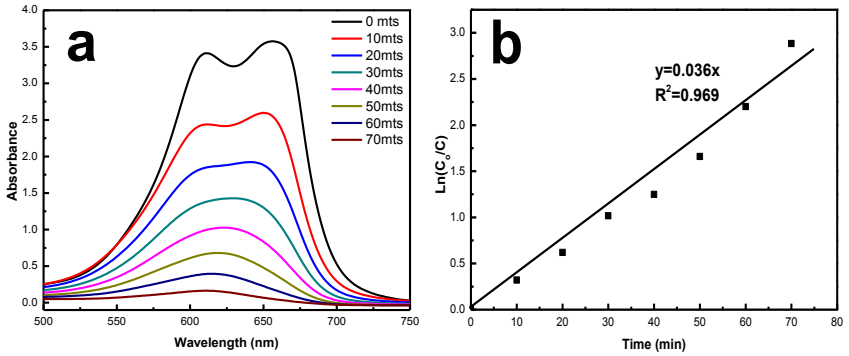

Figure 7.8. Absorption spectra and Kinetic study of methylene blue dye degradation under UV using TiO_2 sample calcined at 500 ˚C.

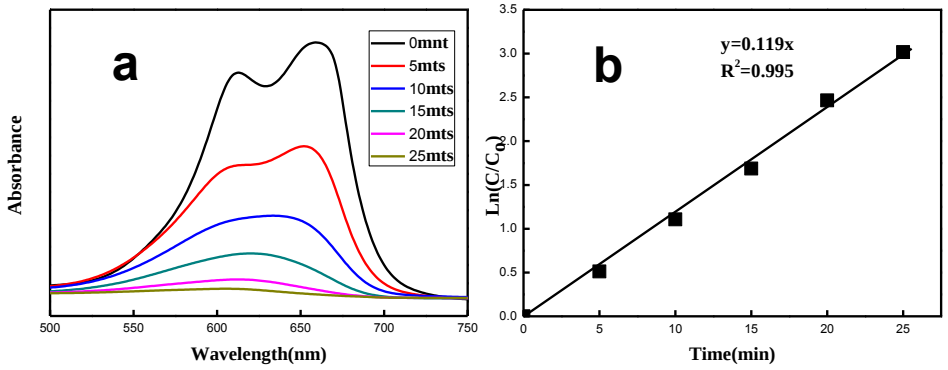

Figure 7.9. Absorption spectra and Kinetic study of methylene blue dye degradation under UV using TEr1 calcined at 500 ˚C.

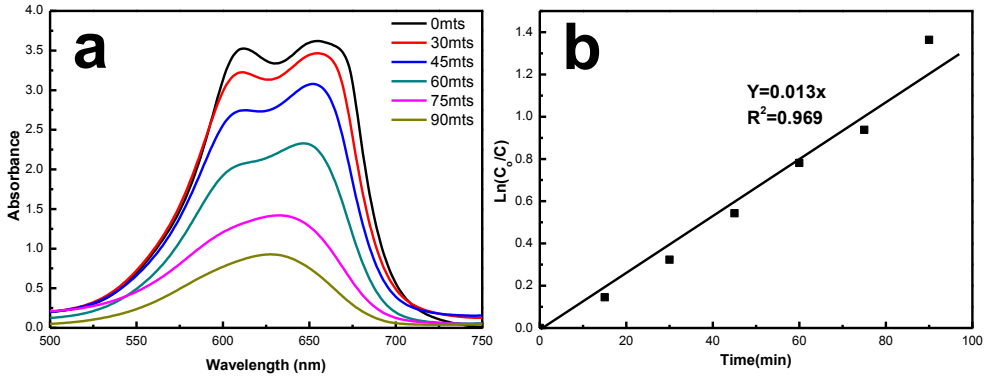

Figure 7.10. Absorption spectra and Kinetic study of methylene blue dye degradation under direct sunlight using Ti sample calcined at 500 ˚C.

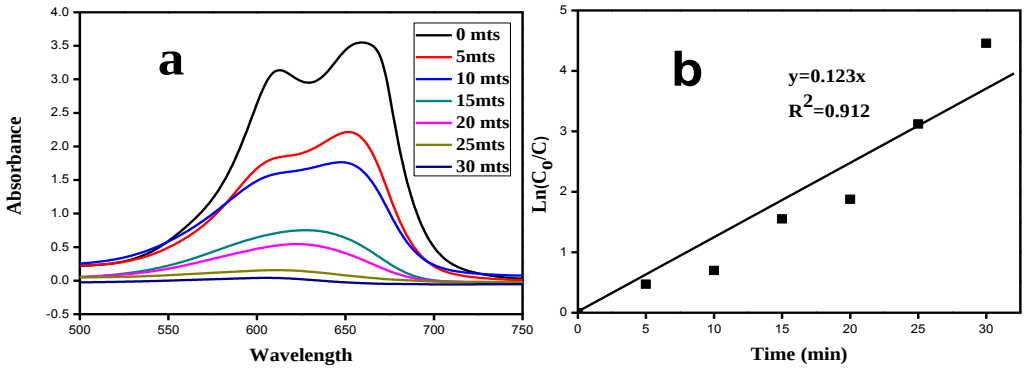

Figure 7.11. Absorption spectra and Kinetic study of methylene blue dye degradation under direct sun light using TEr1 sample calcined at 500 ˚C.

7.4 Conclusions

Nanocrystalline TiO_2 and Er^{3+} doped TiO_2 were synthesized *via* a modified sol-gel strategy. These nano materials are well characterised with FT-IR, XRD, Raman spectroscopy, XPS, SEM and TEM. XRD and TEM study proved the nanocrystalline nature of TiO_2 and Er^{3+} doped TiO_2 and reduction in size of the nano particles as result of Er^{3+} doping in bare TiO_2. XPS study revealed that on introducing Er^{3+} into the crystal lattice of oxygen rich TiO_2 nanocrystals the environment was transmuted from oxygen richness to oxygen deficiency as evidenced by XPS peak shifting. These TiO_2 and Er^{3+} doped TiO_2 nanoparticles calcined at various temperatures were subjected to photocatalytic study under UV and solar illuminations using methylene blue. It was found that TEr1 calcined at 500 ˚C has shown the maximum photoactivity under both UV and sunlight illumination.

7.5. References

1. C. Karunakaran and R. Dhanalakshmi, *Sol. Energy Mater. Sol. Cells*, 2008, 92, 588.

2. R. Xu, J. Li, J. Wang, X. Wang,B.Liu , B. Wang, X. Luan and X. Zhang, *Sol. Energy Mater. Sol. Cells*, 2010,94,1157.

3. M.R. Hoffmann, S. T. Martin, W. Choi and D.W. Bahnemann, *Chem. Rev.*,1995, 95 , 69.

4. P. Periyat, B. Naufal and S. G. Ullattil, *Mater. Sci. Forum*, 2016, 855, 78.

5. Z.L. Ma, G.F. Huang, D.S. Xu, M.G. Xia, W. Q. Huang and Y. Tian, *Mater. Lett.* , 2013, 108, 37.

6. H. Li, Y. Sheng, H. Zhang, J. Xue, K. Zheng, Q. Huo and H. Zou, *Powder Technol.* 2011, 212, 372.

7. Q. Shang, H. Yu, X. Kong, H. Wang, X. Wang, Y. Sun, Y. Zhang and Q. Zeng, *J. Lumin*, 2008, 128, 1211.

8. Y. L. Zheng and W.Z. Wang, *J. Solid State Chem.*, 2014, 210, 206.

9. J. Zhang, X. Wang, W.T. Zheng, X.G. Kong, Y.J. Sun and X. Wang, *Mater. Lett.*, 2007, 61, 1658.

10. X.G. Mao, B.X. Yan, J. Wang and J. Shen, *Vacuum*, 2014, 102, 38.

11. Y. Lia, Y.Wanga, J. Konga and J.Wanga,*Appl. Surf. Sci.*, 2015, 328, 115.

12. [1]X. Zou, F. Zhang, S. Thomas, Prof. G. Zhu, V. Valtchev and S. Mintova, *Chem. Eur. J.*, 2011, 17, 12076.

13. D. G. Huang, S. J. Liao, W. B. Zhou, S. Q. Quan, L. Liu, Z. J. He and J. B. Wan, *J. Phys. Chem. Solids*, 2009, 70, 853.

14. M. F. Hou, F. B. Li, R. F. Li, H. F. Wan, G. Y. Zhou and K. C. Xie, *J. Rare Earths*, 2004, 22, 542.

15. C. H. Liang, F. B. Li, C. S. Liu, J. L. Lu and X. G. Wang, *Dyes Pigm.*, 2008, 76, 477.

16. J. Yan, G. Wu, N. Guan, L. Li, Z. Li and X. Cao,. *Chem. Chem. Phys.*, 2013, 15, 10978.

17. W. Ma, Z. Lu and M. Zhang, *Appl. Phys. A*, 1998, 66, 621.

18. Z. Lu, C. T. Yip, L. Wang, H. Huang and L. Zhou, *Chem. Plus. Chem*, 2012**,** 77, 991.

19. J. Reszczy´nskaa, T. Grzyb, J. W. Sobczak, W. Lisowski, M. Gazda, B. Ohtani and A. Zaleska, *Appl. Surf. Sci.*, 2014, 307, 333.

20. S. G. Ullattil and P. Periyat, *Nanoscale*, 2015, 7, 19184.

21. R. Ren, Z. Wen, S. Cui, Y. Hou and X. Guo, *J. Chen, Sci. Rep.*, 2015, 5, 10714.

22. H. Ogasawara, A. Kotani and B. T. Thole, *Phys. Rev. B: Condens.Matter*, 1994, 50, 12332.

23. D. Barreca, A. Gasparotto, A. Milanov, E. Tondello, A. Devi and R.A. Fischer, *Surf. Sci*., 2007, 14, 52.

24. A. P. Milanov, R. W. Seidel,D. Barreca, A. Gasparotto, M. Winter, J. Feydt, S. Irsen, H.W. Becker and A. Devi, *Dalton Trans*.,2011, 40, 62.

25. E. Borgarello, J. Kiwi , M. Gratzel, E. Pelizzetti and M. Visca, *J. Am. Chem. Soc.*,1982, 104 2996.

26. K. V. Baiju, C. P. Sibu, K. Rajesh, P. K. Pillai, P. Mukundan, K. G. K. Warrier and W. Wunderlich, *Mater. Chem. Phys.*, 2005, 90, 123.

8 Chapter

Self Cleaning and pesticide degradation properties of rare earths doped TiO_2 photocatalyst.

Contents

8.1 Introduction

In this chapter we successfully demonstrating the application of the rare earth doped TiO_2 photocatalyst discussed in chapter 3, 4, 5, 6 and 7 for two practical applications. First application is to utilize best active rare earth doped TiO_2 photocatalyst to develop as a self-cleaning coating on glass bottle to purify the dye contaminated water using the UV/normal sunlight. Second application is to utilize the rare earth doped TiO_2 for the degradation of the pesticide "karate" an organo chlorine pesticide commonly used by the farmers of Kerala.

Photocatalytic materials such as TiO_2, ZnO, CeO_2 *etc.* have attained much relevance in the last few years due to their potential applications in fields such as photo-induced removal of pollutants from water and air, self-cleaning and antibacterial materials.[1,2] TiO_2 is one such photocatalyst due to its high photoactivity, low cost, low toxicity and good chemical and thermal stability.[3,4] Pure TiO_2 cannot utilize the entire light from solar spectra, which results in very low photocatalytic efficiency in day light. As discussed in the chapter 3, 4, 5, 6 and 7 rare earth metal ion (Sm^{3+}, Dy^{3+}, Er^{3+}, Yb^{3+}, Nd^{3+}) doping increased photocatalytic activity of TiO_2 from UV light to visible/normal sunlight and increased photocatalytic efficiency of TiO_2.

The photocatalytic and super hydrophilic properties of TiO_2 discussed in the chapter 1 introduction as section 1.8 and 1.10 can combine together to make for the application of self-cleaning coatings for the

control of organic contaminants such as dyes. These coatings can decompose organic contaminations with the aid of ultraviolet/visible light/normal sunlight suggesting the application of TiO_2 as a novel 'self-cleaning' material. Obviously this technique will have great value because it utilizes the available free solar energy along with nanomaterials coating which undergo self-cleaning process without using any chemicals such as detergents, soaps *etc*. With the help of a stream of water it is able to remove the stain of organic contaminates present on the substrate. Here we have attempted to develop self-cleaning glass bottle to produce clean water from water contaminated with organic dyes such as methylene blue.

Organic pollutants in water shows the presence of non-biodegradable compounds, which can withstand for long period in the environment and act as a risk to the aquatic and mammalian life.[5] The possibility of access of pesticides into water sources are follows: (i) industrial waste or effluents expelled directly into water (ii) seepage from buried toxic wastes into water supplies and (iii) contamination of surface and groundwater directly or from runoff during spraying operations.[6]One of the other major sources for water pollution is the excreting solutions produced during the formulation, dilution, mixing, transfer and application of commercial pesticides may pollute the waste water lines and may reach the sources of fresh water.[7]The amount of pesticides custom applied to agricultural commodities has dramatically increased in recent years which have led to serious anxiety about the increasing risks to human health. The use and production of several organic pesticides has continuously risen since introduction of DDT in the

early 1940s, giving as a result a great family of organo chlorine pesticides.The consequence of the wide spread use and availability of pesticides is the problem of accidental or intentional poisoning. A wide variety of organic compounds are disposed to the water system from various sources such as industrial effluents, agriculture runoffs and chemical spills. Various awareness programs are conducted by authorities and social organizations for the protection of environment from hazardous wastes *etc.* Many conventional techniques were used for the removal of hazardous waste from water. Among the different techniques advanced oxidation technology of photocatalytic degradation with semiconductor oxides is the promising one. TiO_2 and its modified forms have shown to be very active photocatalyst and useful for destroying a wide range of environmental contaminants.

A series of Sm^{3+}, Dy^{3+}, Er^{3+}, Yb^{3+}, Nd^{3+} doped TiO_2 were synthesized using sol-gel method as discussed in chapter 3, 4, 5, 6 and 7 and subjected to study the photocatlytic activity. The best photocatalyst among the each of the dopant were selected for the above applications, *i.e.* TSm1, TDy1, TEr1 and TYb2 calcined at 500 ˚C and TNd1 calcined at 700 ˚C. The self-cleaning glass bottles coated with sol of active photocatalysts were subjected to study the photocatalytic activity under UV and direct sunlight. The photocatalytic degradation of organic pollutant, “karate” the pesticide commonly used in Kerala in aqueous medium was also studied under UV and direct sunlight irradiation using the photoactive catalysts.

8.2 Results and discussion

Glass bottles were coated using the TiO_2 sol of best active photocatalyst of TSm, TDy, TEr, TYb and TNd. Coating was made on the glass bottle as described in section 2.3 in the experimental section of chapter 2. The reason to make coating on the glass bottle is because when powder$TiO_2$was utilized as photocatalyst material, powder form has to be separated from water after photocatalytic reaction, limiting its practical application. Coating will make an excellent way, which gives the surface of glass bottle to self-cleaning function. This glass bottle coated with TSm2, TDy1, TEr1, TYb2 calcined at 500 ˚C and TNd1 calcined at 700 ˚C is filled with 10 ml of methylene blue solution and then irradiated under UV light in photoreactor. Dye degradation was recorded using photography through color change (Figure 8.1-8.5). From the figure it is clear that bottle coated with doped TiO_2 degrades the blue coloured methylene blue dye completely showing its self-cleaning activity. Similar experiment was carried out using normal sunlight (Figure 8.1-8.5). Under direct solar irradiation it degrades more rapidly than under UV light. The reproducibility of dye degradation was also checked. The dye got degraded at the same rate even after three consecutive irradiations. Similar dye degradation experiment was repeated for a glass bottle without any coating (Figure 8.1-8.5 B& D). The color of the dye remains the same after the irradiation of UV/direct sunlight.

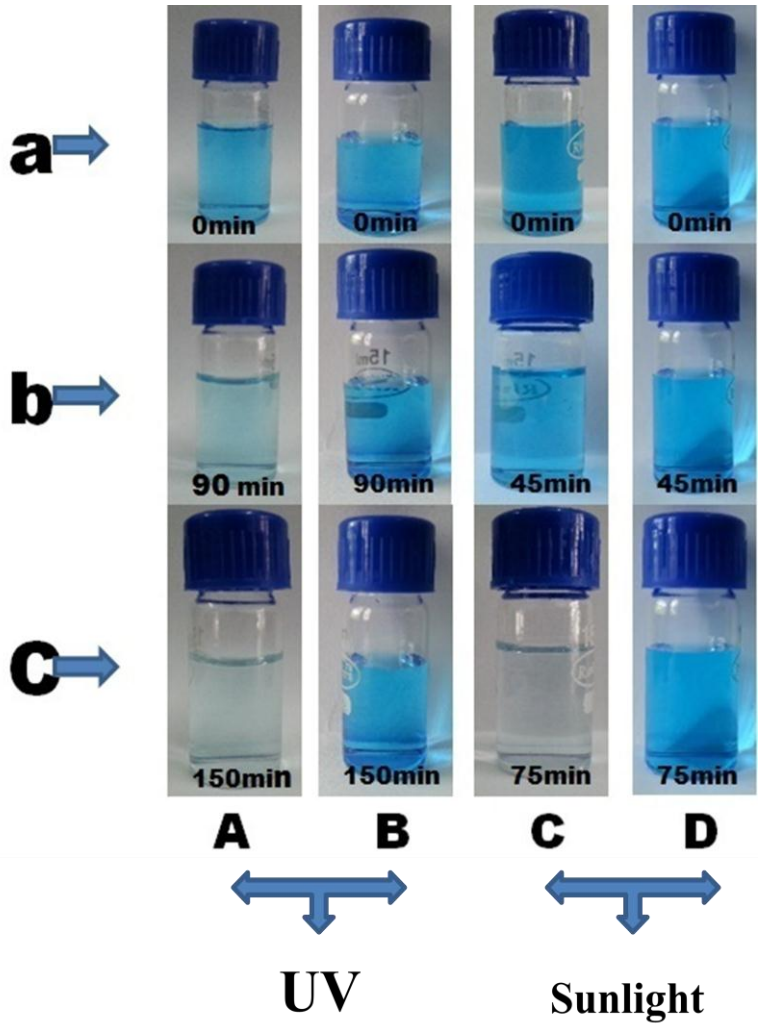

Figure 8.1 A) and C) glass bottle with TSm2 coating B) and D) glass bottle without coating under UV and sunlight illumination respectively at different time intervals.

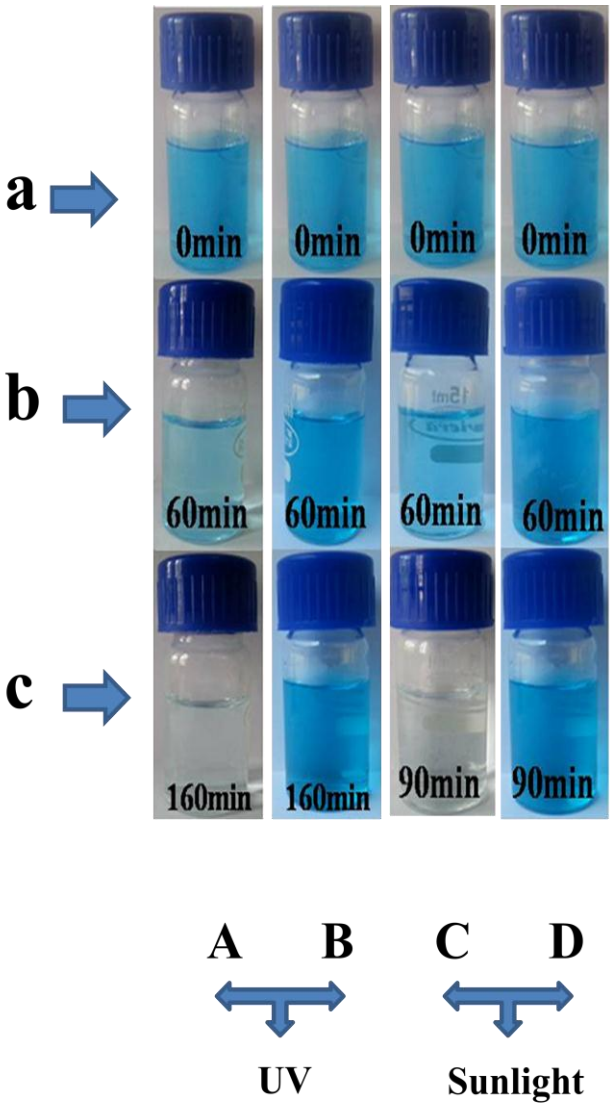

Figure 8.2 A) and C) glass bottle with TDy1 coating B) and D) glass bottle without coating under UV and sunlight illumination respectively at different time intervals.

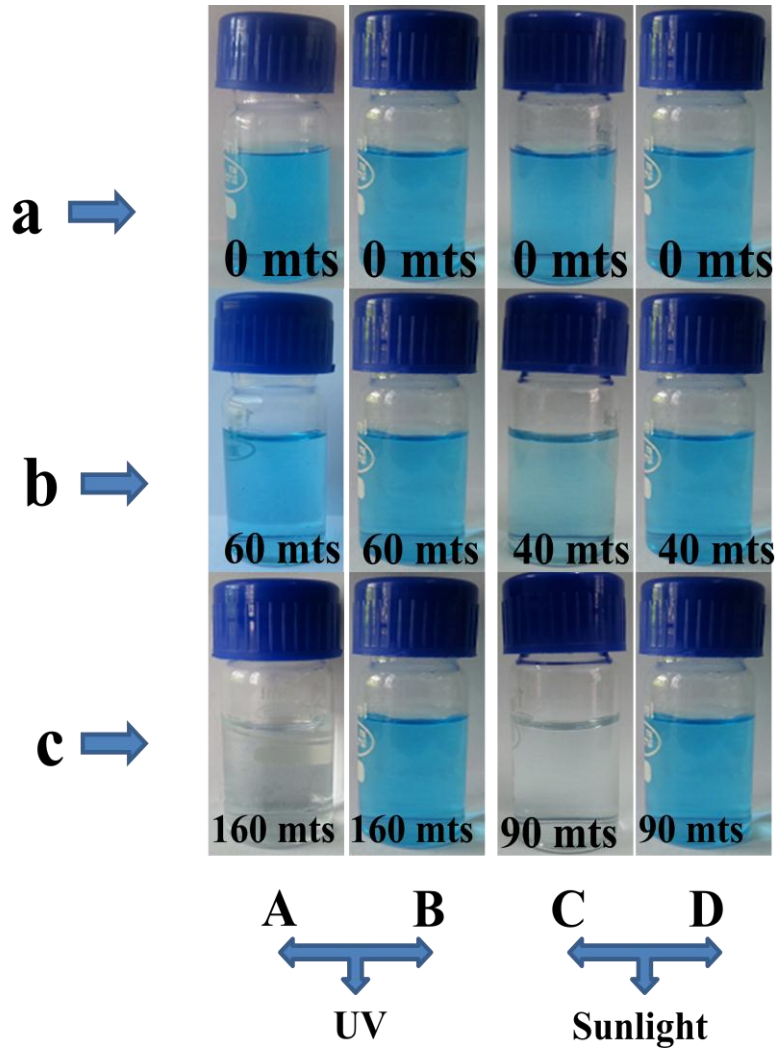

Figure 8.3 A) and C) glass bottle with TEr1 coating B) and D) glass bottle without coating under UV and sunlight illumination respectively at different time intervals.

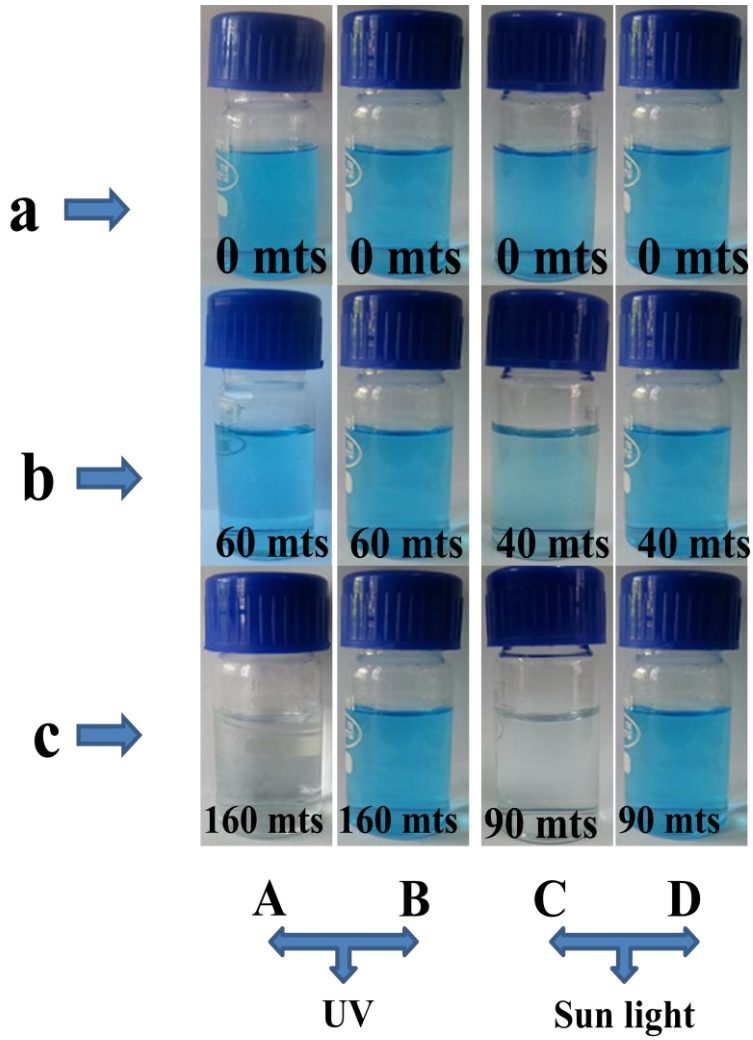

Figure 8.4 A) and C) glass bottle with TYb2 coating B) and D) glass bottle without coating under UV and sunlight illumination respectively at different time intervals.

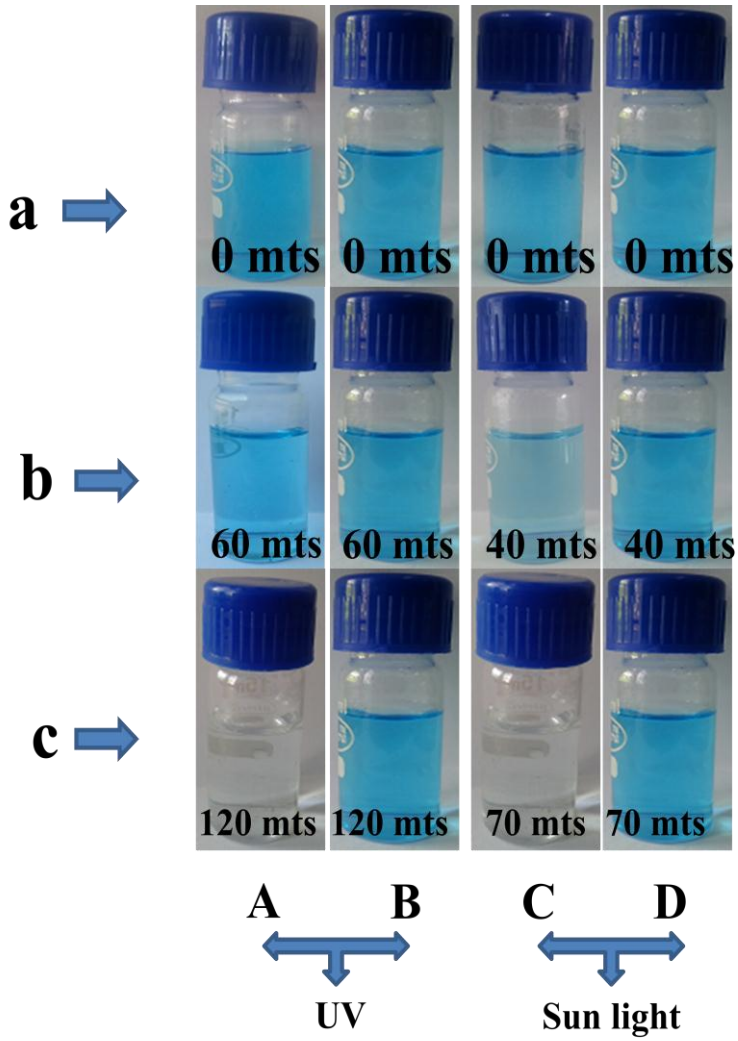

Figure 8.5 A) and C) glass bottle with TNd1 coating B) and D) glass bottle without coating under UV and sunlight illumination respectively at different time intervals.

Photodegradation of karate an organo chlorine pesticide (commonly used by the farmers of Kerala) were done using active catalysts TSm2, TDy1, TEr1, TYb2 calcined at 500 ˚C and TNd1 calcined at 700 ˚C under UV illumination. 50 ml of 1% karate solution with 0.1, 0.2, and 0.3g catalysts were irradiated under UV light in photoreactor. Pesticide degradation was recorded using photography through color change at different time intervals (Figure 8.6-8.10). Figure 8.6- 8.10 shows that the catalysts are ideal for degrading the pesticide. Similar experiment was carried out using normal sunlight with 0.3g doped TiO_2 photocatalyst loading (Figure 8.11). Under direct solar irradiation it degrades more rapidly than under UV light. A representative experiment was done using 0.3g TYb1 under sunlight and the degradation was checked by studying the difference in total organic carbon (TOC) of initial pesticide solution (Figure 8.12A) and final degraded solution (Figure 8.12B).The total organic carbon content of initial solution is 2581 ppm. After irradiation with sunlight it was declined to 669 ppm showing the faster degradation of karate (Table 8.1). This confirms that organic part of the pesticide gets degraded. The result also showed that about 75% of the pesticide was degraded with first 50 minutes under direct sunlight.

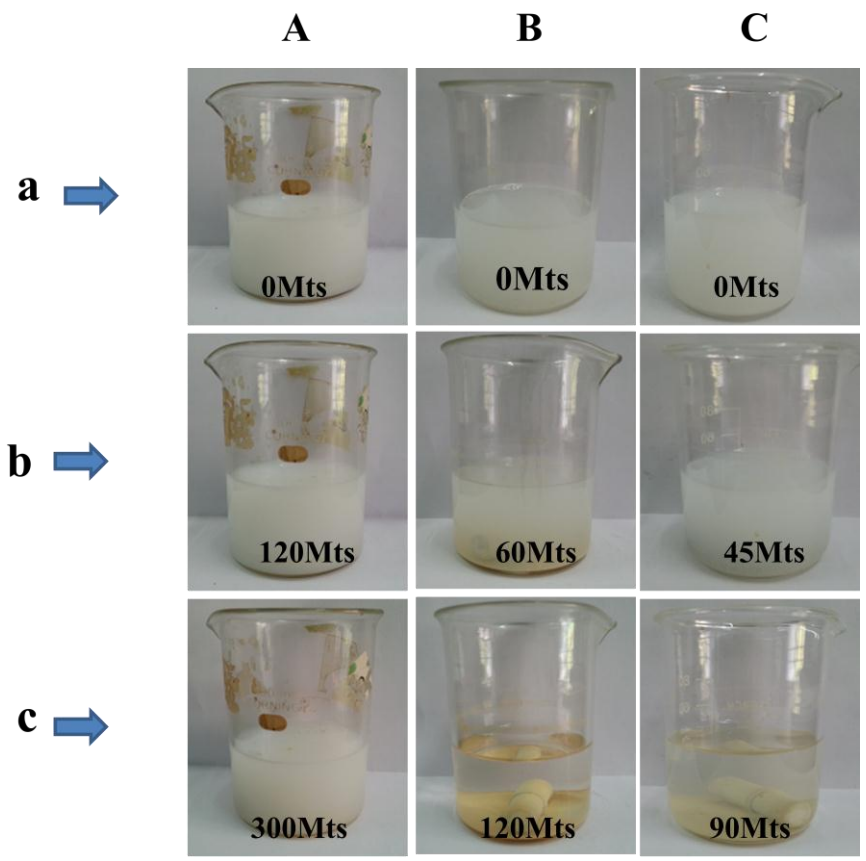

Figure 8.6 Photograph of degradation study of pesticide using (A) 0.1 gm (B) 0.2 gm (C) 0.3 gm TSm2 calcined at 500 ˚C under UV illumination at different time intervals.

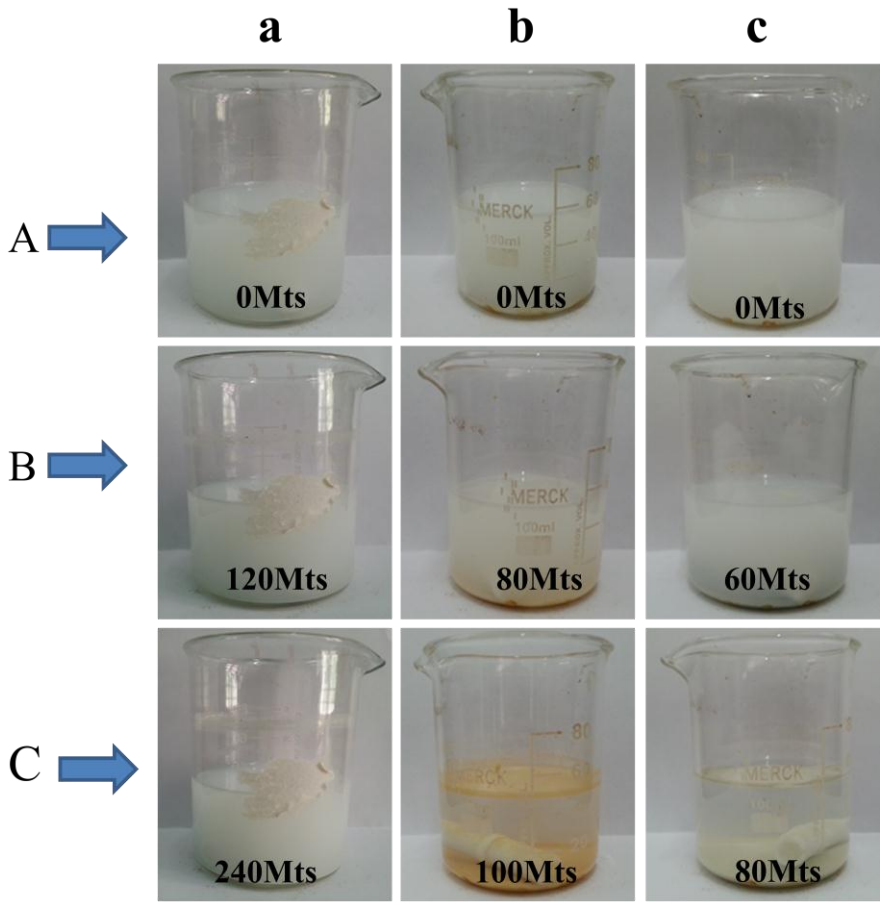

Figure 8.7 Photograph of degradation study of pesticide using (a) 0.1 gm (b) 0.2 gm (b) 0.3 gm TDy1 calcined at 500 ˚C under UV illumination at different time intervals.

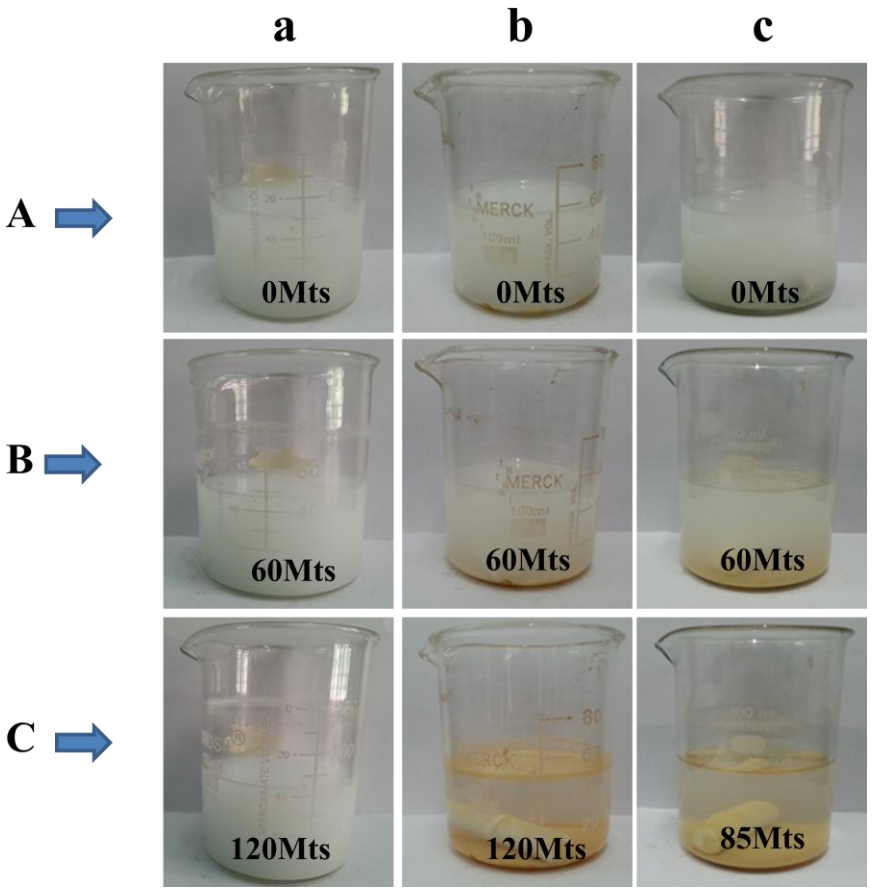

Figure 8.8. Photograph of degradation study of pesticide using (a) 0.1 gm (b) 0.2 gm (c) 0.3 gm TEr1 calcined at 500 ˚C under UV illumination at different time intervals.

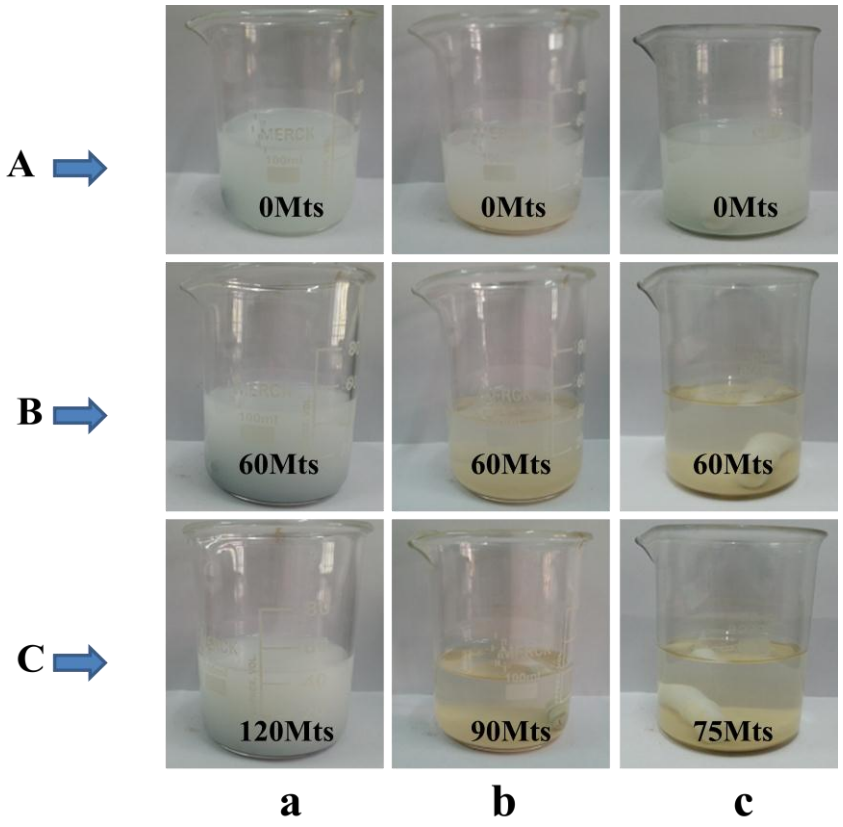

Figure 8.9. Photograph of degradation study of pesticide using (a) 0.1 gm (b) 0.2 gm (c) 0.3 gm TYb2 calcined at 500 ˚C under UV illumination at different time intervals.

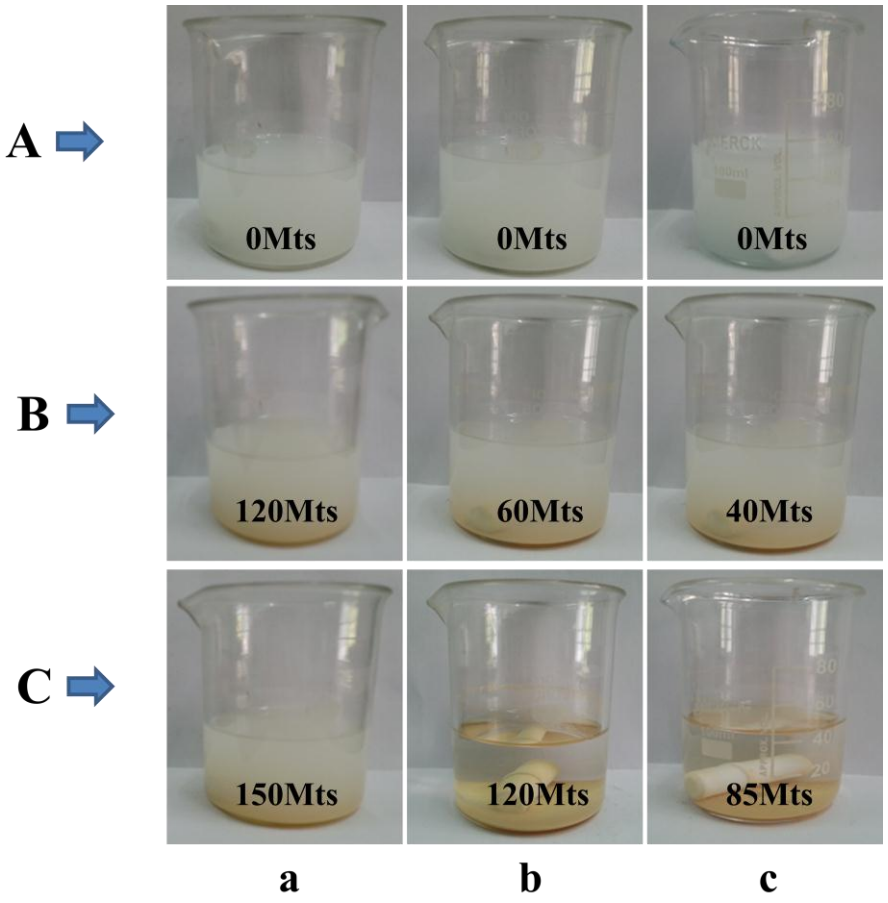

Figure 8.10. Photograph of degradation study of pesticide using (a) 0.1 gm (b) 0.2 gm (c) 0.3 gm TNd1 calcined at 700 ˚C under UV illumination at different time intervals.

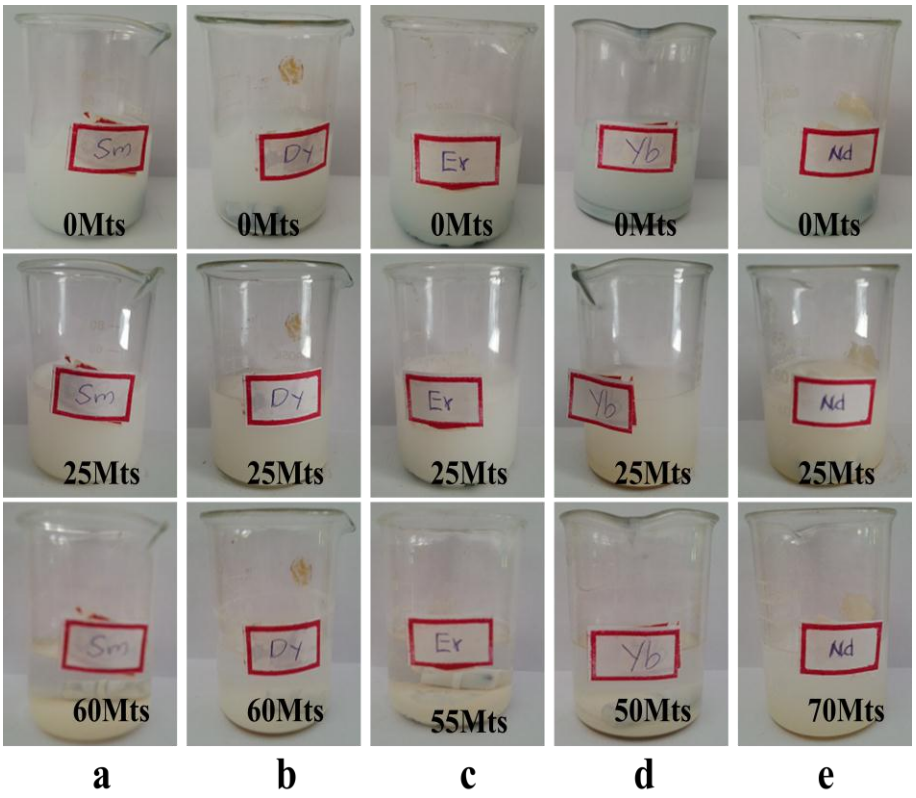

Figure 8.11. Photograph of degradation study of pesticide using 0.3 gm of (a) TSm2 (b) TDy1 (c) TEr1 (d) TYb2 (e) TNd1 under direct sunlight illumination at different time intervals.

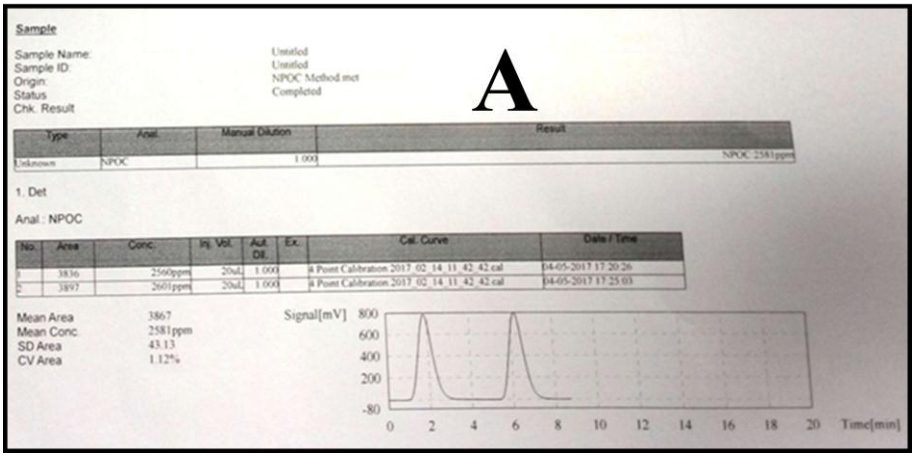

Figure 8.12. A) TOC data of initial pesticide solution.

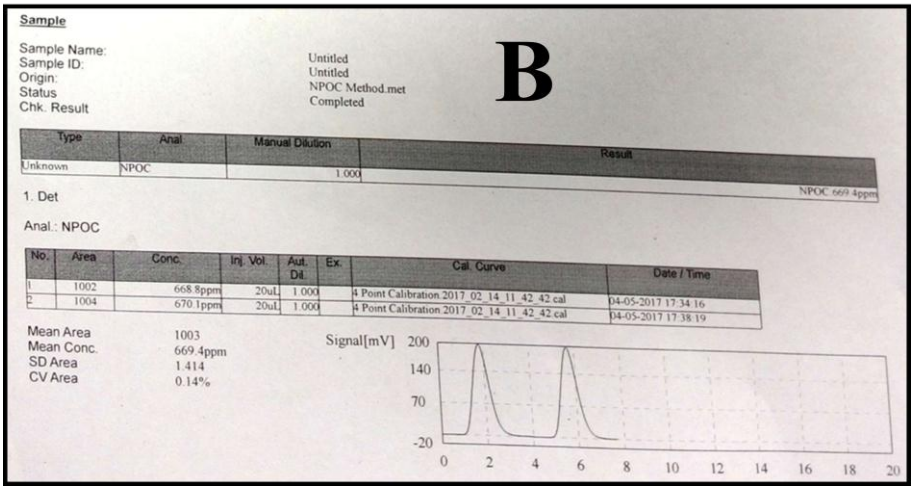

Figure 8.12 B) TOC data of pesticide solution after irradiation.

Table 8.1. TOC data of pesticide solution before and after irradiation.

Sl. No	Sample	Carbon concentration (ppm)
1	Initial pesticide solution	2581
2	Pesticide solution after degradation	669.4

8.4 Conclusions

Here we successfully demonstrated the application of the Sm^{3+}, Dy^{3+}, Er^{3+}, Yb^{3+} and Nd^{3+} doped TiO_2 photocatalyst discussed in chapter 3, 4, 5, 6 and 7 for two practical applications. In first application a self-cleaning coating on glass bottle to purify the dye contaminated water using the normal sunlight. In second application we achieved the degradation of a pesticide "karate" which is an organo chlorine pesticide commonly used by the farmers of Kerala using the Sm^{3+}, Dy^{3+}, Er^{3+}, Yb^{3+} and Nd^{3+} doped TiO_2 photocatalyst. Degradation was more effective in sunlight than UV light, which shows the possibility of using these Sm^{3+}, Dy^{3+}, Er^{3+}, Yb^{3+} and Nd^{3+} doped TiO_2 photocatalyst for the practical and industrial applications such as self-cleaning coating and decomposition of organic pesticides, water purification *etc*.

8.4 References.

1. C. Huang, H. Bai, Y. Huang, S. Liu, S. Yen and Y. Tseng, *INT J PHOTOENERGY*, 2012 ,2012.

2. E. Gonzalez, A. Bonnefond , M. Barrado , A. M. C. Barrasa, J. M. Asua and J. R. Leiza, *Chem. Eng. J*,2015,281, 209.

3. B. Naufal, P. K. Jaseela and P. Periyat, *Mater. Sci. forum*, 2016, 855, 33.

4. L. An-xian, L. Na, L. Xue and T. Chang-you, *J. Cent. South U*niv. *Technol.*2004, 11, 124.

5. L. S. Nikos, R. Despina, K. Eleftheria, M. Dionissios and P. X. Nikolaos, *Desalination*, 2010, 250, 351.

6. D. Branko and S. Matej, *Intern.J. Environ.Anal. Chem.*, 2007, 87, 1079.

7. E. Moctezuma., E. Leyva, E. Monreal, N. Viuuegas and D. Infante, *Chemosphere*, 1999, 39, 511.

9 Chapter

Summary

Overall Conclusion

The first part of chapter 1 explains the basics of nanoscience, semiconducting nanomaterials and its various applications. Second part gives a detailed and precise description about the TiO_2 semiconducting nanomaterials, various synthesis method and its photocatalytic applications along with a literature review on current development of TiO_2 photocatalyst.

Chapter 2 includes the procedure for the sol-gel synthesis of TiO_2 nanomaterials and various lanthanide ions (Sm^{3+}, Dy^{3+}, Yb^{3+} Nd^{3+}, Er^{3+}) doped TiO_2 nanomaterials and the characterisation technique used for the systematic study of all the samples. It also explains the detailed procedure used to compare the photocatalytic activity of various samples synthesised and the procedure adopted for making self-cleaning coating by selecting the best photocatalytic sample.

In working chapter 3,TiO_2 was doped with 1, 2, 5 &10 weight percentage of samarium ion (Sm^{3+}), calcined at 300, 500 and 700 °C and TSm2 calcined at 500 ˚C has shown the maximum photocatalytic activity under both UV and sunlight illumination.The augment activity was connected to the change of surface structure of TiO_2, the raise of ·OH radicals produced by the

unbalance charge, and the production of sub-band gap level by doping Sm^{3+}.

Chapter 4 reveals that Dysprosium ion (Dy^{3+}) with 0.5, 1, 2, 5 &10 weight percentage was doped, calcined at 300, 500 and 700 °C, 8among the various samples TDy1calcined at 500 ˚C has shown the maximum photocatalytic activity under both UV and sunlight illumination.

The chapter 5 discloses TiO_2 was doped with 1, 2, 5 &10 weight percentage of Ytterbium ion (Yb^{3+}), calcined at 300, 500 and 700 °C,the Photocatlytic activity of TYb2 is more in direct sunlight than in UV, which inference that the light absorption capacity of TiO_2 gets enhanced.

Chapter 6 imparts that Neodymium ion (Nd^{3+}) with 0.5, 1, 2, 5 &10 weight percentage was doped, calcined at 300, 500 and 700 °C, It was found that TNd1calcined at 700 ˚C has shown the maximum photoactivity under both UV and sunlight illumination.

Chapter 7 tells that Erbium ion (Er^{3+}) with 0.5, 1, 2, 5 &10 weight percentage was doped, calcined at 300, 500 and 700 °C,and was found that TEr1calcined at 500 ˚C has shown the maximum photocatalytic activity under both UV and sunlight illumination.The comparison of the best photocatalytically active sample among the different rare earth ion doped were shown in the Table 9.1.

Table 9.1. Comparison of the photocatalytic activity of the different rare earth ion doped TiO_2.

Comparison of the rate of degradation of most active catalysts			
Sl.No	**Catalysts**	**Rate constants (min^{-1})**	
		UV	**Direct Sun Light**
1	**TiO_2 calcined at 500 °C**	**0.036**	**0.013**
2	TSm2 calcined at 500 °C	0.092	0.103
3	TDy1 calcined at 500 °C	0.145	0.141
4	**TYb2 calcined at 500 °C**	**0.149**	**0.151**
5	TNd1 calcined at 700 °C	0.128	0.123
6	TEr1 calcined at 500 °C	0.121	0.123

In summary a modified sol-gel strategy has been developed for the synthesis of TiO_2 and various lanthanide ion (Sm^{3+}, Dy^{3+}, Yb^{3+} Nd^{3+}, Er^{3+}) doped TiO_2 nanoparticles. As synthesized nanomaterials are well characterized with X-Ray Diffraction, FT-IR, FT-Raman spectroscopy, Diffuse Reflectance Spectra, X-Ray Photoelectron Spectroscopy, Scanning Electron Microscope and Transmission Electron Microscope. Crystallite size calculation from XRD showed that the crystallite size is decreased as a result of rare earth ions doping and is further supported by TEM also. On introducing ions into the crystal lattice of oxygen rich TiO_2 nanocrystals environment was changed from oxygen richness to

oxygen deficiency *i.e.* rare earth ions induced oxygen deficiency in the crystal lattice of TiO_2. These TiO_2 nanoparticles with oxygen richness and oxygen deficiency (doped and undoped) were subjected photocatalytic degradation of methylene blue dye under UV and solar illuminations and degradation kinetics were systematically examined.

In the final working chapter we successfully demonstrated the two practical applicationsof the Sm^{3+}, Dy^{3+}, Er^{3+}, Yb^{3+} and Nd^{3+} doped TiO_2 photocatalyst discussed in chapter 3, 4, 5, 6 and 7 for. In first application a self-cleaning coating on glass bottle to purify the dye contaminated water using the normal sunlight. In second application we achieved the degradation of a pesticide “karate” which is an organo chlorine pesticide commonly used by the farmers of Kerala using the Sm^{3+}, Dy^{3+}, Er^{3+}, Yb^{3+} and Nd^{3+} doped TiO_2 photocatalyst.Degradation was more effective in sunlight than UV light, which shows the possibility of using these Sm^{3+}, Dy^{3+}, Er^{3+}, Yb^{3+} and Nd^{3+} doped TiO_2 photocatalyst for the practical and industrial applications such as self-cleaning coating and decomposition of organic pesticides, water purification *etc*.

Solar Energy 155 (2017) 1380–1388

Contents lists available at ScienceDirect

Solar Energy

journal homepage: www.elsevier.com/locate/solener

A dual function nanocrystalline TiO_2 platform for solar photocatalysis and self cleaning application

Binu Naufal [a], Sanjay Gopal Ullattil [a,b], Pradeepan Periyat [a,c,*]

[a] Department of Chemistry, University of Calicut, Kerala 673635, India
[b] Department of Nanoscience & Technology, University of Calicut, Kerala 673635, India
[c] Department of Chemistry, Central University of Kerala, Kasaragod 671314, India

ARTICLE INFO

Article history:
Received 19 May 2017
Received in revised form 1 August 2017
Accepted 2 August 2017

Keywords:
Sol–gel
TiO_2
Sm^{3+} doping
Defects
Ti^{3+} doping
Photocatalysis

ABSTRACT

Nanocrystalline anatase TiO_2 and Sm^{3+} doped TiO_2 having defective and non-defective nature were synthesised and systematically examined as photocatalysts with a function of dopant present (1, 2, 5 and 10 wt%) and temperature at 300, 500 and 700 °C using methylene blue dye as model system. A bare TiO_2 nanocrystal has shown oxygen richness and while incorporating Sm^{3+}, oxygen deficiency was induced along with a significant enhancement in the overall photocatalytic activity. Photocatalytic study showed that the Sm^{3+} doped TiO_2 nanostructure calcined at 500 °C with higher defects at the nanosurface has the highest activity under both UV and sunlight irradiation. Finally a dual function nano TiO_2 platform were demonstrated using Sm^{3+} doped TiO_2 sol coated self-cleaning glass bottle.

1. Introduction

Semiconducting TiO_2 nanomaterials have received considerable attention because of their structural, electronic and optical properties and finds potential applications such as photocatalysts, selective photocatalysis and as self-cleaning agents in the form of nanocoatings and nanoceramic membranes (Bahnemann, 2004; Smitha et al., 2016; Chen et al., 2003; Ullattil and Periyat, 2017). Among the various nanocrystallites, TiO_2 is one of the most investigated materials because of their low cost, low toxicity and good chemical and thermal stability. TiO_2 has three phases namely anatase, rutile and brookite where anatase is the most unambiguously accepted phase of TiO_2 in the area of photocatalysis and is widely accepted for its potential application in the complete mineralization of many toxic and non-biodegradable organic pollutants (Natarajan et al., 2014; Fujishima et al., 2000; Hoffmann et al., 1995; Li and Li, 2001; Liang et al., 2008). Generally a photocatalytic reaction takes place initially by the excitation of electron from valence band (VB) to conduction band (CB) of the TiO_2 material that generates holes at the valence band and an excess electron at the conduction band. The oxidation and reduction occur at the VB and CB respectively leading to the formation of super oxide ($O_2^{-\cdot}$) and $OH^{\cdot}$ that facilitate the photomineralization of organic pollutants.

TiO_2 has mainly two drawbacks in achieving high photocatalytic efficiency, the fast electron hole recombination and the limited absorption in the solar spectrum. In order to overcome these drawbacks, various modifications were suggested *via* metal/non-metal doping (Muruganandham and Swaminathan, 2006; Choi et al., 1994; Jin and Shiraishi, 2004; Paola et al., 2002; Wang et al., 2001; Yu et al., 2003a), coupling with low band semiconducting systems (Yu et al., 2003b; Hattori et al., 2000), noble metal deposition (Wang and Xu, 2005; Iliev et al., 2006; Ranjit et al., 2001; Xiaoli et al., 2005; Xie et al., 2005) *etc*. Nanocrystalline TiO_2 doped with rare earth cations were reported by various groups (Ranjit et al., 2001; Xie et al., 2005; Zhang et al., 2005) using different methods. They found that the presence of incomplete f orbital and empty d orbital of rare earth elements will promote the catalytic activity of TiO_2. For *e.g.* Sm^{3+}, Nd^{3+}, Pr^{3+} doped TiO_2 exhibited higher photocatalytic activity in comparison to bare TiO_2 under UV light (Yang et al., 2002; Xiao et al., 2007; Shi et al., 2008). All these methods are using costly chemicals, expensive templates for giving morphology to TiO_2, and finally harsh chemical treatment has to be employed to give crystallinity and shape for TiO_2. Self-cleaning materials can also be achieved by TiO_2 coating on glass surface, textiles *etc* (Park et al., 2013; Gonzalez et al., 2015). In presence of sunlight this coating will clean the surfaces of glass and textile by removing the organic

* Corresponding author at: Department of Chemistry, Central University of Kerala, Kasaragod, Kerala 671314, India.
E-mail addresses: pperiyat@uoc.ac.in, pperiyat@cukerala.ac.in (P. Periyat).

http://dx.doi.org/10.1016/j.solener.2017.08.005
0038-092X/

pollutants and dirt (Parkin and Palgrave, 2005; Smits et al., 2013). Here we report a facile and modified sol-gel method to synthesise Sm^{3+} doped TiO_2 and its application by demonstrating a self-cleaning glass bottle for polluted water purification.

2. Experimental

2.1. Preparation of TiO_2 and Sm^{3+} doped TiO_2

For the synthesis of nano TiO_2 sol, chemicals used were titanium isopropoxide ($Ti(OPr)_4$) (Aldrich 97%), $Sm(NO_3)_3$ (Aldrich 99.9%), glacial acetic acid (Aldrich 99.8%) and de-ionized water. Initially, $Ti(OPr)_4$ was mixed with glacial acetic acid in the ratio 1:10 where acetic acid is used as a stabilizing agent. This is followed by the addition of de-ionized water in small quantity with constant stirring. The overall ratio of $Ti(OPr)_4$: acetic acid: water is 1:10:100. A white sol is obtained after continuous 3 h stirring. For Sm^{3+} doped TiO_2 synthesis, calculated amount of samarium nitrate with different weight percentage (1, 2, 5 and 10%) were added to the TiO_2 sol and the same procedure was followed. The samples were named as TSm1, TSm2, TSm5 and TSm10. The xerogel is made from the above sol by drying on a water bath. The dried powder was calcined at various temperatures (300, 500 and 700 °C) at a heating rate of 5 °C per minute and held at this temperature for 2 h.

X-ray diffraction (XRD) patterns were obtained using Rigaku Miniflex 600 X-ray diffractometer with CuKα radiation. Raman measurements were taken using a MultiRAM spectrometer. The FT IR spectra were measured using a Jasco-FT/IR-4100 spectrometer in the wave number range 4000–400 cm^{-1}. The diffuse reflectance spectra (DRS) were taken using a Jasco-V-550 UV/VIS spectrophotometer. Scanning Electron Microscope (Hitachi, SU-66000) and Transmission electron microscopy (JEOL 2011) of the samples were performed to find out the morphology of the samples. The photocatalytic experiments were performed using the reported procedure earlier (Smits et al., 2013; Naufal and Periyat, 2016) by taking 0.1 g of TiO_2 powder as catalyst in 50 mL of methylene blue solution having a concentration of 1×10^{-4} M.

2.2. Coating on glass bottle

In order to make the nano coating on the normal glass bottle to study the self-cleaning activity, the best photoactive sol sample (2% Sm^{3+} doped TiO_2) was used. 50 mL of the sol was taken in 100 mL beaker with cashew gum (used as a binder; natural binder) in the ratio 10:1 and stirred for further 3 h. Then the solution was poured into the glass bottle to obtain the coating and kept for 1 h. After 1 h the sol was poured out back and the empty bottle was dried in an oven at 80 °C and then calcined at 500 °C at a heating rate of 5 °C per minute and held 2 h at this temperature.

3. Results and discussion

3.1. XRD

XRD patterns of TiO_2 powders calcined at 300, 500 and 700 °C were carried out and the sample at 500 and 700 °C were shown in Fig. 1A and B. From the figures it is clear that all catalysts are completely in the anatase phase. The particle characteristics of the TiO_2 and Sm^{3+} doped TiO_2 samples with different weight percentage of dopant at various temperatures were summarized in Table 1. The relative intensity of (1 0 1) peaks were reduced in the Sm^{3+}doped TiO_2, in comparison with bare TiO_2 calcined at the same temperature (Table 1). XRD patterns didn't show any peaks corresponds to samarium oxide in any of the doped samples, which implies that Sm^{3+} ions are incorporated in the crystal lattice of TiO_2. When the crystallite sizes of the Sm^{3+} doped TiO_2 samples were calculated using the Scherrer formula (Table 1), it was found that the crystallite size was reduced by Sm^{3+} ion doping. It is due to the segregation of the dopant cations at the grain boundary of TiO_2,

Table 1
Crystal structure, Crystal sizes and (1 0 1) peak relative intensity of TiO_2, TSm1, TSm2, TSm5 and TSm10 calcined at 300, 500 and 700 °C.

Sample	Temperature (°C)	Crystal structure	Crystal size
TiO_2	300	Anatase	7.84
	500	Anatase	12.6
	700	Anatase	21.7
TSm1	300	Anatase	7.79
	500	Anatase	10.5
	700	Anatase	15.0
TSm2	300	Anatase	8.20
	500	Anatase	10.6
	700	Anatase	12.4
TSm5	300	Anatase	6.96
	500	Anatase	8.40
	700	Anatase	11.4
TSm10	300	Anatase	6.50
	500	Anatase	7.60
	700	Anatase	15.1

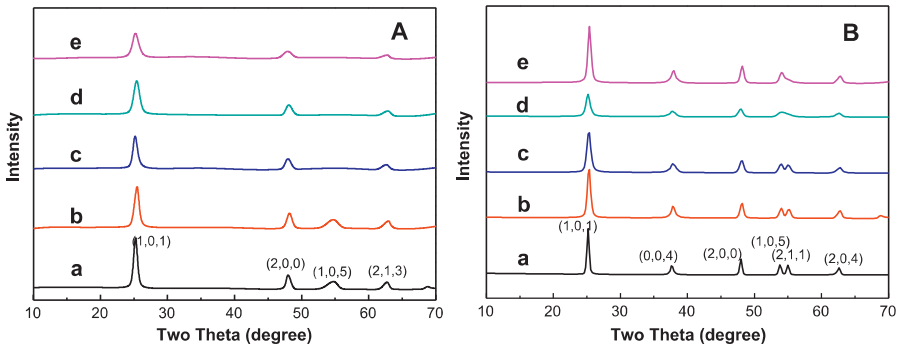

Fig. 1. XRD patterns of (a) TiO_2, (b) TiSm1, (c) TiSm2, (d) TiSm5 and (e) TiSm10 calcined at (A) 500 and (B) 700 °C.

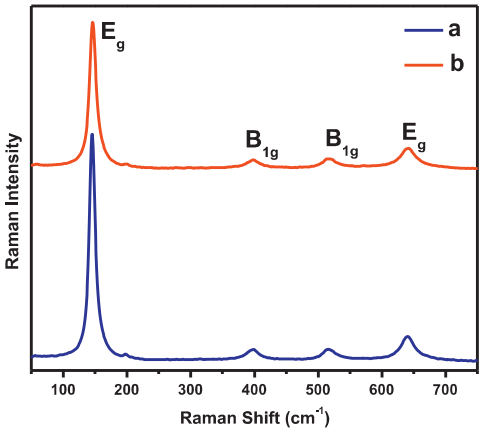

Fig. 2. Raman Spectra of (a) TiO_2 and (b) TSm2 calcined at 500 °C.

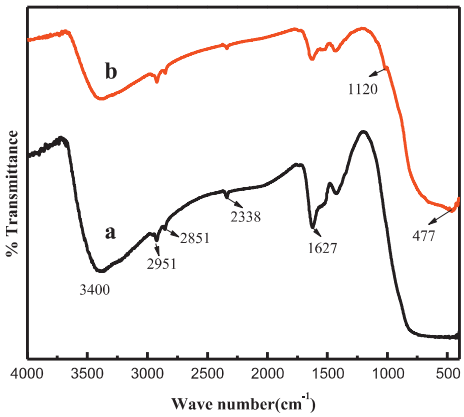

Fig. 3. FTIR spectra of (a) TiO_2, (b) TSm2 calcined at 500 °C.

and the growth of nanocrystallineTiO_2 is then prevented. These smaller crystallites of Sm^{3+} doped TiO_2 delay the transformation of anatase to rutile structure and also have the larger surface area compared to pure TiO_2 (Ullattil and Periyat, 2015; Li and Li, 2001).

3.2. Raman spectroscopy

As shown in Fig. 2, Raman spectra reveal the anatase phase purity of as synthesized TiO_2 nanoparticles. The peaks present at 145 (E_g), 395 (B_{1g}), 514 (B_{1g}) and 639 cm^{-1} (E_g) which are the characteristics of anatase phase of TiO_2 (Hou et al., 2004). The major peak intensity of anatase is decreasing as the dopant was introduced which confirms the incorporation of Sm^{3+} into the crystal lattice and thereby decrease in crystallinity as evidenced from the XRD patterns (Fig. 1). It can also be confirmed that, in addition to decrease in peak intensity the peak get broadened, which is attributed to the presence of oxygen vacancies and thereby Ti^{3+} doping occurred as a result of doping (Yan et al., 2013).

3.3. FTIR Spectroscopy

The FTIR spectra of 1, 2, 5 and 10 wt% doped Sm^{3+} doped TiO_2 and pure TiO_2 calcined at 300, 500 and 700 °C were recorded (Fig. 3). In both spectra of TiO_2 and Sm^{3+} doped TiO_2, the absorption band at 3500–3000 cm^{-1} corresponds to the hydroxyl group stretching vibration and surface adsorbed water molecule. The peak at 1627 cm^{-1} indicates the hydroxyl group bending vibration and the peak at 2951 and 2851 cm^{-1} corresponds to the asymmetric C-H stretching vibration (Lu et al., 2012). Absorbed CO_2 on the surface is indicated by the peak on 2338 cm^{-1} (Pawlak and Mucha, 2003). Ti-O-Sm stretching vibrations were obtained at 1120 cm^{-1} (Pawlak and Mucha, 2003). The broad peak in the range 400–700 cm^{-1} were obtained for both TiO_2 and Sm^{3+} doped TiO_2 is due to the Ti-O-Ti stretching mode (Zou et al., 2011). A new peak at 477 cm^{-1} for Sm^{3+} doped TiO_2 is due to the vibration modes of Ti-O-Sm bonds (Huang et al., 2009; Karakitsou and Verykios, 1993; Parida and Sahu, 2008; Soler-Illia et al., 2002; Wang et al., 2001).

3.4. Diffuse reflectance spectroscopy (DRS)

Diffuse reflectance spectroscopy (DRS) in the range 200–800 nm of TiO_2 and Sm^{3+} doped TiO_2 calcined at different temperature were investigated to study the optical absorption properties. The DRS spectra of TiO_2 and Sm^{3+} doped TiO_2 at 500 and 700 °C were shown in the Fig. 4. Pure TiO_2 had no absorption

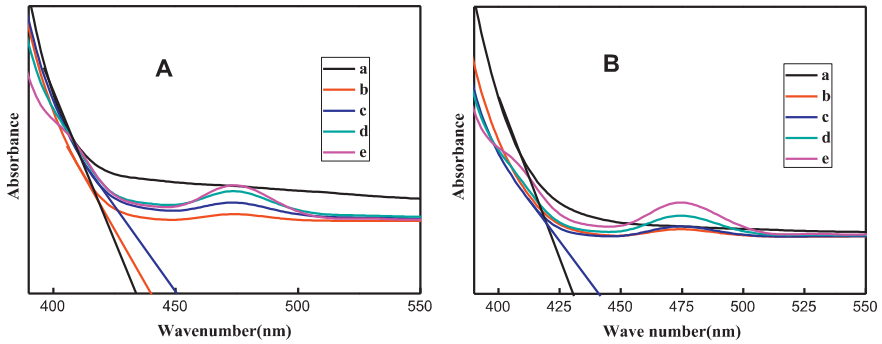

Fig. 4. DRS of (a) TiO_2, (b) TSm1, (c) TSm2, (d) TSm5 and (e) TSm10 calcined at (A) 500 and (B) 700 °C.

Table 2
Band gap energies of TiO_2, TSm1, TSm2, TSm5 and TSm10 calcined at different temperatures.

Sample	Band Gap (eV)		
	300 °C	500 °C	700 °C
TiO_2	3.10	3.00	3.06
TSm1	2.79	2.75	2.76
TSm2	2.76	2.67	2.68
TSm5	2.63	2.59	2.56
TSm10	2.86	2.77	2.77

in the visible region (>400 nm), while Sm^{3+} doped TiO_2 shows an absorption band in the range 400–500 nm (Fig. 4). It is also observed that the absorption edge of sample shifts to higher wavelength, when doping concentration increased from 1 to 10 percent. This red shift can be attributed to the charge-transfer transition between the *f* electrons of Sm^{3+} ion and the TiO_2 conduction band (Huang et al., 2009; Wang et al., 2001), which helps in the generation of electron and hole under visible light irradiation. Similar red shift absorption profile is observed with an increase in calcined temperature from 300 to 700 °C. The band gap energies were calculated by using UV–Vis DRS spectra with Tauc equation shown in Table 2. The band gap energies of Sm^{3+} doped samples are lower than that of TiO_2 due to the red shift that occurred as a result of Sm^{3+} doping.

3.5. X-ray Photoelectron Spectroscopy (XPS)

XPS reveals that the incorporation of Sm^{3+} ion into the lattice of TiO_2. The $2p_{3/2}$ and $2p_{1/2}$ peaks of TiO_2 were observed at 460.2 and 466 eV for bare TiO_2 (Fig. 5a) and the corresponding values for Sm^{3+} doped TiO_2 obtained at 457.5 and 463.3 eV showing notable peak changes are occurred on the surface of TiO_2 as result of doping. The peak 460.2 eV for bare TiO_2 is attributed to the oxygen richness (Naufal and Periyat, 2016). The splitting difference was found to be 5.8 eV in both bare and doped TiO_2 samples, which is attributed to the anatase phase purity of as prepared samples (Wu et al., 2002). When Sm^{3+} enters into the lattice of TiO_2, surface defects originate and is confirmed by the blue shift in the binding energy *i.e.* 457.5 eV ($2p_{3/2}$) and 463.2 eV ($2p_{1/2}$). The peak at 457.5 eV is the characteristic for the presence of Ti^{3+} (Naufal and Periyat, 2016). At the same time, the decrease in valency of Ti^{4+} to Ti^{3+} reveals the presence of oxygen vacancies developed. This reveals the transformation of oxygen rich environment to oxygen deficient environment. From the O1s XPS (Fig. 5b) it can be seen that the peak at 531.5 eV blue shifted to 528.7 eV indicating the change in oxygen environment (Wu et al., 2002). Fig. 5c represents the XPS pattern of Sm3d reveals the incorporation of Sm^{3+} into the crystal lattice. The distinct doublets at 1081.5 and 1106 eV coming from $Sm3d_{5/2}$ and $Sm3d_{3/2}$ attribute the presence of Sm—O—Ti bond (Ren et al., 2015). Even though the ionic radius of Sm^{3+} is

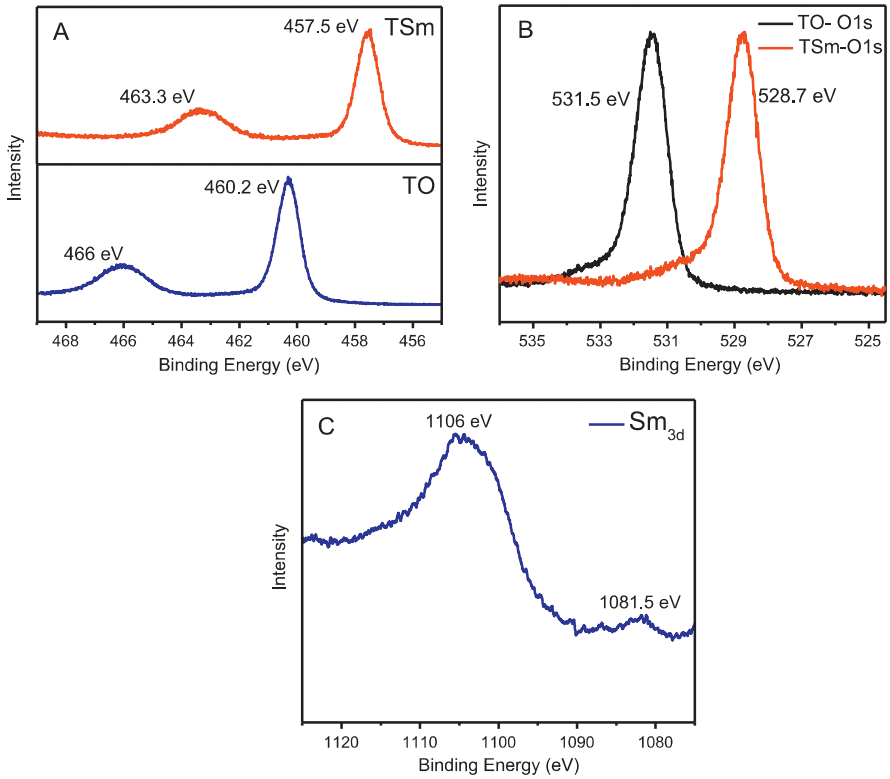

Fig. 5. XPS of (A) Ti2p, (B) O1s and (C) Sm3d.

greater than Ti^{4+}, Sm^{3+} entered into the crystal lattice of TiO_2 and those ions occupy the interstitial position of TiO_2.

3.6. Morphology (SEM and TEM)

Morphological study and EDS analysis of the samples were carried out using SEM and TEM respectively. The results were showed in Figs. 6–8. SEM analysis of the sample showed that the particles underwent agglomeration. Particle size of Sm^{3+} doped TiO_2 is lower than that of TiO_2 which is in good agreement with the crystalline size calculation obtained from XRD. From XRD, pure TiO_2 showed a size of 21.7 nm while Sm^{3+} doped TiO_2 showed only 11.4 nm crystalline size (Table 1) indicating that Sm^{3+} ion doping could hinder the increase of crystallite size during calcinations. Results of EDS analysis (Fig. 7 and Table 3) carried out showed the presence of both Ti and Sm in the lattice of Sm^{3+} doped TiO_2 sample. Fig. 8 shows TEM images of samples calcined at 500 °C, where TiO_2 shows a particle size of 19–23 nm (Fig. 8a) whereas the Sm^{3+} doped TiO_2 has a particle size of 10–12 nm (Fig. 8b).

At 500 °C Sm^{3+} doped TiO_2 showed smaller sized particles, whereas bare TiO_2 showed larger one. This is clearly evidenced from the SAED pattern. SAED pattern of Sm^{3+} doped TiO_2 showed broad band due to the Scherrer line broadening representing small crystalline particles (Ma et al., 2010; Baiju et al., 2005) whereas bare TiO_2 showed distinct spots due to larger sized particles.

4. Photocatalysis

Photocatalytic activity of both TiO_2 and Sm^{3+} doped TiO_2 for methylene blue degradation under UV and sunlight were carried out and the rate constant obtained from the degradation kinetics were summarized in Table 4. Fig. 9 shows the degradation efficiency of methylene blue under the UV and sunlight irradiation usingTiO_2 and 1%, 2%, 5% and 10% Sm-doped TiO_2 calcined at different temperatures. From Table 4 it can be seen that calcination temperature influenced on photocatalytic activity of bare TiO_2 and Sm^{3+} doped TiO_2. The best calcination temperature was at 500 °C irrespective of the light source. However, comparing UV and direct sunlight, rate of degradation under direct sunlight irradiation is more compared to UV light irradiation. This can be attributed to the increase in the absorption edge as a result of narrowing band-gap energy resulted from Sm^{3+} doping in TiO_2. Overall examination of the Table 4 and Fig. 9 (dye degradation curve under UV and sunlight light using TiO_2 and Sm^{3+} doped TiO_2), it can be stated that Sm^{3+} doped TiO_2 have higher photocatalytic activity than bare TiO_2 except the one which is calcined at lower temperature and having lower concentration of Sm^{3+} (1% Sm^{3+} doped TiO_2). Among the different sample prepared, 2% Sm^{3+} doped TiO_2 calcined at 500 °C is the best photocatalyst both under UV and sunlight.

Absorption spectra of methylene blue dye degradation under UV and visible light, using Sm^{3+} doped TiO_2 calcined at 500 °C in comparison to bare TiO_2 were shown in Figs. 10–13. The rate constant calculated from the first order kinetics were shown in Table 4. Among the doped samples highest activity was obtained for 2% Sm^{3+} doped TiO_2 sample calcined at 500 °C. The 2% Sm^{3+} doped TiO_2 calcined at 500 °C showed the highest reaction rate constant of 0.103 min^{-1} while its TiO_2 counterpart has only 0.013 min^{-1}. Hence Sm^{3+} doped TiO_2 photocatalyst is 10 times higher active than that of bare TiO_2. Absorption spectra of methylene blue dye degradation under sunlight using TiO_2 and 2% Sm^{3+} doped TiO_2 at 500 °C were shown in Figs. 12 and 13 respectively.

The higher visible light activity of Sm^{3+} doped TiO_2 compared to pure TiO_2 is due to the ability of Sm^{3+} ion to adsorb as well as complex with methylene blue dye molecule on the surface of theTiO_2 and thereby exciting dye molecule using suitable visible light

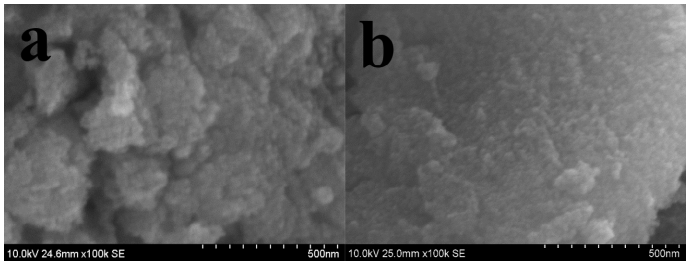

Fig. 6. SEM image of (a) TiO_2, (b) TSm2 calcined at 500 °C.

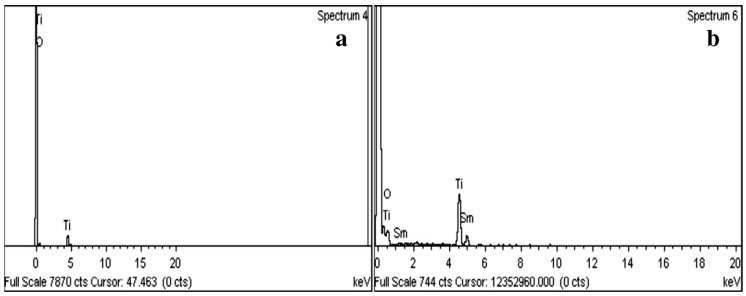

Fig. 7. Energy Dispersive Spectroscopy (EDS) of (a) TiO_2 and (b) TSm2 calcined at 500 °C.

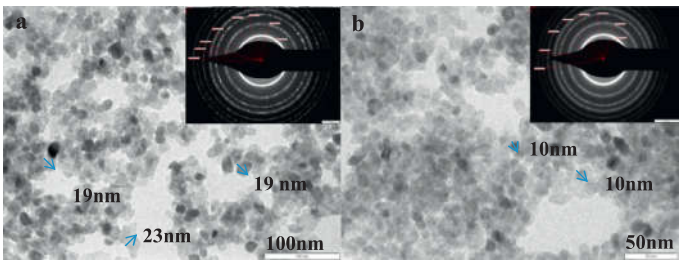

Fig. 8. TEM image of (a) TiO_2, (b) TSm2 at 500 °C.

Table 3
Energy Dispersive Spectroscopy (EDS) elementary analysis TiO_2 and TiSm2 calcined at 500 °C.

Element	TSm2		TiO_2	
	Weight %	Atomic %	Weight %	Atomic %
TiK	57.00	80.03	57.39	80.13
OK	42.40	19.88	42.61	19.87
SmL	0.61	0.09	Nil	Nil

absorption as represented by Eq. (1). The excited dye molecule having an electron in LUMO can be injected it into conduction band (CB) of TiO_2 (Eq. (2)). Sm^{3+} ion present on the TiO_2 surface can now reduce Sm^{3+} to Sm^{2+} as represented by Eq. (3) leading to an electron scavenging activity which will trap the conduction band electrons of TiO_2 obtained as a result of electron injection from methylene blue dye (Eq. (1)). These electrons trapped in Sm^{2+} sites can transfer to the adsorbed O_2 by oxidation process as represented by Eq. (5). This leads to the generation of effective oxidative superoxide (Eq. (4)) species (O_2^{-}) and hydroxyl radicals (Eq. (5)). These superoxide and hydroxyl radical can now attack the nearby dye molecules which lead to a higher photocatlytic activity.

$$MB + h\nu \rightarrow MB^{*} \quad (1)$$

$$MB^{*} + TiO_2 \rightarrow MB + TiO_2 + 1e^{-} \quad (2)$$

$$Sm^{3+} + 1e^{-} \rightarrow Sm^{2+} \quad (3)$$

$$Sm^{2+} + O_2 \rightarrow Sm^{3+} + O_2{\cdot}^{-} \quad (4)$$

$$O_2{\cdot}^{-} + 2H^{+} \rightarrow 2{\cdot}OH \quad (5)$$

There is also a possibility for the light absorption directly by the anatase TiO_2 photocatalyst leading to the photoexcitation of electron from the valence band to the conduction band. This process provides electron-hole separation and thereby effective photocatalysis. In this case the holes that are generated get react with water molecules forming OH'. Also the electrons that present in the conduction band of anatase simultaneously react with oxygen molecules directing towards O_2^{-} (super oxide radical anion). So

Table 4
Rate constant of TiO_2, TSm1, TSm2, TSm5 and TSm10 calcined at different temperatures.

UV light (min^{-1})				Sunlight (min^{-1})			
Sample	300 °C	500 °C	700 °C	Sample	300 °C	500 °C	700 °C
TiO_2	0.021	0.036	0.002	TiO_2	0.007	0.013	0.004
TSm1	0.007	0.03	0.014	1% Sm^{3+}	0.003	0.059	0.28
TSm2	0.007	**0.092**	0.073	2% Sm^{3+}	0.004	**0.103**	0.091
TSm5	0.009	0.051	0.066	5% Sm^{3+}	0.005	0.024	0.026
TSm10	0.012	0.028	0.023	10% Sm^{3+}	0.013	0.025	0.020

The highest rate constants achieved are shown in bold.

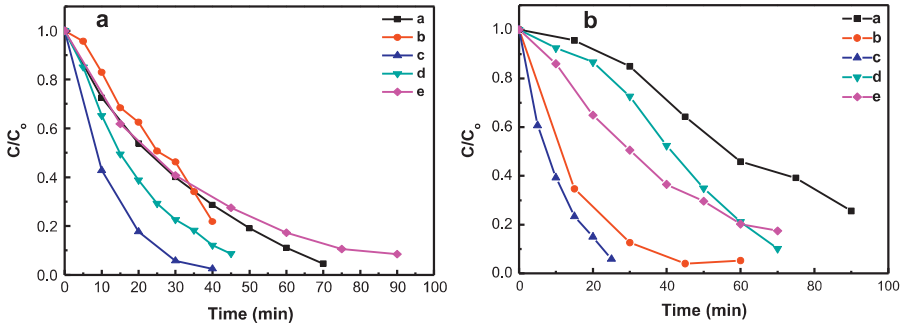

Fig. 9. Degradation curve of (a) TiO_2, (b) TSm1, (c) TiSm2, (d) TSm5 and (e) TSm10 calcined at 500 °C (a) UV light (b) Sunlight.

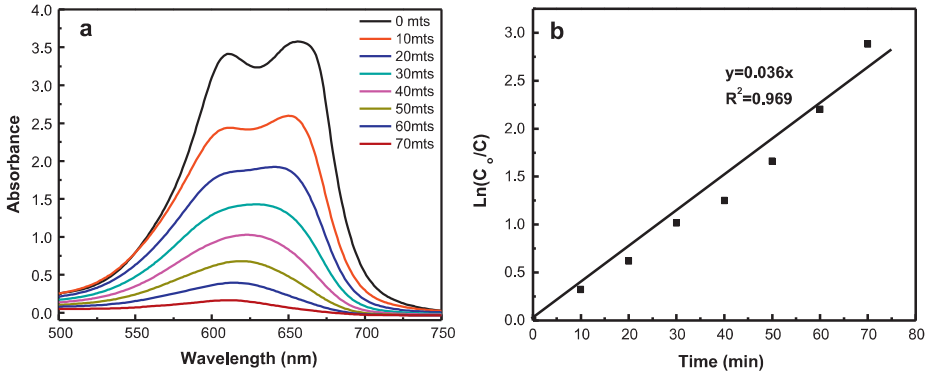

Fig. 10. Absorption spectra and Kinetic study of methylene blue dye degradation under UV using TiO_2 sample calcined at 500 °C, C_o is the Initial absorbance and C is the absorbance after a time of the methylene blue dye degradation.

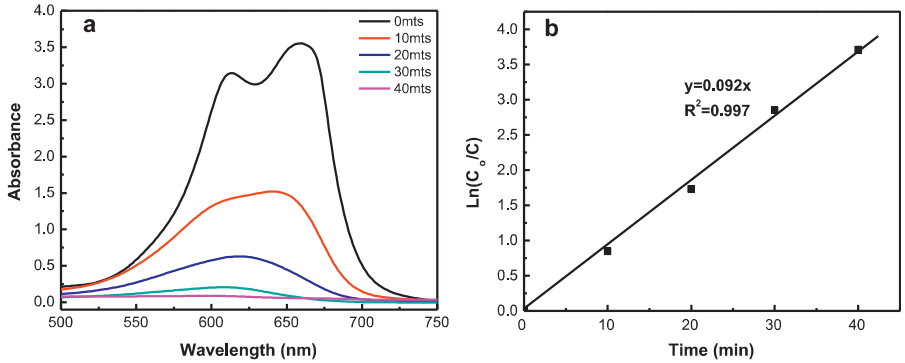

Fig. 11. Absorption spectra and Kinetic study of methylene blue dye degradation under UV using TSm2 sample calcined at 500 °C, C_o is the Initial absorbance and C is the absorbance after a time of the methylene blue dye degradation.

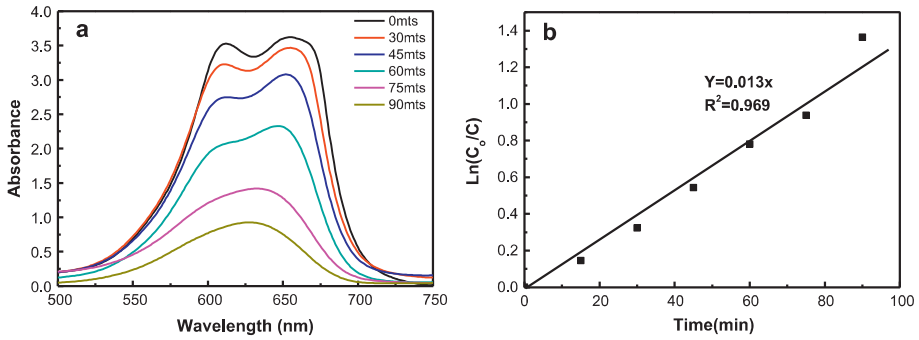

Fig. 12. Absorption spectra and Kinetic study of methylene blue dye degradation under direct sunlight using TiO_2 sample calcined at 500 °C, C_o is the Initial absorbance and C is the absorbance after a time of the methylene blue dye degradation.

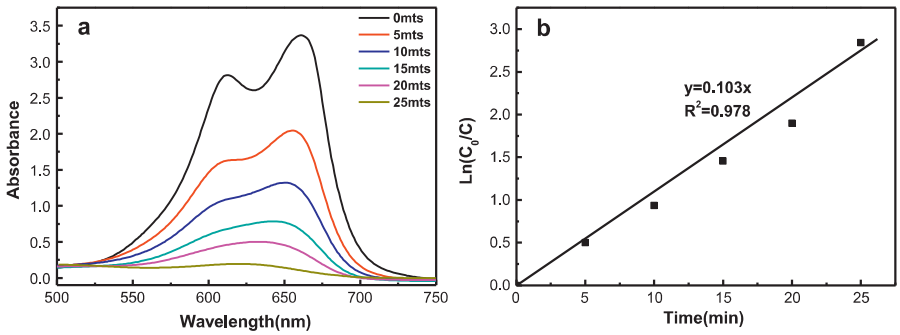

Fig. 13. Absorption spectra and Kinetic study of methylene blue dye degradation under direct sunlight using TSm2 sample calcined at 500 °C, C_o is the initial absorbance and C is the absorbance after a time of the methylene blue dye degradation.

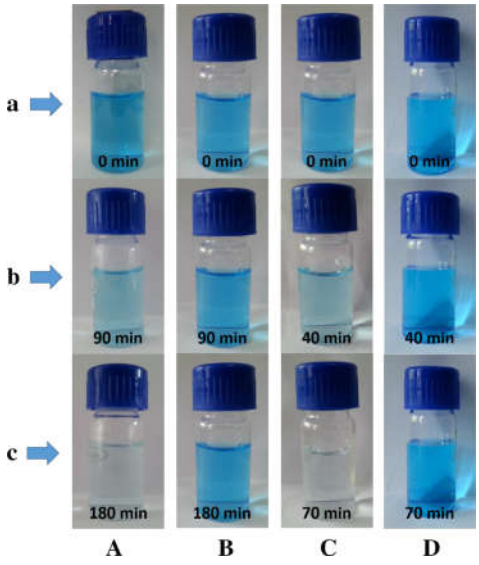

Fig. 14. Photocatalytic Self-cleaning using TSm2 calcined at 500 °C under UV illumination (A) in presence of catalyst (B) absence of catalyst and under Sunlight illumination (C) in presence of catalyst (D) absence of catalyst.

formed ·OH and O_2^- mineralize the methylene blue dye facilitate effective photocatalysis. In the case of Sm^{3+} doped anatase TiO_2, the photoexcitation is more feasible due to the narrowed band gap contributed by the donor levels that are formed by Sm^{3+} doping and thus photodegradation rate was enhanced.

5. Self cleaning TiO_2 coated glass bottle

Photocatalytic study using powder sample showed that the best photocatalytic activity was obtained for 2% Sm^{3+} doped TiO_2 calcined at 500 °C. Using the 2% Sm^{3+} doped TiO_2 sol, coating was made on the glass bottle as described in section 2.4, and then heated to 500 °C. The amount of catalyst coated on the inner side of the glass bottle was measured as 0.01 g of TiO_2 catalyst. The nature and thickness of the TiO_2 coating (Natarajan et al., 2011) were studied using SEM and were shown in Fig. 15. SEM image of the TiO_2 coated glass bottle showed a crack free surface with uniform distributed particles. Cross sectional analysis gave the thickness of the coating and found to be 320 nm. The amount of catalyst coated on glass bottle using TiO_2 the sol was found to be 0.01 g. The glass bottle coated with Sm^{3+} doped TiO_2 is filled with 10 mL of methylene blue solution and then irradiated under UV light in photoreactor. Dye degradation was recorded using photography through color change (Fig. 14). Fig. 14 shows that bottle coated with Sm^{3+} doped TiO_2 sol can act as a self-cleaning bottle. Similar experiment was carried out using normal sunlight (Fig. 14). Under direct solar irradiation it degrades more rapidly than that under UV light. The reproducibility of dye degradation was checked, the dye degraded

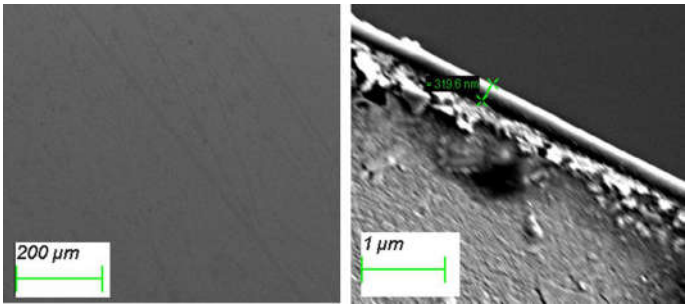

Fig. 15. SEM image of TiO_2 coating on the glass bottle (left) and cross sectional analysis of TiO_2 coating (right).

at the same rate even after three consecutive irradiations. Similar dye degradation experiments were repeated for a glass bottle without any coating (Fig. 14). The color of the dye remains unaltered after the irradiation of UV/direct sunlight.

6. Conclusions

A modified sol-gel strategy has been developed for the synthesis of oxygen rich TiO_2 nanoparticles. On introducing Sm^{3+} into the crystal lattice of oxygen rich TiO_2 nanocrystals, the environment was changed from oxygen richness to oxygen deficiency, *i.e.* Sm^{3+} induced oxygen deficiency in the crystal lattice of TiO_2. These TiO_2 nanoparticles with oxygen richness and oxygen deficiency (doped and undoped) were subjected to various calcination temperatures and their photocatalytic and self-cleaning activity under UV and solar illuminations were systematically examined. It was found that 2% Sm^{3+} induced TiO_2 at 500 °C has shown the maximum photoactivity. Using this photoactive TiO_2 sol self-cleaning bottle were developed to show the practical application of TiO_2 photocatalyst.

Acknowledgements

Authors would like to thank Soumya B.N. for her valuable comments.

References

Bahnemann, D., 2004. Photocatalytic water treatment: solar energy applications. Sol. Energy 77, 445–459.

Baiju, K.V., Sibu, C.P., Rajesh, K., Pillai, P.K., Mukundan, P., Warrier, K.G.K., Wunderlich, W., 2005. An aqueous sol–gel route to synthesize nanosized lanthana doped titania having an increased anatase phase stability for photocatalytic application. Mater. Chem. Phys. 90, 123–127.

Chen, F., Zhao, J., Hidaka, H., 2003. Highly selective deethylation of rhodamine B: Adsorption and photooxidation pathways of the dye on the TiO_2/SiO_2 composite photocatalyst. Inter. J. Photoenergy 5, 209–217.

Choi, W., Termin, A., Hoffmann, M.R., 1994. The role of metal ion dopants in quantum-sized TiO_2: correlation between photoreactivity and charge carrier recombination dynamics. J. Phys. Chem. 98, 13669–13679.

Fujishima, A., Rao, T.N., Tryk, D.A., 2000. Titanium dioxide Photocatalysis. J. Photochem. Photobiol. C Photochem. Rev. 1, 1–21.

Gonzalez, E., Bonnefond, A., Barrado, M., Barrasa, A.M.C., Asua, J.M., Leiza, J.R., 2015. Photoactive self-cleaning polymer coatings by TiO_2 nanoparticle Pickering miniemulsion polymerization. Chem. Eng. J. 281, 209–217.

Hattori, A., Tokihisa, Y., Tada, H., Ito, S., 2000. Acceleration of oxidationsand retardation of reductions in photocatalysis of a TiO_2/SnO_2 bilayer-type catalyst. J. Electrochem. Soc. 147, 2279–2283.

Hoffmann, M.R., Martin, S.T., Choi, W., Bahnemann, D.W., 1995. Environmental applications of semiconductor Photocatalysis. Chem. Rev. 95, 69–96.

Hou, M.F., Li, F.B., Li, R.F., Wan, H.F., Zhou, G.Y., Xie, K.C., 2004. Mechanisms of enhancement of photocatalytic properties and activity of Nd^{3+} doped TiO_2 for methyl orange degradation. J. Rare Earths 22, 542–546.

Huang, D.G., Liao, S.J., Zhou, W.B., Quan, S.Q., Liu, L., He, Z.J., Wan, J.B., 2009. Synthesis of samarium- and nitrogen-co-doped TiO_2 by modified hydrothermal method and its photocatalytic performance for the degradation of 4-chlorophenol. J. Phys. Chem. Solids 70, 853–859.

Iliev, V., Tomova, D., Bilyarska, L., Eliyas, A., Petrov, L., 2006. Photocatalytic properties of TiO_2 modified with platinum and silver nanoparticles in degradation of oxalic acid in aqueous solution. Appl. Catal. B: Environ. 63, 266–271.

Jin, S., Shiraishi, F., 2004. Photocatalytic activities enhanced for decompositions of organic compounds over metal- photodepositing titanium dioxide. J. Chem. Eng. 97, 203–211.

Karakitsou, K., Verykios, X., 1993. Effects of altervalent cation doping of TiO_2 on its performance as a photocatalyst for water. J. Phys. Chem. 97, 1184–1189.

Li, X.Z., Li, F.B., 2001. Study of Au/Au^{3+}-TiO_2 photocatalysts toward visible photooxidation for water and wastewater treatment. Environ. Sci. Technol. 35, 2381–2387.

Liang, C.H., Li, F.B., Liu, C.S., Lu, J.L., Wang, X.G., 2008. The enhancement of adsorption and photocatalytic activity of rare earth ions doped TiO_2 for the degradation of Orange I. J. Dyes Pigm. 76, 477–484.

Lu, Z., Yip, C.T., Wang, L., Huang, H., Zhou, L., 2012. Hydrogenated TiO_2 nanotube arrays as high-rate anodes for lithium-ion microbatteries. Chem. Plus. Chem. 77, 991–1000.

Ma, Y., Zhang, J., Tian, B., Chen, F., Wang, L., 2010. Synthesis and characterization of thermally stable Sm, N co-doped TiO_2 with highly visible light activity. J. Hazard Mater. 182, 386–393.

Muruganandham, M., Swaminathan, M., 2006. Photo-catalytic decolourisation and degradation of Reactive Orange 4 by TiO_2-UV process. Dyes Pigm. 68, 133–142.

Natarajan, K., Natarajan, T.S., Bajaj, H.C., Tayade, R.J., 2011. Photocatalytic reactor based on UV-LED/TiO_2 coated quartz tube for degradation of dyes. Chem. Eng. J. 178, 40–49.

Natarajan, T.S., Bajaj, H.C., Tayade, R.J., 2014. Preferential adsorption behavior of methylene blue dye onto surface hydroxyl group enriched TiO_2 nanotube and its photocatalytic regeneration. J. Colloid Inter. Sci. 433, 104–114.

Naufal, B., Periyat, P., 2016. High temperature stable dysprosium modified nano TiO_2 photocatalyst. J. Chem. Pharm. Sci. 1, 68–74.

Paola, A.D., Marci, G., Palmisano, L., Schiavello, M., Uosaki, K., Ikeda, S., 2002. Preparation of polycrystalline TiO_2 photocatalysts impregnated with various transition metal ions: characterization and photocatalytic activity for the degradation of 4-nitrophenol. J. Phys. Chem. B 106, 637–645.

Parida, K.M., Sahu, N., 2008. Visible light induced photocatalytic activity of rare earth titania nanocomposites. Appl. Catal. A 287, 151–158.

Park, D.J., Sekino, T., Tsukuda, S., Tanaka, S., 2013. Synthesis of Sm-Doped TiO_2 nanotube and analysis of its methylene blue removal properties under dark and UV irradiated conditions. Res. Chem. Intermed. 39, 1581–1591.

Parkin, I.P., Palgrave, R.G., 2005. Self-cleaning coatings. J. Mater. Chem. 15, 1689–1695.

Pawlak, A., Mucha, M., 2003. Erratum to Thermogravimetric and FTIR studies of chitosan blends. Thermochim. Acta 396, 153–166.

Ranjit, K.T., Willner, I., Bossmann, S.H., Braun, A.M., 2001. Lanthanide oxide doped titanium dioxide photocatalysts: effective photocatalyst for the enhanced degradation of salicyclic acid and t-cinnamic acid. J. Catal. 204, 305–313.

Ren, R., Wen, Z., Cui, S., Hou, Y., Guo, X., Chen, J., 2015. Controllable synthesis and tunable photocatalytic properties of Ti^{3+} doped TiO_2. Sci. Rep. 5, 10714.

Shi, J., Zheng, J., Hu, Y., Zhao, Y., 2008. Photocatalytic degradation of methyl orange in water by samarium-doped TiO_2. Environ. Eng. 25, 451–460.

Smitha, V.S., Vidya, K., Jayasankar, M., Peer Mohamed, A., Hareesh, U.S., Warrier, K.G. K., 2016. Energy revamping of solar panels through titania nanocomposite coatings; influence of aqueous silica precursor. RSC Adv. 6, 31114–31121.

Smits, M., Chan, C.K., Tytgat, T., Craeye, B., Costarramone, N., Lacombe, S., Lenaerts, S., 2013. Photocatalytic degradation of soot deposition: self-cleaning effect on titanium dioxide coated cementitious materials. Chem. Eng. J. 222, 411–418.

Soler-Illia, G.J.A.A., Louis, A., Sanchez, C., 2002. Synthesis and characterization of mesostructured titania-based materials through evaporation- induced self-assembly. Chem. Mater. 14, 750–759.

Ullattil, S.G., Periyat, P., 2015. Green microwave switching from oxygen rich yellow anatase to oxygen vacancy rich black anatase TiO_2 solar photocatalysts using Mn (II) as 'anatase purifier'. Nanoscale 7, 19184–19192.

Ullattil, S.G., Periyat, P., 2017. Microwave-power induced green synthesis of randomly oriented mesoporous anatase TiO_2 nanoparticles for efficient dye sensitized solar cells. Sol. Energy 147, 99–105.

Wang, C., Xu, B.Q., 2005. Preparation and photocatalytic activity of $ZnO/TiO_2/SnO_2$ mixture. J. Solid State Chem. 178, 3500–3506.

Wang, J.A., Ballesteros, R.L., Lopez, T., Moreno, A., Gomez, R., Novaro, O.X., 2001. Quantitative determination of titanium lattice defects and solid-state reaction mechanism in iron-doped TiO_2 photocatalysts. J. Phys. Chem. B 105, 9692–9698.

Wu, X.A., Gao, Y., Liu, H.Q., 2002. The preparation, characterization and their photocatalytic activities of rare-earth doped TiO_2 nanoparticle. J. Catal. 207, 151–157.

Xiao, Q., Si, Z., Yu, Z., Qiu, G., 2007. Sol–gel auto-combustion synthesis of samarium-doped TiO_2 nanoparticles and their photocatalytic activity under visible light irradiation. Mater. Sci. Eng. B 137, 189–195.

Xiaoli, Y., He, J., Evans, D.G., Duan, X., Zhu, Y., 2005. Effect of TiO_2 thin film thickness and specific surface area by low-pressure metal–organic chemical vapor deposition on photocatalytic activities. Appl. Catal. B: Environ. 55, 243–252.

Xie, Y.B., Yuan, C.W., Li, X.Z., 2005. Photosensitized and photocatalyzed degradation of azo dye using Ln^{n+}-TiO_2 sol in aqueous solution under visible light irradiation. Appl. Catal. B: Environ. 55, 243–252.

Yan, J., Wu, G., Guan, N., Li, L., Li, Z., Cao, X., 2013. Understanding the effect of surface/bulk defects on the photocatalytic activity of TiO_2: anatase versus rutile. Phys. Chem. Chem. Phys. 15, 10978–10988.

Yang, P., Lu, C., Hua, N.P., 2002. Titanium dioxide nanoparticles co-doped with Fe^{3+} and Eu^{3+} ions for Photocatalysis. Mater. Lett. 57, 794–801.

Yu, J., Zhang, L., Zheng, Z., Zhao, J., 2003a. Synthesis and characterization of phosphated mesoporous titanium dioxide with high photocatlytic activity. Chem. Mater. 15, 2280–2286.

Yu, J.G., Yu, H.G., Cheng, B., Zhao, X.J., Yu, J.C., Ho, W.K., 2003b. The effect of calcinations temperature on the surface microstructure and photocatalytic activity of TiO_2 thin films prepared by liquid phase deposition. J. Phys. Chem. B 107, 13871–13879.

Zhang, Y., Xu, H., Xu, Y., Zang, H., Wang, Y., 2005. The effect of lanthanide on the degradation of RB in nanocrystalline Ln/TiO_2 aqueous solution. J. Photochem. Photobiol. A: Chem. 170, 279–285.

Zou, X., Zhang, F., Thomas, S., Zhu, G., Valtchev, V., Mintova, S., 2011. $Co_3(HCOO)_6$ microporous metal-organic framework membrane for separation of CO_2/CH_4 mixtures. Chem. Eur. J. 17, 12076–12083.

Journal of Chemical and Pharmaceutical Sciences ISSN: 0974-2115

High Temperature Stable Dysprosium modified Nano TiO_2 Photocatalyst

B. Naufal, P. Periyat*

Department of Chemistry, University of Calicut, Kerala, India - 673635.

***Corresponding author: E-Mail: pperiyat@uoc.ac.in**

ABSTRACT

TiO_2 and Dy^{3+} doped TiO_2nanocrystalline has been successfully synthesized by a modified sol-gel method. As synthesised samples of TiO_2 and Dy^{3+} doped TiO_2 were calcined at 300, 500 and 700 ^oC and their photocatalytic activity was compared. Characterization of the samples was carried out by various techniques such as XRD, UV/Vis Reflectance spectroscopy, FTIR and TEM. The photocatalytic activity of TiO_2 and Dy^{3+} doped TiO_2were investigated by the degradation of methylene blue solution under UV light irradiation. The results showed that the Dy^{3+} doped TiO_2 sample calcined at 700 ^oC shows the highest photocatalytic activity.

KEY WORDS: Sol-gel method, photocatalyst, advanced oxidation process.

1. INTRODUCTION

Dye waste coming from textiles and food industry are one of the largest group of pollutants found in the drinking water and its colour is easily recognizable in water stream. They are either toxic or become toxic when being gradually decomposed in the ecosystem and undergo bio magnification in living organisms due to its low rate of natural degradation and also cause severe health problems. Hence many physical, chemical and biological treatment technologies are currently being employed to remove dyes waste or degrade them into non-toxic ones. However most of the organic dye waste cannot be removed using these technologies. Advanced Oxidation Processes (AOPs) is a prominent technique to remove organic dye in which the organic compounds are completely degrading into ultimate products as CO_2 and H_2O.

Among all the AOPs, photo catalytic oxidation (PCO) is the most promising one.**Error! Bookmark not defined.** **Error! Bookmark not defined.** **Error! Bookmark not defined.**Photocatalytic oxidation is a process where degradation of organic dyes and/or compounds occur by the illumination of photocatalyst without introducing any other chemicals. TiO_2, ZnO, CeO_2 and ZrO_2 are the commonly used photocatalysts. Among these TiO_2 is the promising photocatalyst because of its unique optical and physical properties and also due to its easy availability, in-expensiveness and non-toxicity.TiO_2 crystallizes mainly in to three – anatase, rutile and brookite. Majority of research work has been carried out with either anatase or rutile. Many physical, chemical and biological treatment technologies are currently being employed to remove dyes using anatase and/or rutile phase. However among these three different forms of TiO_2, anatase, rutile and brookite, generally anatase has the highest photocatalytic activity than the other two. It can be due to the high indirect band gap (Eg=3.2 eV) of anatase that enables the exited electrons to stabilize at lower level in the conduction band leading to high mobility and longer life of the exited electrons. The photocatalytic activity of semiconducting nanoparticles (TiO_2 and ZnO) is improved by doping with various rare earth dopant source.

In this work a simple modified sol-gel method was used to synthesize TiO_2 and Dy^{3+}doped TiO_2calcined at different temperature and characterized with XRD, FTIR, DRS and TEM. Photo catalytic activities of these samples were studied by photo degradation of methylene blue under UV light. The effect of calcination temperatures on the photo catalytic activity was also been discussed.

2. EXPERIMENTAL

TiO_2 and Dy^{3+} doped TiO_2 catalysts were prepared with the raw materials of analytical grade. The raw materials used are titanium isopropoxide ($Ti(OPr)_4$, Aldrich, 97%), $Dy(NO_3)_3$Aldrich,glacial acetic acid (Aldrich, 99.8%) and deionized water. In a typical experiment to synthesize nano TiO_2, $Ti(OPr)_4$ was mixed with glacial acetic acid followed by the addition of de-ionized water in small quantity with constant stirring. The $Ti(OPr)_4$:acetic acid : water ratio was kept as 1:10:100. The homogenous solution was stirred for 3 hrs. It was dried at 100^o C on water bath for 12 hrs. The dried powder was calcined at 300, 500 and 700^o Cat a heating rate of 5^o C per minute and held at this temperature for 2 hrs. For the Dy^{3+} doped TiO_2 synthesis, along with the above reacting mixture calculated amount of Dysprosium (III) nitrate for 5 weight percentage were added and the same procedure is followed.

X-ray diffraction (XRD) patterns of the calcined gels were obtained with a Miniflex 600 X-ray diffractometer with CuKα radiation, λ=1.54 A^o, Voltage 40 KV and current 15mA in the diffraction angle range 2θ

Journal of Chemical and Pharmaceutical Sciences ISSN: 0974-2115

= 10–70º. The FT IR spectra of the gel dried at 100 ºC was measured by using a Jasco-FT/IR-4100 spectrometer in the wave number range 4000-400 cm^{-1} using 70 scans for each sample. The diffuse reflectance spectra (DRS) of the catalysts in the wavelength range of 200-800 nm were obtained using a UV-Vis reflectance spectrophotometer using a Jasco-V-550 UV/VIS spectrophotometer. Morphology of the samples was examined using Transmission Electron Microscope using Hitachi SU-66000.

2.1. Photocatalytic activity evaluation: In a typical experiment 0.1 g of sample was dispersed in 50 ml of methylene blue solution having concentration of 1 x 10^{-4} M. This solution was stirred for 10 minutes in dark for the chemisorptions on the surface of the catalyst to avoid any absorption error. The methylene blue solution containing catalyst was then irradiated under UV photo reactor (LZC-4x Luzchem Photo reactor) with continuous and uniform stirring. The degradation of methylene blue dye was monitored by taking 5 ml aliquots at different intervals of time. These aliquots were centrifuged at 4500 rpm for 15 minute and absorption spectra of the samples were recorded using UV/Visible spectrophotometer. Methylene blue concentration was used to determine at a wavelength range of 650 – 660nm. The absorbance set at 650 – 660nm is due to the color of the dye solution and it is used to monitor the degradation of dye. The rate of degradation was assumed to obey first order kinetics and hence the rate constant for degradation k was obtained from the first order plot using equation 1.

$$\ln(A_o/A) = kt \qquad (1)$$

Where A_o is initial absorbance, A is absorbance after a time and k is the first order rate constant.

3. RESULTS AND DISCUSSION

The nano $TiO_2$where synthesized by the hydrolysis of titanium tetra isopropoxide $(Ti(OPr)_4$with water. Acetic acid was used as a stabilizing and catalyzing agent. Dysprosium (III) nitrate was used as a dopant source of Dy^{3+} ion.

3.1. X-ray Diffraction (XRD): XRD patterns of TiO_2 and Dy^{3+} doped TiO_2 powder calcined at a temperature of 300, 500 and 700 °C were shown in Figure 1. For TiO_2 the major peaks obtained at 2θ value at 25.18º, 37.94º, 48.07º and 54.15º were assigned to diffraction from the planes (101) , (103), (200), (105), and (213) respectively. Dy^{3+} doped TiO_2 possess peaks at 2θ value at 25.52º, 38.00º, 48.20º,54.52º, 62.80º, and 75.2º were corresponds to (101), (103), (200), (105) ,(213) and (107) planes respectively. These results are consistent with the data base of (JCPDS No 75-1537) of an anatase TiO_2. From the XRD pattern it is confirmed that both $TiO_2$and Dy^{3+}doped TiO_2 are in anatase structure and Dy^{3+} doped TiO_2calcined at 700ºC shows more relative intensity of (101) peak than others. From Figure 1A,XRD patterns of Dy^{3+} doped TiO_2 at calcination temperature of 700ºC shows a doublet at 2θ= 53.79 and 54.98º corresponding to the planes (105) and (211) where as in the TiO_2 sample this is turned to singlet peak at 2θ= 54.01ºcorresponding to (105) plane in the Dy^{3+} doped TiO_2 sample. From XRD spectra, it is clear thatTiO_2 and Dy^{3+}doped TiO_2showed complete anatase phase at all temperatures. Presence of complete anatase phase is due to the formation of Dy-O-Ti bond which inhibit the movement of Ti atoms for the phase transformation and that of bare TiO_2 may be due to the addition of acetic acid while synthesis, which stabilize the TiO_2sol formed after hydrolysis. The relative intensity of (101) peaks increased significantly in Dy^{3+} doped TiO_2 with respect to the TiO_2. This confirms the Dy^{3+} doping induced higher crystallinity and phase purity in doped TiO_2.

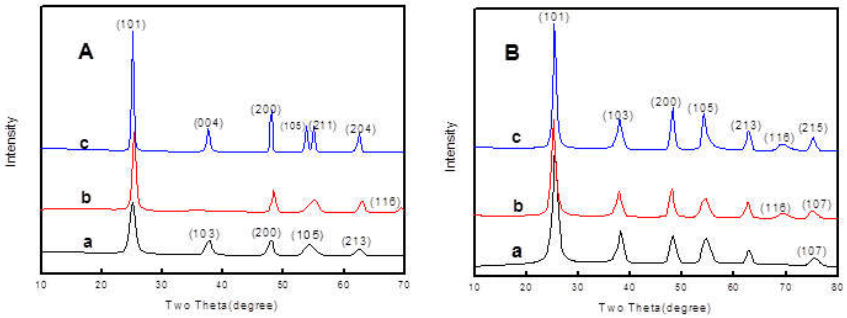

Figure.1.XRD pattern of A) TiO_2 B) Dy^{3+}dopeTiO_2at a) 300 b) 500 and c) 700 ºC

Crystalline size calculated for TiO_2 and Dy^{3+} doped TiO_2 using Sherr's equation were shown in Table 1. Crystallite sizes of TiO_2calcined at temperature 300, 500and 700°C are 7.84, 12.6, and 21.7 nm respectively. Similarly crystallite size of Dy^{3+} doped TiO_2calcined at 300, 500 and 700 °C was7.2, 8.6 and 11.1 nm respectively. It is found that the crystallite size decreased by Dy^{3+} doping confirms the improvement in the nanocrystalline nature of TiO_2 as a result of Dy^{3+} doping. ForTiO_2 crystallite size increases with calcination temperature. Dy^{3+} doped TiO_2 doped sample showed increase in crystallite size with all calcined temperature. From Table 1 it is clear that a drastic change in crystallite size occurs in the case of 700 °C calcined sample of TiO_2 to Dy^{3+} doped TiO_2. TiO_2 possess 21.7 nm, however Dy^{3+} doped TiO_2 possess only 11.1 nm. It indicates that upon doping crystallite size decreases and thus improves nano behavior of Dy^{3+}doped TiO_2.The decrease in crystalline size may attributed to the presence of Ti-O-Dybond formation in the Dy^{3+} doped sample, which inhibits the growth of crystal grains.

Table 1.Crystallite size of TiO_2 and Dy^{3+} doped TiO_2calcined at different temperatures

Sample	Crystallite size (nm)		
	300 °C	500 °C	700 °C
TiO_2	7.84	12.6	21.7
Dy^{3+} doped TiO_2	7.2	8.6	11.1

3.2. FTIR Spectroscopy: The FTIR spectra of TiO_2 and Dy^{3+}doped TiO_2calcined at 300 °C were shown in Figure 2. TiO_2 and Dy^{3+} doped TiO_2 sample possess strong and broad band in the range of 400-700 cm^{-1} which were attributed to Ti-O stretching and Ti-O-Ti bridging stretching modes, which is a characteristic peaks of observable in the anatase phase of TiO_2. A new band at 405 $cm^{-1}$was observed in the spectra of Dy^{3+}doped TiO_2 samples. This band is attributed to the Dy–O bond and it arises due to the reason that Dy^{3+} ions dispersed on the surface of TiO_2 in the form of metal oxides, formed during the calcination process. The peak at 1425, 1540 cm^{-1} in both TiO_2 and Dy^{3+} doped TiO_2 is due to the symmetric and asymmetric stretching vibration of acetate groups. The band at 1625 cm^{-1} and broad band at 3400 cm^{-1} in both sample corresponding to the O–H bending and stretching modes of water indicative of the presence of residual water and hydroxyl groups present in the sample. Absorbed CO_2 on the surface is indicated by the peak on 2337 cm^{-1}.The peak at 2920 and 2855 cm^{-1} is the asymmetric C-H stretching vibration. Absorbed CO_2 on the surface is indicated by the peak on 2337 cm^{-1}. The broad peak in the range 400-700 $cm^{-1}$is due to Ti-O stretching vibration modes, which can be observable in the anatase phase of TiO_2. Band at 543cm^{-1} observed, attributes the Dy-O bond. Similar type of observation was also seen in the FTIR spectra of TiO_2 and Dy^{3+} doped TiO_2calcined at 500 and 700 °C.

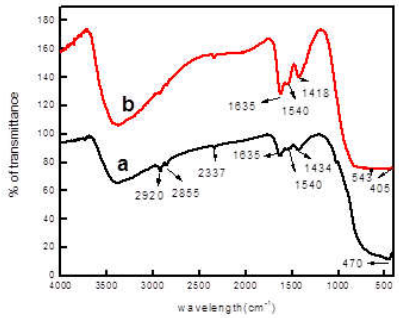

Figure.2.FTIR spectra of a) TiO_2b) Dy^{3+} doped TiO_2calcined at 300 °C

3.3. Optical Characterization: Diffuse Reflectance spectroscopy (DRS) was used to obtain the band gap energy value of TiO_2 and Dy^{3+} doped $TiO_2$and were shown in Table 3.From DRS, it is clear that the bare TiO_2 has no absorption in the visible region (>400 nm), however the Dy^{3+}-doped TiO_2 has showed significant absorption between 400 and 500 nm. Dy^{3+} doped TiO_2 sample (Figure 3) showed a significant shift to longer wavelengths and an extension of the absorption in to the visible region due to the doping effect of Dysprosium. Hence band gap energy of Dy^{3+}doped TiO_2samples is lesser compared to TiO_2 at different calcinations temperature. Lin (1998), reported that the band gap of TiO_2nanoparticles was reduced by Nd^{3+} doping and the band gap narrowing

was primarily attributed to the substitution Nd^{3+} ions which introduced electron states into the band gap of TiO_2 to form the new lowest unoccupied molecular orbital. Here FTIR already confirmed the presence of Dy^{3+} ion doped in the lattice of TiO_2. The Dy^{3+} ion in TiO_2 lattice will introduce new electronic states into the band gap of TiO_2 to form the new lowest unoccupied molecular orbital that will expected to lead to the higher photocatalytic activity of Dy^{3+} doped TiO_2.

Table 2. Band gap of TiO_2 and Dy^{3+} doped TiO_2calcined at different temperatures.

Temperature (^oC)	Band gap(eV)	
	TiO_2	Dy^{3+} dopedTiO_2
300	3.34	2.54
500	3.32	2.51
700	3.05	2.49

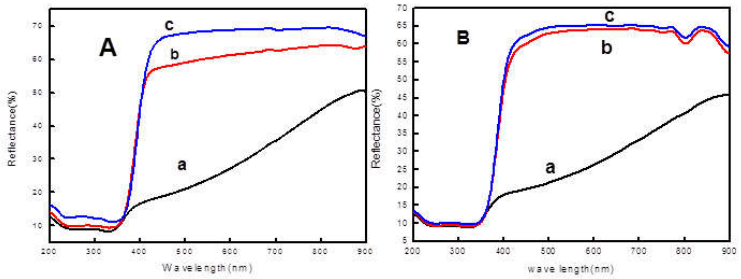

Figure.3.Diffuse Reflectance Spectra of A) TiO_2 B) Dy^{3+}doped TiO_2 at a) 300 b) 500 c) 700^o C

3.4. Transmission Electron Microscope (TEM): TEM images of $TiO_2$and Dy^{3+} doped TiO_2calcined at 700^o C were shown in Figure 4.TiO_2 shows a crystallite size of 18–28nm (Fig. 4a) at 700^{o}C. On the other hand, the Dy^{3+} doped TiO_2has a crystallite size of 7-14nm (Fig. 4b), and thus the TEM observations support the conclusions derived from the XRD data. The electron diffraction image of Dy^{3+} doped TiO_2calcined at 700^{o}C shows broad bands due to the Scherrerline broadening which is attributed to the small crystallite sizehowever TiO_2, at same temperature, showed distinct spots due to the high crystallinity and larger size of the crystals.

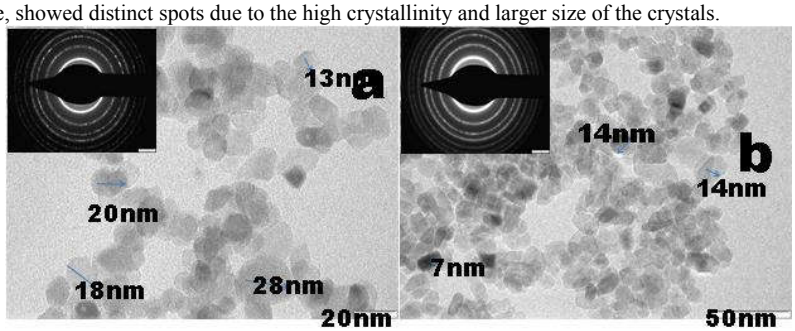

Figure.4.TEM image of a) TiO_2 b) Dy^{3+} doped TiO_2 at 700^{o}C

3.5. Photocatalytic activity of TiO_2 and Dy^{3+} doped TiO_2: Under irradiation from a suitable light source applied to the TiO_2 material, the electrons in theTiO_2 valence band will be excited, causing the electron to jump to the conduction band resulting in formation of a positive hole in the valence band and a free electron in the conduction band. These photogenerated electrons are able to reduce the dioxygen molecule to produce superoxide radicals and the hole can simultaneously oxidize water to produce hydroxyl radicals. These radicals are highly reactive and are able to break chemical bonds. This makes TiO_2, a suitable photocatalyst useful in the field of environmental

Journal of Chemical and Pharmaceutical Sciences ISSN: 0974-2115

purification. Textile dyes and other industrial dye stuffs constitute one of the largest groups of organic compounds that represent an increasing environmental danger. Methylene Blue is a kind of typical azo dye used in the textile dye industry. Here we selected methylene blue dye as a target of photodegradation due to these practical values. The photo catalytic activity of the samples is executed by the degradation using aqueous solution of methylene blue. Before irradiating with a UV lamp light, the samples were stirred in the dark for fifteen minutes. Results of absorption spectra showed that the methylene blue concentration has negligible decrease caused by the slight absorption on photocatalysts surface, which indicates that there is no degradation in the absence of irradiation. When photocatalytic reaction is conducted in aqueous medium, the holes were effectively scavenged by the water and generated hydroxyl radicals OH•, which are strong and unselected oxidant species in respect of total oxidative degradation for organic substrates. The holes, free electron, superoxide and hydroxyl radicals have been proposed as the oxidizing and reducing species responsible for the degradation (mineralization)of the organic substrates.

$TiO_2 + hv \rightarrow h^+ + e^-$

$H^+ + H_2O \rightarrow OH\bullet + H^+$

$h^+ + dye \rightarrow products$

$OH\bullet + dye \rightarrow products$

$MB + TiO_2 \rightarrow CO_2 + H_2O + NO^-_3 + NH_4^+ + SO_4^{2-}$

Table.3.Degradation time and rate constant in min under UV light of samples at different calcination temperatures

Temperature (°C)	TiO_2		Dy^{3+} doped TiO_2	
	Time (min)	Rate constant	Time (min)	Rate constant
300	150	0.021	105	0.007
500	70	0.037	40	0.051
700	210	0.003	60	0.070

Photocatalytic activity of both TiO_2 and Dy^{3+} doped TiO_2 for methylene blue degradation under UV light are summarized in the Table 3. From the Table 3, it is observed that at Dy^{3+} doped TiO_2 sample showed greater photocatalytic activity than TiO_2 under UV light. The rate constant calculated from the first order kinetics were also shown in the Table 3. Among the Dy^{3+}doped TiO_2maximum activity was obtained for sample calcined at 700° C. The highest rate constant 0.070 min^{-1} corresponds to the Dy^{3+} doped TiO_2 at 700°C while its TiO_2counterpart has only 0.003 min^{-1}. Absorption spectra of methylene blue dye degradation under UV using TiO_2 and Dy^{3+} doped TiO_2 at 700° C were shown in Figure 6. Therefore it can be concluded that the Dy^{3+} doped TiO_2calcined at 700° C is the best photocatalyst among these samples under UV light irradiation, showing the fastest decolourization of methylene blue and has the maximum degradation rate constant.

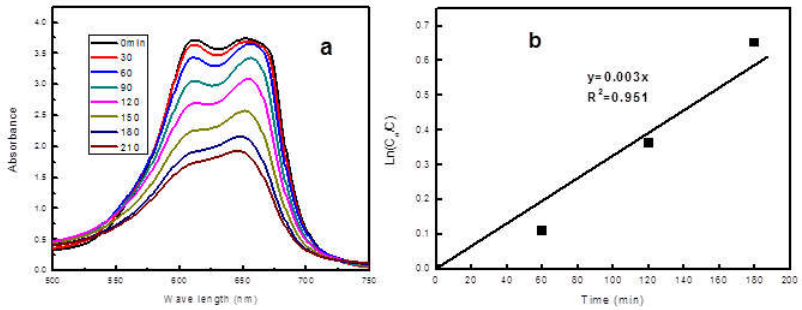

Figure.5.Absorption spectra and Kinetic study of methylene blue dye degradation under UV using TiO_2 sample calcined at 700°C, C_o is the Initial absorbance and C is the absorbance after a time of the methylene blue dye degradation

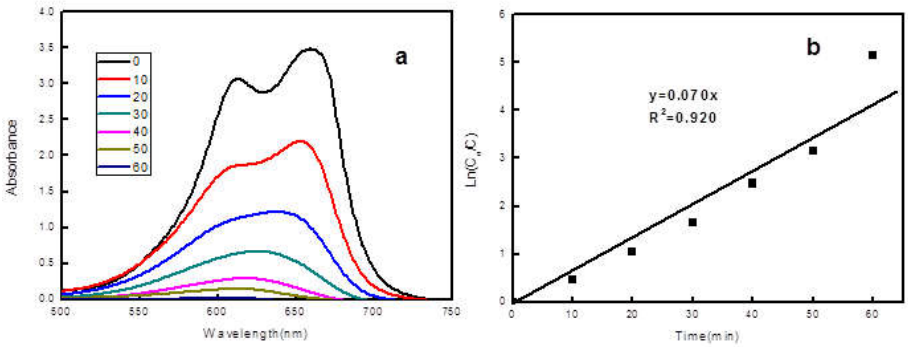

Figure.6.Absorption spectra and Kinetic study of methylene blue dye degradation under UV using Dy^{3+} doped TiO_2 sample calcined at 700ºC,C_o is the Initial absorbance and C is the absorbance after a time of the methylene blue dye degradation

4. CONCLUSIONS

Nanocrystalline TiO_2 and Dy^{3+} doped TiO_2 has been successfully synthesized using a modified sol-gel method. The samples were calcined at 300, 500 and 700ºC and characterized by various techniques such as XRD, UV/Vis Reflectance spectroscopy, FTIR and TEM. XRD study proved that both TiO_2 and Dy^{3+} doped TiO_2 sample synthesised are in the form of anatase phase. TEM study confirmed that TiO_2 has a crystallite size of 18–28 nm, on the other hand, the Dy^{3+}doped TiO_2has a size of 7-14 nm, revealed that the doping Dy^{3+} ion decreased the crystallite size of $TiO_2$and thereby induced more nano behavior. FTIR spectroscopy confirmed Ti-O and Ti-O-Ti bond in TiO_2, in Dy^{3+} doped TiO_2 presence of Dy-O and Ti-O-Dy bonds are also been confirmed along with Ti-O and Ti-O-Ti bond. Diffuse reflectance spectra showed that the Dy^{3+}doped TiO_2 have a significant red shift and an extension of the absorption in the visible region compared to the TiO_2. Finally the photocatalytic activity of TiO_2 and Dy^{3+} doped TiO_2 at various calcination temperatures was investigated by the degradation of methylene blue solution under UV light. Doping with the Dy^{3+} significantly enhanced the overall photocatalytic activity for MB degradation under UV light irradiations. The results showed that the Dy^{3+} doped TiO_2 sample calcined at 700º C shows the highest photocatalytic activity under UV light irradiation. These high temperature stable and higher photoactive Dy^{3+} doped anatase TiO_2 may be used for the self-cleaning, white light emitting and antibacterial coatings on high temperature processed ceramic materials.

REFERENCES

Arslan-Aloton, Advanced oxidation of textile industry dyes, S. Parsons (Ed.), IWA Publishing, London, 2004, 302–308.

Ayca Kambur, Gulin Selda Pozan, Ismail Boz, Preparation, characterization and photocatalytic activity of TiO_2–ZrO_2 binary oxide nanoparticles, Appl. Catal. B: Environ., 115, 2012, 149– 158.

Baiju K.V, Sibu C.P, Rajesha K, Pillai P.K, Mukundan P, Warrier K.G.K, Wunderlich W, An aqueous sol–gel route to synthesize nanosized lanthana-doped titania having an increased anatase phase stability for photocatalytic application, Mater. Chem. Phy., 90, 2005, 123–127.

Borgarello E, Kiwi J, Gratzel M, Pelizzetti E, Visca M, Visible light induced water cleavage in colloidal solutions of chromium-doped titanium dioxide particles, J. Am. Chem. Soc., 104, 1982, 2996-3002.

Chockalingam Karunakaran, Binu Naufal, and Paramasivan Gomathisankar, Efficient Photocatalytic Degradation of Salicylic Acid by Bactericidal ZnO. J.Kor.Chem.Soc., 56, 2012, 108-114.

Journal of Chemical and Pharmaceutical Sciences ISSN: 0974-2115

Houas A, Lachheb H, Ksibi M, Elalooui E, Guillard C, Herrmann J.M, Photocatalytic degradation pathway of methylene blue in water, App. Catal. B Environ., 31, 2001, 145–157.

Karkmaz M, Puzenat E, Guillard C, Herrmann J.M, Photocatalytic degradation of the alimentary azo dye amaranth - Mineralization of the azo group to nitrogen, App.Catal. B Environ., 51, 2004, 183–194.

Lin J, Yu J.C, An investigation on photocatalytic activities of mixed TiO_2-rare earth oxides for the oxidation of acetone in air, J. Photochem. Photobiol. Chem.A, 116, 1998, 63-67.

Parida K.M, Sahu N, Visible light induced photocatalytic activity of rare earth titania nanocomposites, J. Mol. Catal. A: Chem., 287, 2008, 151-158.

Periyat P, Mccormack D.E, Colreavy J, Hinder S.J, Pillai S.C, Improved High-Temperature Stability and Sun-Light-Driven Photocatalytic Activity of Sulfur-Doped Anatase TiO_2, J. Phys. Chem. C, 112, 2008, 7644-7652.

Periyat P, Mccormack D.E, Hinder S.J, Pillai S.C, One-Pot Synthesis of Anionic (Nitrogen) and Cationic (Sulfur) Codoped High-Temperature Stable, Visible Light Active, Anatase Photocatalysts, J.Phys.Chem.C, 113, 2009, 3246-3253.

Periyat P, Saeed P.A, Ullattil S.G, Anatase titania nanorods by pseudo-inorganic templating. Mater, Sci. Semicond. Process., 31, 2015, 658-664.

Sudha M, Senthilkumar S, Hariharan R, Suganthi A, Rajarajan M, Synthesis, characterization and study of photocatalytic activity of surface modified ZnO nanoparticles by PEG capping, J.Sol-Gel Sci.Technol., 65, 2013, 301–310.

Tayade R.J, Bajaj H.C, Jasra R.V, Transition Metal Ion Impregnated Mesoporous TiO_2 for Photocatalytic Degradation of Organic Contaminants in Water, Ind. Eng. Chem. Res., 45, 2006, 5231-5238.

Xiao Q, Si Z, Zhang J, Xiao C, Tan X, Photo induced hydroxyl radical and photocatalytic activity of samarium-doped TiO_2 nanocrystalline, J. Hazard. Mater., 150, 2008, 62-67.

Materials Science Forum
ISSN: 1662-9752, Vol. 855, pp 33-44
doi:10.4028/www.scientific.net/MSF.855.33

Online: 2016-05-19

Direct Sunlight Active Sm^{3+} doped TiO_2 photocatalyst

Binu Naufal, P.K.Jaseela, Pradeepan Periyat*

Department of Chemistry, University of Calicut, Kerala, India - 673635.

*pperiyat@uoc.ac.in

Keywords: Nanoparticles, Sol–gel, TiO_2, Photocatalysis.

Abstract: TiO_2 and Sm^{3+} doped TiO_2 nanocrystalline has been successfully synthesized by a modified sol-gel method. As synthesized samples of TiO_2 and Sm^{3+} doped TiO_2 were calcined at 300, 500, 700 and 800^{o}C and characterized by various techniques such as XRD, UV/Vis Reflectance spectroscopy, FTIR, SEM-EDS and TEM. The crystallite size of Sm^{3+} doped TiO_2 at all calcination temperature is lower than that of TiO_2 due the doping Sm^{3+} ion and thereby induced more nano behavior. FTIR spectroscopy confirmed the presence of Ti-O and Ti-O-Ti bond in TiO_2, in Sm^{3+} doped TiO_2 along with Ti-O and Ti-O-Ti, the presence Sm-O and Ti-O-Sm bonds are confirmed. Diffuse reflectance spectra showed that the Sm^{3+} doped TiO_2 have a significant shift to longer wavelengths and an extension of the absorption in the visible region compared to the TiO_2. SEM images confirmed that the particles are agglomerated and the particle size was decreased in the Sm^{3+} doped TiO_2 in comparison with the TiO_2. EDS analysis showed the presence of Sm^{3+} ion present in the lattice of TiO_2 in doped sample. Finally the photocatalytic activity of TiO_2 and Sm^{3+} doped TiO_2 at various calcinations temperatures was investigated by the degradation of methylene blue solution under UV light and visible light. Doping with the samarium ions significantly enhanced the overall photocatalytic activity for MB degradation under both UV and visible light irradiation. The results showed that the Sm^{3+} doped TiO_2 sample calcined at 700 ^{o}C shows the highest photocatalytic activity under UV light and visible light irradiation.

1. Introduction

Dyes are one of the largest groups of pollutants found in the drinking water and its colour is easily recognizable in water stream [1,2,3]. It is mainly coming from the food and textile industries [1]. These dyes are either toxic or become toxic when being gradually decomposed in the ecosystem and undergo biomagnification in living organisms due to its low rate of natural degradation. These dyes come in contact with certain drugs in the human body they can induce allergic and asthmatic reactions [1]. It is necessary to remove these contaminants to protect our water resources and aquatic organisms. Many physical, chemical and biological treatment technologies are currently being employed to remove dyes or degrade them into non-toxic ones. Unfortunately, many types of organic dyes in water are not removable by these conventional technologies. Advanced Oxidation Processes (AOPs) show the potential to become a preferred treatment technology, attributed to their capability of completely degrading almost all organic dyes into the ultimate products as CO_2 and H_2O.

Among all the AOPs, photo catalytic oxidation (PCO) is the most promising one [1,2,3]. Photocatalytic oxidation is a process where degradation of organic dyes and/or compounds occur by the illumination of photocatalyst without introducing any other chemicals. Under such circumstances, it can be concluded that a new material is needed to degrade the contaminants into non-toxic products by using UV lamps and/or solar light. For this purpose nano TiO_2 is found to be the best photocatalyst [4]. Thus the choice of TiO_2 in the present work was based on its importance in environmental purification and waste water treatment.

TiO_2 is one of the very interesting metal oxide nano material used as a photocatalyst because of its unique optical and physical properties and also due to its easy availability, in-expensiveness and

non-toxicity [4,5,6]. TiO_2 crystallizes mainly in to three – anatase, rutile and brookite [7,8]. Majority of research work has been carried out with either rutile or anatase phase [9]. Among these three different forms of TiO_2, anatase, rutile and brookite, generally anatase has the highest photocatalytic activity than the other two [10]. Due to the large band gap of anatase TiO_2 (Eg=3.2 eV), it absorbs light only in UV region [11]. However, solar energy spectrum contains only 3-5% of UV light, limiting the application of TiO_2 in normal sunlight. In order to overcome this metal doped TiO_2 was synthesized and these metal ion doped TiO_2 shows an appreciable photo activity than bare TiO_2 under normal sunlight [12]. Transition and lanthanide metal ions, have been doped into TiO_2 nanomaterials in order to extend its absorption in the visible region. Liang *et. al.* [13] reported the photocatalytic activity of rare earth ions (Sm^{3+}, Nd^{3+}, Pr^{3+}) doped TiO_2 catalysts for Orange I degradation under both UV and visible light irradiations. Xiao *et. al.* [14] reported the synthesis of Sm^{3+} doped TiO_2 nano crystalline under visible light by auto-combustion technique shift to longer wavelengths compared to bare TiO_2 sample. Shi *et al* [15] reported a series of Sm^{3+} doped TiO_2 for the photocatalytic degradation of methyl orange. Park *et al* [16] reported that the photoluminescence emission of Sm^{3+}doped TiO_2nano tubes with UV light irradiation.

However, all these method required expensive chemicals, templates for structure direction of TiO_2, harsh chemical/heat treatment for removal of the template to obtain pure TiO_2 and induce crystallinity into TiO_2. In this work a simple modified sol-gel method was used to synthesise TiO_2 and Sm^{3+}doped TiO_2 and characterized with XRD, FTIR, DRS, SEM and TEM. Photo catalytic activity of these samples were studied by photo degradation of methylene blue under UV and direct sun light. The effect of calcination temperatures on the photo catalytic activity was also been discussed.

2. Experimental

TiO_2 and Sm^{3+} doped TiO_2 catalysts were prepared with the raw materials of analytical grade. The raw materials used are titanium isopropoxide ($Ti(OPr)_4$, Aldrich, 97%), Sm $(NO_3)_3$, glacial acetic acid (Aldrich, 99.8%) and deionized water. In a typical experiment to synthesize nano TiO_2, $Ti(OPr)_4$ was mixed with glacial acetic acid followed by the addition of de-ionized water in small quantity with constant stirring. $Ti(OPr)_4$:acetic acid : water ratio was kept as 1:10:100. The homogenous solution was stirred for 3 hrs. It was dried at 100 ^oC on water bath for 12 hrs. The dried powder was calcined at 300, 500, 700 and 800 ^oC at a heating rate of 5 ^oC/ minute and held at this temperature for 2 hrs in the absence of air. For the Sm^{3+} doped TiO_2 synthesis, calculated amount of samarium (III) nitrate for 5 weight percentage were added and the same procedure is followed.

X-ray diffraction (XRD) patterns of the calcined gels were obtained with a Miniflex 600 X-ray diffractometer with CuKα radiation, λ=1.54 A°, Voltage 40 KV and current 15mA in the diffraction angle range 2θ = 10–70º. The FT IR spectra of the gel dried at 100 ºC was measured by using a Jasco-FT/IR-4100 spectrometer in the wave number range 4000-400 cm^{-1} using 70 scans for each sample. The diffuse reflectance spectra (DRS) of the catalysts in the wavelength range of 200-800 nm were obtained using a UV-Vis reflectance spectrophotometer using a Jasco-V-550 UV/VIS spectrophotometer. The BET (Brunauer, Emmett and Teller) surface area measurements and porosity analysis were carried out by nitrogen adsorption using a Quantachrome NOVA 2000e surface area analyzer. The measurements were carried out at liquid nitrogen temperature after degassing the powder samples for 2 h at 200 °C.
Morphology of the samples were examined using Scanning Electron Microscope using Hitachi,SU-66000 and elements Ti and Sm present in the samples were determined using Energy Dispersive Spectroscopy.

2.1 Photocatalytic activity

In a typical experiment 0.1 g of sample was dispersed in 50 ml of methylene blue solution having concentration of 1 x 10^{-4} M. This solution was stirred for 10 minutes in dark for the chemisorptions on the surface of the catalyst to avoid any absorption error. The methylene blue solution containing catalyst was then irradiated under UV photo reactor (LZC-4x Luzchem Photo reactor) with continuous and uniform stirring. The degradation of methylene blue dye was monitored by taking 5 ml aliquots at different intervals of time. These aliquots were centrifuged at 4500 rpm for 15 minute and absorption spectra of the samples were recorded using UV/Visible spectrophotometer. The photo catalytic activity in the presence of sunlight was determined by carrying out the reaction under direct normal sunlight. Intensity of sunlight was measured using lux meter from 9 am to 4 pm with a time interval of one hour. The result shows that from 9 am to 12 noon intensity increases and upto 2 pm intensity remains constant and then decreases. In this work the experiment was carried out (sunlight irradiation) at 12 to 2 pm. During that time intensity remains constant showed a value between 75000±100 lux. Methylene blue concentration was used to determine at a wavelength range of 650 – 660 nm. The absorbance set at 650 – 660 nm is due to the color of the dye solution and it is used to monitor the degradation of dye. The rate of degradation was assumed to obey first order kinetics and hence the rate constant for degradation k was obtained from the first order plot using equation 1.

$$\ln(A_o/A)=kt \quad (1)$$

Where A_o is initial absorbance, A is absorbance after a time and k is the first order rate constant.

3. Results and Discussion

Titanium tetraisopropoxide ($Ti(OPr)_4$) undergo very fast hydrolysis with water. When $Ti(OPr)_4$ reacts with water, the Ti metal ion increases its coordination from 4 to 6 by employing its vacant d-orbitals to accept oxygen lone pairs from ligands like OH groups[12]. This fast hydrolysis will generate only ill-defined TiO_2. Hence required a pre-stabilization step against hydrolysis with water. Therefore glacial acetic acid was used as a stabilizing and catalyzing agent. $Ti(OPr)_4$ stabilized with acetic acid usually follows a condensation pattern producing linear chain, enclosing small pores in the gel network and a stable sol is obtained. This will lead to improve the textural properties such as surface area, crystallinity *etc* during the calcination of the TiO_2 powder. To this stabilized sol samarium (III) nitrate was used as a dopant source of Sm^{3+} ion.

3.1 X-ray Diffraction (XRD)

XRD patterns of TiO_2 and Sm^{3+} doped TiO_2 powder calcined at a temperature of 300, 500, 700 and 800^{o}C were shown in Figure 1. For TiO_2 the major peaks obtained at 2θ value at 25.18º, 37.94º, 48.07º,54.15º and 62.52º were assigned to diffraction from the planes (101) , (103), (200), (105), and (213) respectively. Sm^{3+} doped TiO_2 possess peaks at 2θ value at 25.39º, 37.56º, 47.85º, 54.17ºand 62.5ºwere corresponds to (101), (103), (200), (105) and(213) planes respectively. These results are consistent with the data base of (JCPDS No 75-1537) of an anatase TiO_2. From the XRD pattern it is confirmed that both $TiO_2$and Sm^{3+}doped TiO_2 are in anatase structure and there is no change in relative intensities of all peaks in the TiO_2 and Sm^{3+} doped TiO_2.From Figure 1C,XRD patterns of Sm^{3+} doped TiO_2 at calcination temperature of 800ºC shows a doublet at 2θ= 53.83 and 55.12º corresponding to the planes (105) and (211) where as in the TiO_2 sample this is turned to singlet peak at 2θ= 54.01ºcorresponding to (105) plane in the Sm^{3+} doped TiO_2 sample.

From these results of XRD spectra, it is clear that both TiO_2 and Sm^{3+}doped TiO_2 consist of only anatase structure ,it may be due to the formation of Sm-O-Ti bond which inhibit the movement of Ti atoms for the phase transformation [17] and that of bare TiO_2 may be due to the addition of acetic acid while synthesis, which follows a condensation pattern producing linear chain, enclosing small pores in the gel network and a stable sol is obtained after hydrolysis and the relative intensity

of dominant (101) peaks increased significantly in Sm^{3+} doped TiO_2 with respect to the TiO_2. This confirms the Sm^{3+} doping induced higher crystallinity and phase purity in TiO_2.

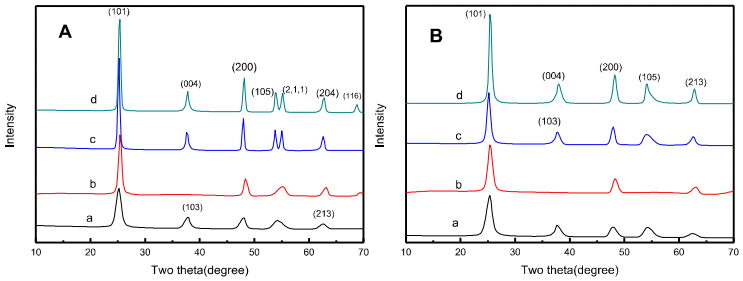

Fig. 1. XRD pattern of A) TiO_2 B) Sm^{3+}doped TiO_2at a) 300 b) 500 c) 700 and d) 800 ^oC

From these results of XRD spectra, it is clear that both TiO_2 and Sm^{3+}doped TiO_2 consist of only anatase structure ,it may be due to the formation of Sm-O-Ti bond which inhibit the movement of Ti atoms for the phase transformation [17] and that of bare TiO_2 may be due to the addition of acetic acid while synthesis, which follows a condensation pattern producing linear chain, enclosing small pores in the gel network and a stable sol is obtained after hydrolysis and the relative intensity of dominant (101) peaks increased significantly in Sm^{3+} doped TiO_2 with respect to the TiO_2. This confirms the Sm^{3+} doping induced higher crystallinity and phase purity in TiO_2.

Crystalline size calculated for TiO_2 and Sm^{3+} doped TiO_2 using Sherr's equation were shown in Table 1. Crystallite sizes of TiO_2 calcined at temperature 300, 500, 700 and 800 ^oC are 7.84, 12.6, 21.7 and 19.3 nm respectively. Similarly crystallite size of Sm^{3+} dopedTiO_2 calcined at 300, 500, 700 and 800 ^oC were 6.96, 8.02, 11.4 and 15.2 nm respectively. It is found that the crystallite size decreased by Sm^{3+} doping confirms the improvement in the nano crystalline nature of TiO_2 as a result of Sm^{3+} doping. For TiO_2upto 700 ^oC crystallite size increases with calcination temperature. Sm^{3+} doped TiO_2 doped sample showed increase in crystalline size with all calcined temperature. From table 1 it is clear that a drastic change in crystallite size occurs in the case of 700 ^oC calcined sample of TiO_2 to Sm^{3+} doped TiO_2. TiO_2 possess 27.4 nm, however Sm^{3+} doped TiO_2 possess only 11.4 nm. It indicates that upon doping crystallite size decreases and thus improves nano behavior of Sm^{3+}doped TiO_2. This decrease in crystallite size may be due to the distribution of dopant cations at the crystal lattice or it may be on the grain boundary of TiO_2 which inhibits grain growth by providing a barrier between the TiO_2grains[18]. In addition to this the decrease in crystalline size may attributed to the presence of Ti-O-Sm bond formation in the Sm^{3+} doped sample, which inhibits the growth of crystal grains[19].

Table 1. Crystallite size of TiO_2 and Sm^{3+} doped TiO_2 calcined at different temperatures.

Sample	Crystallite size [nm]			
	300 [^oC]	**500[^oC]**	**700 [^oC]**	**800 [^oC]**
TiO_2	7.84	12.6	21.7	19.3
Sm^{3+} doped TiO_2	6.96	8.02	11.4	15.4

3.2 FTIR Spectroscopy

The FTIR spectra of TiO_2 and Sm^{3+}doped TiO_2 calcined at 300 °C were shown in Figure 2. TiO_2 and Sm^{3+} doped TiO_2 sample possess strong and broad band in the range of 400-700 cm^{-1} which were attributed to Ti-O stretching and Ti-O-Ti bridging stretching modes, which is a characteristic peaks of observable in the anatase phase of TiO_2. A new band at 490 cm^{-1} was observed in the spectra of Sm^{3+}doped TiO_2 samples. This band is attributed to the Sm–O bond[20]. This bond arises due to the reason that Sm^{3+} ions dispersed on the surface of TiO_2 in the form of metal oxides, formed during the calcination process. The presence of peak at 1120 cm^{-1} in Sm^{3+}doped TiO_2sample may be due to the Ti-O-Sm stretching vibrations. The peak at 1425, 1532 cm^{-1} in both TiO_2 and Sm^{3+} doped TiO_2 is due to the symmetric and asymmetric stretching vibration of acetate groups. The band at 1632 cm^{-1} and broad band at 3400 cm^{-1} in both sample corresponding to the O–H bending and stretching modes of water indicative of the presence of residual water and hydroxyl groups present in the sample. Similar type of observation were also seen in the FTIR spectra of TiO_2 and Sm^{3+} doped TiO_2 calcined at 500, 700 and 800 °C.

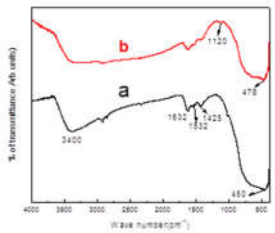

Fig. 2. FTIR spectra of a) TiO_2b) Sm^{3+} doped TiO_2calcined at 300 °C.

3.3 BET Surface area measurements

BET surface areas and total pore volumes were calculated by BET method for the sample calcined at 700 $^{\circ}C$ of TiO_2 and Sm^{3+} doped TiO_2 were measured. The results showed that the surface area of the sample was strongly dependent on Sm^{3+} doping. TiO_2 calcined at 700 $^{\circ}C$ shows a surface area value 1.14 m^2/g and the Sm^{3+} doped TiO_2 calcined at same temperature shows a value of 68.7 m^2/g, which is very much higher than TiO_2. The higher amount of Sm^{3+} going in to the TiO_2 matrix will increase the defects in the TiO_2 matrix and hence it will increase the surface area. This sol-gel method leads to a thermally stable anatase TiO_2 having a significantly higher surface area. This higher surface area of Sm^{3+} doped TiO_2 can help to absorb more number of dye molecules compared to bare TiO_2 during the photocatalytic reaction and hence contribute towards higher photocatalytic effiency.

3.4 Scanning Electron Microscopy (SEM)

The morphology of the TiO_2 and Sm^{3+} doped TiO_2 sample was analyzed using Scanning Electron Microscopy (SEM). SEM images of TiO_2 and Sm^{3+} doped TiO_2 calcined at a temperature 700 ^{0}C showed in the Fig 3. SEM analysis indicated that the particles undergo agglomeration in both TiO_2 and Sm^{3+} doped TiO_2 samples. It is clear from the Figure 3 that the particle size of Sm^{3+} doped TiO_2 sample is lower than that of TiO_2. This observation is in agreement with the crystalline size calculation from XRD where TiO_2 showed a size of 21.7 nm whereas Sm^{3+} doped TiO_2 showed only 11.4 nm crystalline size (Table 2) at calcination temperature 700 °C. That means the Sm^{3+} ion doping could hinder the increase of crystallite size during calcinations. The average grain diameter was measured as being in the range of a few nanometers. Also SEM images showed the uniform nature of particles with no change in particle morphology due to samarium doping with well defined clear boundaries. EDS analysis was carried out for the TiO_2 and Sm^{3+}doped TiO_2 to

determine the chemical composition. Strong X-ray peaks associated with Ti and oxygen are present in TiO_2 where as strong peaks of Sm were found in the Sm^{3+} doped TiO_2 along with Ti and oxygen. Quantitative analysis by the EDS software package was used to determine the respective weight percentages of each element in the TiO_2 and Sm^{3+} doped TiO_2shown in Table 2 confirms the presence of both Ti and Sm in the lattice of Sm^{3+} doped TiO_2.

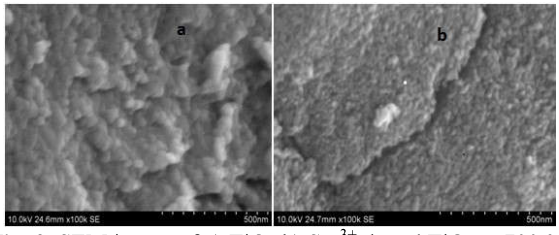

Fig. 3. SEM image of a) TiO_2 b) Sm^{3+} doped TiO_2 at 700 °C

Table 2. EDS elementary analysis of TiO_2 and Sm^{3+} doped TiO_2 calcined at 700 °C.

Element	TiO_2[%]	Sm^{3+} doped TiO_2[%]
Ti	45.76	55.4
O	54.24	43.29
Sm	0	1.32

3.5. Optical Characterisation

Diffuse Reflectance spectroscopy (DRS) was used to obtain the band gap energy value of TiO_2 and Sm^{3+} doped $TiO_2$and were shown in Table 3.From DRS, it is clear that the bare TiO_2 has no absorption in the visible region (>400 nm), however the Sm^{3+}-doped TiO_2 has showed significant absorption between 400 and 500 nm. Sm^{3+} doped TiO_2 sample (Figure 4) showed a significant shift to longer wavelengths and an extension of the absorption in to the visible region due to the doping effect of samarium. Hence band gap energy of Sm^{3+}doped TiO_2samples is lesser compared to TiO_2 at different calcinations temperature. Li *et al* [21] reported that the band gap of TiO_2nanoparticles was reduced by Nd^{3+} doping and the band gap narrowing was primarily attributed to the substitution Nd^{3+} ions which introduced electron states into the band gap of TiO_2 to form the new lowest unoccupied molecular orbital. Here FTIR and EDS analysis already confirmed the presence of Sm^{3+} ion in the lattice of TiO_2. The Sm^{3+} ion in TiO_2 lattice will introduce new electronic states into the band gap of TiO_2 to form the new lowest unoccupied molecular orbital that will expected to lead to the visible light photocatalytic activity of Sm^{3+} doped TiO_2[14].

Table 3. Band gap of TiO_2 and Sm^{3+} doped TiO_2 calcined at different temperatures.

Temperature [^oC]	Band gap[eV]	
	TiO_2	Sm^{3+} dopedTiO_2
300	3.34	2.57
500	3.22	2.52
700	3.05	2.50
800	3.00	2.46

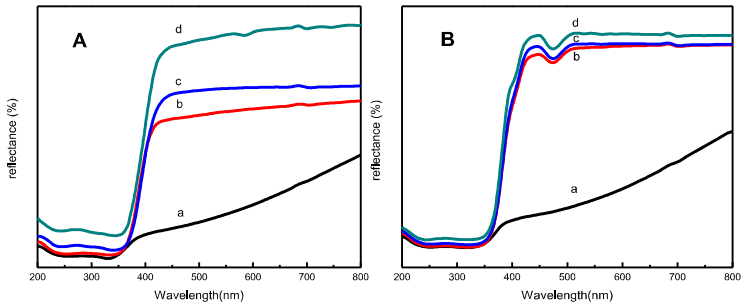

Figure 4. Diffuse Reflectance Spectra of A) TiO_2 B) Sm^{3+}doped TiO_2 at a) 300 b) 500 c) 700 d) 800 ^oC

3.6. Transmission Electron Microscope (TEM)

Fig. 5 shows TEM images of $TiO_2$and Sm^{3+} doped TiO_2 calcined at 700 $^{\circ}C$.TiO_2 shows a crystallite size of 16–28 nm(Fig. 5a) at 700 $^{\circ}C$. On the other hand, the Sm^{3+} doped TiO_2has a crystallite size of 7-12 nm (Fig. 5b), and thus the TEM observations support the conclusions derived from the XRD data. The electron diffraction image of Sm^{3+} doped TiO_2calcined at 700 $^{\circ}C$ shows broad bands due to the Scherrer line broadening which is attributed to the small crystallite size [22,23]however TiO_2, at same temperature, showed distinct spots due to the high crystallinity and larger size of the crystals.

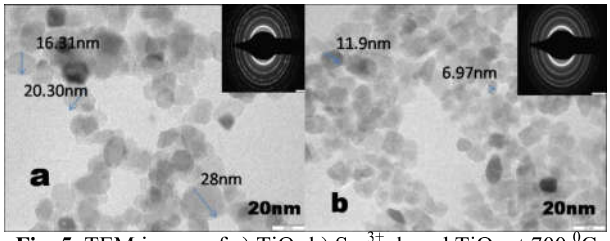

Fig. 5. TEM image of a) TiO_2 b) Sm^{3+} doped TiO_2 at 700 ^0C

3.7. Photocatalytic Activity of TiO_2 and Sm^{3+} doped TiO_2

Under irradiation from a suitable light source applied to the TiO_2 material, the electrons in theTiO_2 valence band will be excited, causing the electron to jump to the conduction band resulting in formation of a positive hole in the valence band and a free electron in the conduction band. These photogenerated electrons are able to reduce the dioxygen molecule to produce superoxide radicals and the hole can simultaneously oxidize water to produce hydroxyl radicals. These radicals are highly reactive and are able to break chemical bonds. This makes TiO_2, a suitable photocatalyst useful in the field of environmental purification. Textile dyes and other industrial dye stuffs constitute one of the largest groups of organic compounds that represent an increasing environmental danger. Methylene Blue is a kind of typical azo dye used in the textile dye industry. Here the selected organic pollutant methylene blue dye as a target of photodegradation due to these practical values. The photo catalytic activity of the samples is executed by the degradation of methylene blue aqueous solution. Before irradiating with a lamp light, the samples were stirred in the dark for fifteen minutes. Detection results show that the methylene blue concentration has negligible decrease caused by the slight absorption on photocatalysts surface, which indicates that there is no degradation in the absence of irradiation. When photocatalytic reaction is conducted in

aqueous medium, the holes were effectively scavenged by the water and generated hydroxyl radicals OH•, which are strong and unselected oxidant species in respect of totally oxidative degradation for organic substrates. The holes, free electron, superoxide and hydroxyl radicals have been proposed as the oxidizing and reducing species responsible for the degradation (mineralization)of the organic substrates [24,25,26]

$$TiO_2 + hv \rightarrow h^+ + e^- \quad (1)$$
$$H^+ + H_2O \rightarrow OH\bullet + H^+ \quad (2)$$
$$h^+ + dye \rightarrow products \quad (3)$$
$$OH\bullet + dye \rightarrow products \quad (4)$$
$$MB + TiO_2 \rightarrow CO_2 + H_2O + NO^-_3 + NH_4^+ + SO_4^{2-} \quad (5)$$

Photocatalytic activity of both TiO_2 and Sm^{3+} doped TiO_2 for methylene blue degradation under UV light are summarized in the Table 4. From the Table 4, it is observed that at all given temperature, Sm^{3+} doped TiO_2 sample showed greater photocatalytic activity than TiO_2 under UV light.

Table 4. Degradation time and rate constant in min under UV light of samples at different calcination temperatures

Temperature (^oC)	TiO_2		Sm^{3+} doped TiO_2	
	Time (min)	Rate constant	Time (min)	Rate constant
300	150	0.021	90	0.009
500	70	0.037	45	0.051
700	210	0.003	50	0.066
800	>210	0.002	60	0.050

The rate constant calculated from the first order kinetics were also shown in the Table 4. Among the Sm^{3+}doped TiO_2 maximum activity was obtained for sample calcined at 700 ^oC. The highest rate constant 0.066 min^{-1} corresponds to the Sm^{3+} doped TiO_2 at 700 ^oC while its TiO_2 counterpart has only 0.002 min^{-1}. Absorption spectra of methylene blue dye degradation under UV using TiO_2 and Sm^{3+} doped TiO_2 at 700 ^oC were shown in Figure 6. Therefore it can be concluded that the Sm^{3+} doped TiO_2 calcined at 700 ^oC is the best photocatalyst among these samples under UV light irradiation, showing the fastest decolourization of methylene blue and has the maximum degradation rate constant. The reusability of the best photocatalyst Sm^{3+} doped TiO_2 calcined at 700 ^oC is checked by repeating the photocatalytic experiment using the used catalyst. The result showed that same activity was observed for three consecutive cycles, thereafter a small decrease in activity was observed. However, after the third cycle same catalyst was washed with methanol, dried and reused exhibited the same activity as that of the first experiment.

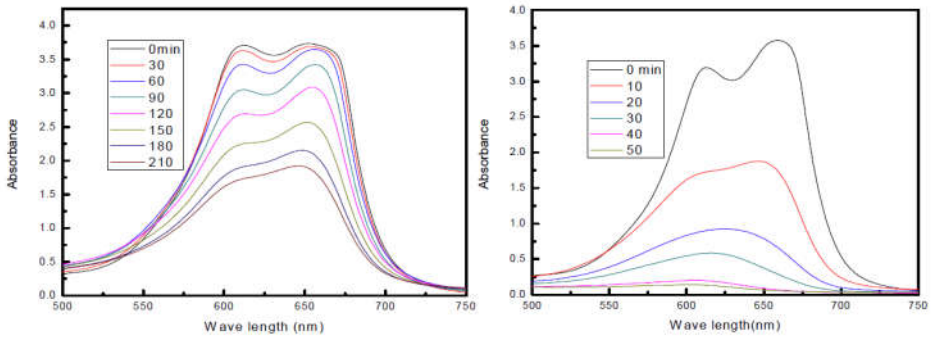

Fig. 6. Absorption spectra of methylene blue dye degradation under UV using A) TiO_2 B) Sm^{3+} doped TiO_2calcined at 700 ^oC.

Generally when TiO_2 excited by visible light, it will not undergo photocatalysis. However, from the experimental details it could be seen that TiO_2 showed photocatalytic activity, due to dye sensitization, which led to photocatalytic activity of TiO_2 as presented in equations [27].

$$Dye + hv \rightarrow dye^* \quad (6)$$

$$TiO_2 + dye^* \rightarrow TiO_2(e^-) + dye^{+\bullet} \quad (7)$$

$$O_2 + TiO_2(e^-) \rightarrow O_2^{\cdot-} + TiO_2 \quad (8)$$

$$O_2^{\cdot-} + H_2O \rightarrow HO_2^{\cdot} + OH^- \quad (9)$$

$$HO_2^{\cdot} + H_2O + TiO_2(e^-) \rightarrow H_2O_2 + OH^- + TiO_2 \quad (10)$$

$$H_2O_2 + TiO_2(e^-) \rightarrow OH^- + OH^{\cdot} + TiO_2 \quad (11)$$

The visible light activity of TiO_2 and Sm^{3+} doped TiO_2 under direct sunlight using the methylene blue degradation experiment were carried out and the times taken for degradation of methylene blue using TiO_2 and Sm^{3+} doped TiO_2 under visible light results were shown in Table 5. From the Table 5, it is found that Sm^{3+} doped TiO_2 sample undergo methylene blue degradation much faster than compared to TiO_2 at all calcinations temperatures under visible light irradiation. The rate constant calculated from the first order kinetics were shown in Table 5.Among the doped sample maximum activity was obtained for sample calcined at and 700^oC. The maximum reaction rate 0.028 min^{-1} corresponds to the Sm^{3+} doped TiO_2 at 700 ^oC while its TiO_2 counterpart has only 0.004 min^{-1}. Therefore it can be concluded that the Sm^{3+} doped TiO_2 calcined at 700 ^oC is the best photocatalyst among the samples, which is showing the fastest decolourization of methylene blue and has the maximum degradation rate. Absorption spectra of methylene blue dye degradation under visible light using TiO_2 and Sm^{3+} doped TiO_2 at 700 ^oC were shown in Figure 7.

Table 5. Degradation time and rate constant of TiO_2 and Sm^{3+} doped TiO_2calcined at different temperatures under sunlight.

Temperature (^oC)	TiO_2		Sm^{3+} doped TiO_2	
	Time (min)	Rate constant	Time (min)	Rate constant
300	150	0.007	140	0.005
500	90	0.009	70	0.024
700	>105	0.004	70	0.028
800	>105	0.001	70	0.028

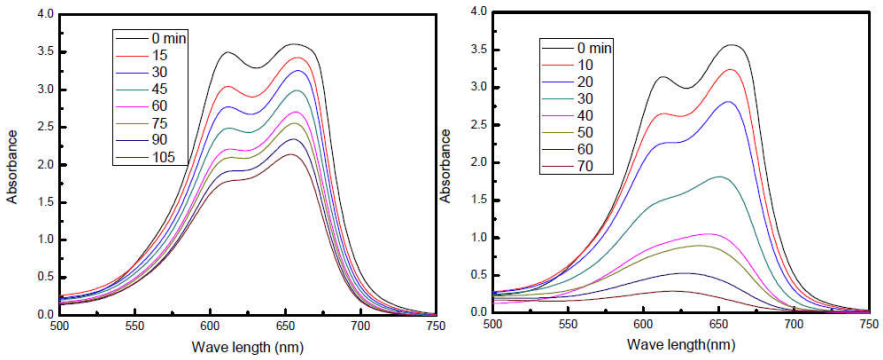

Fig.7. Absorption spectra of methylene blue dye degradation under visible using A) TiO_2B) Sm^{3+} doped TiO_2calcined at 700°C.

The reason why the Sm^{3+} doped sample showed higher activity than the TiO_2 can be explained as follows. The methylene blue dye is adsorbed as well as complexes with the Sm (III) ions on the surface of the catalyst, then the dye molecule is excited by absorption of a suitable visible light photon (Figure 8). The electrons of excited dye molecule can be injected into conduction band (CB) of TiO_2.The Sm (III) species can then act as an effective electron scavenger to trap the conduction band electrons of TiO_2, which were injected from the excited dye molecule. The electrons trapped in Sm (III) sites were subsequently transferred to the surrounding adsorbed $O_2$by oxidation process leading to generation of effective oxidative hydroxyl radical species capable of attacking the nearby dye molecules. Ti(III) can also form a defect level and act as the hole-trap to promote the charge transfer[28,29]. These defects on the TiO_2 surface or in its bulk can suppress the recombination of electron–hole pairs and hence extend their lifetime. The processes described above can be expressed by

$$Dye + h\upsilon \rightarrow Dye^{*} \quad (12)$$

$$Dye^{*} + TiO_2 \rightarrow Dye + TiO_2(e^{-}) \text{ (electron injection)} \quad (13)$$

$$Sm^{3+} + e^{-} \rightarrow Sm^{2+} \quad \text{(electron trapping)} \quad (14)$$

$$Sm^{2+} + O_2 \rightarrow Sm^{3+} + O_2^{\bullet -} \quad \text{(electron trapping)} \quad (15)$$

$$O_2^{\bullet -} + 2\,H^{+} \rightarrow 2\,^{\bullet}OH \quad \text{(Generation of oxidative species)} \quad (16)$$

$$Ti^{4+} + e^{-} \rightarrow Ti^{3+} \quad (17)$$

$$Ti^{3+} + h^{+} \rightarrow Ti^{4+} \quad (18)$$

Sm^{3+} might trap the photogenerated electrons and then transfer them to O_2 adsorbed on the surface of TiO_2 to produce the very oxidant superoxide radical ion O_2^{-} according to the following reactions.

$$Sm^{3+} + e \rightarrow Sm^{2+} \text{ (electron trapping)} \quad (19)$$

$$Sm^{2+} + O_2 \rightarrow Sm^{3+} + O_2^{-} \text{ (electron transfer)} \quad (20)$$

$$O_2^{-} + 2H^{+} \rightarrow 2OH^{\cdot} \quad (21)$$

Sm^{2+} with 6f electrons is unstable and the electrons can be easily de-trapped and transferred to the oxygen molecules. Therefore it reduced the recombination rate of the photogenerated electron and hole, which enhanced the rate photocatalytic degradation of methylene blue dye. The mechanism of dye degradation using Sm^{3+} doped TiO_2 is schematically represented in Figure 8.

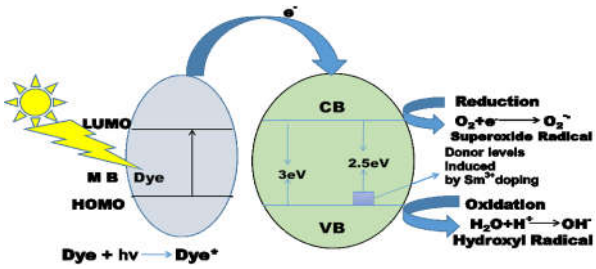

Fig. 8. Photocatalytic mechanism of dye degradation using Sm^{3+} doped TiO_2.

4. Conclusions

Nanocrystalline TiO_2 and Sm^{3+} doped TiO_2 e has been successfully synthesized using a modified sol-gel method. The samples were calcined at 300, 500, 700 and 800 ^{o}C and characterized by various techniques such as XRD, UV/Vis Reflectance spectroscopy, FTIR, SEM-EDS and TEM. TEM study confirmed that TiO_2 has a crystallite size of 16–20 nm, on the other hand, the Sm^{3+}doped TiO_2has a size of 7-12 nm, revealed that the doping Sm^{3+} ion decreased the crystallite size of TiO_2 and thereby induced more nano behavior. FTIR spectroscopy confirmed Ti-O and Ti-O-Ti bond in TiO_2, in Sm^{3+} doped TiO_2 presence of Sm-O and Ti-O-Sm bonds are also been confirmed along with Ti-O and Ti-O-Ti bond. Diffuse reflectance spectra showed that the Sm^{3+}doped TiO_2 have a significant red shift and an extension of the absorption in the visible region compared to the TiO_2. SEM images confirmed that the particles are agglomerated and EDS analysis confirmed the presence of Sm^{3+} ion in lattice of TiO_2. Finally the photocatalytic activity of TiO_2 and Sm^{3+} doped TiO_2 at various calcinations temperatures was investigated by the degradation of methylene blue solution under UV light and visible light. Doping with the samarium ions significantly enhanced the overall photocatalytic activity for MB degradation under both UV and visible light irradiation. The results showed that the Sm^{3+} doped TiO_2 sample calcined at 700 ^{o}C shows the highest photocatalytic activity under UV light and visible light irradiation. These high temperature stable and higher photoactive Sm3+ doped anatase TiO_2 may be used for the self-cleaning and antibacterial coatings on high temperature processed ceramic materials such as tiles, glass and sanitary wares.

References:

[1] I. Arslan-Aloton, *Advanced oxidation of textile industry dyes*, S. Parsons (Ed.), IWA Publishing, London. (2004) 302–308.
[2] A. Houas, H. Lachheb, M. Ksibi, E. Elalooui, C. Guillard, J.M. Herrmann, *App. Catal. B Environ.* 31 (2001)145–157.
[3] M. Karkmaz, E. Puzenat, C. Guillard, J.M. Herrmann, *App.Catal. B Environ.* 51 (2004)183–194.
[4] X. Wang, Z. Li, J. Shi, Y. Yu, *Chem. Rev.* 114 (2014) 9346−9384
[5] R.J. Tayade, H.C. Bajaj, R.V. Jasra, *Ind. Eng. Chem. Res.* 45 (2006) 5231-5238.
[6] R.J. Tayade, H.C. Bajaj, R.V. Jasra, *Desalination.* 275 (2011) 160-165.
[7] R.J. Tayade, P.K. Surolia, M.A. Lazar, R.V. Jasra, *Ind. Eng. Chem. Res.* 47 (2008) 7545-7551.
[8] P. Periyat, D. E. Mccormack,S. J. Hinder, S. C. Pillai,*J. Phys. Chem. C.* 113 (2009) 3246-3253.
[9] P. Periyat, D. E. Mccormack, J.Colreavy, S. J. Hinder, S. C. Pillai. *J. Phys. Chem. C.* 112(2008) 7644-7652.

[10] P. Periyat, K.V. Baiju, P. Mukundan, KGK Warrier, *Applied Cata. A: Gen.*349 (2008) 349-354.
[11] P. Periyat, P.A. Saeed, S.G.Ullattil, *Mater. Sci. Semicond. Process.*31 (2015) 658-664.
[12] S.C. Pillai, P. Periyat, R. G. Kutty, D.E. McCormack, M. K. Seery, H. Hayden, J. Colreavy, D. Corr and S.J. Hinder, *J. Phys. Chem. C.*111 (2007) 1605-1612.
[13] C. Liang, F. Li, C. Liu, J. Lu, X. Wang, *Dyes and Pigments*. 76 (2008) 477-484.
[14] Q. Xiao, Z. Si , Z. Yu , G. Qiu, *Mater. Sci. Eng.B.*137 (2007)189-195.
[15] J. Shi, J. Zheng, Y. Hu and Y. Zhao, *Environ. Eng. Sci.* 25(2008) 489-496.
[16] D. J. Park, T. Sekino, S. Tsukuda S. Tanaka,*Res. Chem. Intermed,* 39 (2013) 1581–1591.
[17] A.M. Ferrari-Lima,R.G. Marques, M.L. Gimenes, N.R.C. Fernandes-Machado, *Catal. Today* 254(2015) 119–128.
[18] X. Z. Ding, X. H. Liu*, J. Mater. Res*. 13 (1998) 2556-2562.
[19] J. Lin, J. C. Yu, *J. Photochem. Photobiol. Chem.A.* 116 (1998) 63-67.
[20] Y. P. Yang, K. L. Huang, *J. Rare Earth.* 4 (1996) 20-22.
[21] W. Li, Y. Wang, H. Lin, S. I. Shah, C.P. Doren, S.A. Rykov, J.G. Chen,M.A. Barteau, *Appl. Phys. Lett.* 83 (2003)4143-4145.
[22] E. Borgarello, J. Kiwi, M. Gratzel,, E. Pelizzetti, M. Visca, *J. Am. Chem. Soc.*104 (1982)2996-3002.
[23] K.V. Baiju, C. P. Sibu, K. Rajesha, P. K. Pillai, P. Mukundan, K. G. K. Warrier, W. Wunderlich,*Mater. Chem. Phy.* 90 (2005) 123–127.
[24] K.M. Parida, N. Sahu*, J. Mol. Catal. A: Chem.* 287 (2008) 151-158.
[25] V. Stengl, S. Bakardjieva, N.Murafa*, Mater. Chem. Phys.*114 (2008) 217-226.
[26] Q. Xiao ,Z. Si, J. Zhang, C. Xiao, X. Tan*, J.Hazard.Mater.* 150 (2008)62-67.
[27] Chun-Hua Liang , Fang-Bai Li , Cheng-Shuai Liu , Jia-Long Lu, Xu-Gang Wang, *Dyes and pigments.* 76 (2008) 477-484.
[28] M. Saif, M.S.A. Abdel-Mottaleb,*Inorg. Chim. Acta.* 360 (2007) 2863-2874.
[29] D. G. Huang, S.J. Liao, W.B. Zhou, S.Q. Quan, L. Liu, Z.J. He, J.B. Wan, *J. Phys. Chem.Solids* 70 (2009) 853-859.